



**University of  
Reading**

# **Novel Strategies to Treat Snake Venom Induced Muscle Damage**

**Medha Sonavane**

This thesis was submitted for the degree of Doctor of  
Philosophy

**School of Chemistry, Food and Pharmacy  
Institute for Cardiovascular and Metabolic Research**

December 2023

*Snakebite is the most important tropical disease you've never heard of.*

*-Kofi Annan*

## Table of Contents

Declaration of Original Work	
Acknowledgement.....	
Abbreviations .....	
List of Antibodies.....	
Abstract.....	
1. Introduction .....	1
1.2 Evolution of snakes .....	2
1.3. Snake venoms .....	3
1.3.1 Structure and functions of major snake venom toxins.....	5
1.4. Skeletal muscle .....	13
1.5. Skeletal muscle regeneration .....	17
1.6. Venom-induced muscle damage .....	21
1.7. Pathologies caused by venoms relating to muscle damage .....	22
1.8. Current treatment approaches for SBE-induced local tissue damage.....	26
1.9. Alternative treatments for SBE venom-induced local muscle damage .....	27
1.10. Regenerative medicine to improve muscle regeneration .....	30
1.11. Improving muscle regeneration by reducing fibrosis.....	33
1.12. Rationale of this study.....	34
1.13. Hypothesis, aim and objectives .....	35
References .....	36
2. Experimental Chapters.....	48
2.1 Impact of small molecule inhibitors on the attenuation of venom-induced muscle damage .....	48
Abstract.....	49
1. Introduction .....	50
2. Material and Methods.....	52
3. Results.....	55
4. Discussion .....	70
References .....	73
2.2 Soluble activin receptor type IIB-mediated inhibition improves muscle regeneration following <i>Crotalus atrox</i> venom-induced damage.....	77
Abstract.....	78
1. Introduction .....	78

2. Materials and methods.....	80
3. Results.....	83
4. Discussion .....	94
References .....	97
2.3 Mesenchymal stem cells-derived secretome improves skeletal muscle regeneration following Russell's Viper-induced muscle damage.....	102
Abstract.....	102
1. Introduction .....	103
2 Material and Methods.....	105
3 Results.....	108
4 Discussion .....	114
References .....	118
2.4 Intramuscular bleeding and formation of microthrombi during skeletal muscle damage caused by a snake venom metalloprotease and a cardiotoxin.....	122
Abstract:.....	123
1. Introduction .....	124
2. Materials and Methods.....	125
3. Results.....	128
4. Discussion .....	137
References .....	143
3. Conclusions .....	149
4. PUBLICATIONS AND PRESENTATIONS .....	156

## **Declaration of Original Work**

I confirm that this is my own work and the use of all material from other sources has been properly and fully acknowledged.

Medha Sonavane

## **ACKNOWLEDGEMENT**

First and foremost, I would like to thank my Baba (father) and Aai (Mother), who made me capable enough to take this leap of faith and pursue this PhD. You taught me to be brave, you taught me to dream, always loved and supported me unconditionally, and for that I will be entirely grateful.

I thank my supervisors, Prof. Sakthivel Vaiyapuri. Thank you, Sakthi, for being a kind person and my mentor through the journey of my PhD. I also thank my second supervisor, Prof. Ketan Patel. Thank you, Ketan, for your guidance and for being 'YODA' when I struggled otherwise. Thank you for being two strong pillars of my PhD journey. Thank you for being a solid support and providing expert guidance and encouragement during this entire process.

I would also like to thank my lab members, Dina Albadawi, Anika Salim, Sohail Gilabadi, Pradeep Kumar, Elancherian Rajan and Jose Rafael Almeda, Jarred Williams for supporting me academically and emotionally. I would also like to thank Ali Aqalaf and Robert Mitchell for helping me with my animal experiments.

I would express my love for sisters Apurva and Manasi for being my biggest support system. I wouldn't be the person I am without you guys.

Finally, the person without whose support I wouldn't even be here is my husband, Rushikesh Nikam. Thank you for moving to a different continent for me to pursue my dream. It was a risk, and you took it for me. You always kept one side strong, allowing me to walk this path towards my doctorate. You took care of me, our daughter our home, and I could never thank you enough for that.

My acknowledgement section will be incomplete without the mention of my daughter Hridnya, and I dedicate my PhD to her. Hridu baby, 'In this chaos of uncertainties, you have been my peace.' Love you till Rigel and back!!!!

## Abbreviations

<b>Abbreviation</b>	<b>Acceptations</b>
3FTx	Three finger toxins
5'NUC	5'-nucleotidase
ActRIIB	Activin type IIB receptor
ADAM	A Disintegrin and metalloprotease
ADMSC	Adipose-derived mesenchymal stem cells
AKT	Protein Kinase B
ANOVA	Analysis of Variance
ASC	Adipose-derived stem cell secretome
BMD	Becker Muscular Dystrophy
CAMP	Crotalus atrox P-III metalloprotease
CLN	Centrally located nuclei
CRISP	Cysteine-rich secretory protein
CSA	Cross section area
CTX	Cardiotoxin - 1
DAPI	4,6-diamidino-2-phenylindole
DMD	Duchenne Muscular Dystrophy
DPX	Dysterine, Plastisizer and Xylene
ECM	Extracellular matrix
FAPs	fibro-adipogenic progenitors
FGF	Fibroblast growth factor
FITC	Fluorescein isothiocyanate
H&E	Haematoxylin & Eosin
HGF	Hepatocyte growth factor
IC50	Half maximal inhibitory concentration

IF	Interferon
IGF	Insulin-like growth factor
IL	Interleukin
INF	Interferon
LAAO	L-amino acid oxidase
MAPK	Mitogen-activated protein kinase
MCP	Monocyte chemoattractant protein
MMPs	Matrix metalloprotease
MYHII	Myosin heavy chain/ embryonic myosin III
NGF	Nerve growth factor
NO	Free radical nitric oxide
NTD	Neglected Tropical Disease
OCT	Optimal Cutting Temperature
PBS	Phosphate buffer saline
PDE	Phosphodiesterase
PLA2	Phospholipase A <sub>2</sub>
PTSD	Post-traumatic stress disorder
RGD	Arginine-Glycine-Aspartate
ROTEM	Rotational thromboelastometry
RV	Russell's viper
sActRIIB	Soluble activin receptor II B
SBE	Snakebite envenomation
SC	Satellite cells
SMI	Small molecule inhibitor
SVMP	Snake venom metalloproteases
SVSP	Snake venom serin proteases
TA	Tibialis anterior



TGF	Transforming growth factor
TIMPs	Tissue inhibitor metalloprotease
TNF	Tumour necrosis factor
Tregs	Regulatory T cells
VICC	Venom-induced consumption coagulopathy
WHO	World health organisation

## List of Antibodies

### Primary Antibodies

Antigen	Type	Immunoglobulin	Host Species	Dilution Ratio	Supplier
MYHIII	Monoclonal	IgG	Mouse	1:200	DSHB
Collagen IV	Polyclonal	IgG	Rabbit	1:200	Abcam
Dystrophin	Polyclonal	IgG	Rabbit	1:200	Santa Cruz Biotechnology
<i>C.atrox</i> venom	Polyclonal	IgG	Sheep	1:200	Toxiven
Laminin	Polyclonal	IgG	Mouse	1:200	Sigma L9393
CD31	Monoclonal	IgG2a	Rat	1:200	AbD serctec

### Secondary Antibodies

Antibody	Immunoglobulin	Host Species	Dilution Ratio	Supplier
Alexa flour 488 anti-mouse	IgG	Goat	1:200	Invitrogen
Alexa flour 594 anti-rabbit	IgM	Goat	1:200	Invitrogen
Alexa flour 594 anti-rat	IgG	Goat	1:200	Invitrogen
Fibrinogen-FITC	IgG	Rabbit	1:50	Dako

anti-human				
------------	--	--	--	--

## **Abstract**

Snakebite envenoming is a propriety neglected tropical disease that annually claims a life of around 150,000 and is responsible for 500,000 disabilities. Skeletal muscle damage is a primary factor for snake venom-induced permanent disabilities. The only treatment available for snakebite envenoming is anti-venoms produced against venomous snake species. These anti-venoms are raised against the geographical venom variant and effectively treat the systemic effects of envenoming. However, they fail to treat local tissue damage. Most research in the snake venom field is focused on improving anti-venom understanding of venom chemistry and physiology. Studies on local effects, pathologies, and treatment of local tissue damage are limited. This thesis investigates skeletal muscle pathologies inflicted by snake venom, especially snake venom metalloprotease-rich viper venoms. The viper venoms and some species of elapids can cause local tissue damage and tissue necrosis. These venoms are rich in snake venom metalloproteases (SVMP), three-finger toxins (3FTxs), and phospholipase A<sub>2</sub>, which can induce local damaging effects on the skeletal muscle of the bite victim. The elapid venom-mediated damage is often self-resolved; however, in the case of viper envenoming, the muscle damage is often permanent. Here, we aim to narrow down niche areas in skeletal muscle regeneration affected by viper envenomation. We can use innovative methods to target and eliminate the hindrance in the normal regeneration of skeletal muscle damage. The factors contributing to impaired muscle regeneration in the case of SBE are: 1. The venom proteins are present in the muscle tissue and cause persistent damage. 2. The impaired muscle regeneration often results in fibrotic/scar tissue formation that hampers muscle regeneration. 3. The snake venom toxins, especially SVMPs, can affect the function of muscle stem cells and alter the immune response post-muscle injury, which then dysregulated the muscle regeneration process. We selected different approaches to target each problem area. We used small molecular inhibitors marimastat and varespladib specific for SVMPs and PLA<sub>2</sub>s to inhibit the initial trigger of active venom proteins. These inhibitor molecules improved muscle regeneration, reduced venom pathological effects and restored

immune response balance. Secondly, we tested the effect of a known anti-fibrotic molecule soluble activin receptor IIB to minimise muscle fibrosis, which improved muscle regeneration and reduced fibrosis with persistent dosing. Lastly, we have used stem cell-derived condition media to boost the innate regeneration mechanism and restore the dysregulation of the immune response. The presence of secretome was found effective in enhancing myoblast proliferation, differentiation and maturation of muscle cells. All the individual approaches achieved effective muscle regeneration. However, there is a possibility of gaining more benefits from the combination of these molecules. The Circulatory system also plays a vital role in wound healing and regeneration. Hence, we studied the effects of P-III metalloprotease from *Crotalus atrox* (CAMP) venom and a cardiotoxin -I (CTX) from *Naja pallida* concerning intramuscular bleeding and microthrombus formation in the tissue. CAMP affected  $\alpha\text{IIb}\beta\text{3}$  integrin-mediated thrombus formation, whereas CTX exhibited effects on extrinsic and intrinsic clotting pathways. All the approaches tested and validated in this thesis target specific areas of muscle regeneration. The small molecule inhibitors target particular proteins in the whole venom, soluble activin receptor IIB, target the specific pathological outcome and condition media targeted modulation of immune response and muscle stem cells. Hence, these treatment molecules may have global application and potential to tackle the crucial pathological outcome of envenoming: SBE-induced muscle damage.

## 1. Introduction

Fear of snakes, which is a primordial instinct and innate human emotion has fascinated experimental psychologists, evolutionists, and scientists to spend decades researching snakebites and their pathological effects. Snakebite envenoming (SBE, i.e. when the venom is injected into the body) has recently gained much-needed attention from medical and scientific communities as well as policymakers. The World Health Organisation (WHO) has reinstated SBE as a high-priority neglected tropical disease (NTD) and has established a strategic roadmap to reduce SBE-induced mortalities by 50% by 2030 [1]. According to the WHO, SBE affects around 1.8 to 2.7 million people annually, with mortality cases of 81,410 to 137,880 and around 500,000 permanent disabilities [2]. SBE primarily affects rural populations in Africa, South Asia, Latin America, and Oceania [3]. SBE is an occupational health hazard for agricultural workers in many developing countries [3-5]. The bites and fatalities are often common in younger, productive age groups [6]. For example, in Myanmar, SBE is the leading cause of death in rice-growing agricultural workers [7]. In countries like India, Sri Lanka, and South Africa, people are often exposed to snakebites while working as tea pickers, rubber tappers and sugar cane harvesters. Fishermen handling nets and lines in warmer tropical seas are also at risk for bites from sea snakes. Snakebites also affect nomadic tribes and hunters whose livelihood largely depends on collecting wood and indigenous products [5].

In addition to mortalities, a large population of SBE victims develops chronic medical conditions, permanent disabilities and profound psychological effects following SBE [5, 8]. Some of the severe consequences of SBE include post-traumatic stress disorder (PTSD), foetal loss, blindness, contractures, malignant ulcers, chronic infections, and amputation of limbs [8]. In sub-Saharan Africa alone, more than 6000 amputations occur every year due to SBE-induced permanent muscle damage [9]. The socioeconomic impacts of permanent disabilities affect not only the livelihood of the victims but also their families [10]. Since SBE-related morbidities significantly impact the emotional and financial well-being of the communities, finding an effective solution for this issue is highly desirable. Antivenoms produced against the venoms of regionally specific snakes are the only treatment available for SBE. Antivenoms often have limitations due to high variability in venoms among the same species living in different geographical locations. Antivenoms are raised against whole venoms, whereas local tissue damage is mainly caused by specific toxin families (discussed

in detail later). These toxin families affect particular areas of muscle regeneration. Hence, focusing on the specific areas to improve impaired muscle regeneration would be a better solution for SBE-induced tissue damage. SBE-related morbidities contribute to a high number of permanent disabilities worldwide; however, the treatment options are limited. This project aims to identify and target the main areas to overcome pathological outcomes of SBE-induced skeletal muscle damage.

## **1.2 Evolution of snakes**

The journey of snake evolution spans millions of years. Along with lizards, snakes belong to the order of Squamata. The earliest snake fossils date back to the Cretaceous period, around 130 million years ago [11]. Limb loss is one of the significant steps in snake evolution. Modern snakes are completely limbless; however, early snakes had hind limbs, and as snakes evolved, they gradually lost their limbs. The loss of limbs and elongated body allow them to move efficiently for their adopted burrowing lifestyle [12]. The skull of a snake has undergone significant changes. The mandibles are loosely connected at the back of the skull, allowing for a much greater rotation angle than most animals, so a snake can open its mouth wider than its body and swallow larger prey. The mandibles move independently of each other, slowly inching the prey into the throat [13]. Snake fangs are an example of complex adaptation. Snakes exhibit a variety of tooth structures depending on their diet. Some are equipped with rear-facing teeth to help grasp and swallow prey. Venomous snakes have specialised fangs for injecting venom [14]. There are two main types of fangs: grooved fangs, where venom spreads down an open anterolateral or lateral groove and tubular fangs, where venom runs through a canal or a duct [15]. The tubular fangs evolved independently in three front-fanged clades: Viperidae, Elapidae and Atractaspidae [16]. The grooved fangs are posterior to the maxillary bone and are found in Colubridae, homolapsid and lamprophiid snake lineages [17].

Some snakes from the Viperidae family, specifically 'pit vipers', possess specialised sensory organs in their head that can detect heat emitted by objects/prey in their environment. This heat-sensing organ allows these snakes to locate the heat source precisely and gives them a hunting advantage [18]. Jacobson's or vomeronasal organ is vital for detecting pheromones during mating [19]. These evolutionary adaptations have made modern snakes one of our planet's most feared and fascinating animals. Venomous and non-venomous snakes are believed to share a common

ancestry. Over time, different snake lineages adopted to different ecological roles leading to the divergence of venomous and non-venomous snakes. Non-venomous snakes evolved a constriction strategy to capture their prey. On the other hand, venomous snakes use their venom to capture their prey. This adaptation has given venomous snakes a selective advantage in survival and hunting.

The evolution of venomous snakes has equipped them with venom delivery systems. It is fascinating that a small and physically weak animal can deploy a toxic cocktail that can inflict life-threatening pathological complications on its prey and much larger animals, including humans. Venom evolution studies often provide insights towards natural selection, molecular evolution, protein neofunctionalisation (duplication of genes that result in new or additional function of the resultant protein) and, interestingly, predator and prey interactions. Phylogenetic and evolutionary data suggest that the snake venom gland evolved 60-80 million years ago, still undergoing subsequent evolutionary changes. The most popular hypothesis for the evolution of toxin families is the duplication of non-toxic genes. Such duplications have occurred multiple times throughout the evolution of snakes, including parallel expression of gene families in different snake lineages [20].

The main families of venomous snakes are a) Viperidae - vipers often have triangular heads. The snakes from this family have well-developed venom glands and hinged tubular fangs for venom delivery. Viper venoms mostly exert haemotoxic and myotoxic effects. b) Elapidae - snakes in this venom family have neurotoxic venom. These snakes have short, fixed tubular fangs in the front of their mouth. c) Colubridae - most snakes in this family are non-venomous, but a few have venom glands and rear-faced groove teeth for venom delivery. Their venoms are usually mildly toxic (except some, which are highly lethal species) and used for subduing prey. d) Atractaspididae (burrowing asps) - these snakes have short rear-facing grooved fangs for venom delivery. Their venoms are cytotoxic and may cause tissue damage [21, 22]. The most medically important venomous snakes are from the Elapidae and Viperidae families.

### **1.3. Snake venoms**

The snake venom proteomes suggest that typical snake venom may consist of around 20 primary toxin families and up to 57 secondary (comprising in small amounts of total proteins) protein families [23]. Some components in snake venoms such as metalloproteases, serine proteases

(SVSP), phospholipase A<sub>2</sub> (PLA<sub>2</sub>), and three-finger toxins (3FTx), can directly alter normal physiological conditions in their prey or SBE victims. The remaining venom components include disintegrins, cysteine-rich secretory proteins, Kunitz peptides, L-amino acid oxidase, natriuretic peptides, and C-type lectins [20, 21]. The non-toxic components facilitate venom delivery and spreading of venom in host tissues, help with the digestion of the prey, modulate the immune response, and inflict inflammation.

Depending on their specific toxicities, venoms are classified as a) haemotoxic venoms; they primarily target the cardiovascular system and blood. The toxins in haemotoxic venoms can damage blood vessels, interfere with blood clotting, and lead to several adverse effects on the circulatory system. The effect of haemotoxins may lead to excessive bleeding, tissue damage and altered blood clotting mechanism [24]. b) neurotoxic venoms; these venoms target nerve cells, disrupting the transmission of nerve impulses that may lead to breathing difficulties and other neurological impairments. c) myotoxic venoms; these venoms primarily target skeletal muscle. The breakdown of the muscle cells may lead to the release of specific proteins into the bloodstream, and they can lead to kidney damage. d) cardiotoxic venoms; these venoms affect the cardiovascular system, particularly the heart. They can cause cardiac arrhythmias and hypotension [25]. Elapid venoms are mainly neurotoxic; however, some have myotoxic effects. Viper venoms have haemotoxic effects and strong myotoxic effects that contribute to local tissue damage and permanent disabilities [26, 27]. The clinical manifestations and pathophysiological consequences of envenoming may vary depending on the species and the amount of venom injected.

Elapid venoms consist of two major toxin families: 3FTx and PLA<sub>2</sub>. However, many elapid species exhibit a 3FTx/PLA<sub>2</sub> dichotomy, with one family comprising most of the venom [21, 28]. However, elapids appear to have greater toxin diversity than vipers [29, 30]. In contrast to elapids, viper venoms predominately comprise three protein families, SVMPs, PLA<sub>2</sub> and SVSPs. Viper venoms also include a much more significant proportion of secondary protein families than elapids [31-33]. The structure and functions of individual toxins are explained in further detail in the next section.

### **1.3.1 Structure and functions of major snake venom toxins**



### 1.3.1.1 SVMPs

SVMPs are Zn<sup>2+</sup>-dependent proteolytic enzymes. They are closely related to the ADAM (A Disintegrin and Metalloprotease) family of proteins found in humans and belong to the M12 B' metzincin family. The molecular mass of SVMPs ranges from 25 kDa to 150 kDa depending on their structure.

There are four classes of SVMPs:

1) P-I: it comprises only a metalloproteinase domain with molecular weight ranging from 20-30 kDa [34, 35]. The metalloprotease domain has a conserved zinc-binding sequence (HEXXHXXGXXH) and methionine turn [36, 37]. P-I metalloproteases can co-localise with the extracellular matrix (ECM) and can degrade components of the basement membrane.

2) P-II: This class is structurally more complex than the P-I. In addition to the metalloprotease domain, it contains a disintegrin-like domain although the protein contains a single chain. The molecular weight of P-II ranges from 30-40 kDa [35]. P-II metalloproteases are only found in the viper venoms, suggesting that during venom evolution, this protein family diverged from the Elapidae snakes [38, 39]. The unique feature of P-II SVMPs is the integrin-binding RGD (arginine-glycine-aspartate) motif [40, 41]. RGD motif is embedded in the flexible loop abutted to the metalloprotease's C-terminus region. This RGD motif interacts significantly with the integrin molecules, e.g. integrin  $\alpha$ IIb $\beta$ 3 to inhibit platelet aggregation [42, 43].

3) P-III: This class has a higher molecular mass ranging from 60-100 kDa [44]. In addition to the metalloprotease domain, P-III contains a disintegrin-like and a cysteine-rich domain on the same polypeptide chain. Due to structural complexity, the P-III class is further classified into P-IIIa, P-IIIb, P-IIIc and P-IIId [45]. P-III SVMPs can cleave basement membrane and ECM proteins such as collagen IV, laminin, and fibronectin. Some P-III SVMPs can also cleave prothrombin and factor-X. The cysteine-rich domain and the disintegrin domains can decrease cell adhesion and inhibit angiogenesis [46, 47].

4) P-IV: It contains two C-type lectin-like domains connected by disulphide bonds to the other PIII domains. The C-type lectin-like domains can cause platelet activation through tyrosine kinase receptor clustering [48].

SVMPs have proteolytic and collagenolytic activities and can affect the proteins involved in the blood coagulation cascade, affecting the balance of the cardiovascular system. The disintegrin-like domain in class II and III inhibits platelet aggregation by binding to fibrinogen receptors, integrin  $\alpha\text{IIb}\beta\text{3}$ , on the plasma membrane of platelets. According to some recent studies, in addition to haemolytic activities, SVMPs have other properties like fibrinogenolytic activities, prothrombin activation and the activation of factor X. In addition, they also possess apoptotic and pro-inflammatory activities and inactivate serine proteinase inhibitors in blood [49] (**Figure 1**). SVMPs are abundant in viper venoms and are responsible for myotoxicity, a well-known characteristic symptom of viper bites. Along with systemic and local effects, SVMPs damage blood vessels, reduce cell adhesion, degrade major ECM proteins, and affect angiogenesis. These conditions may lead to extensive tissue necrosis and muscle damage.

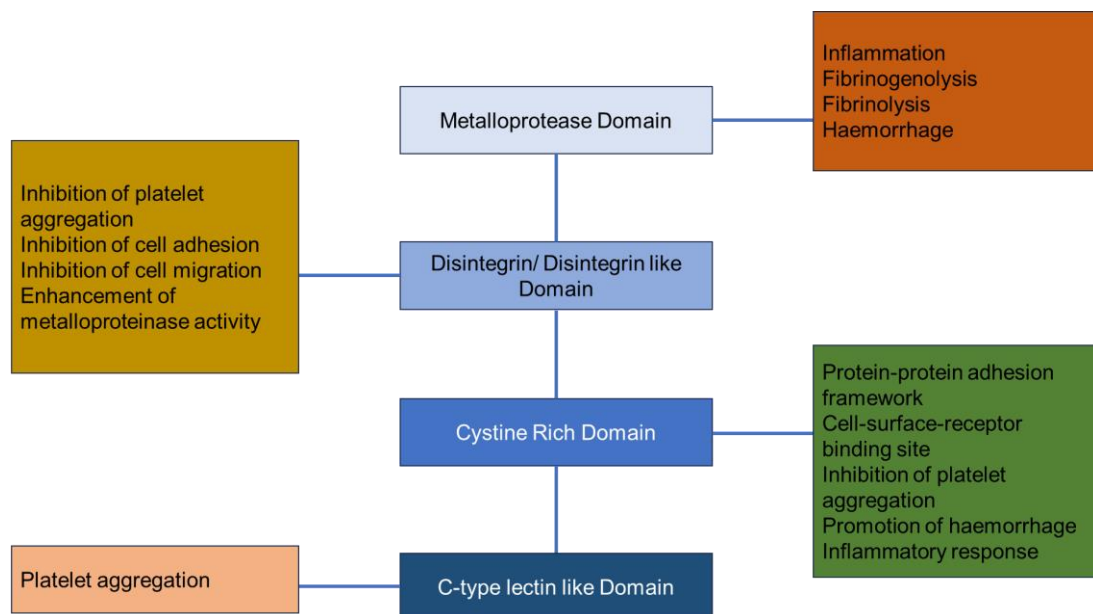


**Figure 1:** Various domains present in SVMPs and their functions. Diagram adapted from [35]. The figure lists the general functions of each domain of SVMPs.

### 1.3.1.2 SVSPs

SVSPs are one of the major components of snake venoms and are mainly found in the venoms of the Viperidae family. However, a few SVSPs are also found in the venoms of the Elapidae family members. In addition to their contribution to the digestion of the prey, these enzymes exhibit specific pharmacological effects. Many SVSPs are described as ‘thrombin-like’ enzymes because they cleave fibrinogen, mimicking the action of thrombin. However, unlike thrombin, SVSPs typically do not activate factor XIII, which is important for cross-linking soluble fibrin into insoluble clots. SVSPs primarily target fibrinogen, a crucial protein in the coagulation cascade. At the same time, SVSPs can induce dysfibrinogenemia, preventing normal blood clot formation [50, 51]. Some SVSPs are described as ‘kallikrein-like’ enzymes, as they alter blood pressure by releasing kinin/bradykinin from kininogen. SVSPs can also activate factor V, contributing to the coagulation cascade by subsequent prothrombin activation. In contrast, some SVSPs exhibit anti-coagulation properties by activating protein C, which negatively regulates the coagulation cascade by inactivating factors V and VII. Moreover, they convert plasminogen to plasmin, facilitating clot degradation [52, 53] (**Figure 2**).

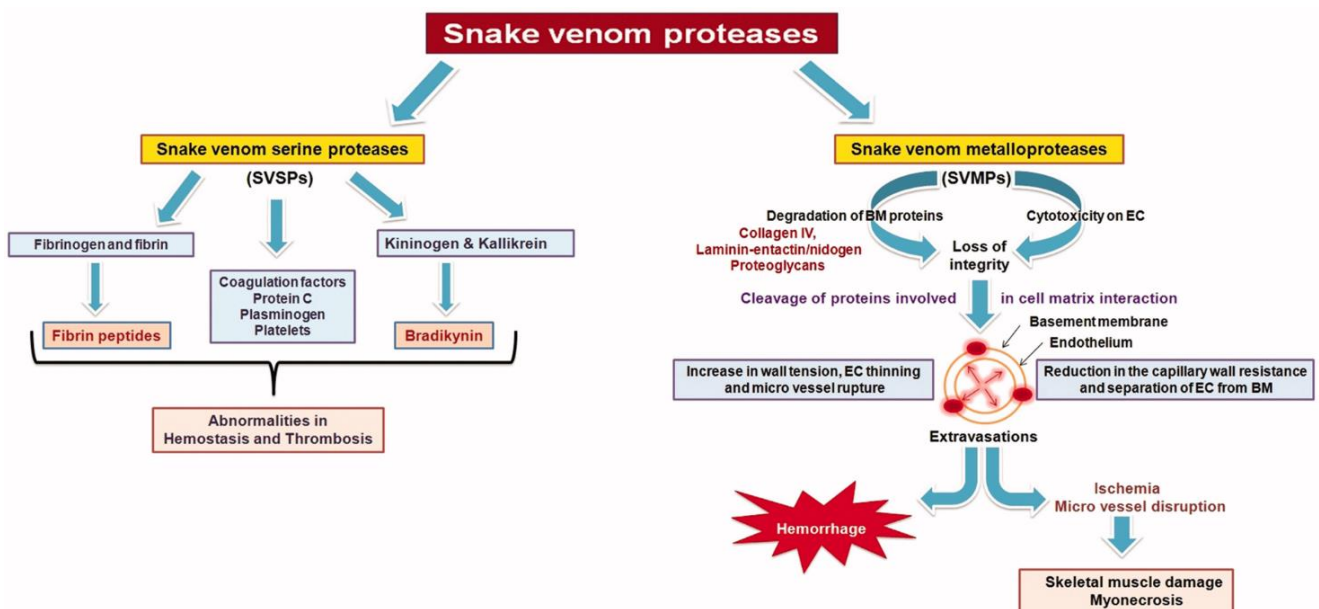


**Figure 2:** Mechanism of action of snake venom proteases on various components involved in blood coagulation cascades. The diagram is adopted from [54]. The above figure indicates the action of

snake venom proteases (SVSPs and SVMs) on different factors and cell types, leading to abnormalities in haemostasis and thrombosis.

#### 1.3.1.3 Snake venom PLA<sub>2</sub>

PLA<sub>2</sub>s are abundant in the venoms of Elapidae family members and are also one of the main components of viper venoms. PLA<sub>2</sub>s exhibit a range of systemic and local effects and contribute significantly to snake venom-induced pathologies. They are classified based on their three-dimensional structures, amino acid sequences and catalytic activities. Broadly, snake venoms PLA<sub>2</sub> are classified into group I and II enzymes. The group I PLA<sub>2</sub> are found in the elapid and colubrid families and primarily has neurotoxic effects. They act by blocking neurotransmission by irreversible binding to nerve terminals. Group II PLA<sub>2</sub>s are found mainly in the venoms of viper snakes and possess myotoxic or cytotoxic activities, although some can affect the blood coagulation [55, 56]. Group II PLA<sub>2</sub> are subdivided into catalytically active Asp 49 enzymes and Lys 49 containing catalytically inactive enzymes. Catalytically active PLA<sub>2</sub>s hydrolyse the ester bonds of phospholipids at Sn-2 positions present in the plasma membranes of various cells [57]. Catalytically inactive PLA<sub>2</sub> act through perturbation of the membrane resulting in alteration in membrane potential, leading to unrestrained gradient of ions such as Ca<sup>2+</sup> and causing hypercontraction of myofibers, swelling in mitochondria, and disorganisation, leading to mitochondrial dysfunction [57]. Both catalytic and non-catalytic PLA<sub>2</sub>s cause alterations in membrane structures. The inflammatory responses triggered by PLA<sub>2</sub> are primarily because of the release of arachidonic acid and lysophospholipids in the cell membrane due to their actions [58, 59].

#### 1.3.1.4 Hyaluronidase

Hyaluronidases are another class of venom enzymes and are mainly responsible for spreading the injected venom into tissues by breaking the tissue barriers. Hyaluronidases can hydrolyse hyaluronic acid present in the intercellular barriers. Hyaluronic acid is essential for maintaining the structural integrity of tissue structures. Loss of hyaluronic acid facilitates the diffusion of venom toxins from the bitten area to surrounding tissues. Therefore, hyaluronidase is also called a 'spreading factor' in venoms [60]. Due to its unique mechanism of action, hyaluronidase plays an

essential role in increasing the efficacy of venoms. This venom component is also suspected to induce inflammatory responses [61] (**Figure 3**).

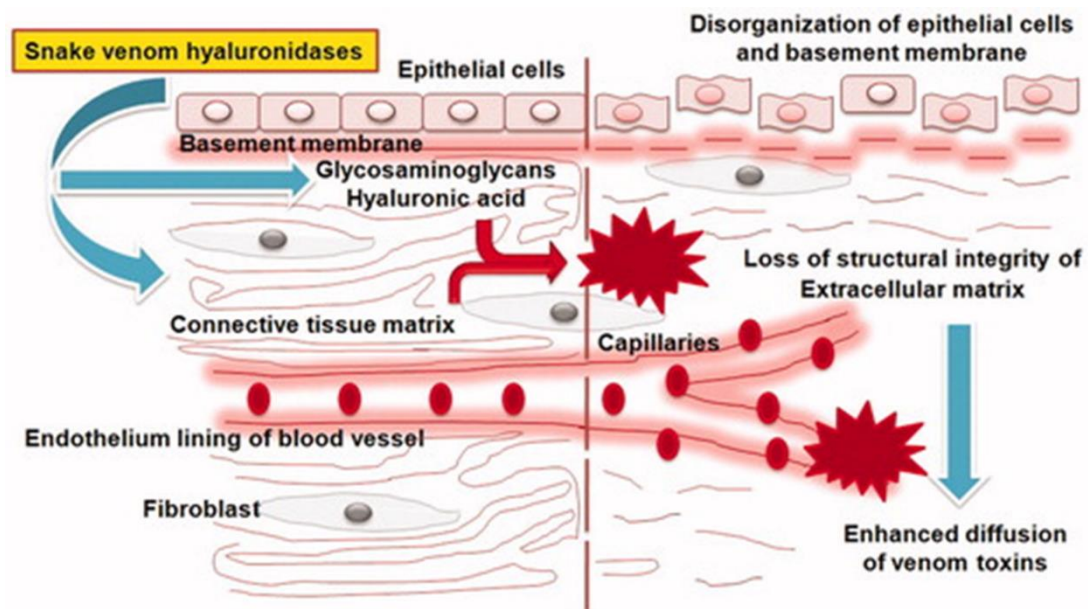


**Figure 3:** Mechanism of action of snake venom hyaluronidases. This figure is adapted from [54]. The hyaluronidase acts on hyaluronic acid, causing loss of structural integrity of epithelial cells, connective tissue, and endothelial lining of blood vessels. This action facilitates the diffusion and absorption of snake venom into the victim's body.

### 1.3.1.5 3FTxs

3FTXs	Target	Biological activities
$\alpha$ -neurotoxins	Inhibit muscle acetylcholine receptors (nAChR) [66]	Flaccid or spastic paralysis [66-69]
$\kappa$ -neurotoxins	Inhibit neuronal AChR [67]	
Muscarinic toxins	Inhibit neuronal AChR [69]	
Fasciculins	Inhibit acetylcholinesterase (AChE) [68]	
Calciseptine	Modulates L-type calcium channels [70]	Tissue necrosis[70]
Cardiotoxins	Interact non-specifically with phospholipids [71] or induce insulin secretion [72]	
Mambin	Interacts with platelet receptors [73]	Alteration in haemostasis [73, 74]
Exactin	Inhibits Factor X [74]	
$\beta$ -cardiotoxins	Inhibit $\beta$ -adrenoreceptors [75]	Alteration of cardiac rates [75-77]
MT $\alpha$	Inhibits $\alpha$ -adrenoreceptors [76]	
Mambalgins	Inhibit ASIC channels [77]	
Tx7335	Activates potassium channels [78]	Neuromuscular paralysis [78, 79]
Calliotoxin	Activates voltage-gated sodium channels [79]	

**Table 1:** Examples of short and long-chain 3FTxs, their targets and biological activities.

3FTxs are non-enzymatic proteins containing sixty to seventy-four amino acids and include a three-finger-like fold in their structures stabilised by disulfide bridges. The 3FTxs have a characteristic structure of three loops that project from the core region and resemble three finger-like projections [62, 63]. The 3FTxs are abundantly present in elapid venoms. Many 3FTxs are neurotoxins, although their mechanisms of toxicity vary significantly even among proteins of high sequence identity. The typical targets for 3FTxs include those involved in cholinergic signalling, such as the nicotinic acetylcholine receptors. The  $\alpha$ -neurotoxins are one group of 3FTxs that operate post-synaptically by targeting nicotinic acetylcholine receptors in skeletal muscles in vertebrates [64]. They are present mainly in the venoms of elapid and colubrid snakes. They exert their neurotoxic effects by binding post-synaptically at the neuromuscular junctions to induce flaccid paralysis in snakebite victims [65]. 3FTxs differ in length, with short-chain 3FTxs including  $\alpha$ -neurotoxins,  $\beta$ -cardiotoxins, cytotoxins, fasciculins and mambalgins, comprising 57– 62 residues and 4 disulfide bridges, and long-chain 3FTxs including  $\gamma$ -neurotoxins, hannalgesin and  $\kappa$ -neurotoxins, contain 66– 74 residues and five disulfide bridges. The 3FTxs have diverse targets and biological activities despite the shared three-finger fold.

Another large subfamily of 3FTxs is cardiotoxins (CTX) (cytolysins). CTXs form a reasonably homogeneous group of toxins in cobra venoms. CTX consist of three beta-sheet loops similar to neurotoxins. However, CTXs are classified into two types, namely S-type and P-type. This classification is based on the position of two amino acid residues in toxins. All S-type CTXs contain a serine residue at position 28 in the phospholipid binding site near the hydrophobic region of loop 2, while in all P-type CTXs, a proline residue is present at position 30 near the tip of the second loop. P-type and S-type CTX have a phospholipid binding site near loop 1, however, P-type CTX exhibits higher binding and fusion activity due to additional binding sites on loop 2. S-type CTX exhibits higher muscle cell depolarisation activity, while P-type CTX possesses higher haemolytic activity. The primary target of CTX is the heart and associated tissues. The systemic effects of CTX include changes in blood pressure, heart rate and other haemodynamic parameters.

Meanwhile, the local effects are exhibited due to phospholipase activity that may induce cellular damage. *In vitro* experiments using model membranes have shown that the hydrophobic core of cytotoxins represents the principal membrane-binding motif. Upon binding, cytotoxins produce structural defects in lipid bilayers by hydrophobic interaction in the phospholipid bilayer [80].

#### 1.3.1.6 Other toxins

Along with main toxin families, snake venoms also contain small quantities of CRiSP, Cysteine-rich secretory protein; LAAO, L-amino acid oxidase; VEGF, vascular endothelial growth factor; PDE, phosphodiesterase, NGF, nerve growth factor; 5'NUC, 5'-nucleotidase, and snake C-type lectins (snaclecs). The composition and percentage of these components have species-specific variations. Some of these components may affect blood coagulation and vasculature, such as snaclecs binding to various receptors on platelets, blood coagulation factor IX/X and endothelial cells. They have been reported to both activate and inhibit platelets via binding to integrin  $\alpha 2\beta 1$ , GPIb, and GPVI and may induce thrombocytopenia [81].

Skeletal muscle is the main target for snake venom-induced local tissue damage. Snake venoms can cause structural alterations in skeletal muscle and affect innate muscle regeneration. These effects on skeletal muscle lead to permanent loss of structure and function of the affected

muscle. Before discussing venom-induced muscle damage in detail, learning about the basic structure and function of skeletal muscles is essential. Therefore, here, I present some basic information about the structure and functions of skeletal muscle.

#### **1.4. Skeletal muscle**

Skeletal muscle comprises approximately 40% of total body weight and accounts for 50% to 70% of total protein contents in the human body. Skeletal muscles function under voluntary control to perform their roles. They play essential roles in movement, structure, stability, protection, wound healing, metabolism, thermogenesis, and the secretion of numerous molecules to communicate with other tissues [82-84].

Skeletal myofibers and associated connective tissues represent the basic cellular unit of muscle structure. An individual skeletal muscle comprises numerous cylindrical muscle cells called 'muscle fibres' (**Figure 4**). These muscle fibres are wrapped in a covering of connective tissues. Each muscle fibre is surrounded by a connective tissue sheath called epimysium. The epimysium possesses inward projections, which divide the muscle into compartments. Muscle fibres are assembled as a bundle called fasciculus. These fasciculi are surrounded by a layer of connective tissue called 'perimysium'. At the same time, each muscle fibre is surrounded by connective tissue called 'endomysium'. This connective tissue covering supports and protects the muscle cells. The cover also provides passage for nerves and blood vessels. An artery and at least one vein accompany each nerve that penetrates the epimysium of a skeletal muscle. The epimysium, perimysium and endomysium extended to form a thick thread-like structure, called tendon. The tendon and aponeurosis form indirect attachments from muscles to the periosteum of bones or the connective tissue of other muscles. A cell membrane (sarcolemma) surrounds each muscle fibre. Sarcolemma connects several protein complexes to the myofilament structure, such as actin and myosin in the filament [85].



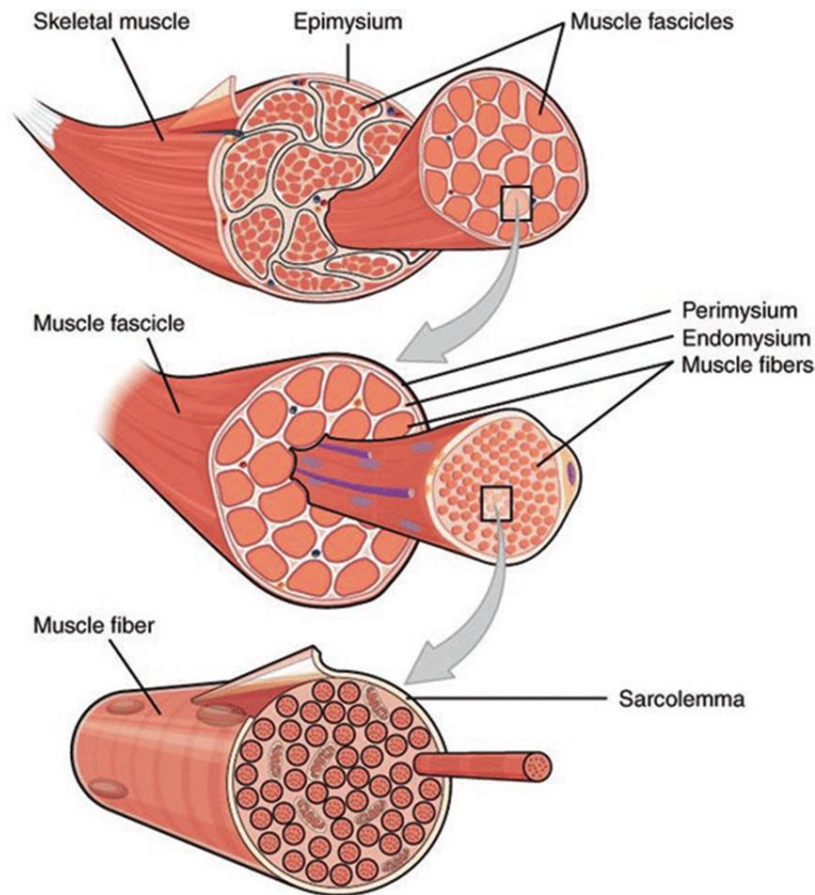


**Figure 4:** Basic structure of skeletal muscle. This figure was adapted from [86]. The basic structure unit of skeletal muscle is ‘muscle fibre’, which is surrounded by sarcolemma. Furthermore, there are different layers of connective tissue sheath called epimysium, perimysium, and endomysium (outer to inner layer).

In normal muscles, a population of muscle stem cells known as ‘satellite cells’ (SC) is present at the periphery of muscle fibres between the sarcolemma and basal lamina [87]. These cells remain quiescent under normal conditions. In case of injury, SCs become activated, proliferate, and then differentiate into new myotubes or fuse with (or replace) injured muscle fibres [88]. These multinucleated cells then differentiate into adult muscle fibres. The ECM is an integral part of skeletal muscle structure, and it forms the framework that holds blood vessels and nerves in place in myofibres. The ECM plays a vital role in maintaining and repairing the muscle fibres post-injury [89].

### 1.4.1 The ECM

Skeletal muscles have a complex meshwork of the ECM containing collagen, glycoproteins, proteoglycans, and elastin [90]. Studies over the past decade indicate that the ECM, the scaffolding structure surrounding the cells, plays an influential role during cellular signalling and tissue responses to injury and disease. The functions of the ECM in skeletal muscle include the maintenance of muscle, myogenesis, regeneration and adaptations to the surrounding environment and atrophy after periods of disuse [90, 91].

The basement membrane is a sheath-like, thick form of ECM that surrounds skeletal muscle. The basement membrane consists primarily of type IV collagen and laminin [92]. Collagen IV is present in the epimysial, perimysial, and endomysial interstitium, particularly around the basement membrane [93]. Collagen IV forms a mesh-like structure with laminin, which is a ligand for two sarcolemmal receptors – the dystrophin-associated glycoprotein complex and the integrin  $\alpha7\beta1$ . These are membrane-bound protein structures aligned in line with the Z-disks of myofibrils. Integrins act bidirectionally, allowing intracellular signalling molecules to regulate the external adhesion and transfer external stimuli to alter cellular processes. Dystrophin is a structural protein and is an essential component in the dystrophin-associated glycoprotein complex, that plays a critical role in the structural integrity of the ECM [94]. The conformational changes in the integrin receptor creates an extracellular change, and this high-affinity upright state facilitates the binding of ECM proteins, such as laminin, collagen, or fibronectin [95]. The dystrophin-associated glycoprotein complex is another crucial factor in providing a mechanical linkage between the contractile components of skeletal muscle [96, 97] (**Figure 5**).

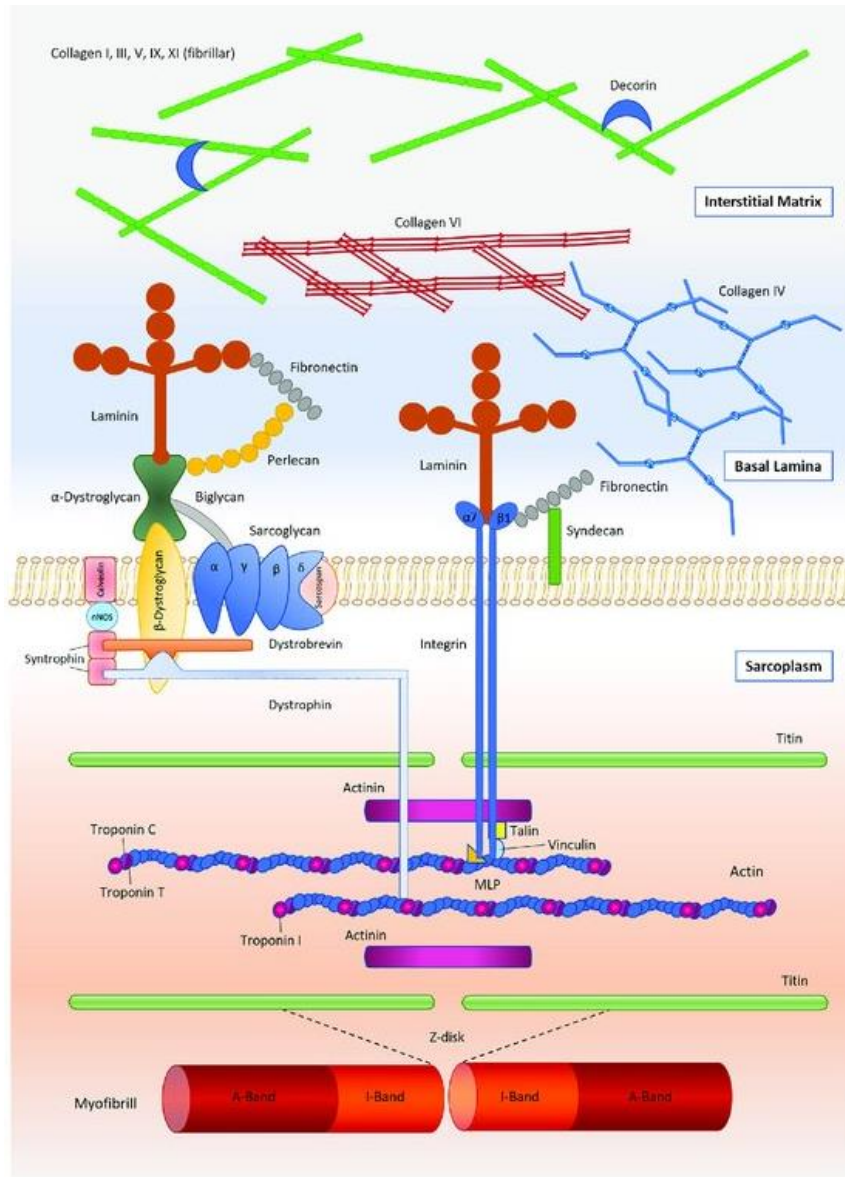


**Figure 5:** Basic structure of the ECM in skeletal muscle. This figure was adapted from [98]. The main structural component in the skeletal muscle ECM is collagen IV, which forms cross-linking with laminin which is important to maintain the structural integrity. The laminin acts as a binding ligand for receptors on sarcolemma and membrane-bound protein structures. Dystrophin plays an important role in maintaining the structural integrity of the ECM by binding laminin and other ECM proteins through the dystrophin-glycoprotein complex.

Homeostasis of the ECM is maintained through a robust mechanism involving various proteoglycans, growth factors, and enzymes. Collagen production results from downstream gene transcription governed by the transforming growth factor beta (TGF- $\beta$ ) superfamily. TGF- $\beta$  induces the phosphorylation of Smad proteins, leading to the formation of activated Smad complex. This

complex translocates into the nucleus and regulates transcription signals involving collagen and synthesis and remodelling of the ECM [99]. Small leucine-rich proteoglycans interact with collagen and may influence the assembly, organisation and stability of collagen fibres [100]. The transcription rate for collagen production is slow, and it may take up to three days for complete translation. In contrast, the secretion rates are quick, and their levels are elevated in less than one hour in the extracellular space. The secretion rates are regulated, and post-transcriptional regulation controls high collagen-producing cells by negative feedback control between the secretion and translation rates [101]. Two families of enzymes govern the remodelling and homeostasis of the ECM: matrix metalloproteinases (MMPs) and tissue inhibitors of metalloproteinases (TIMPs) [102]. TIMPs can inhibit MMPs that degrade distinct types of collagens. Specifically, MMP-1 and MMP-8 initiate the degradation of collagens I and III (prevalent in endo-, peri-, and epimysium), whereas MMP-2 and MMP-9 break down type IV collagen (the major collagenous component of the basement membrane in skeletal muscle) [103, 104].

### 1.5. Skeletal muscle regeneration

The regeneration of skeletal muscles is a complex process involving a series of well-coordinated steps (**Figure 6**). I briefly explained these steps here.

- a) *Degeneration/ tissue necrosis* - Muscle degeneration is a process of progressive deterioration or breakdown of muscle tissues. Tissue necrosis refers to the premature death of the cells within living muscle. These processes can trigger an immune response. Chemical or mechanical trauma, ischemia, toxins including venoms, infections, and diseases can trigger tissue necrosis or degradation.
- b) *Inflammatory responses* - The first wave of immune response post-injury is the arrival of mast cells and neutrophils at the injury site. The complement system, the first line of defence, is activated within seconds after injury and leads to the arrival of the neutrophils and macrophages at the injury site [105]. The muscle injury leads to rapid activation of resident mast cells and releases pro-inflammatory cytokines such as tumour necrosis factor  $\alpha$  (TNF $\alpha$ ) and interleukin (IL)-1. These secreted factors recruit more neutrophils, mast cells and other immune cells to the injury site [106]. Neutrophils are an essential cell type in the first wave of

the pro-inflammatory phase. Like mast cells, neutrophils release pro-inflammatory cytokines including TNF $\alpha$ , interferon (IF)- $\gamma$ , and IL-1 $\beta$ . In two hours, this mechanism attracts many neutrophils to the extracellular space around the damaged fibre [107]. Neutrophil-released factors facilitate the clearance of necrotic tissues, which is essential for muscle regeneration. Neutrophils are also a significant source of reactive oxygen species after the injury [108]. Neutrophils trim down the edges of the lesion to facilitate muscle regeneration. This action temporarily worsens the injury site to move the muscle regeneration process to the next level.

Macrophages and T-cells mark the second step of muscle regeneration post-injury. The number of macrophages significantly increases two days after the injury, along with the rapid decline of the neutrophils [109]. During the process of muscle regeneration, these cells undergo two different stages of activation: classically activated macrophage, M1 and alternatively activated macrophage, M2. The M1 macrophages are pro-inflammatory, while M2 macrophages are anti-inflammatory to promote resolution [110]. M1 macrophages remove muscle debris and secrete TNF $\alpha$ , IL-6, and IL-1 $\beta$ . TNF $\alpha$  attracts muscle stem cells to the damaged site and facilitates myoblast proliferation. It has been suggested that IL-6 can stimulate myoblast migration, proliferation, and differentiation. M1 macrophages recruit T cells to infiltrate the injury site. T cells express a high amount of TNF $\alpha$ , INF- $\gamma$ , IL-1 $\beta$ , IL-4, IL-12, IL-14, and several other cytokines. In addition, M1 macrophages are responsible for generating nitric oxide (NO). A high concentration of NO can induce apoptosis [111].

- c) *Myogenesis* – The transition from pro-inflammatory to anti-inflammatory after differentiation is marked by a switch from M1 to M2 macrophages. Here, the pro-inflammatory microenvironment is converted to an anti-inflammatory one [112]. M2 macrophages produce anti-inflammatory cytokines including IL-4, IL-10, and IL-13 to control local inflammatory responses at the injury site. M2 macrophages also promote muscle stem cell differentiation to myotubes, thus promoting late-stage myogenesis and regeneration [113]. The absence of M2 macrophages causes a delay in muscle growth and inhibits muscle differentiation and regeneration. Regulatory T cells (T regs) have potent abilities to control immune responses. T regs secrete IL-10 and other cytokines to facilitate M1 to M2 conversion. T regs also help slow the proliferation of SCs and promote the myoblast differentiation [114, 115]. The muscle

regeneration process depends upon pro-inflammatory and anti-inflammatory pathways and the presence and absence of inflammatory cells and their secretome. The contents of the secretome provide a suitable microenvironment for the initiation, proliferation, and differentiation of SCs into muscle fibres [116].

- d) *Myofiber maturation* - The skeletal muscle is a complex, multifaceted tissue. The complete maturation of the skeletal muscle involves the reconstruction of the ECM, angiogenesis, and innervation. Matrix deposition begins within a week post-injury, driven by TGF- $\beta$ -mediated fibroblast response [117]. Fibroblasts play a critical role in the reconstruction of the ECM. Fibroblasts promote the deposition of the ECM proteins, including collagen, which form the structural framework necessary for tissue repair. The maturation and growth of the newly regenerated muscle fibres are governed by various growth factors, including insulin-like growth factor 1 (IGF-1), fibroblast growth factor (FGF), and hepatocyte growth factor (HGF), which play important roles in promoting the growth and maturation of muscle fibres [118].
- e) *Functional recovery of the muscle* - The muscle regeneration is only beneficial if the muscle can regain its functional ability. The enlargement of muscle fibres (hypertrophy) contributes to restoring muscle strength. Structural and functional recovery marks the final step of muscle regeneration.

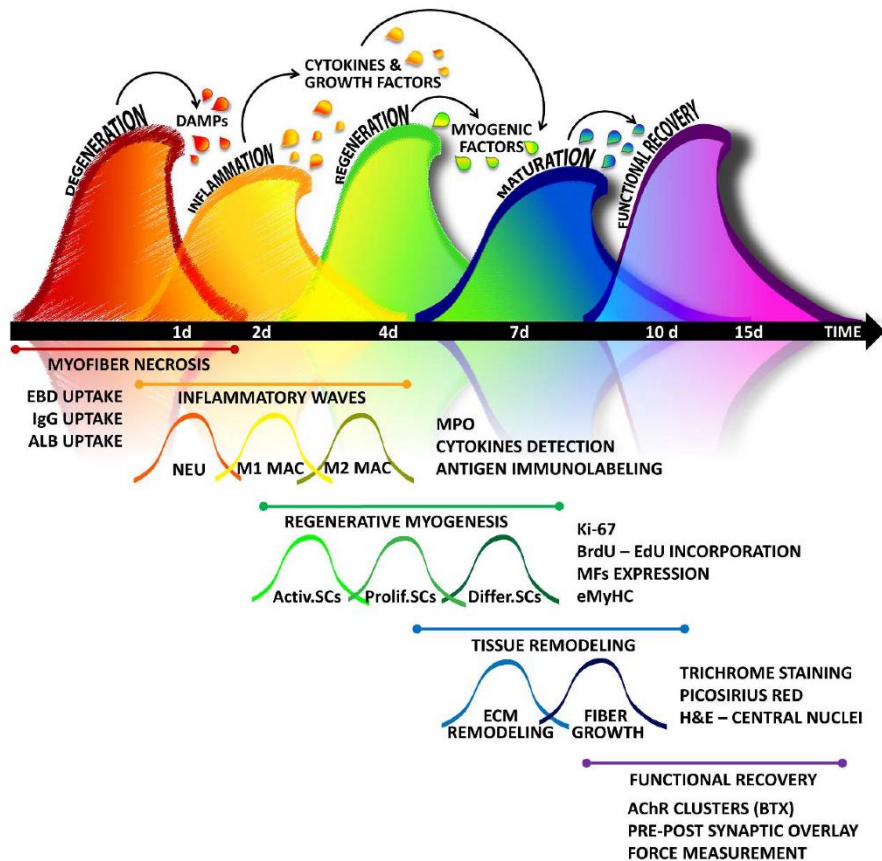


**Figure 6:** Different stages of muscle regeneration following skeletal muscle damage. This figure was adapted from [119]. A series of timely, interlinked processes outline the muscle regeneration process. Regeneration can be briefly divided into different stages including tissue degeneration, inflammatory responses, muscle regeneration, remodelling and functional recovery. The damage caused activates inflammatory responses involving the release of various cytokines and growth factors that activate SCs. These SCs undergo fusion and differentiation into myofibers. The maturation of myofibers involves the remodelling of the ECM and hypertrophy of the regenerated myofibres. The final stage of muscle regeneration is functional recovery of the muscle.

Dysregulation of muscle regeneration is common in muscle disorders such as Duchenne Muscular Dystrophy (DMD), which is a degenerative disorder caused by a genetic defect that leads to the absence of dystrophin. The lack of dystrophin leads to instability and fragility of sarcolemma. Due to this, the degenerative stage persists in DMD patients, which leads to progressive muscle loss. Repeated degeneration and regeneration cycles lead to muscle wasting and scar tissue formation in the skeletal muscles of DMD patients [120]. Like DMD, Becker Muscular Dystrophy (BMD) is also caused by a mutation in the dystrophin gene but it has a late onset. The common aspect of various muscle dystrophies is that they are chronic muscle degenerative disorders and

result in dysregulated muscle degeneration and fibrosis that leads to muscle wasting and loss of muscle function.

The effect of snake venom on the muscle tissue causes persistent damage due to the prolonged presence and effects of venom proteins. This condition mimics similar to chronic muscle degeneration. Hence, like muscle degenerative disorders, SBE victims are presented with conditions such as muscle fibrosis and wasting.

### **1.6. Venom-induced muscle damage**

Venom-induced muscle damage is a rapid degeneration (myonecrosis) caused by venom toxins at the site of injection and surrounding tissues. Snake venoms cause extensive pathological changes in skeletal muscles following envenomation. The victims with elapid envenoming are often presented with local tissue necrosis. The viper envenoming causes swelling, ischemia, blister formation, tissue necrosis, and muscle fibrosis or scar tissue formation as long-term repercussions in the bite victims. Muscle regeneration after venom-induced myonecrosis does not follow the normal muscle regeneration process. Snake venoms often destroy the plasma membrane, connective tissues, ECM, blood capillaries, and nerves. These components are crucial for the normal regeneration of muscle. Myonecrosis is one of the most severe aspects of tissue damage induced by SBE and a major factor in permanent disabilities [121].

In SBE, skeletal muscle damage is mainly caused by PLA<sub>2</sub> and SVMPs from elapid and viper venoms. Experimental evidence shows that PLA<sub>2</sub> affect muscle fibres by disrupting the integrity of the plasma membrane through enzymatic hydrolysis of membrane phospholipids. They also have a catalytically independent mechanism, where they can penetrate and disrupt the membrane bilayer by clustering hydrophobic and cationic residues located at the C-terminal region and neighbouring molecular regions by Lys49 PLA<sub>2</sub> homologues [122, 123]. Studies indicate that the size of the regenerated muscle fibre post PLA<sub>2</sub> mediated muscle damage is similar to typically mature muscle fibre, indicating that the impact of myotoxic PLA<sub>2</sub>s (or cardiotoxin) on muscle regeneration is not permanent and damaged muscles can be restored to their normal structure. When myotoxins from the venom of *Agkistrodon contortix* were injected subcutaneously into the hind limb of the mice, there was an increase in abnormal muscle fibre formation after myonecrosis [124, 125]. Venoms of elapid



snakes mainly contain 3FTXs including cardiotoxins and PLA<sub>2</sub> and low quantities of other toxins, such as hyaluronidase. Cardiotoxin acts on sarcolemma through enzymatically independent mechanisms. The damage in the plasma membrane results in a rapid influx of calcium ions from the extracellular fluid, and a steep gradient occurs across this membrane [126]. Consequently, a series of intracellular degenerative events, such as myofibrillar hypercontraction, mitochondrial damage, and activation of calcium-dependent intracellular proteases and PLA<sub>2</sub>s, thus rapidly causing cell damage [127].

In addition to PLA<sub>2</sub>, viper venoms contain haemorrhagic SVMPs, which act by degrading proteins in the basement membrane of blood vessels, collagen, ECM, and surrounding capillaries. In addition, they induce blistering, dermonecrosis, myonecrosis and a prominent inflammatory reaction with the release of diverse inflammatory mediators [26].

## **1.7. Pathologies caused by venoms relating to muscle damage**

### *1.7.1 Vascular damage*

During the muscle regeneration process, adequate blood supply and timely removal of damaged cells and debris are critical for effective regeneration [128]. SVMPs can degrade the basement membranes in blood capillaries. This weakening of the vessel wall results in capillary disruption and blood leaking in surrounding tissues [129]. The weakening of capillaries also leads to necrosis of intramuscular arteries and smooth muscles [130]. The lack of adequate blood supply and a hypoxic environment could contribute to poor muscle regeneration after the injection of viper venoms. Hypoxia during the early stage and persistent loss of angiogenesis can lead to impaired muscle regeneration. [131, 132]. The lack of microvasculature can also affect the arrival and activation of inflammatory cells in a timely manner. An adequate supply of oxygen is vital for cell survival. The absence of microvascular tissue harms the essential microenvironment, which can affect muscle stem cells and the regeneration of muscle tissues [133]. Ischemia and hypoxia caused by SVMPs affect the oxygen levels of the muscle tissue, harming the progress of muscle regeneration. Experimental evidence also suggests the death of myogenic cells and smaller regenerating fibres after the myonecrosis caused by viper venoms [131]. The compartment syndrome results from vascular endothelial damage caused by the cytotoxic and haemorrhagic

effects of venoms. Locally increased vascular permeability allows fluid build-up and increased fluid pressure within limited space. The untreated compartment syndrome can compromise vascularity, leading to ischemic contracture [134]. SVMPs have been demonstrated to reduce the density of capillaries in muscle. A study showing the effects of a P-III metalloprotease from *C. atrox* venom demonstrated that this reduction in capillary density persists even at day 10 [135].

#### *1.7.1.1 Inflammatory responses due to vascular damage*

A well-coordinated inflammatory response is required for effective muscle regeneration. Immune cells like macrophages, T lymphocytes, T reg (regulatory T cells) lymphocytes, and T-CD8+ cells are known to activate and differentiate myoblasts (muscle precursor cells) [116]. Moreover, in the initial wave of inflammatory cells, neutrophils followed by macrophages are responsible for clearing necrotic tissue debris and preparing the microenvironment by releasing cytokines and growth factors for muscle regeneration [136]. Macrophages are proven to be a key component for effective muscle regeneration. An orchestrated mechanism between pro-inflammatory M1 macrophages, and anti-inflammatory M2 macrophages is critical for regeneration [137]. The anti-inflammatory environment alters the landscape from myoblast proliferation to myoblast fusion and myotube formation [138]. The lack of a vascular network can hinder the timely arrival of cells, and persistent damage caused by SVMPs can push the muscle into a constant degeneration-regeneration cycle. The lack of coordination between M1 and M2 macrophages can jeopardise the process of regeneration and can also alter the equilibrium between myogenic cells and fibro-adipogenic progenitor cells [139]. Myogenic cells eventually give rise to myofibers, leading to normal muscle structure, whereas fibro-adipogenic prolonged survival of progenitor cells leads to fibrotic tissue formation [138]. This imbalance can lead to excessive formation of fibroblasts instead of myoblasts and results in fibro-adipose tissue deposition or muscle fibrosis, a known pathological condition resulting from viper envenomation [140, 141]. When the muscle is affected by SVMPs, the microcapillary network is destroyed around the affected tissues, which leads to the absence of the infiltration of inflammatory cells [141, 142]. In this case, the standard actions of neutrophils followed by active macrophages, which remove the necrotic tissues and release growth factors and cytokines, cannot take place in an intended way. The crucial switch from M1 to M2 macrophages to complete

myoblast proliferation and myotube formation is vastly affected. As a result, muscle regeneration does not follow the ordinary course of the regeneration pathway. Instead, there is a formation of fibro-adipose tissues. Another study speculated that apoptotic signals required for regular renewal are either absent or have a minimal presence within the first few days of myonecrosis caused by viper envenoming, which may lead to abnormal muscle fibres. However, in some cases, SCs are activated while expressing Pax-7 after muscle damage, a regular shift in the reparative program from muscle regeneration to fibro-adipose tissue formation, which is affecting the regenerative cells [143, 144].

### *1.7.2 Damage to the ECM structure and modification*

The damage to the ECM structure plays a vital role in muscle regeneration, and permanent skeletal muscle damage is associated with the alterations in the ECM structure [145]. SVMPs have been known to have the ability to cause extensive and long-term damage to the ECM. P-I metalloproteases can co-localise with collagen IV, a significant component of ECM, whereas the enzymatic activity of P-III SVMPs can vastly affect collagen IV, laminin, and dystrophin [135, 146]. Because of high SVMP contents, viper venoms can degrade the most prominent ECM structural components such as collagen. The lack of structural scaffolding during the regeneration process results in abnormal distribution of the ECM, leading to impaired muscle regeneration and fibrosis [145]. Simultaneously, the onset of acute inflammatory action and tissue necrosis results in the overexpression of MMPs, contributing to excessive turnover of the ECM [147]. As the cascade of tissue destruction and the pathological changes in the tissue continue, the release of cellular contents from the disrupted cells causes more damage. ECM also contains essential cells such as fibro-adipogenic progenitors, mesenchymal progenitor cells, and connective tissue growth factors. These are essential for ECM reconstruction, remodelling and maintenance [148].

### *1.7.3 Damage to intramuscular nerves*

An adequate nerve supply is another crucial requirement for skeletal muscle regeneration [149]. Prominent nerve damage is often observed in cases of viper envenomation, which is associated with myelin breakdown, axon loss and damage to perineural structure [150]. A study conducted using *Bothrops jararacussu* venom demonstrated that after a sublethal dose of

intramuscular venom injection, all intramuscular nerve bundles were depleted entirely [151]. Some reports have demonstrated reduced intramuscular nerve supply, especially upon exposure to myotoxic and neurotoxic PLA<sub>2</sub>. Studies carried out with *Bothrops asper* venom have shown that the necrotic zone after the acute phase of damage reduced the number of intramuscular nerves. However, by day 28, the nerve density was increased, suggesting a reinnervation [152]. These findings indicate that both PLA<sub>2</sub> and SVMPs-rich whole venoms induce extensive nerve damage; however, PLA<sub>2</sub>-mediated nerve damage has better recovery than SVMPs-mediated damage.

In summary, SBE may result in extensive and permanent muscle damage due to ischemia, tissue necrosis, microvasculature and nerve damage, ECM degradation, hampering SC action in the muscle, and imbalance in immune response. These conditions lead to impaired muscle regeneration and the development of permanent pathological conditions such as muscle fibrosis (**Figure 7**).

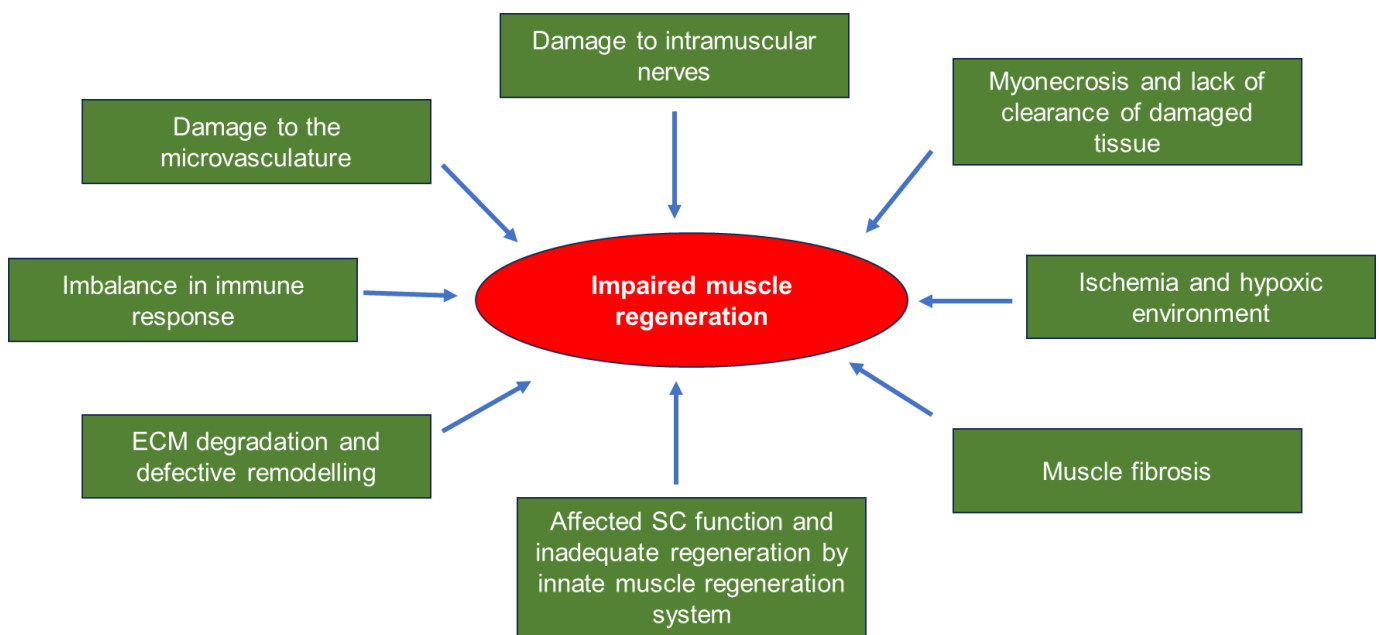


**Figure 7:** Summary of factors determining impaired muscle regeneration following SBE-induced damage. The diagram was adapted and modified from [121].

## 1.8. Current treatment approaches for SBE-induced local tissue damage

The first antivenom was developed against the Indian cobra in 1895, and until now, the only available treatment for SBE is the anti-snake venom (ASV or antivenom) [153]. Antivenoms are usually raised against the venoms of medically important snakes in a specific region or country. Even though antibodies are raised against geographical venom variants to provide more specific antibodies, they are also a limiting factor for cost and broader applications. Although antivenom has been proven effective in treating the systemic effects of envenomation, there are several issues associated with antivenom treatment. For example, antivenoms are mostly available in lyophilised form as they suffer stability issues in liquid form. The victims may suffer adverse reactions due to antivenom administration as they originate from animals. The production cost involved often makes antivenoms too expensive for those in need. The antivenoms are produced in large mammals due to the availability of large blood volume. Traditionally, the venom is extracted from selected specimens by 'milking'. The collected venom is injected into large animals (e.g. Horses). Then, the blood from the injected animal is collected, and the total IgG is purified. The F(ab)<sub>2</sub>/Fab fractions are produced from isolated IgG and used in antivenom therapy to reduce serum sickness. Over the years, the procedure to produce antivenoms remained the same. This process involves capturing and maintaining snake species and large facilities for holding and maintaining the well-being of the production animals [154]. Most antivenoms available today are equine immunoglobulins or their fragments. However, sheep, donkeys, and camels are sometimes used for antivenom production [155].

Sometimes, whole immunoglobulins (IgG) can cause anaphylactic reactions in humans. Therefore, the fragmented (Fab) antibodies can lower the risk of allergic reactions, but they have faster renal clearance [156]. Fab-based antivenom has also shown better reach and neutralisation abilities but has reduced half-life [157]. In some cases, recombinant antivenoms are also available for F(ab)<sub>2</sub> (CroFab). The pharmacokinetic properties of these antivenoms are better than whole IgG but less than Fab fragments [157]. The antivenom is available either in monovalent (raised against a single species) or polyvalent (raised against a mixture of different species) forms [4].

In local tissue damage, the microvasculature is often damaged [102, 135]. In this situation, the intravenous administration of antivenom is ineffective as the antibodies may not reach the site of damage. Antibodies are also bulky molecules that fail to reach the site of local tissue damage with intravenous administration due to their inability to penetrate the damaged tissues. The antivenoms are raised against whole venoms. Even though tissue damage results from the synergetic effects of venom toxins present in the whole venom, only a few specific toxin families, such as SVMPs, PLA<sub>2</sub>, and 3FTx, play critical roles in tissue damage. Therefore, the antibodies produced against the whole venoms may not act specifically against these toxins. Without specific treatment, the local tissue damage is often managed by surgical procedures such as fasciotomy- a process of releasing compartment pressure built up in the tissues, debridement- surgical removal of necrotic/damaged tissues followed by skin grafting, and, in worse scenarios, amputation of affected limbs. These are still the most popular or only available options to tackle SBE-mediated local tissue damage, which often results in muscle loss and permanent disabilities [158].

### **1.9. Alternative treatments for SBE venom-induced local muscle damage**

Due to the disadvantages of antivenoms, a range of research activities are underway to develop better therapeutics for SBE, including muscle damage. Several studies have been carried out using different small molecule inhibitors or peptides to neutralise the effects of venoms *in vivo*. A recent study explored the impact of small molecule inhibitors and metal chelators to counteract the effects of viper and elapid venom toxins such as SVMPs and PLA<sub>2</sub>. Varespladib was initially developed to neutralise high levels of PLA<sub>2</sub> for conditions like acute coronary syndrome, rheumatoid arthritis, asthma, and sepsis. The structure, function, and efficacy studies for varespladib have directly addressed its potential for SBE therapy [159]. Therefore, this is being tested for various applications in SBE-induced systemic and local effects.

Similarly, marimastat, a broad-spectrum MMP inhibitor, was initially tested in clinical trials as a cancer treatment, specifically in inhibition of tumour metastasis. This drug failed the trial because the prolonged treatment with this drug resulted in severe side effects [160]. However, in SBE, the treatment period is shorter. Therefore, due to their potential specific inhibition of snake venom PLA<sub>2</sub> and SVMPs, these drugs have been repurposed and tested against SBE. A study demonstrated that

by using combinations of varespladib and marimastat, dimercaprol or DMPS (SVMP inhibitors), it was possible to reduce the systemic haemotoxic effects of viper envenomation. This study supports a combination therapy using small molecule inhibitors such as varespladib and marimastat [161]. Another study achieved *in vitro* and *in vivo* neutralisation of viper venoms from different geographical locations including the West African and South Asian saw-scaled vipers (*Echis ocellatus* and *Echis carinatus*), the Central American ferde-lance or terciopelo (*Bothrops asper*), the African puff adder (*Bitis arietans*) and the South Asian Russell's viper (*Daboia russelii*). They used clinical-grade metal chelators that can reduce the availability of Zn<sup>2+</sup> required for SVMP bioactivity and phase-II approved peptidomimetic hydroxamate inhibitors, which can directly bind the Zn<sup>2+</sup> ion present in the catalytic core of the metalloproteinases. The research outcome from this study provided strong evidence suggesting that the combination of marimastat and varespladib has the potential as a pre-hospital treatment for SBE-induced systemic effects by achieving cross-species venom neutralisation in the geographically different viper species [162].

In another approach, a published study proposed using these inhibitor molecules to tackle the local effects of *Bothrops asper* venom. This viper venom is rich in myotoxins, especially myotoxin II, a Lys49 non-enzymatic PLA<sub>2</sub> analogue crucial in exhibiting myotoxic effects. However, this toxin is moderately immunogenic and fails to raise a strong antibody response during animal immunisation. A peptide inhibitor molecule (JB006) targeting myotoxin II was tested for its selective binding and functional neutralisation efficacy. This peptide reduced myotoxin-II-induced cytotoxicity in the C2C12 cell line. Pre-incubation of myotoxin II and different concentrations of JB006 peptide showed a dose-dependent reduction in myotoxicity in an *in vivo* mouse model by completely inhibiting the release of creatine kinase at the highest tested concentration (900 µM). The data from structural modelling suggested that the peptide-myotoxin II interactions could be due to electrostatic interactions. This questions the specificity of JB006 towards myotoxin II. There is a hypothesis based on peptide-myotoxin interaction, which needs further experimental research. The study suggested further investigation, structural modification to increase specificity, and studies on half-life and bioavailability, which are required to support the current data [163].

Scientists have explored using traditional medicine and plant extracts for years for SBE treatment. Medicinal plants are a rich source of bioactive compounds. These natural compounds, such as alkaloids, proteins, and phenolic compounds, have been used in experiments to test their effects against whole venoms or purified toxins. Compounds like atropine (cholinergic blocker), Azadirachta indica (PLA<sub>2</sub> inhibitor), Aristolochic acid (reduction in oedema), Rosmarinic acid (anti-inflammatory, anti-myotoxic),  $\beta$ -sitosterol (anti-myotoxic) and many more have been shown to reduce or inhibit the effect of different venom toxins. Most of these experiments have proven effective in *in vitro* studies but lack evidence of *in vivo* data [164]. These alternative treatment options primarily focus on systemic neutralising of whole venoms or specific venom toxins. However, treatment for SBE-mediated local tissue damage is relatively unexplored. There is an enormous scope for research and improvement in treating venom-induced muscle damage.

Successful inhibition of venom toxins may result in the effective regeneration of damaged muscle. The tissue damage begins when the venom enters the victim's system. An early stage of muscle regeneration decides the outcome of the post-damage repair. Hence, an early restriction of SVMPs and PLA<sub>2</sub> toxins will vastly improve muscle regeneration options. Batimastat and marimastat are known inhibitors of MMPs. These are phase II-approved drugs, following rigorous safety and efficacy studies. However, higher water solubility makes marimastat a more desirable candidate [165]. At the same time, varespladib has been effective in reducing the systemic effects of venom PLA<sub>2</sub> [166].

SVMPs and PLA<sub>2</sub> have specific target components in the tissue but also indirectly affect the entire regeneration process. The metalloprotease domain of SVMPs has an affinity towards collagen IV in the ECM. Research suggests that with the help of this domain, SVMPs can co-localise themselves with the ECM components, and the additional enzymatic domain can degrade different ECM components [146]. SVMP's action on microcapillary networks affects the blood and oxygen supply in the damaged tissue. The absence of capillaries reduces oxygen levels in the damaged tissue, and blood supply is also essential to maximise the reach of immune cells to remove and repair damaged and necrotic tissue. SVMPs also directly affect SC mobility, and lack of ECM scaffolding affects SC action and ECM remodelling [44, 129, 135]. Hence, SVMPs, directly and



indirectly, affect tissue regeneration and repair. PLA<sub>2</sub>s on the other hand, includes tissue necrosis either by directly acting on the phospholipid bilayer or inducing calcium reflex promoting tissue necrosis [56, 167]. If we can block the action of these two toxin families *in vivo*, we can control the tissue damage caused by viper venoms. Hence, using small molecule inhibitors specific for SVMPs and PLA<sub>2</sub>s can be a viable option to stop the actions of these two toxins *in vivo*.

### **1.10. Regenerative medicine to improve muscle regeneration**

For effective muscle regeneration, a suitable microenvironment is essential [168]. Our current and previous research demonstrates that the enzymatic action of venom toxins, lack of blood supply to the damaged tissues and inability of immune cells to act promptly creates an unfavourable or rather hostile environment for tissue regeneration [135].

Stem cells have proven their use and importance in regenerative medicine. They form a clonal cell population and differentiate into various cells/tissue types. Stem cells can be divided into three main categories: a) Embryonic stem cells are pluripotent stem cells derived from the inner mass of developing blastocytes. Pluripotent stem cells can develop into any cell type in the human body. Due to their ability to differentiate into any cell type, these cells have developed significant interest in tissue engineering and regenerative medicine; however, embryonic cells have been the subject of ethical debate. b) Induced pluripotent stem cells- like embryonic stem cells, these cells are also pluripotent. Unlike embryonic stem cells, the generation of these stem cells does not involve the destruction of an embryo. Induced pluripotent stem cells are generated by reprogramming adult cells, such as skin cells or blood cells, back into pluripotent cells. This programming is achieved by inducing specific transcription factors into the cells. c) Adult stem cells are multipotent stem cells and can develop into the same tissue lineage in which they are located. Adult stem cells are often used for autologous transplants. These cells include haematopoietic, neural & mesenchymal stem cells. Even with limited plasticity, adult stem cells are attractive tools for regenerative medicine due to the easier availability and ethical feasibility of obtaining these stem cells [169]. The therapeutic use of stem cells is mainly because of three essential qualities: Homing, where cells migrate to the site of injury due to chemical or chemo-attraction mediated by cell surface receptors. 2. Ability to

differentiate into multiple tissues/cell types. 3. Secretion of numerous bioactive factors affecting local and systemic physiological processes [170].

Studies have shown that stem cells significantly promote the repair of injured tissues. Typically, functional recovery of an organ achieved by stem cells was considered part of the stem cell differentiation process. A recent study has revealed that the outcome of tissue repair depends upon the local microenvironment of surrounding cells and the secreted products of stem cells [171]. Stem cell secretome is a term collectively used for soluble paracrine factors, including various cytokines, growth factors, and extracellular vesicles produced and released by stem cells under stressful conditions. The stem cell secretome contains cytokines, growth factors, ECM components, extracellular vesicles, exosomes, microvesicles, membrane particles and peptides [172]. They are mainly utilised for inter-cell communications, angiogenesis, and growth of new cells [173]. In addition, they are also responsible for tissue development, homeostasis, and regeneration. This potent combination of trophic factors can modulate the molecular composition of the environment to evoke a response from resident cells, and this phenomenon is called the paracrine effect. Studies have shown that stem cells contribute to tissue repair and regeneration by releasing a spectrum of paracrine factors that can lead to cell regeneration, repair, angiogenesis, tissue remodelling, and cell survival. Most studies demonstrating the paracrine activity of stem cells for cardiac repair have utilised adult stem cells. These cell types include mesenchymal stem cells, bone marrow stem cells, cardiac progenitor cells, and endothelial progenitor cells. Experimental investigation of the paracrine activity of mesenchymal stem cells revealed that administration of mesenchymal cell-derived, cell-free condition media increases the survival of cardiomyocytes *in vivo* and *in vitro* settings [174]. The paracrine factors secreted by mesenchymal stem cells, such as vascular endothelial growth factor, are effective in stem cell-mediated myocardial recovery in case of ischemia [175]. Mesenchymal cells have been applied as a therapeutic strategy for chronic muscle degeneration caused by muscular dystrophies, such as Duchenne muscular dystrophy. These cells are primarily examined for their antifibrotic and immunoregulatory properties. Secretory factors of mesenchymal stem cells were effective in enhancing the proliferation and differentiation of muscle stem cells, ECM

modulation, reduction of muscle fibrosis and muscle mass gain in chronic muscle degeneration studies [176-178]

Although it is well known that muscle tissues have SCs, in many cases of traumatic injury or diseases, including SBE, the quantity and potency of endogenous stem cell population are insufficient to regenerate compromised tissues due to dampening of proliferation and fusion potential. The traditional treatment option to achieve effective muscle regeneration is to transplant stem cells directly. However, in SBE-induced damage, the microenvironment is not favourable for the growth and development of stem cells. Stem cell secretome proved to be useful in many applications because of its different properties, including immunomodulatory, anti-inflammatory, anti-apoptotic, wound healing, tissue repair, neuroprotective, angiogenesis, and anti-microbial effects. Preclinical studies with mesenchymal cell secretome have shown the effects on immune cells' proliferation, activation, and function [179]. It is well established that the anti-inflammatory effects are mediated by soluble immunoregulatory molecules, which consist of tumour necrosis factors, interleukins, and anti-inflammatory cytokines. The balance between anti-inflammatory and pro-inflammatory cytokines helps the outcome [180]. Therefore, the paracrine effects of the cell secretome play a significant role in wound healing [181].

Several studies have reported the presence of growth factors in cell secretomes that contribute to the regeneration of damaged tissues. It also has anti-fibrotic and angiogenic effects that can reduce scar formation [182, 183]. Pro-inflammatory stimuli were largely studied using adipose-derived stem cell secretome (ASC). When TNF- $\alpha$  was stimulated, ASC was applied to the rodent wound healing model, where the analysis showed elevated levels of IL-6, IL-8, and MCP-I, which increased monocyte migration at the injury site. It also showed prominent levels of cathepsin, which is crucial in ECM remodelling and angiogenesis. After applying ASC, the wounded area showed increased capillary density and a fast overall wound recovery [184, 185]. Some factors have been reported that enhance clinically important properties of ASC. Microarray analysis has shown that some scaffold-free spheroids upregulate the genes responsible for transforming collagen, laminin, fibronectin, tenascin, and many other growth factors [183]. These enhanced growth factors provide improved effects than natively secreted growth factors. Platelet secretome also has

abundant cytokines that can offer a hospitable and nourishing microenvironment in the affected muscle area, and it has been used in wound healing.

### **1.11. Improving muscle regeneration by reducing fibrosis**

Earlier studies have shown that SBE-induced muscle damage presents with fibrotic tissue deposition [117, 141, 186]. Muscle fibrosis affects muscle regeneration and hinders the restoration of structural and functional characteristics of damaged tissues. In viper venom-induced muscle damage, the regenerated tissue is often fibrotic [150]. Fibrosis can permanently lose the structure and function of that part of the muscle. This issue shares a similar pathology to that of muscle degenerative disorders, where constant degeneration and regeneration takes place to replace normal muscle fibres with fibrotic tissues. Anti-fibrotic molecules such as decorin, imatinib, soluble activin receptor IIB, and losartan have proven effective in controlling fibrosis.

Myostatin is an extracellular cytokine belonging to the TGF- $\beta$  family expressed in skeletal muscle lineage. Myostatin is a well-studied promotor of muscle fibrosis and is secreted from fibroblast after proteolytic fusion. Activin IIB is a punitive receptor for myostatin binding. After binding with activin receptor IIB, they form a complex with activin receptor I. This complex acts through the Smad signalling pathway blocks the expression of the myogenesis gene and promotes fibrosis while reducing muscle growth [187]. An anti-fibrotic molecule, the recombinant soluble activin receptor IIB counterpart is an inhibitor for myostatin. Soluble activin receptor IIB acts as a competitive inhibitor for myostatin, reducing myostatin binding to innate activin IIB receptors, thus promoting muscle growth and reducing muscle fibrosis [187, 188]. Another inhibitor is suramin, a TGF- $\beta$  inhibitor that has been studied as an anti-fibrotic molecule. Studies suggest that suramin treatment can improve the differentiation of muscle SCs to myoblasts. Suramin can indirectly inhibit myostatin, reduce muscle fibrosis, and enhance muscle strength [189, 190]. Some studies have also explored the anti-fibrotic effects of nilotinib. This drug reduces muscle fibrosis by promoting tumour necrotic factor-mediated apoptosis of fibro-adipogenic progenitors during chronic muscle injury [191].

## 1.12. Rationale of this study

As evident from all the previous research, SBE-mediated skeletal muscle damage leads to permanent muscle loss and often results in disabilities. Viper venom can cause an impairment in the innate muscle regeneration process. Viper venom proteins last longer in the tissues, inducing persistent damage. They can alter the trajectory of the innate immune responses, hinder the functions of muscle stem cells, and alterations in the ultrastructure of the skeletal muscle cells. Hence, we must develop potential therapy focused on local tissue damage repair. For the global treatment applications, it is better to focus on the specific areas that result in impaired tissue regeneration rather than developing a therapy based on species-specific venoms or venom toxins. Hence, in this study, we have focused on three primary areas to improve muscle regeneration in viper venom-induced skeletal muscle damage. We use small-molecule inhibitors, antifibrotic molecules, and regenerative medicine to rectify these issues. We have developed animal models and examined the progress of skeletal muscle regeneration based on the analysis of various biomarkers. This analysis leads us towards comprehending muscle regeneration, different stages of muscle regeneration, secretion and remodelling of the ECM, and progress towards angiogenesis, intramuscular bleeding, and muscle fibrosis. We aimed to gather as much information as possible to see the effects of a given treatment.

We have analysed these treatment molecules individually; however, the information gathered would help develop a stand-alone or combinational therapy to treat SBE-induced skeletal muscle damage. This project provides exciting new opportunities for the prevention/treatment of SBE-induced skeletal muscle damage. With specific treatment options, there is a hope to lower the impact of SBE-induced permanent muscle damage and morbidities.

The two venoms used in this study are *Crotalus atrox* (*C. atrox*) venom, a prominent snake species in southwestern America and northern Mexico. The venom of *C. atrox* is potent cocktail of SVMPs, SVSPs, PLA<sub>2</sub>, LAAO, C-type lectin-like proteins. SVMPs constitute for around 69.5 % of total venom proteins [176]. Which makes it an ideal venom to study muscle damage. The second venom included in the study is from *Daboia russelii* (Russell's Viper- RV). This species is medically important in Indian sub-continent and responsible for maximum mortality and morbidity cases in snake bite victims. This venom is rather interesting. Unlike most viper venom, the predominant toxic family in RV venom is PLA<sub>2</sub>. The percentage of PLA<sub>2</sub>, varies vastly due to regional variations in the

venom. Recent analysis confirmed that the percentage of PLA<sub>2</sub> ranges from 38% to 56% [192]. Despite of the huge difference in venom composition in the venom proteins, both venoms have been reported to cause extensive skeletal muscle damage up on administration.

### **1.13. Hypothesis, aim and objectives**

We hypothesise that neutralising major venom toxins, providing a favourable microenvironment for muscle regeneration, and reducing fibrosis will result in successful muscle regeneration following SBE-induced muscle damage.

This study aims to develop specific treatment approaches to rectify the difficulties regarding impaired muscle regeneration post-viper envenoming.

The specific objectives are to:

- 1) Neutralise the major venom toxins such as SVMPs and PLA<sub>2</sub> using selective small molecule inhibitors and assess their impact on muscle regeneration.
- 2) Provide a suitable environment using stem-cells-derived secretome to enhance muscle regeneration following venom-induced damage and
- 3) Reduce muscle fibrosis using a recombinant soluble activin receptor IIB to regenerate muscle following venom-induced damage.

## References

1. Bhaumik, S., et al., *How and why snakebite became a global health priority: a policy analysis*. *BMJ Glob Health*, 2023. **8**(8).
2. Williams, D.J., et al., *Strategy for a globally coordinated response to a priority neglected tropical disease: Snakebite envenoming*. *PLoS Negl Trop Dis*, 2019. **13**(2): p. e0007059.
3. Longbottom, J., et al., *Vulnerability to snakebite envenoming: a global mapping of hotspots*. *Lancet*, 2018. **392**(10148): p. 673-684.
4. Warrell, D.A., *Snake bite*. *Lancet*, 2010. **375**(9708): p. 77-88.
5. Gutierrez, J.M., et al., *Snakebite envenoming*. *Nat Rev Dis Primers*, 2017. **3**: p. 17063.
6. Satyanarayan, B., et al., *Clinical and epidemiological profile of snakebite cases - A study from an industrial teaching hospital at Jamshedpur, Jharkhand, India*. *J Family Med Prim Care*, 2022. **11**(12): p. 7652-7656.
7. Mahmood, M.A., et al., *Inadequate knowledge about snakebite envenoming symptoms and application of harmful first aid methods in the community in high snakebite incidence areas of Myanmar*. *PLoS Negl Trop Dis*, 2019. **13**(2): p. e0007171.
8. Williams, S.S., et al., *Delayed psychological morbidity associated with snakebite envenoming*. *PLoS Negl Trop Dis*, 2011. **5**(8): p. e1255.
9. Chippaux, J.P., *Estimate of the burden of snakebites in sub-Saharan Africa: a meta-analytic approach*. *Toxicon*, 2011. **57**(4): p. 586-99.
10. Vaiyapuri, S., et al., *Snakebite and its socio-economic impact on the rural population of Tamil Nadu, India*. *PLoS One*, 2013. **8**(11): p. e80090.
11. Infante, C.R., A.M. Rasys, and D.B. Menke, *Appendages and gene regulatory networks: Lessons from the limbless*. *Genesis*, 2018. **56**(1).
12. Yi, H. and M.A. Norell, *The burrowing origin of modern snakes*. *Sci Adv*, 2015. **1**(10): p. e1500743.
13. Da Silva, F.O., et al., *The ecological origins of snakes as revealed by skull evolution*. *Nat Commun*, 2018. **9**(1): p. 376.
14. Palci, A., et al., *Plicidentine and the repeated origins of snake venom fangs*. *Proc Biol Sci*, 2021. **288**(1956): p. 20211391.
15. Vonk, F.J., et al., *Evolutionary origin and development of snake fangs*. *Nature*, 2008. **454**(7204): p. 630-3.
16. Jackson, K., *The evolution of venom-conducting fangs: insights from developmental biology*. *Toxicon*, 2007. **49**(7): p. 975-81.
17. Young, B.A. and K.V. Kardong, *Dentitional surface features in snakes (Reptilia: Serpentes)*. *Amphibia-Reptilia*, 1996. **17**(3): p. 261-276.
18. Clark, R.W., et al., *Pit viper thermography: the pit organ used by crotaline snakes to detect thermal contrast has poor spatial resolution*. *J Exp Biol*, 2022. **225**(24).

19. Halpern, M., *The organization and function of the vomeronasal system*. Annual review of neuroscience, 1987. **10**(1): p. 325-362.
20. Casewell, N.R., et al., *Complex cocktails: the evolutionary novelty of venoms*. Trends in ecology & evolution, 2013. **28**(4): p. 219-229.
21. Tasoulis, T. and G.K. Isbister, *A Review and Database of Snake Venom Proteomes*. Toxins (Basel), 2017. **9**(9).
22. Junqueira-de-Azevedo, I.L., et al., *Colubrid Venom Composition: An -Omics Perspective*. Toxins (Basel), 2016. **8**(8).
23. Tasoulis, T., T.L. Pukala, and G.K. Isbister, *Investigating toxin diversity and abundance in snake venom proteomes*. Frontiers in Pharmacology, 2022. **12**: p. 768015.
24. Slagboom, J., et al., *Haemotoxic snake venoms: their functional activity, impact on snakebite victims and pharmaceutical promise*. Br J Haematol, 2017. **177**(6): p. 947-959.
25. Chan, Y.S., et al., *Snake venom toxins: toxicity and medicinal applications*. Appl Microbiol Biotechnol, 2016. **100**(14): p. 6165-6181.
26. Gutierrez, J.M. and A. Rucavado, *Snake venom metalloproteinases: their role in the pathogenesis of local tissue damage*. Biochimie, 2000. **82**(9-10): p. 841-50.
27. Gasanov, S.E., R.K. Dagda, and E.D. Rael, *Snake Venom Cytotoxins, Phospholipase A(2)s, and Zn(2+)-dependent Metalloproteinases: Mechanisms of Action and Pharmacological Relevance*. J Clin Toxicol, 2014. **4**(1): p. 1000181.
28. Hiremath, K., et al., *Three finger toxins of elapids: structure, function, clinical applications and its inhibitors*. Molecular Diversity, 2023: p. 1-18.
29. Ainsworth, S., et al., *The medical threat of mamba envenoming in sub-Saharan Africa revealed by genus-wide analysis of venom composition, toxicity and antivenomics profiling of available antivenoms*. Journal of proteomics, 2018. **172**: p. 173-189.
30. Tan, K.Y., et al., *Quantitative proteomics of Naja annulifera (sub-Saharan snouted cobra) venom and neutralization activities of two antivenoms in Africa*. International journal of biological macromolecules, 2020. **158**: p. 605-616.
31. Weinstein, S.A. and D.E. Keyler, *Local envenoming by the Western hognose snake (Heterodon nasicus): A case report and review of medically significant Heterodon bites*. Toxicon, 2009. **54**(3): p. 354-360.
32. de Medeiros, C.R., et al., *Bites by Tomodon dorsatus (serpentes, dipsadidae): Clinical and epidemiological study of 86 cases*. Toxicon, 2019. **162**: p. 40-45.
33. Castro, F.C., et al., *Bites by Philodryas olfersii (Lichtenstein, 1823) and Philodryas aestiva (Duméril, Bibron and Duméril, 1854)(serpentes, dipsadidae) in São Paulo, Brazil: a retrospective observational study of 155 cases*. Toxicon, 2021. **197**: p. 55-64.
34. Markland Jr, F.S. and S. Swenson, *Snake venom metalloproteinases*. Toxicon, 2013. **62**: p. 3-18.



35. Olaoba, O.T., et al., *Snake venom metalloproteinases (SVMPs): a structure-function update*. *Toxicon*: X, 2020. **7**: p. 100052.
36. Ching, A.T., et al., *Venomomics profiling of *Thamnodynastes strigatus* unveils matrix metalloproteinases and other novel proteins recruited to the toxin arsenal of rear-fanged snakes*. *Journal of proteome research*, 2012. **11**(2): p. 1152-1162.
37. Herrera, C., et al., *Tissue localization and extracellular matrix degradation by PI, PII and PIII snake venom metalloproteinases: clues on the mechanisms of venom-induced hemorrhage*. *PLoS neglected tropical diseases*, 2015. **9**(4): p. e0003731.
38. Carbajo, R.J., et al., *NMR structure of bitistatin—a missing piece in the evolutionary pathway of snake venom disintegrins*. *The FEBS Journal*, 2015. **282**(2): p. 341-360.
39. Tan, K.Y., et al., *Comparative venom gland transcriptomics of *Naja kaouthia* (monocled cobra) from Malaysia and Thailand: elucidating geographical venom variation and insights into sequence novelty*. *PeerJ*, 2017. **5**: p. e3142.
40. Cesar, P.H., et al., *Snake venom disintegrins: an overview of their interaction with integrins*. *Current Drug Targets*, 2019. **20**(4): p. 465-477.
41. Rivas-Mercado, E. and L. Garza-Ocañas, *Disintegrins obtained from snake venom and their pharmacological potential*. *Medicina Universitaria*, 2017. **19**(74): p. 32-37.
42. Masuda, S., et al., *cDNA cloning and characterization of vascular apoptosis-inducing protein 1*. *Biochemical and Biophysical Research Communications*, 2000. **278**(1): p. 197-204.
43. Boukhalfa-Abib, H. and F. Laraba-Djebari, *CcMP-II, a new hemorrhagic metalloproteinase from *Cerastes cerastes* snake venom: purification, biochemical characterization and amino acid sequence analysis*. *Comparative Biochemistry and Physiology Part C: Toxicology & Pharmacology*, 2015. **167**: p. 65-73.
44. Markland, F.S., Jr. and S. Swenson, *Snake venom metalloproteinases*. *Toxicon*, 2013. **62**: p. 3-18.
45. Fox, J.W. and S.M. Serrano, *Insights into and speculations about snake venom metalloproteinase (SVMP) synthesis, folding and disulfide bond formation and their contribution to venom complexity*. *The FEBS journal*, 2008. **275**(12): p. 3016-3030.
46. Sajevic, T., A. Leonardi, and I. Križaj, *Haemostatically active proteins in snake venoms*. *Toxicon*, 2011. **57**(5): p. 627-645.
47. Sajevic, T., et al., *VaH3, one of the principal hemorrhagins in *Vipera ammodytes ammodytes* venom, is a homodimeric P-IIIc metalloproteinase*. *Biochimie*, 2013. **95**(6): p. 1158-1170.
48. Clemetson, K.J., *Snaclecs (snake C-type lectins) that inhibit or activate platelets by binding to receptors*. *Toxicon*, 2010. **56**(7): p. 1236-46.
49. Sajevic, T., A. Leonardi, and I. Krizaj, *Haemostatically active proteins in snake venoms*. *Toxicon*, 2011. **57**(5): p. 627-45.
50. Stocker, K., H. Fischer, and J. Meier, *Thrombin-like snake venom proteinases*. *Toxicon*, 1982. **20**(1): p. 265-73.

51. Serrano, S.M. and R.C. Maroun, *Snake venom serine proteinases: sequence homology vs. substrate specificity, a paradox to be solved*. *Toxicon*, 2005. **45**(8): p. 1115-32.
52. Latinović, Z., et al., *The procoagulant snake venom serine protease potentially having a dual, blood coagulation factor V and X-Activating activity*. *Toxins*, 2020. **12**(6): p. 358.
53. Matsui, T., Y. Fujimura, and K. Titani, *Snake venom proteases affecting hemostasis and thrombosis*. *Biochim Biophys Acta*, 2000. **1477**(1-2): p. 146-56.
54. Urs, N.A., et al., *Implications of phytochemicals in snakebite management: present status and future prospective*. *Toxin Reviews*, 2014. **33**(3): p. 60-83.
55. Xiao, H., et al., *Snake Venom PLA(2), a Promising Target for Broad-Spectrum Antivenom Drug Development*. *Biomed Res Int*, 2017. **2017**: p. 6592820.
56. Castro-Amorim, J., et al., *Catalytically Active Snake Venom PLA2 Enzymes: An Overview of Its Elusive Mechanisms of Reaction: Miniperspective*. *Journal of Medicinal Chemistry*, 2023. **66**(8): p. 5364-5376.
57. Burke, J.E. and E.A. Dennis, *Phospholipase A2 structure/function, mechanism, and signaling1*. *Journal of lipid research*, 2009. **50**: p. S237-S242.
58. Mayer, R.J. and L.A. Marshall, *New insights on mammalian phospholipase A2 (s); comparison of arachidonoyl-selective and-nonselctive enzymes*. *The FASEB Journal*, 1993. **7**(2): p. 339-348.
59. Bonventre, J.V., *Phospholipase A2 and signal transduction*. *Journal of the American Society of Nephrology*, 1992. **3**(2): p. 128-150.
60. Girish, K., et al., *Hyaluronidase and protease activities from Indian snake venoms: neutralization by Mimosa pudica root extract*. *Fitoterapia*, 2004. **75**(3-4): p. 378-380.
61. Kemparaju, K. and K. Girish, *Snake venom hyaluronidase: a therapeutic target*. *Cell Biochemistry and Function: Cellular biochemistry and its modulation by active agents or disease*, 2006. **24**(1): p. 7-12.
62. Osipov, A.V. and Y.N. Utkin, *Snake venom toxins targeted at the nervous system*. *Snake Venoms-Toxinology*: Springer, Dordrecht, 2017: p. 189-214.
63. Kessler, P., et al., *The three-finger toxin fold: a multifunctional structural scaffold able to modulate cholinergic functions*. *Journal of Neurochemistry*, 2017. **142**: p. 7-18.
64. Heyborne, W.H. and S.P. Mackessy, *Identification and characterization of a taxon-specific three-finger toxin from the venom of the Green Vinesnake (Oxybelis fulgidus; family Colubridae)*. *Biochimie*, 2013. **95**(10): p. 1923-32.
65. Barber, C.M., G.K. Isbister, and W.C. Hodgson, *Alpha neurotoxins*. *Toxicon*, 2013. **66**: p. 47-58.
66. Changeux, J.-P., *The TiPS lecture the nicotinic acetylcholine receptor: an allosteric protein prototype of ligand-gated ion channels*. *Trends in pharmacological sciences*, 1990. **11**(12): p. 485-492.

67. Grant, G.A. and V.A. Chiappinelli, . *kappa*-Bungarotoxin: complete amino acid sequence of a neuronal nicotinic receptor probe. *Biochemistry*, 1985. **24**(6): p. 1532-1537.
68. Marchot, P., et al., *Inhibition of mouse acetylcholinesterase by fasciculins: crystal structure of the complex and mutagenesis of fasciculins*. *Toxicon*, 1998. **36**(11): p. 1613-1622.
69. Marquer, C., et al., *Structural model of ligand-G protein-coupled receptor (GPCR) complex based on experimental double mutant cycle data: MT7 snake toxin bound to dimeric hM1 muscarinic receptor*. *Journal of Biological Chemistry*, 2011. **286**(36): p. 31661-31675.
70. Garcia, M., et al., *Calciseptine, a Ca<sup>2+</sup> channel blocker, has agonist actions on L-type Ca<sup>2+</sup> currents of frog and mammalian skeletal muscle*. *The Journal of Membrane Biology*, 2001. **184**: p. 121-129.
71. Konshina, A.G., N.A. Krylov, and R.G. Efremov, *Cardiotoxins: functional role of local conformational changes*. *Journal of Chemical Information and Modeling*, 2017. **57**(11): p. 2799-2810.
72. Nguyen, T.T.N., et al., *Cardiotoxin-I: An Unexpectedly Potent Insulinotropic Agent*. *ChemBioChem*, 2012. **13**(12): p. 1805-1812.
73. McDowell, R.S., et al., *Mambin, a potent glycoprotein IIb-IIIa antagonist and platelet aggregation inhibitor structurally related to the short neurotoxins*. *Biochemistry*, 1992. **31**(20): p. 4766-4772.
74. Girish, V.M. and R.M. Kini, *Exactin: A specific inhibitor of Factor X activation by extrinsic tenase complex from the venom of Hemachatus haemachatus*. *Scientific Reports*, 2016. **6**(1): p. 32036.
75. Rajagopalan, N., et al.,  *$\beta$ -Cardiotoxin: a new three-finger toxin from Ophiophagus hannah (king cobra) venom with beta-blocker activity*. *The FASEB Journal*, 2007. **21**(13): p. 3685-3695.
76. Koivula, K., S. Rondinelli, and J. Näsman, *The three-finger toxin MT $\alpha$  is a selective  $\alpha$ 2B-adrenoceptor antagonist*. *Toxicon*, 2010. **56**(3): p. 440-447.
77. Diochot, S., et al., *Black mamba venom peptides target acid-sensing ion channels to abolish pain*. *Toxicon*, 2013(75): p. 212.
78. Rivera-Torres, I.O., et al., *Discovery and characterisation of a novel toxin from Dendroaspis angusticeps, named Tx7335, that activates the potassium channel KcsA*. *Scientific Reports*, 2016. **6**(1): p. 23904.
79. Yang, D.C., et al., *The snake with the scorpion's sting: Novel three-finger toxin sodium channel activators from the venom of the long-glanded blue coral snake (Calliophis bivirgatus)*. *Toxins*, 2016. **8**(10): p. 303.
80. Chien, K.Y., et al., *Two distinct types of cardiotoxin as revealed by the structure and activity relationship of their interaction with zwitterionic phospholipid dispersions*. *J Biol Chem*, 1994. **269**(20): p. 14473-83.

81. de Queiroz, M.R., et al., *The role of platelets in hemostasis and the effects of snake venom toxins on platelet function*. *Toxicon*, 2017. **133**: p. 33-47.
82. Rowland, L.A., N.C. Bal, and M. Periasamy, *The role of skeletal-muscle-based thermogenic mechanisms in vertebrate endothermy*. *Biological Reviews*, 2015. **90**(4): p. 1279-1297.
83. Csapo, R., M. Gumpenberger, and B. Wessner, *Skeletal muscle extracellular matrix—what do we know about its composition, regulation, and physiological roles? A narrative review*. *Frontiers in physiology*, 2020. **11**: p. 253.
84. Pedersen, B.K. and M.A. Febbraio, *Muscles, exercise and obesity: skeletal muscle as a secretory organ*. *Nature Reviews Endocrinology*, 2012. **8**(8): p. 457-465.
85. Frontera, W.R. and J. Ochala, *Skeletal muscle: a brief review of structure and function*. *Calcified tissue international*, 2015. **96**: p. 183-195.
86. Cretoiu, D., et al., *Myofibers*. *Adv Exp Med Biol*, 2018. **1088**: p. 23-46.
87. Dayanidhi, S. and R.L. Lieber, *Skeletal muscle satellite cells: mediators of muscle growth during development and implications for developmental disorders*. *Muscle Nerve*, 2014. **50**(5): p. 723-32.
88. Munoz-Canoves, P. and A.L. Serrano, *Macrophages decide between regeneration and fibrosis in muscle*. *Trends Endocrinol Metab*, 2015. **26**(9): p. 449-50.
89. Gillies, A.R. and R.L. Lieber, *Structure and function of the skeletal muscle extracellular matrix*. *Muscle Nerve*, 2011. **44**(3): p. 318-31.
90. Takala, T.E. and P. Virtanen, *Biochemical composition of muscle extracellular matrix: the effect of loading*. *Scand J Med Sci Sports*, 2000. **10**(6): p. 321-5.
91. Halper, J. and M. Kjaer, *Basic components of connective tissues and extracellular matrix: elastin, fibrillin, fibulins, fibrinogen, fibronectin, laminin, tenascins and thrombospondins*. *Adv Exp Med Biol*, 2014. **802**: p. 31-47.
92. Kjaer, M., *Role of extracellular matrix in adaptation of tendon and skeletal muscle to mechanical loading*. *Physiol Rev*, 2004. **84**(2): p. 649-98.
93. McLoon, L.K., et al., *Composition, Architecture, and Functional Implications of the Connective Tissue Network of the Extraocular Muscles*. *Invest Ophthalmol Vis Sci*, 2018. **59**(1): p. 322-329.
94. Boppart, M.D. and Z.S. Mahmassani, *Integrin signaling: linking mechanical stimulation to skeletal muscle hypertrophy*. *Am J Physiol Cell Physiol*, 2019. **317**(4): p. C629-C641.
95. Boppart, M.D. and Z.S. Mahmassani, *Integrin signaling: linking mechanical stimulation to skeletal muscle hypertrophy*. *American Journal of Physiology-Cell Physiology*, 2019. **317**(4): p. C629-C641.
96. Ervasti, J.M. and K.P. Campbell, *A role for the dystrophin-glycoprotein complex as a transmembrane linker between laminin and actin*. *J Cell Biol*, 1993. **122**(4): p. 809-23.
97. Peter, A.K., et al., *The costamere bridges sarcomeres to the sarcolemma in striated muscle*. *Prog Pediatr Cardiol*, 2011. **31**(2): p. 83-88.

98. Csapo, R., M. Gumpenberger, and B. Wessner, *Skeletal Muscle Extracellular Matrix - What Do We Know About Its Composition, Regulation, and Physiological Roles? A Narrative Review*. Front Physiol, 2020. **11**: p. 253.
99. Panahipour, L., et al., *TGF-beta Activity Related to the Use of Collagen Membranes: In Vitro Bioassays*. Int J Mol Sci, 2020. **21**(18).
100. Brandan, E. and J. Gutierrez, *Role of proteoglycans in the regulation of the skeletal muscle fibrotic response*. FEBS J, 2013. **280**(17): p. 4109-17.
101. Schwarz, R.I., *Collagen I and the fibroblast: high protein expression requires a new paradigm of post-transcriptional, feedback regulation*. Biochem Biophys Rep, 2015. **3**: p. 38-44.
102. Visse, R. and H. Nagase, *Matrix metalloproteinases and tissue inhibitors of metalloproteinases: structure, function, and biochemistry*. Circ Res, 2003. **92**(8): p. 827-39.
103. Corcoran, M.L., et al., *MMP-2: expression, activation and inhibition*. Enzyme Protein, 1996. **49**(1-3): p. 7-19.
104. Christensen, S. and P.P. Purslow, *The role of matrix metalloproteinases in muscle and adipose tissue development and meat quality: A review*. Meat Sci, 2016. **119**: p. 138-46.
105. Hawke, T.J. and D.J. Garry, *Myogenic satellite cells: physiology to molecular biology*. J Appl Physiol (1985), 2001. **91**(2): p. 534-51.
106. Frenette, J., B. Cai, and J.G. Tidball, *Complement activation promotes muscle inflammation during modified muscle use*. Am J Pathol, 2000. **156**(6): p. 2103-10.
107. Gordon, J.R. and S.J. Galli, *Mast cells as a source of both preformed and immunologically inducible TNF-alpha/cachectin*. Nature, 1990. **346**(6281): p. 274-6.
108. Arango Duque, G. and A. Descoteaux, *Macrophage cytokines: involvement in immunity and infectious diseases*. Front Immunol, 2014. **5**: p. 491.
109. Semple, J.W., et al., *Intravenous immunoglobulin prevents murine antibody-mediated acute lung injury at the level of neutrophil reactive oxygen species (ROS) production*. PLoS One, 2012. **7**(2): p. e31357.
110. Chazaud, B., et al., *Dual and beneficial roles of macrophages during skeletal muscle regeneration*. Exerc Sport Sci Rev, 2009. **37**(1): p. 18-22.
111. Palmieri, E.M., et al., *Nitric Oxide in Macrophage Immunometabolism: Hiding in Plain Sight*. Metabolites, 2020. **10**(11).
112. Mantovani, A., et al., *The chemokine system in diverse forms of macrophage activation and polarization*. Trends Immunol, 2004. **25**(12): p. 677-86.
113. Gordon, S., *Alternative activation of macrophages*. Nat Rev Immunol, 2003. **3**(1): p. 23-35.
114. Arnold, L., et al., *Inflammatory monocytes recruited after skeletal muscle injury switch into antiinflammatory macrophages to support myogenesis*. J Exp Med, 2007. **204**(5): p. 1057-69.

115. Villalta, S.A., et al., *Interleukin-10 reduces the pathology of mdx muscular dystrophy by deactivating M1 macrophages and modulating macrophage phenotype*. Hum Mol Genet, 2011. **20**(4): p. 790-805.
116. Ziemkiewicz, N., et al., *The Role of Innate and Adaptive Immune Cells in Skeletal Muscle Regeneration*. Int J Mol Sci, 2021. **22**(6).
117. Garg, K., B.T. Corona, and T.J. Walters, *Therapeutic strategies for preventing skeletal muscle fibrosis after injury*. Front Pharmacol, 2015. **6**: p. 87.
118. Ahmad, S.S., et al., *The roles of growth factors and hormones in the regulation of muscle satellite cells for cultured meat production*. J Anim Sci Technol, 2023. **65**(1): p. 16-31.
119. Forcina, L., M. Cosentino, and A. Musaro, *Mechanisms Regulating Muscle Regeneration: Insights into the Interrelated and Time-Dependent Phases of Tissue Healing*. Cells, 2020. **9**(5).
120. Grounds, M.D., et al., *Towards developing standard operating procedures for pre-clinical testing in the mdx mouse model of Duchenne muscular dystrophy*. Neurobiol Dis, 2008. **31**(1): p. 1-19.
121. Gutierrez, J.M., et al., *Why is Skeletal Muscle Regeneration Impaired after Myonecrosis Induced by Viperid Snake Venoms? Toxins (Basel)*, 2018. **10**(5).
122. Montecucco, C., J.M. Gutierrez, and B. Lomonte, *Cellular pathology induced by snake venom phospholipase A2 myotoxins and neurotoxins: common aspects of their mechanisms of action*. Cell Mol Life Sci, 2008. **65**(18): p. 2897-912.
123. Gutierrez, J.M. and C.L. Ownby, *Skeletal muscle degeneration induced by venom phospholipases A2: insights into the mechanisms of local and systemic myotoxicity*. Toxicon, 2003. **42**(8): p. 915-31.
124. Salvini, T.F., et al., *Long-term regeneration of fast and slow murine skeletal muscles after induced injury by ACL myotoxin isolated from Agkistrodon contortrix laticinctus (broad-banded copperhead) venom*. Anat Rec, 1999. **254**(4): p. 521-33.
125. Morini, C.C., et al., *Injury and recovery of fast and slow skeletal muscle fibers affected by ACL myotoxin isolated from Agkistrodon contortrix laticinctus (Broad-Banded copperhead) venom*. Toxicon, 1998. **36**(7): p. 1007-24.
126. Ownby, C.L., J.E. Fletcher, and T.R. Colberg, *Cardiotoxin 1 from cobra (Naja naja atra) venom causes necrosis of skeletal muscle in vivo*. Toxicon, 1993. **31**(6): p. 697-709.
127. Bickler, P.E., *Amplification of Snake Venom Toxicity by Endogenous Signaling Pathways*. Toxins (Basel), 2020. **12**(2).
128. Eming, S.A., P. Martin, and M. Tomic-Canic, *Wound repair and regeneration: mechanisms, signaling, and translation*. Sci Transl Med, 2014. **6**(265): p. 265sr6.
129. Escalante, T., et al., *Key events in microvascular damage induced by snake venom hemorrhagic metalloproteinases*. J Proteomics, 2011. **74**(9): p. 1781-94.

130. Gutierrez, J.M., et al., *Hemorrhage Caused by Snake Venom Metalloproteinases: A Journey of Discovery and Understanding*. Toxins (Basel), 2016. **8**(4): p. 93.
131. Chaillou, T., et al., *Effect of hypoxia exposure on the recovery of skeletal muscle phenotype during regeneration*. Mol Cell Biochem, 2014. **390**(1-2): p. 31-40.
132. Neto, H.S. and M.J. Marques, *Microvessel damage by B. jararacussu snake venom: pathogenesis and influence on muscle regeneration*. Toxicon, 2005. **46**(7): p. 814-9.
133. Yin, H., F. Price, and M.A. Rudnicki, *Satellite cells and the muscle stem cell niche*. Physiol Rev, 2013. **93**(1): p. 23-67.
134. Dhar, D., *Compartment Syndrome Following Snake Bite*. Oman Med J, 2015. **30**(2): p. e082.
135. Williams, H.F., et al., *Mechanisms underpinning the permanent muscle damage induced by snake venom metalloprotease*. PLoS Negl Trop Dis, 2019. **13**(1): p. e0007041.
136. Janakiram, N.B., et al., *The Role of the Inflammatory Response in Mediating Functional Recovery Following Composite Tissue Injuries*. Int J Mol Sci, 2021. **22**(24).
137. Perez, S. and S. Rius-Perez, *Macrophage Polarization and Reprogramming in Acute Inflammation: A Redox Perspective*. Antioxidants (Basel), 2022. **11**(7).
138. Tidball, J.G., *Regulation of muscle growth and regeneration by the immune system*. Nat Rev Immunol, 2017. **17**(3): p. 165-178.
139. Yu, Y., et al., *Macrophages play a key role in tissue repair and regeneration*. PeerJ, 2022. **10**: p. e14053.
140. Chapman, M.A., R. Meza, and R.L. Lieber, *Skeletal muscle fibroblasts in health and disease*. Differentiation, 2016. **92**(3): p. 108-115.
141. Queiroz, L.S., et al., *Muscle necrosis and regeneration after envenomation by Bothrops jararacussu snake venom*. Toxicon, 1984. **22**(3): p. 339-46.
142. Gutierrez, J.M., C.L. Ownby, and G.V. Odell, *Skeletal muscle regeneration after myonecrosis induced by crude venom and a myotoxin from the snake Bothrops asper (Fer-de-Lance)*. Toxicon, 1984. **22**(5): p. 719-31.
143. Li, Y., et al., *Transforming growth factor-beta1 induces the differentiation of myogenic cells into fibrotic cells in injured skeletal muscle: a key event in muscle fibrogenesis*. Am J Pathol, 2004. **164**(3): p. 1007-19.
144. Giuliani, G., M. Rosina, and A. Reggio, *Signaling pathways regulating the fate of fibro/adipogenic progenitors (FAPs) in skeletal muscle regeneration and disease*. FEBS J, 2022. **289**(21): p. 6484-6517.
145. Lu, P., et al., *Extracellular matrix degradation and remodeling in development and disease*. Cold Spring Harb Perspect Biol, 2011. **3**(12).
146. Baldo, C., et al., *Mechanisms of vascular damage by hemorrhagic snake venom metalloproteinases: tissue distribution and in situ hydrolysis*. PLoS Negl Trop Dis, 2010. **4**(6): p. e727.

147. Cabral-Pacheco, G.A., et al., *The Roles of Matrix Metalloproteinases and Their Inhibitors in Human Diseases*. Int J Mol Sci, 2020. **21**(24).
148. Wang, X., et al., *Diverse effector and regulatory functions of fibro/adipogenic progenitors during skeletal muscle fibrosis in muscular dystrophy*. iScience, 2023. **26**(1): p. 105775.
149. Schiaffino, S. and T. Partridge, *Skeletal muscle repair and regeneration*. Vol. 3. 2008: Springer Science & Business Media.
150. Arce, V., F. Brenes, and J.M. Gutierrez, *Degenerative and regenerative changes in murine skeletal muscle after injection of venom from the snake Bothrops asper: a histochemical and immunocytochemical study*. Int J Exp Pathol, 1991. **72**(2): p. 211-26.
151. de Souza Queiroz, L., M.J. Marques, and H. Santo Neto, *Acute local nerve lesions induced by Bothrops jararacussu snake venom*. Toxicon, 2002. **40**(10): p. 1483-6.
152. Hernandez, R., et al., *Poor regenerative outcome after skeletal muscle necrosis induced by Bothrops asper venom: alterations in microvasculature and nerves*. PLoS One, 2011. **6**(5): p. e19834.
153. Pucca, M.B., et al., *History of Envenoming Therapy and Current Perspectives*. Front Immunol, 2019. **10**: p. 1598.
154. Ramos, H.R. and P.L. Ho, *Developing Snake Antivenom Sera by Genetic Immunization: A Review*, in *Clinical Toxinology in Asia Pacific and Africa*, P. Gopalakrishnakone, et al., Editors. 2015, Springer Netherlands: Dordrecht. p. 401-414.
155. Gutiérrez, J.M., *Global Availability of Antivenoms: The Relevance of Public Manufacturing Laboratories*. Toxins, 2019. **11**(1): p. 5.
156. Kang, T.H. and S.T. Jung, *Boosting therapeutic potency of antibodies by taming Fc domain functions*. Exp Mol Med, 2019. **51**(11): p. 1-9.
157. Gutierrez, J.M., G. Leon, and B. Lomonte, *Pharmacokinetic-pharmacodynamic relationships of immunoglobulin therapy for envenomation*. Clin Pharmacokinet, 2003. **42**(8): p. 721-41.
158. Jayawardana, S., et al., *Chronic Musculoskeletal Disabilities following Snake Envenoming in Sri Lanka: A Population-Based Study*. PLoS Negl Trop Dis, 2016. **10**(11): p. e0005103.
159. Lewin, M.R., et al., *Varespladib in the Treatment of Snakebite Envenoming: Development History and Preclinical Evidence Supporting Advancement to Clinical Trials in Patients Bitten by Venomous Snakes*. Toxins (Basel), 2022. **14**(11).
160. Ikonomidou, C., *Matrix metalloproteinases and epileptogenesis*. Mol Cell Pediatr, 2014. **1**(1): p. 6.
161. Xie, C., et al., *Neutralizing Effects of Small Molecule Inhibitors and Metal Chelators on Coagulopathic Viperinae Snake Venom Toxins*. Biomedicines, 2020. **8**(9).
162. Albulescu, L.O., et al., *A therapeutic combination of two small molecule toxin inhibitors provides broad preclinical efficacy against viper snakebite*. Nat Commun, 2020. **11**(1): p. 6094.



163. Laustsen, A.H., et al., *In Vivo Neutralization of Myotoxin II, a Phospholipase A(2) Homologue from Bothrops asper Venom, Using Peptides Discovered via Phage Display Technology*. ACS Omega, 2022. **7**(18): p. 15561-15569.
164. Singh, P., et al., *A Review on Venom Enzymes Neutralizing Ability of Secondary Metabolites from Medicinal Plants*. J Pharmacopuncture, 2017. **20**(3): p. 173-178.
165. Winer, A., S. Adams, and P. Mignatti, *Matrix Metalloproteinase Inhibitors in Cancer Therapy: Turning Past Failures Into Future Successes*. Mol Cancer Ther, 2018. **17**(6): p. 1147-1155.
166. Zinenko, O., I. Tovstukha, and Y. Korniyenko, *PLA(2) Inhibitor Varespladib as an Alternative to the Antivenom Treatment for Bites from Nikolsky's Viper Viper a berus nikolskii*. Toxins (Basel), 2020. **12**(6).
167. Lomonte, B. and J.M. Gutierrez, *Phospholipases A2 from viperidae snake venoms: how do they induce skeletal muscle damage?* Acta Chim Slov, 2011. **58**(4): p. 647-59.
168. Nguyen, J.H., et al., *The Microenvironment Is a Critical Regulator of Muscle Stem Cell Activation and Proliferation*. Front Cell Dev Biol, 2019. **7**: p. 254.
169. Kolios, G. and Y. Moodley, *Introduction to stem cells and regenerative medicine*. Respiration, 2013. **85**(1): p. 3-10.
170. Watt, F.M. and B.L. Hogan, *Out of Eden: stem cells and their niches*. Science, 2000. **287**(5457): p. 1427-30.
171. Vizoso, F.J., et al., *Mesenchymal Stem Cell Secretome: Toward Cell-Free Therapeutic Strategies in Regenerative Medicine*. Int J Mol Sci, 2017. **18**(9).
172. Baraniak, P.R. and T.C. McDevitt, *Stem cell paracrine actions and tissue regeneration*. Regenerative medicine, 2010. **5**(1): p. 121-143.
173. Daneshmandi, L., et al., *Emergence of the Stem Cell Secretome in Regenerative Engineering*. Trends Biotechnol, 2020. **38**(12): p. 1373-1384.
174. Gnecci, M., et al., *Evidence supporting paracrine hypothesis for Akt-modified mesenchymal stem cell-mediated cardiac protection and functional improvement*. FASEB J, 2006. **20**(6): p. 661-9.
175. Markel, T.A., et al., *VEGF is critical for stem cell-mediated cardioprotection and a crucial paracrine factor for defining the age threshold in adult and neonatal stem cell function*. Am J Physiol Heart Circ Physiol, 2008. **295**(6): p. H2308-14.
176. Lang, F.M., et al., *Mesenchymal stem cells as natural biofactories for exosomes carrying miR-124a in the treatment of gliomas*. Neuro Oncol, 2018. **20**(3): p. 380-390.
177. Goolaerts, A., et al., *Conditioned media from mesenchymal stromal cells restore sodium transport and preserve epithelial permeability in an in vitro model of acute alveolar injury*. Am J Physiol Lung Cell Mol Physiol, 2014. **306**(11): p. L975-85.
178. Madaro, L., et al., *Denervation-activated STAT3-IL-6 signalling in fibro-adipogenic progenitors promotes myofibres atrophy and fibrosis*. Nat Cell Biol, 2018. **20**(8): p. 917-927.

179. Keating, A., *Mesenchymal stromal cells: new directions*. Cell Stem Cell, 2012. **10**(6): p. 709-716.
180. Caplan, A.I., *Adult mesenchymal stem cells for tissue engineering versus regenerative medicine*. J Cell Physiol, 2007. **213**(2): p. 341-7.
181. Drago, D., et al., *The stem cell secretome and its role in brain repair*. Biochimie, 2013. **95**(12): p. 2271-85.
182. Kim, J., et al., *Stem cell recruitment factors secreted from cord blood-derived stem cells that are not secreted from mature endothelial cells enhance wound healing*. In Vitro Cell Dev Biol Anim, 2014. **50**(2): p. 146-54.
183. Cargnoni, A., et al., *Conditioned medium from amniotic mesenchymal tissue cells reduces progression of bleomycin-induced lung fibrosis*. Cytotherapy, 2012. **14**(2): p. 153-61.
184. Heo, S.C., et al., *Tumor necrosis factor-alpha-activated human adipose tissue-derived mesenchymal stem cells accelerate cutaneous wound healing through paracrine mechanisms*. J Invest Dermatol, 2011. **131**(7): p. 1559-67.
185. Lee, M.J., et al., *Proteomic analysis of tumor necrosis factor-alpha-induced secretome of human adipose tissue-derived mesenchymal stem cells*. J Proteome Res, 2010. **9**(4): p. 1754-62.
186. Head, S.I., et al., *Properties of regenerated mouse extensor digitorum longus muscle following notexin injury*. Exp Physiol, 2014. **99**(4): p. 664-74.
187. Pistilli, E.E., et al., *Targeting the activin type IIB receptor to improve muscle mass and function in the mdx mouse model of Duchenne muscular dystrophy*. Am J Pathol, 2011. **178**(3): p. 1287-97.
188. Cadena, S.M., et al., *Administration of a soluble activin type IIB receptor promotes skeletal muscle growth independent of fiber type*. J Appl Physiol (1985), 2010. **109**(3): p. 635-42.
189. Chan, Y.S., et al., *The use of suramin, an antifibrotic agent, to improve muscle recovery after strain injury*. Am J Sports Med, 2005. **33**(1): p. 43-51.
190. Nozaki, M., et al., *Improved muscle healing after contusion injury by the inhibitory effect of suramin on myostatin, a negative regulator of muscle growth*. Am J Sports Med, 2008. **36**(12): p. 2354-62.
191. Lemos, D.R., et al., *Nilotinib reduces muscle fibrosis in chronic muscle injury by promoting TNF-mediated apoptosis of fibro/adipogenic progenitors*. Nat Med, 2015. **21**(7): p. 786-94.
192. Senji Laxme, R.R., et al., *Biogeographic venom variation in Russell's viper (Daboia russelii) and the preclinical inefficacy of antivenom therapy in snakebite hotspots*. PLoS Negl Trop Dis, 2021. **15**(3): p. e0009247.



## 2. Experimental Chapters

## **2.1 Impact of small molecule inhibitors on the attenuation of venom-induced muscle damage**

### **Authors**

Medha Sonavane<sup>1</sup>, Ali Alqallaf<sup>2,3</sup>, Robert D. Mitchel<sup>4</sup>, Matthew R. Lewin<sup>5</sup>, Ketan Patel<sup>2\*</sup>, and Sakthivel Vaiyapuri<sup>1\*</sup>

<sup>1</sup>School of Pharmacy, University of Reading, Reading, RG6 6UB, United Kingdom

<sup>2</sup>School of Biological Sciences, University of Reading, Reading, RG6 6UB, United Kingdom

<sup>3</sup>Medical Services Authority, Ministry of Defence, Kuwait

<sup>4</sup>Micregen Ltd, Thames Valley Science Park, Reading, RG2 9LH, United Kingdom

<sup>5</sup>California Academy of Sciences, USA

\*Corresponding authors

*In preparation for publication*

### **Contribution to this chapter**

#### **Experimental contribution**

- Study design
- Animal work: dosing, dissections
- Tissue preparation: Muscle blocking, cryo-sectioning
- Staining and imaging- Staining muscle for histology and immunohistochemistry using various antibodies, imaging the sections

#### **General contribution**

- Data collection and analysis
- Preparing original figures
- Writing original manuscript

## Abstract

Skeletal muscle damage is a severe complication arising due to snakebite envenoming (SBE). Currently, the only available treatment for SBE is antivenom produced against regionally specific venomous snakes. While the antivenoms are helpful in neutralising the systemic effects of venom toxins, they cannot prevent/treat local muscle damage as they are unable to penetrate through the damaged tissues and blocked blood vessels/capillaries. In the absence of any specific treatment, the muscle damage is often treated by surgical procedures, such as debridement and fasciotomy and, in worse cases, amputation. Therefore, there is an urgent need to develop novel treatment strategies for snake venom-induced muscle damage. Recently, small molecule inhibitors have been effectively assessed for the systemic neutralisation of specific venom toxins, including metalloproteases and phospholipase A<sub>2</sub>. In this study, we used marimastat and varespladib as metalloprotease and phospholipase A<sub>2</sub> inhibitors, respectively, to determine their efficacy in attenuating *Crotalus atrox* (*C. atrox*) venom-induced muscle damage in mice. We have studied the effect of these molecules on inflammatory responses, muscle regeneration, extracellular matrix synthesis, and remodelling of the damaged muscle. Our findings suggest that both marimastat and varespladib can effectively neutralise metalloproteases and phospholipase A<sub>2</sub>, respectively, under *in vivo* settings, and they promote muscle regeneration by reducing fibrotic tissues and inducing the reconstruction and remodelling of the extracellular matrix. Therefore, they can act as potential therapeutic candidates to treat/prevent SBE-induced muscle damage in human patients.

## 1. Introduction

Snakebite envenoming (SBE) is a life-threatening condition that primarily affects impoverished communities worldwide. The only treatment available for SBE is the antivenom produced against regionally specific, medically important venomous snakes. While antivenoms effectively neutralise circulating venom toxins, they are proven to be ineffective in treating local tissue damage induced by SBE, one of the most severe repercussions of SBE [1]. Due to the lack of any specific therapy, venom-induced muscle damage is often tackled by surgical approaches such as tissue debridement, fasciotomy, and, in extreme cases, amputation [2]. These methods fundamentally involve the removal of the affected tissues and not recovering the damaged muscle,

resulting in permanent disabilities. Annually, around 400,000 people suffer from permanent disabilities following SBE [1]. Adjusting back to life with physical disabilities after SBE affects the victims' well-being and socioeconomic status [3]. Moreover, SBE-induced muscle damage mainly affects the most productive age group in rural communities and causes long-term health consequences and socioeconomic ramifications [4]. Hence, novel diagnostic and innovative treatment options that can help mitigate the severe damage caused by SBE are critically important [5].

The class of snakes most likely to cause permanent tissue damage are vipers - medically important snakes distributed widely across Asia, Africa, Latin America, and Oceania [6]. While the venoms of some elapid snakes are responsible for inducing muscle damage, elapid-induced muscle damage is often self-resolved and does not turn into permanent muscle damage. On the contrary, viper envenoming is predominantly associated with permanent tissue damage. Viper venom primarily consists of metalloproteases (SVMPs), phospholipase A<sub>2</sub> (PLA<sub>2</sub>), serine proteases and other toxins. SVMPs and PLA<sub>2</sub> form roughly ~60% of the venom proteins in several viper snakes [7]. SVMPs are zinc metalloproteases divided into four classes, PI, PII, PIII and PIV, depending on their structural domains and molecular weights [8]. PLA<sub>2</sub>s are smaller molecular weight Ca<sup>2+</sup>-dependent proteins, with a catalytic activity to hydrolyse cell membranes [9]. These two toxin families cause muscle damage and impairment to muscle regeneration by inducing myotoxicity, necrosis, and degradation of the extracellular matrix (ECM), affecting blood capillaries and angiogenesis [10]. A previous study from our laboratory shows that the PIII SVMPs stay active in the damaged tissue for a long time after initial administration [11].

Small molecule inhibitors against specific toxins such as metalloproteases and PLA<sub>2</sub> have recently gained much attention in direct inhibition and attenuation of venom effects [12, 13]. For example, marimastat is a broad-spectrum matrix metalloproteinase inhibitor that has been demonstrated to inhibit SVMPs from several species. Similarly, varespladib is a potent PLA<sub>2</sub> inhibitor that has proven effective in neutralising venom PLA<sub>2</sub>s from many species. Intravenous administrations of these inhibitors neutralise the systemic effects of venom toxins *in vivo* settings [14-16]. Most studies so far have explored the systemic effects of these molecules, whereas we have

tested their effects on local tissue damage. In this study, we used *C. atrox* venom which comprises ~ 50% of SVMPs and 7.9% of PLA<sub>2</sub> [17]. The victims suffering from *C. atrox* envenomation show myotoxic and haemotoxic symptoms. We hypothesised that neutralising the SVMPs and PLA<sub>2</sub>s in this model viper venom could prevent venom-induced muscle damage and promote innate muscle regeneration. Hence, in this study, we focused on neutralising SVMPs and PLA<sub>2</sub> in *C. atrox* venom using varespladib and marimastat and determining their effects on venom-induced muscle damage.

## **2. Material and Methods**

### *2.1 Materials used*

Lyophilised *C. atrox* venom, marimastat, and varespladib were purchased from Sigma Aldrich (UK). Unless otherwise stated, all other chemicals were obtained from Sigma Aldrich, UK.

### *2.2 Enzymatic assays*

The metalloprotease (MP) activity of *C. atrox* venom was assessed using DQ-gelatin (ThermoFisher Scientific, UK), a fluorogenic substrate for collagenolytic enzymes. Different venom concentrations were mixed with phosphate buffer saline (PBS) and 2 µg DQ gelatin in a 100 µL total reaction volume. The reaction mix was incubated at 37°C, and the level of fluorescence was measured at various time points using a spectrofluorometer (FLUOstar OPTIMA, Germany) at an excitation wavelength of 485 nm and emission wavelength of 520 nm.

Similarly, the PLA<sub>2</sub> activity of the venom was assessed using an EnzChek™ Phospholipase A<sub>2</sub> assay kit. The level of fluorescence was measured at different time points with an excitation wavelength of 460 nm and an emission wavelength of 515 nm by spectrofluorimetry.

### *2.3 Administration of C. atrox venom into the tibialis anterior (TA) muscle of mice*

All the procedures on the experimental mice were performed in line with the principles and guidelines approved by the British Home Office and the Animals (Scientific Procedures) Act 1986. The study protocols were also approved by the University of Reading Ethics Committee. The C57BL/6 (8-12 weeks old) mice were obtained from Charles Rivers, UK. The mice were assigned into four cohorts: a) CA (venom only) group with no inhibitors, ii) CA with marimastat, iii) CA with varespladib and iv) CA with a combination of marimastat and varespladib. The mice were



anaesthetised using 3.5% (v/v) isoflurane in oxygen. *C. atrox* venom was dissolved in sterile PBS and injected intramuscularly into their right TA muscle (30  $\mu$ L of total volume injected) at the dose of 5  $\mu$ g/20 g animal weight ( 0.25  $\mu$ g/ g which is  $\sim$  10 times less than LD<sub>50</sub>) . This dose was selected based on the metalloprotease activity of this venom as analysed above. The inhibitors were injected (4 mg/kg) intraperitoneally, with the first dose given one hour after venom injection followed by further injections every 24 hours until the muscle was dissected. The mice were sacrificed using carbon dioxide on day 5 or 10 after the venom injection to collect tissues for further analysis. The blood samples were collected by cardiac puncture with ethylenediamine tetraacetic acid (EDTA) as an anticoagulant. The TA muscles were dissected, weighed, and frozen using liquid nitrogen-cooled isopentane and then stored at -80° C until further use.

The IC<sub>50</sub> of inhibitors was calculated by using constant venom concentration against serial dilution of inhibitors. The graph and IC<sub>50</sub> values were generated using GraphPad Prism 8.

#### *2.4 Histological examination*

The frozen TA muscles were mounted using the Tissue-TEK<sup>®</sup> OCT compound, and sections of 13  $\mu$ m thickness were obtained using cryo-microtome to examine the internal structures of the muscle. The muscle sections were then subjected to histological examination using haematoxylin and eosin (H&E) staining. Briefly, the slides were submerged in PBS to wash away the OCT. Next, slides were treated with Harris haematoxylin stain for 2 minutes and then rinsed under running tap water. Slides were then dipped twice in acidic alcohol [70% (v/v) ethanol and 0.1% (v/v) HCl] and rinsed with running tap water. Tissues were then stained with 1% (w/v) eosin, followed by gradual dehydration steps using 70%, 90% and 100% ethanol. As a last step, slides were treated with Xylene and mounted using Distyrene Plasticiser Xylene (DPX) mounting media. Sections were imaged using an Axioscope Epifluorescent microscope. The size of regenerated fibres was calculated by taking the area of 50 fibres that displayed centrally located nuclei from each section using ImageJ (version 1.52a) and were then averaged.

The distribution of collagen and tissue fibrosis was analysed using picrosirius red staining. The staining was performed according to the manufacturer's instructions (Abcam, UK). Slides were immersed in Bouin solution and incubated for 15 minutes at 56° C in a water bath. Then, the slides

were washed with distilled water for 15 minutes and then immersed in a picosirius red stain jar for 1 hour in the dark, followed by dipping the slides twice in acidified water [0.5 % (v/v) glacial acetic acid) in two separate jars. The muscle sections were dehydrated with 100% ethanol three times for 5 minutes. Lastly, the slides were cleaned by immersing them in Xylene for 5 minutes. Slides were mounted in the DPX mounting media and kept in a fume cupboard for drying. Sections were imaged using an Axioscope Epifluorescent microscope. The level of fibrosis was calculated using threshold analysis. A set area (200  $\mu\text{m}^2$ ) was selected from the undamaged muscle and a baseline was set using the ImageJ threshold analysis tool. This value was compared to that from a 200  $\mu\text{m}^2$  area of a damaged muscle region to give a relative value (%) of picosirius red coverage.

### 2.5 Immunohistochemistry

The tissue sections were incubated in a permeabilisation buffer [20 mM HEPES, 3 mM  $\text{MgCl}_2$ , 50 mM NaCl, 0.05% (w/v) sodium azide, 300 mM sucrose and 0.5% (v/v) Triton X-100] for 15 minutes, then washed three times with PBS. Slides were then incubated in a blocking buffer [PBS with 5% (v/v) foetal bovine serum and 0.05% (v/v) Triton X-100] for 30 minutes at room temperature. Primary antibodies were prepared in washing buffer (1:200), and then sections were incubated with the primary antibodies overnight at 4°C. The unbound primary antibodies were washed with wash buffer and then incubated with secondary antibodies (1:200) prepared in blocking buffer for 1 hour in the dark, at room temperature. Slides were mounted using a fluorescent mounting medium (Dako, UK) with 4,6-diamidino-2-phenylindole (DAPI) to visualise myonuclei. Tissue images were obtained using a Zeiss AxioImager-fluorescence microscope. All the images were analysed for different markers using ImageJ. In addition, automated ImageJ plug-ins were used to perform threshold and whole-section analyses. The size of IgG infiltrated, or MYHIII-expressing fibres was determined by measuring the area of 30 fibres from each section of each animal. The thickness of collagen IV, laminin, and dystrophin was measured and compared with thickness of the undamaged muscle fibres. 30 fibres with centrally located nuclei from the damaged region of one section of each animal were measured using ImageJ. The intramuscular bleeding and presence of venom in tissues were calculated using threshold analysis in sections stained for fibrinogen and anti-*C. atrox* antibodies.

An area of 200  $\mu\text{m}^2$  section was selected from the damaged region of the muscles and compared to baseline threshold value from undamaged muscle.

## 2.6 Cytokine analysis

A range of cytokines and chemokines was analysed in serum samples collected on day 5 using Multiplex 44 assay at EVE Technologies, Canada.

## Statistical analysis

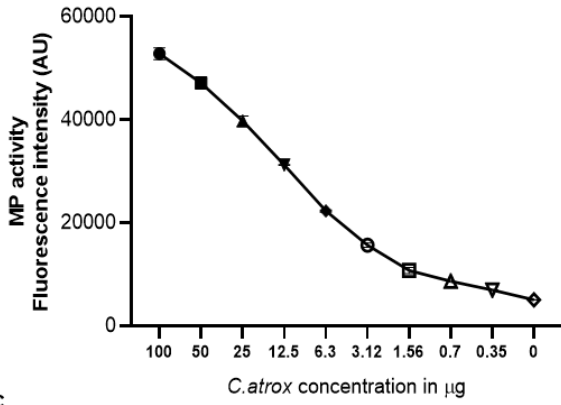
All statistical analyses were performed using GraphPad Prism 8, and P-values were calculated using one-way ANOVA followed by Tukey's multiple comparison test.

## 3. Results

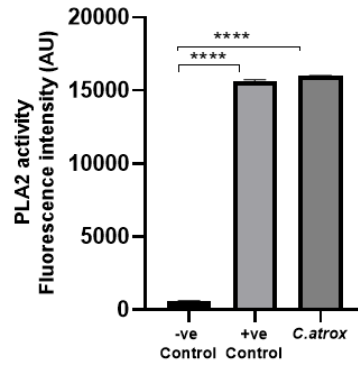
### 3.1 *C. atrox* venom displays both MP and PLA<sub>2</sub> activities

Appropriate fluorogenic enzyme assays confirmed that *C. atrox* venom displayed a significant level of SVMP (**Figure 1A**) and PLA<sub>2</sub> (**Figure 1B**) activities. Marimastat reduced the metalloprotease activity of *C. atrox* venom with concentrations from 0.78 – 100  $\mu\text{M}$  (**Figure 1C**). Similarly, varespladib showed a dose-dependent decrease in PLA<sub>2</sub> activity of *C. atrox* venom (**Figure 1D**). The IC<sub>50</sub> values of these inhibitors were calculated as 0.75  $\mu\text{M}$  for marimastat (**Figure 1E**) and 1.5  $\mu\text{M}$  for varespladib (**Figure 1F**). When these inhibitors were tested together (with the IC<sub>50</sub> concentration of each inhibitor with a dose-response of another inhibitor), they did not show any synergistic effects (**Figure 1G & 1H**). These results confirm that *C. atrox* venom displays high levels of MP and PLA<sub>2</sub> activities that are sensitive to inhibition by marimastat and varespladib, respectively.

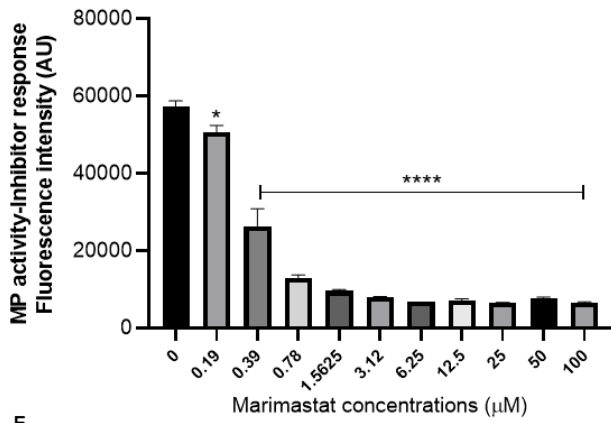
A



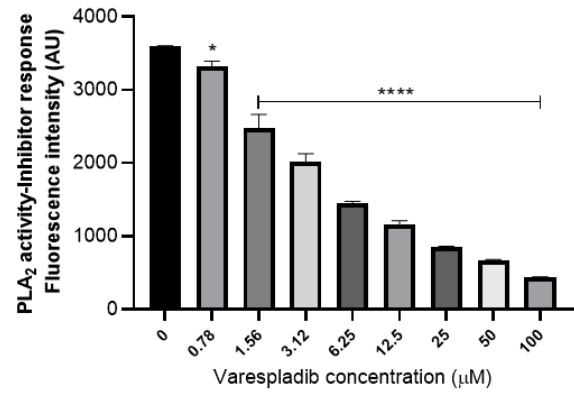
B



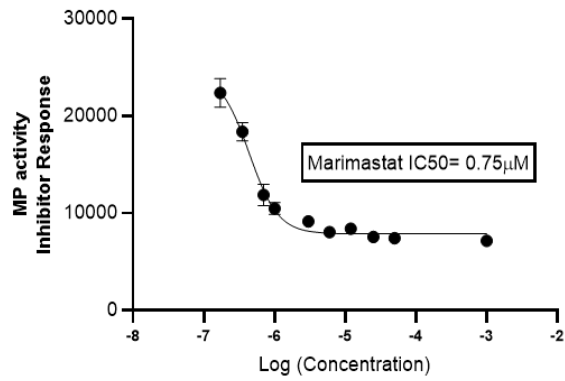
C



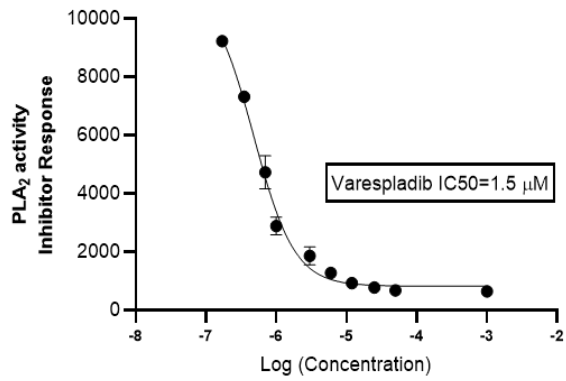
D



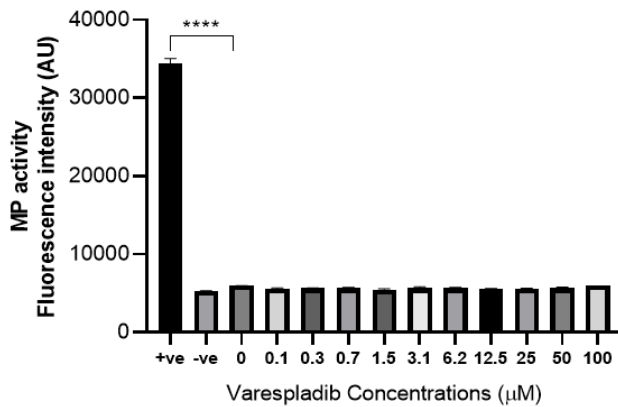
E



F



G



H

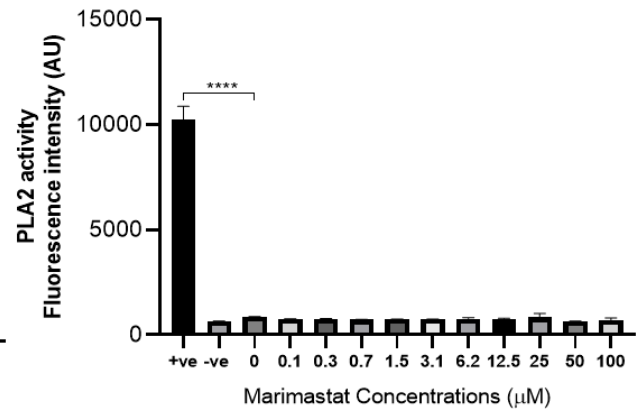


**Figure 1. Metalloprotease and PLA<sub>2</sub> activities of *C. atrox* venom.** **A)** Concentration-dependent metalloprotease activity of *C. atrox* venom. **B)** PLA<sub>2</sub> activity of *C. atrox* venom 5 µg/ 100µL reaction volume (50µg/mL). Inhibitory effects of various concentrations of marimastat on the metalloprotease activity of 50µg/mL *C. atrox* venom. **D)** Inhibitory effects of varespladib on PLA<sub>2</sub> activity of 5 µg/mL *C. atrox* venom. **E)** IC<sub>50</sub> concentration of marimastat for inhibiting PLA<sub>2</sub> activity. **F)** IC<sub>50</sub> concentration of varespladib. **G)** The synergetic effect with varied concentrations of varespladib against marimastat IC<sub>50</sub>. **H)** The synergetic effect with varied concentrations of marimastat against varespladib IC<sub>50</sub>. (+ve is positive control. -ve is negative control). The *p* values are calculated by one-way ANOVA multiple comparison followed by Tukey's post hoc test using GraphPad Prism (\*\**p*<0.01 and \*\*\**p*<0.001, \*\*\*\**p*<0.0001) . In figure B, C, and D the values are compared against -ve control. In G and H values are compared against +ve control. All the experiments performed in triplicates (n=3)

### 3.2 Marimastat and varespladib reduce muscle fibrosis and promote regeneration

We next determined whether marimastat and varespladib had any impact on *C. atrox* venom-induced muscle damage in mice. Mice were injected with either *C. atrox* venom alone (CA), *C. atrox* venom + marimastat (CA+M), *C. atrox* venom + varespladib (CA+V), or *C. atrox* venom, marimastat, and varespladib (CA+M/V). The contralateral muscle from CA was used as an undamaged muscle. On days 5 and 10 following the injection of venom, TA muscles were collected and processed for further analysis (**Figure 2A**). To examine if the effect of venom is contributing towards skeletal muscle loss, we examined the weight of the dissected TA muscles. While there was a weight loss in venom-treated muscle, there was no significant difference between the controls and any of the inhibitors-treated muscles on day 5 (**Figure 2B**). On day 10, there was no difference between the control and venom-treated muscles as well as with inhibitors (**Figure 2C**). These results suggest that *C. atrox* venom induces a slight muscle loss, which is not rescued by any of the inhibitors used.

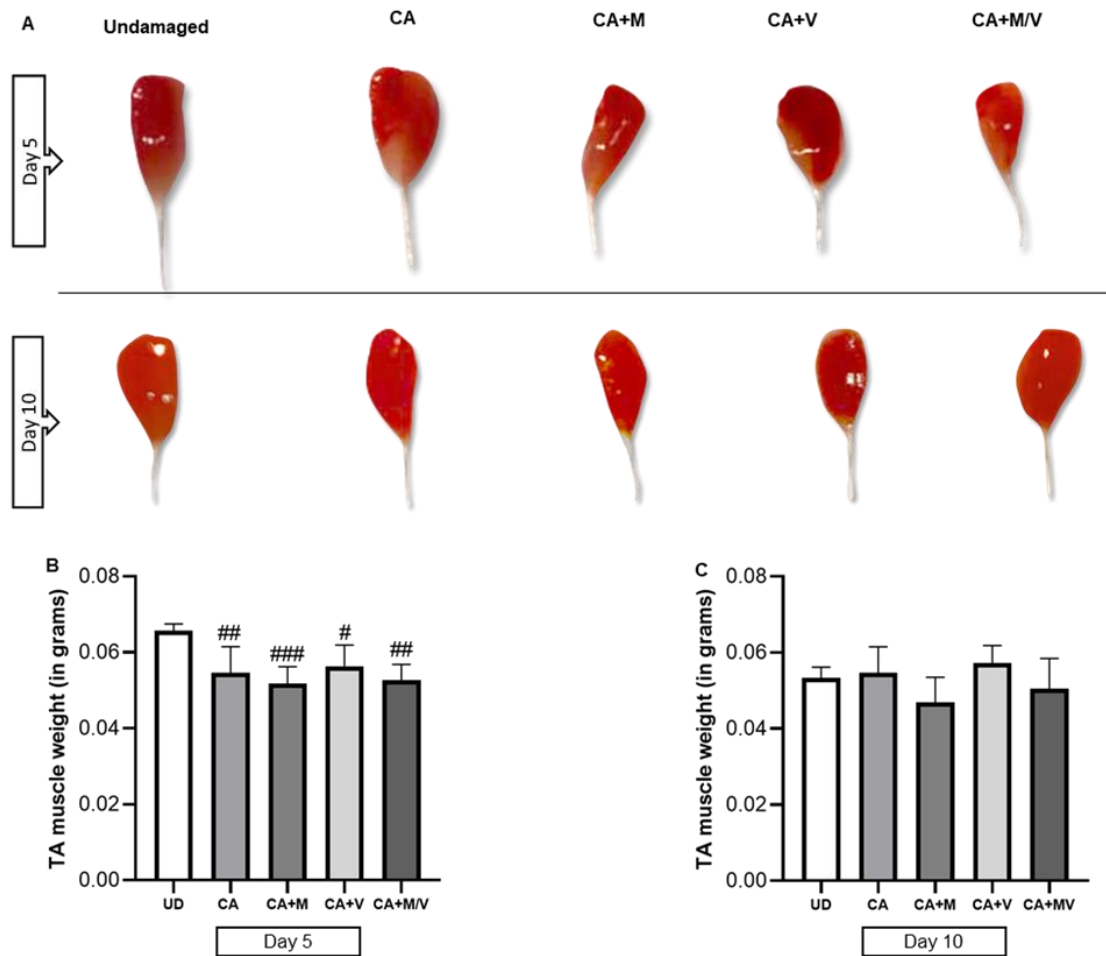


**Figure 2: Dissected TA muscles and their weight comparisons.** **A)** Dissected TA muscles at days 5 and 10 from different cohorts of mice treated with venom in the presence and absence of inhibitors. From Left to the right, negative control [Undamaged (UD)], venom-treated (CA), marimastat with venom (CA + M), varespladib with venom (CA + V), and a combination of these inhibitors with venom (CA + M/V). **B)** TA muscle weight comparison between the cohorts on day 5 and the undamaged muscle. **C)** TA muscle weight comparison between the cohorts on day 10 and the undamaged muscle. Data represent mean  $\pm$  S.D. ( $n=5$  mice in each cohort). The  $p$  values are calculated by one-way ANOVA followed by Tukey's post hoc test using GraphPad Prism (# $p < 0.05$  and ## $p < 0.01$  and ### $p < 0.001$ ). The values in B and C are compared with UD.

The muscle sections were then analysed using histological examinations such as H&E (**Figure 3A**) and picrosirius red (**Figure 3B**) staining. Centrally located nuclei (CLN) are indicative of regenerating fibres following damage. Therefore, we analysed the total area of the fibres with CLN in H&E-stained muscle sections. The area of regenerating fibres with CLN was greater in mice that were treated with the combination of marimastat and varespladib on day 5 (**Figure 3C**). The average increase in fibre size was around twofold compared to the venom-treated muscles. In contrast, mice

treated with individual drugs did not show a significant difference in fibre size compared to venom-treated muscles. On day 10, muscles treated with marimastat or varespladib individually displayed significantly larger fibres than venom-treated muscles, while their combination showed no increase in fibre size (**Figure 3E**). These data suggest that both marimastat and varespladib are beneficial in promoting muscle fibre size following venom-induced damage. The combination of these drugs promotes muscle fibre growth at an early stage whereas individual drugs are beneficial at later time points.

Fibrosis is known to attenuate muscle regeneration following damage. Picrosirius red staining was used to visualise the distribution of collagen and the formation of fibrotic tissues in muscle sections. The mice treated with varespladib alone and the combination of marimastat and varespladib showed significantly higher muscle fibrosis on day 5 than in venom-treated muscle on day 5 (**Figure 3D**). However, on day 10, marimastat largely reduced muscle fibrosis compared to the venom-treated muscles. Varespladib or its combination with marimastat had no effect on muscle fibrosis at day 10 (**Figure 3F**).

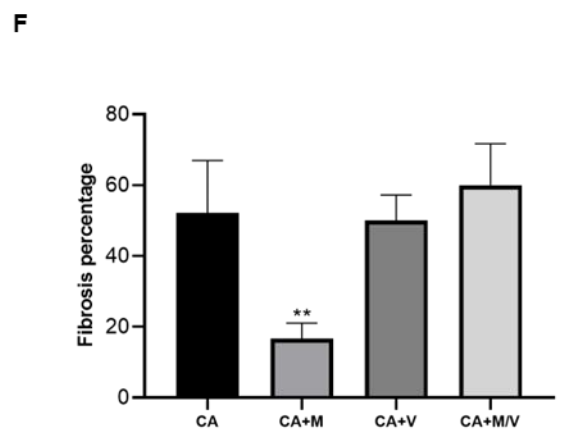
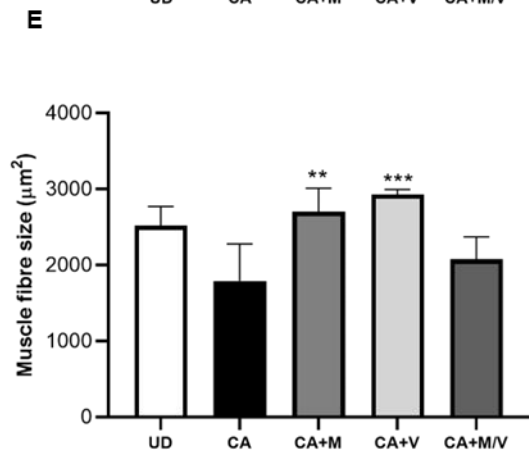
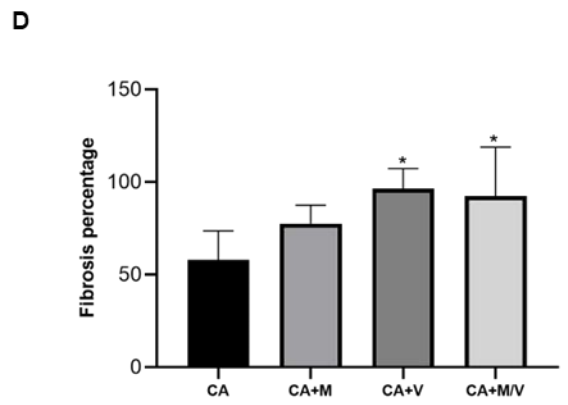
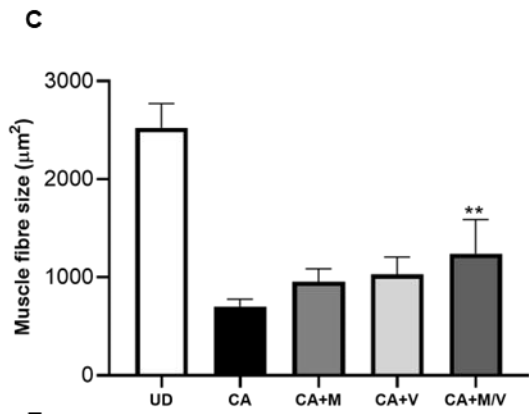
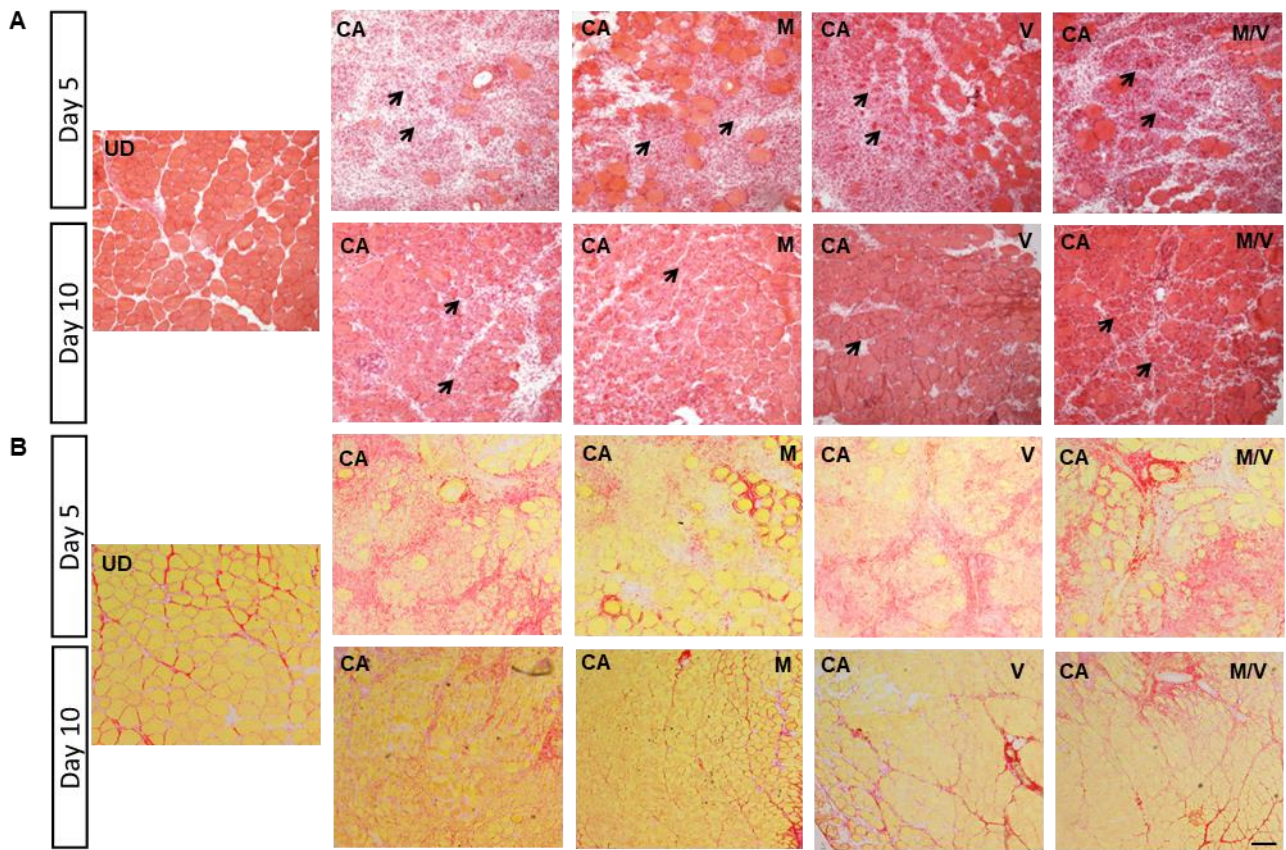




**Figure 3: H&E and picosirius red staining in the muscle sections.** **A)** H&E staining for TA muscles collected on days 5 and 10. The black arrows represent regenerating fibres. **B)** TA muscle sections collected on days 5 and 10 were stained using picosirius red to visualise fibrosis/scar tissue formation. Area measured for regenerating fibres with centrally located nuclei on days 5 (**C**) and 10 (**E**). Percentage of fibrotic tissues at day 5 (**D**) and 10 (**F**). Data represent mean  $\pm$  S.D. (n=5 mice in each cohort). The values in C, D, E, F compared with CA. The *p* values in are calculated by one-way ANOVA followed by Tukey's post hoc test using GraphPad Prism (\*\**p*<0.01 and \*\*\**p*<0.001). The UD bar in C and E is for the representation of undamaged muscle fibre and CA, CA+M, CA+V and CA+M/V are measurement of the cross-section area of regenerating fibres with CLN. The scale bar represents 100 $\mu$ M.

We also assessed the overall improvement of the damaged tissues by calculating the percentage of unhealthy tissues in the entire muscle section using a previously established protocol [18]. On day 5, all the muscles had a significantly higher percentage of unhealthy tissue (**Figure 4A-4D**). On day 10, the unhealthy tissue percentage decreased to an average of 20% across all cohorts (**Figure 4E**). This analysis indicates that even with inhibitors, the muscle damage was not entirely resolved by day 10.

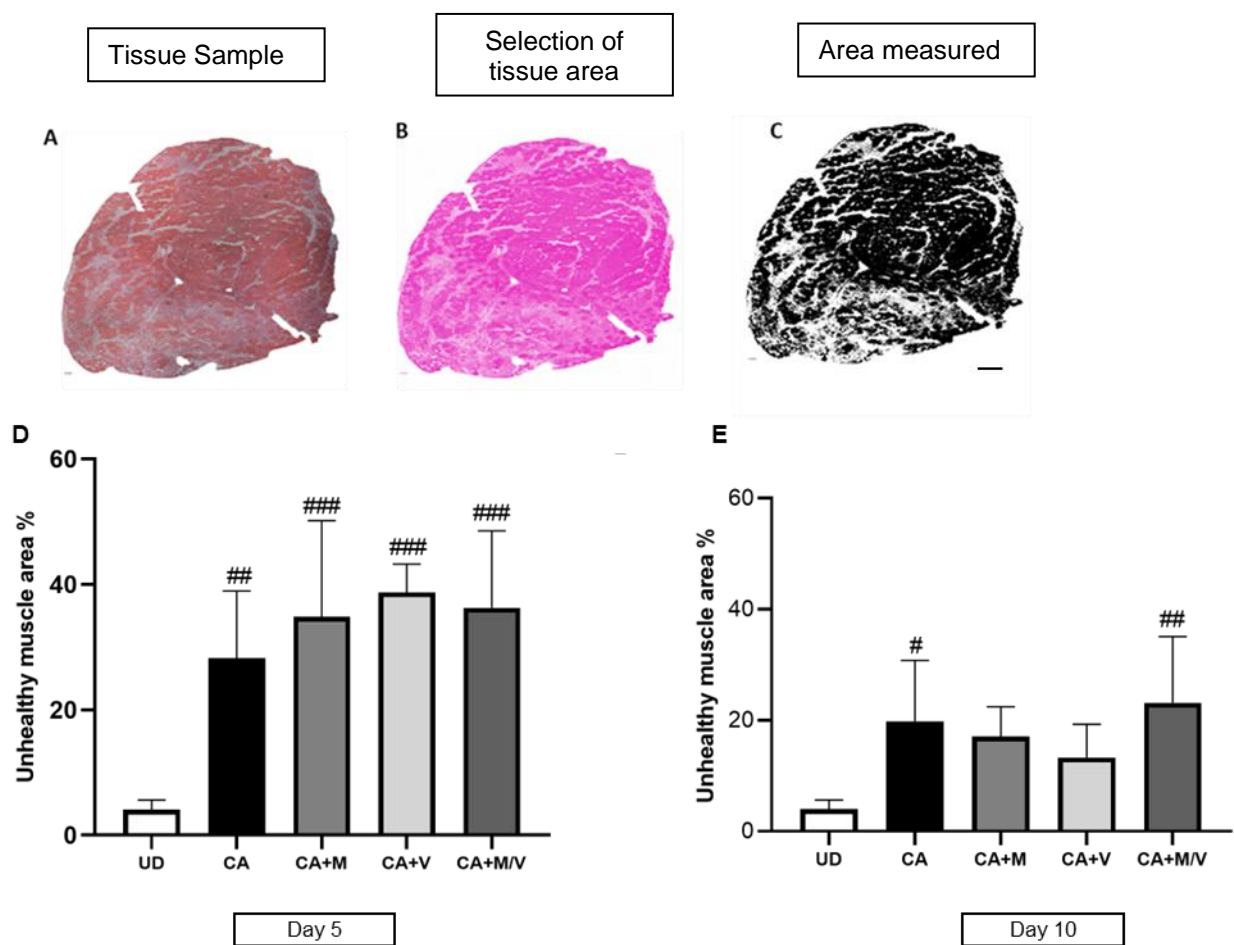


**Figure 4: Unhealthy tissue percentage and frequency distribution based on muscle size.** **A,B,C** Representative stages in the process of whole tissue analysis tissue analysis. Percentage of unhealthy tissue on days 5. A is the image of tissue to be analysed, B is the tissue image when applying the threshold parameters and C is the final stage where area counted after threshold analysis is highlighted in black. **(D)** and 10 Data represent mean  $\pm$  S.D. (n=5 mice in each cohort). The *p* values are calculated by One-way ANOVA followed by post hoc Tukey's test using GraphPad Prism (<sup>#</sup>*p*<0.05 and <sup>##</sup>*p*<0.01 and <sup>###</sup>*p*<0.001). Values in D and E are compared with UD and are represented #. The scale bar represents 100 $\mu$ M.

### 3.4 Marimastat and varespladib improve angiogenesis and reduce pathological effects in muscle

The effects of venom and the inhibitors on angiogenesis were analysed by staining muscle sections with CD31 antibodies (**Figure 5A**). The number of capillaries around damaged fibres was significantly reduced in venom-treated muscles (**Figure 5C**). Notably, the treatment with inhibitors did not improve the angiogenesis compared to the venom-treated muscles even on day 10 (**Figure 5E**). Furthermore, the presence of venom toxins in the damaged muscles was analysed by staining the sections with anti-*C. atrox* venom antibodies (**Figure 5B**). The mice treated with marimastat, and the combination of inhibitors displayed a large decrease in the presence of venom on day 5 (**Figure 5D**). By day 10, the venom was not present in any muscles including the venom-treated samples (**Figure 5F**).

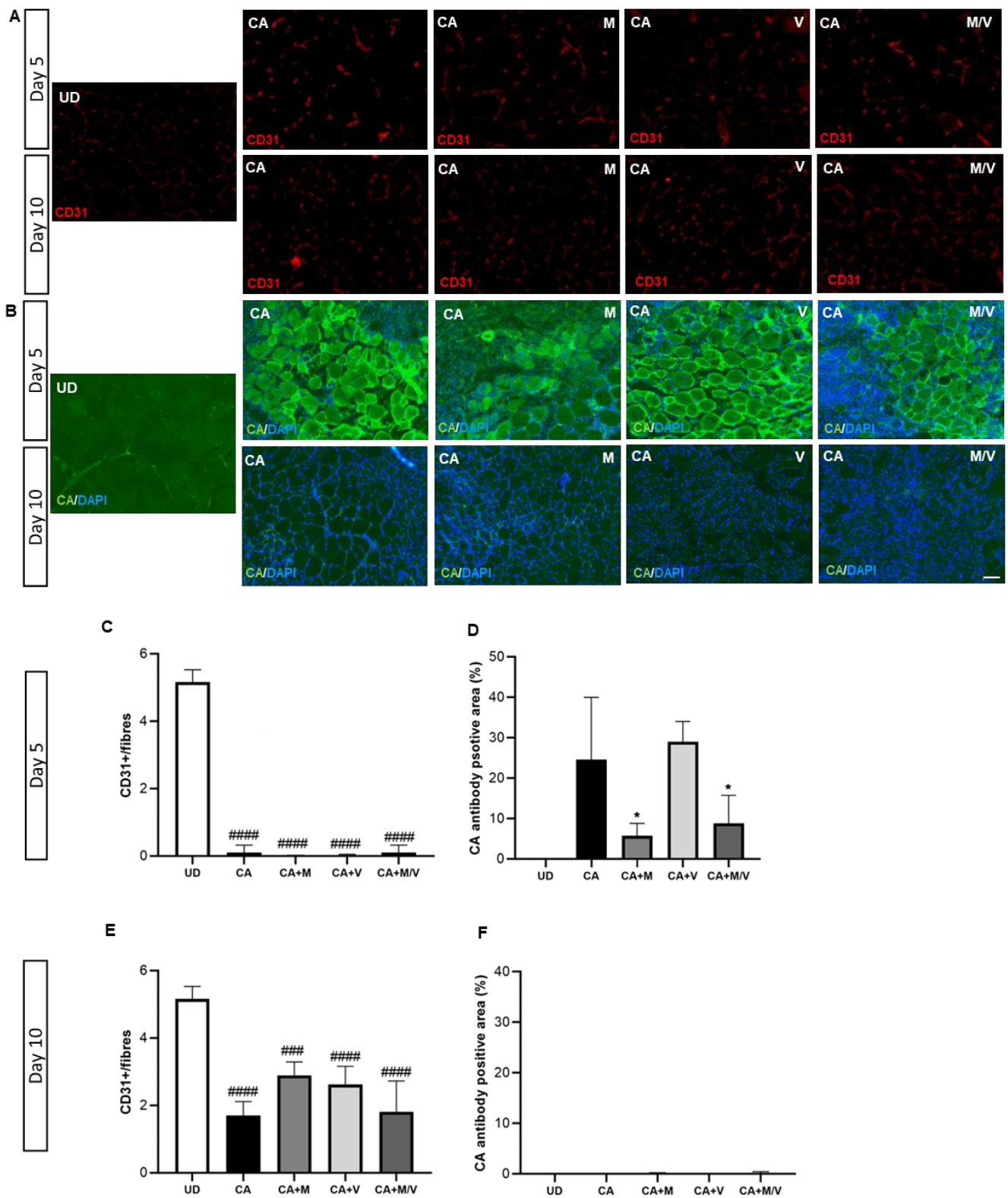


**Figure 5: Analysis of angiogenesis and venom presence.** A) TA muscle sections collected on days 5 and 10 were stained using CD31 antibodies. B) TA muscle sections were stained using CA antibodies to detect the presence of venom. The number of blood vessels was measured on muscle sections on days 5 (C) and 10 (E). The CA antibody-positive area was measured on days 5 (D) and 10 (F). The *p* values are calculated by One-way ANOVA followed by post hoc Tukey's test using

GraphPad Prism (\* $p < 0.05$ , \*\*\*\* $p < 0.0001$ ,  $n = 5$ ). The values in C and D are compared with UD. D and F values are compared with CA. The scale bar represents 100 $\mu$ M.

The damaged muscle fibres facilitate the infiltration of immunoglobulins into the affected regions. We therefore determined the presence of dying/necrotic fibres by analysing the amount of immunoglobulins in the affected muscle (**Figure 6A**). On day 5, treatment with marimastat or varespladib alone resulted in a significantly smaller necrotic area than venom-treated muscles (**Figure 6D**), although the combination of inhibitors showed no impact. On day 10, muscle from all cohorts showed the clearance of necrotic fibres (**Figure 6G**).

The presence of embryonic myosin heavy chain (MYHIII) indicates regenerating muscle fibres. Upon examination, the damaged muscle region showed regenerating fibres across all study groups (**Figure 6B**). The size of these newly formed fibres was measured to assess the advancement of muscle regeneration. On Day 5, treatment with marimastat or varespladib alone or in combination showed no increase in the size of the regenerating fibres compared to the venom-treated muscles (**Figure 6E**). However, on day 10, the area of regenerating fibres was significantly smaller in marimastat-treated muscles compared to the venom-treated ones although varespladib-treated muscle showed larger fibres (**Figure 6H**).

Viper venoms are known to induce intra-muscular bleeding. The presence of fibrinogen within the muscle sections indicates damage to the blood capillaries and subsequent bleeding. Therefore, the fibrinogen level was assessed in muscle sections using specific FITC-labelled anti-fibrinogen antibodies to determine venom-induced bleeding in muscle sections (**Figure 6C**). The results showed that marimastat-treated samples reduced the fibrinogen level compared to the venom-treated muscles (**Figure 6F**). In contrast, the varespladib and marimastat/varespladib combination did not reduce the fibrinogen level. On day 10, fibrinogen levels were reduced across all the cohorts (**Figure 6I**).

These results demonstrate that the inhibitors may attenuate several impacts caused by the venom and promote muscle regeneration.

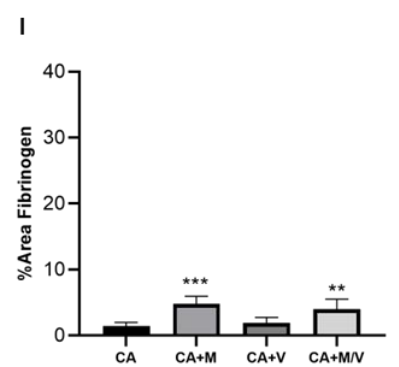
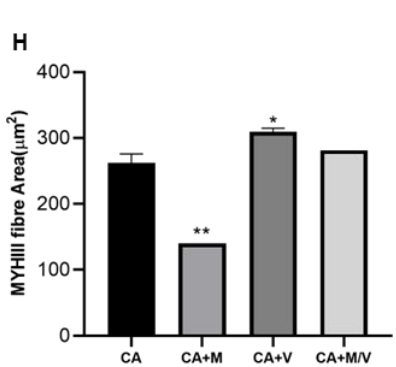
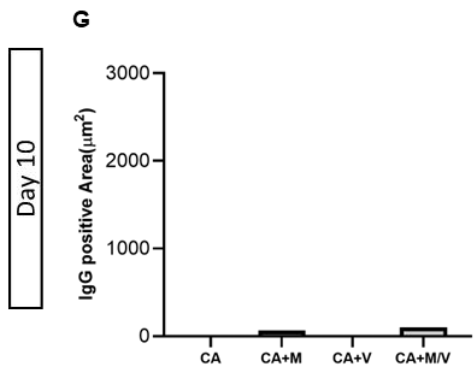
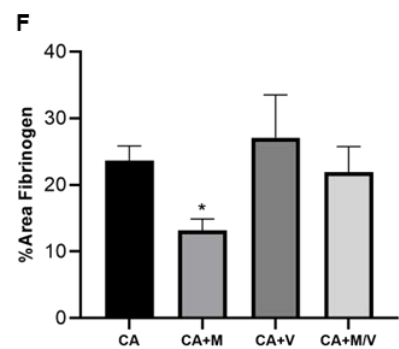
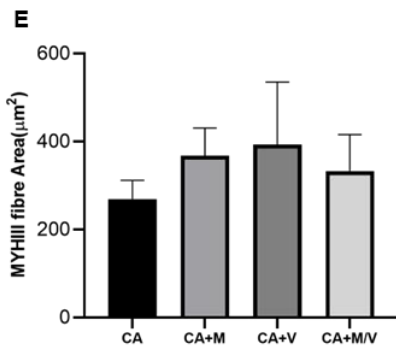
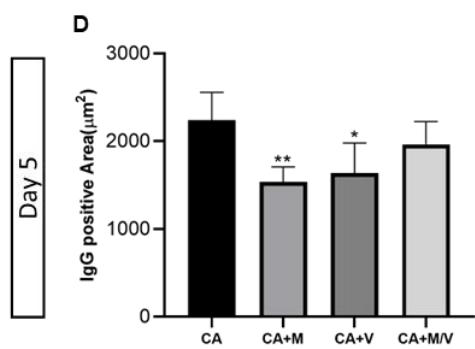
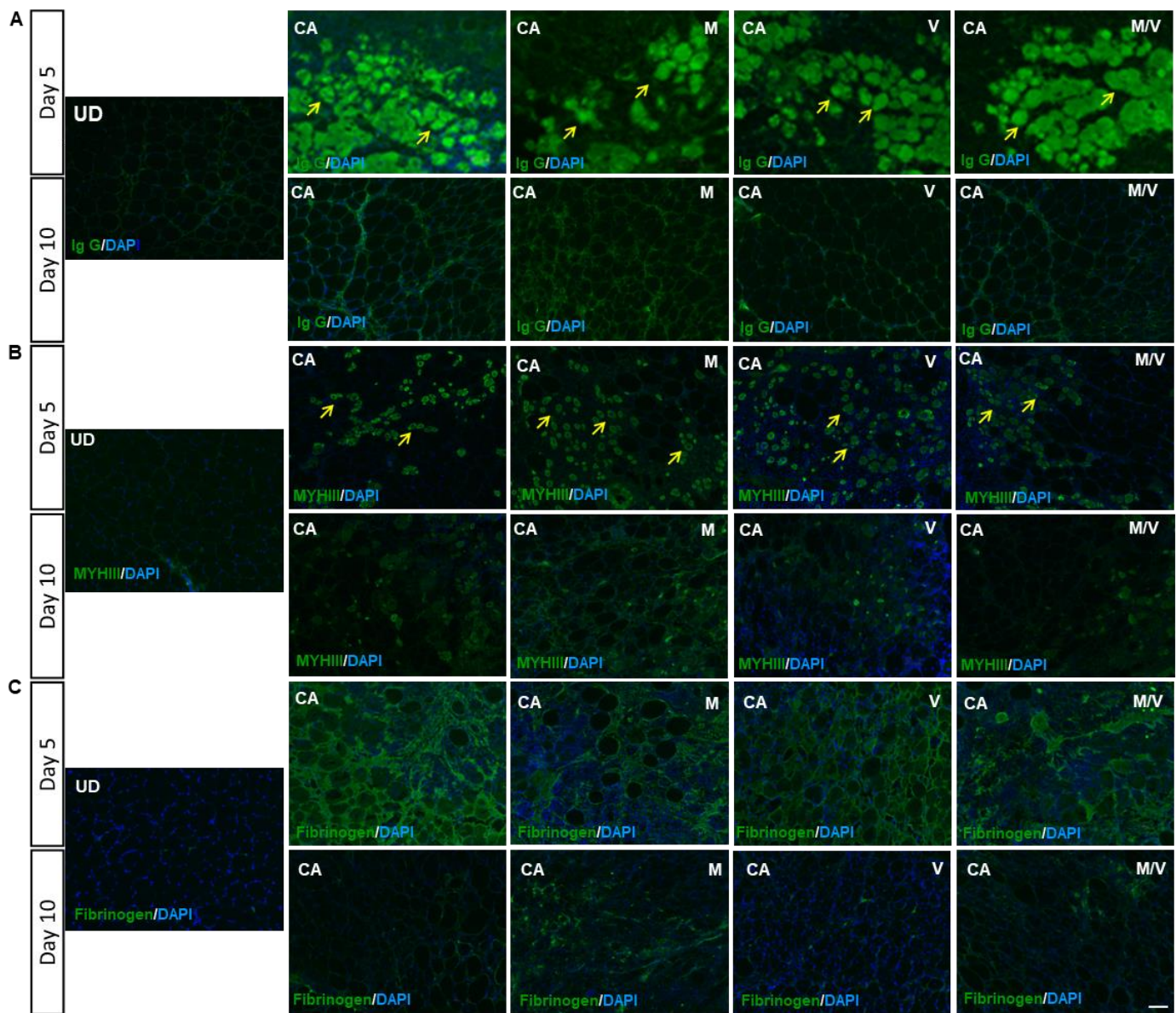


**Figure 6: Immunohistochemistry analysis of the muscle sections.** **A)** TA muscle sections collected on days 5 and 10 were stained using anti-mouse IgG antibodies. The arrows are pointing towards the necrotic fibres. **B)** Muscle sections were stained using MYHIII antibodies. The arrows shown in the figure represent newly regenerating fibres expressing MYHIII. **C)** Muscle sections were stained using anti-fibrinogen antibodies. Analysis of necrotic fibres on days 5 (**D**) and 10 (**G**). The area of the fibres expressing MYHIII on days 5 (**E**) and 10 (**H**). Area of percentage for intramuscular bleeding at days 5 (**F**) and 10 (**I**). The *p* values are calculated by One-way ANOVA followed by post hoc Tukey's test using GraphPad Prism (\**p*<0.05,\*\**p*<0.01 *n*=5). Values represented in D, E, F, G, H, I are compared with CA. The scale bar represents 100µM.

### *3.5 Marimastat and varespladib promote the reconstruction of the ECM in damaged muscle*

The *C. atrox* venom is rich in SVMPs, and the ECM is reported to be the main target for them. Reconstruction of the ECM is one of the critical elements in the progression of muscle regeneration. To determine the impact of venom and the inhibitors on the ECM in damaged muscle, collagen IV (**Figure 7A**), dystrophin (**Figure 7B**) and laminin (**Figure 7C**) was analysed as important ECM components in muscle sections. The thickness of the ECM structures directly reflects the maturity of the ECM. For example, thicker structures indicate immature ECM and its ongoing synthesis, whereas thinner and well-aligned ECM indicates mature ECM. On day 5, mice treated with marimastat or varespladib or in combination showed collagen IV structure that is similar to the undamaged muscles although venom-treated muscle showed thicker collagen (**Figure 7D**). Therefore, marimastat and varespladib positively impacted the reconstruction of collagen IV. Similarly, on day 5, dystrophin was significantly thicker in muscles treated with marimastat or varespladib alone or in combination (**Figure 7E**), and no regenerating fibres showed the presence of dystrophin in venom-treated muscles. The combination of drugs showed close structural thickness of dystrophin to the undamaged muscles, indicating their structural maturity. Similar results were obtained with laminin on day 5, i.e., the inhibitors-treated muscles showed similar laminin structures to the undamaged muscles (**Figure 7F**).

On day 10, there was no significant difference between any cohorts for collagen (**Figure 7G**). However, dystrophin structures in venom-treated muscles are still thicker than the undamaged muscles although the inhibitors largely reduced its thickness (**Figure 7H**). On day 10, laminin thickness measured for all experiment cohorts showed thinner laminin than undamaged laminin (**Figure 7I**).

These data suggest that the inhibitors either alone or in combination displayed a positive effect on the regeneration of the ECM components.

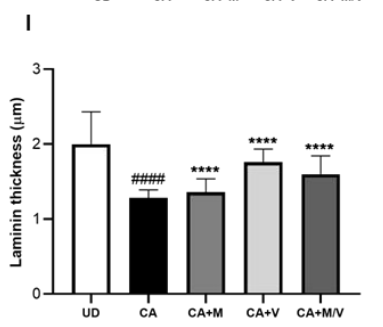
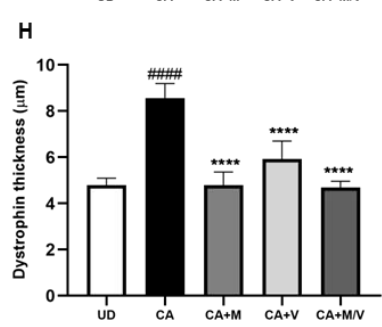
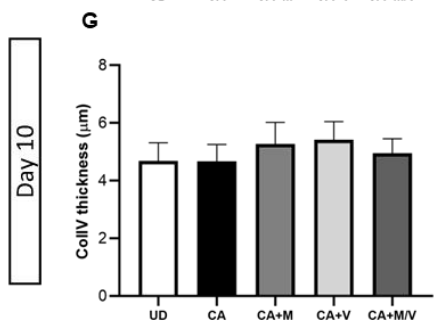
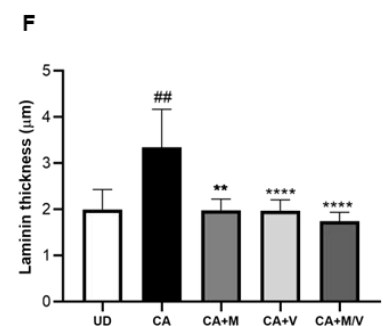
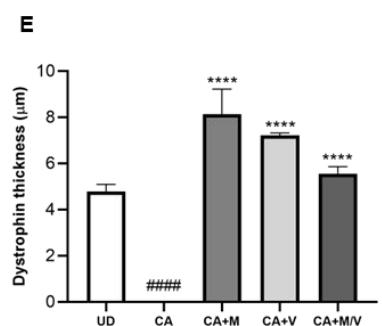
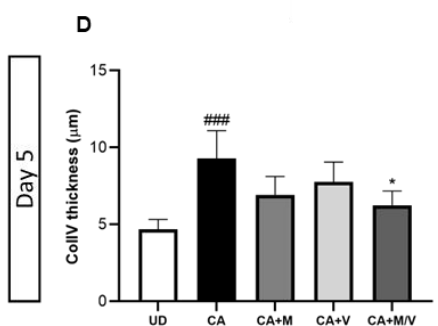
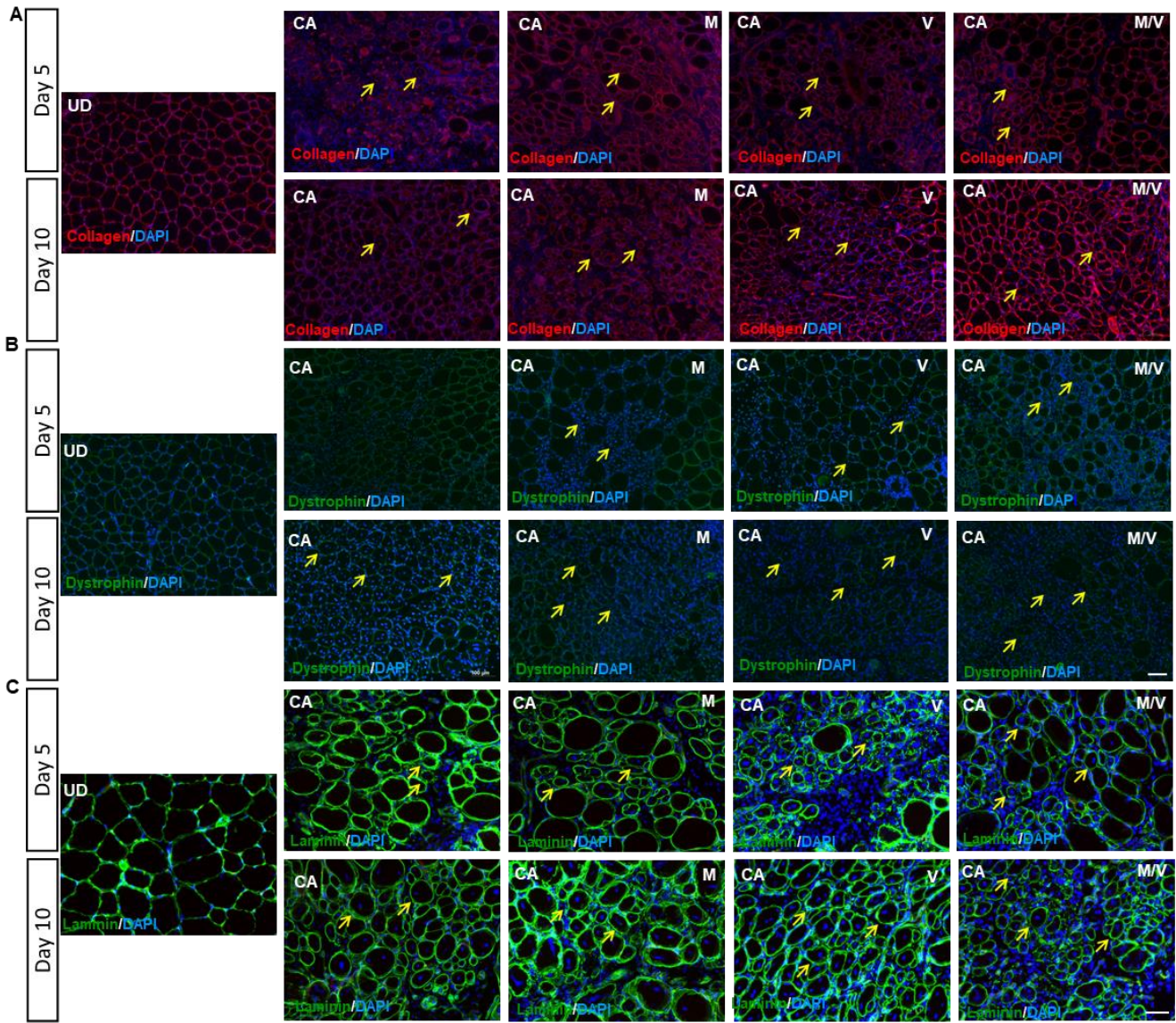




**Figure 7: Immunostaining for ECM markers in TA muscle sections.** TA muscle sections were collected on days 5 and 10 and stained using collagen IV (**A**), dystrophin (**B**) and laminin (**C**) antibodies. The thickness of the collagen IV was measured around the fibres with CLN at days 5 (**D**) and 10 (**G**). The thickness of the dystrophin was measured around the fibres with CLN at days 5 (**E**) and 10 (**H**). The thickness of the laminin was measured around the fibres with CLN at days 5 (**F**) and 10 (**I**). The  $p$  values are calculated by One-way ANOVA followed by post hoc Tukey's test using GraphPad Prism (\* $p$ <0.05, \*\* $p$ <0.01 and \*\*\* $p$ <0.001, \*\*\*\* $p$ <0.0001,  $n=5$ ) (comparison between UD and all other cohorts is represented with # whereas CA and all the treatment groups is represented by \*). The scale bar in represents 100 $\mu$ M. The yellow arrows in the image correlate to ECM proteins around CLN fibres, in figure-A collagen IV, figure B- Dystrophin and figure C- Laminin.

### 3.6 Venom-induced muscle damage alters the levels of various cytokines

The balance between pro-inflammatory and anti-inflammatory responses is critical for effective muscle regeneration [19]. This balanced response results in a structurally intact and functionally active muscle. Different secretory factors are known to play an essential role in the muscle regeneration process. Based on the above data, the effects of inhibitors are evident on day 5. Hence, we examined the serum samples obtained on day 5 from all the cohorts to quantify the levels of various cytokines including pro-inflammatory and anti-inflammatory markers. As shown in **Figure 8**, the venom has increased the levels of several cytokines, but they are reversed by marimastat and varespladib. In the anti-inflammatory panel (**Figure 8A**), IL-4, IL-5, and IL-13 showed no significant difference between treated and untreated samples, whereas IL-10 level was elevated in venom-treated samples, but its levels were reversed by marimastat or varespladib alone or in combination. TNF $\alpha$ , IL-1 $\beta$ , and IL-6 levels were also reduced in samples treated with inhibitors compared to venom-treated samples (**Figure 8B**). The venom has also increased several chemokines, but they are also reduced by the inhibitors (**Figure 8C**). The data indicate that the inhibitors are not only promoting muscle regeneration following venom-induced damage but also restoring the balance between anti-inflammatory and pro-inflammatory responses, which further supports regeneration. Total 44 markers were analysed, however the figures include markers that showed significant changes.

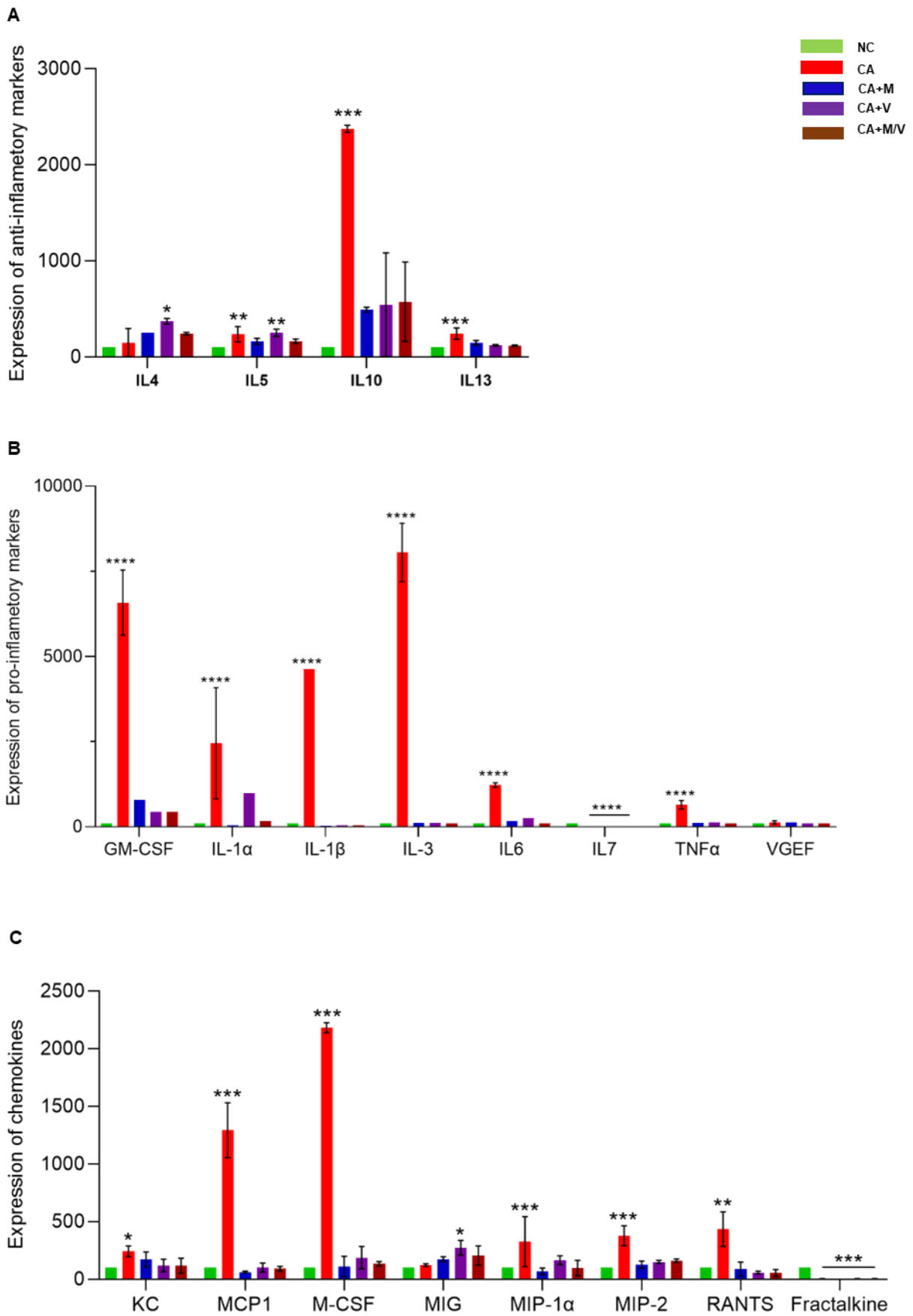


**Figure 8. Inhibitor treatment restored the balance between anti-inflammatory and pro-inflammatory markers: A)** Expression of pro-inflammatory markers. **B)** Expression of anti-inflammatory markers. **C).** Expression of chemokines. The graphs are plotted using GraphPad

Prism. For the statistical analysis all treatments were compared with NC by One-way ANOVA followed by post hoc Tukey's test using GraphPad Prism. (\* $p < 0.05$ , \*\* $p < 0.01$  and \*\*\* $p < 0.001$ , \*\*\*\* $p < 0.0001$ ,  $n=3$ )

#### 4. Discussion

Snake venom-induced muscle damage is one of the severe consequences of SBE, which often results in extensive tissue damage and subsequent permanent disabilities in victims. The number of people suffering from SBE-induced disabilities is three times more than the number of SBE-induced deaths. Therefore, research on SBE-induced muscle damage is essential to understand the pathological processes better and develop new treatment strategies for this condition. The two major venom toxin families responsible for muscle damage are SVMPs and PLA<sub>2</sub>. PLA<sub>2</sub> causes cell membrane damage, which results in tissue necrosis [20]. Tissue necrosis is often self-resolved and does not result in permanent muscle loss due to the innate regenerative capacity of skeletal muscle. SVMPs of viper venoms are reported to cause systemic haemotoxic effects and extensive tissue necrosis and muscle degeneration [21]. The metalloprotease domain of SVMPs has a high affinity to the ECM components of the tissues, and therefore, they can degrade the ECM components, especially collagen IV [22]. ECM acts as the scaffolding for the regenerating muscle fibres. During muscle regeneration following damage, the damaged ECM is repaired. The lack of scaffolding structure can severely affect the muscle regeneration [23]. Moreover, SVMPs can attenuate the migration and proliferation of the resident satellite cells indirectly by disrupting the ECM [11]. Together, SVMPs cause impairment to the innate regenerative capacity of skeletal muscle following viper envenoming, resulting in extensive damage and permanent disabilities.

In this study, we have used *C. atrox* venom and examined its effect on skeletal muscle. We hypothesised that by mitigating the actions of major toxin families, we can prevent excessive damage and promote the regeneration of affected muscle. A broad-spectrum matrix metalloprotease inhibitor, marimastat and PLA<sub>2</sub> inhibitor, varespladib have been proven to be effective in neutralising the systemic effects of venoms to a great extent. Hence, we investigated their impacts in neutralising SVMPs and PLA<sub>2</sub>s under *in vivo* settings in mice [16]. Marimastat inhibits the action of SVMPs via binding with zinc ions present in the catalytic domain [24, 25]. Similarly, varespladib blocks the allosteric activation of the PLA<sub>2</sub> [26]. The *in vitro* assay data confirmed the inhibitory action of

marimastat and varespladib individually, although no synergetic effects were observed. Therefore, we have tested marimastat and varespladib individually and in combination to determine their impacts on venom-induced muscle damage.

The present data shows direct evidence of the correlation between inflammatory responses and tissue regeneration. The typical sequences of action that cause regeneration impairment post-venom-induced damage are: (a) the venom is active in the tissue for a longer time and causes persistent damage; (b) imbalance in the standard regeneration cycle; (c) adipose and fibrotic tissue deposition in the damaged area; and (d) lack of scaffolding affects ECM regeneration and remodelling. We aimed to break this chain of reaction, starting with neutralising the active venom toxins. In line with our previous study, we established the presence of venom in tissues using venom-specific antibodies. Marimastat has significantly reduced the levels of venom in damaged muscle sections. As SVMPs contribute to a large percentage of the *C. atrox* venom, this result confirmed that by inhibiting the action of SVMPs, the overall effects of *C. atrox* venom on muscle could be minimised. A similar effect was observed with the drug combination treatment but not with individual varespladib. These observations suggest that the presence of marimastat can largely affect venom activity on muscles. Viper venoms are known for their haemotoxic effects and can cause intramuscular bleeding. The presence of fibrinogen in the muscle indicates intramuscular bleeding. The treatment with marimastat reduced intramuscular bleeding, suggesting that inhibition of SVMPs can help reduce bleeding in tissues [27]. Tissue necrosis is the first step of muscle damage, progressing towards more pathological indications. It is known that SVMPs and PLA<sub>2</sub> induce tissue necrosis [28, 29]. Individual inhibitors effectively reduced tissue necrosis at the early stage of tissue repair. Untreated, persistent muscle damage results in fibrosis [30]. When SVMPs are blocked with marimastat, it reduces intramuscular bleeding and tissue necrosis, ultimately reducing fibrotic tissue deposition.

Injection of venom often affects a larger muscle area around the injection site. One of this study's key findings was that treatment with the inhibitors dampens the initial muscle-damaging properties of the venom and then, after damage has taken place, acts to promote regeneration. Either inhibitor alone or their dual treatment led to an increase in the size of regenerated fibres.

Furthermore, we show an impact on the initial phase of muscle damage (IgG infiltration). The presence of ECM reconstruction is essential for the progress of skeletal muscle regeneration. It is well established that in the absence of ECM scaffolding, satellite cells fail to promote the regeneration of muscle fibres [31]. The impact of marimastat on the reconstruction and remodelling of ECM was astounding, again a strong indication that marimastat can effectively mitigate the effects of SVMPs. In the presence of marimastat, other ECM components, including laminin and dystrophin, also progressed in the regeneration and remodelling cycle. The reconstruction of ECM may be the key to repairing long-term muscle damage caused by viper venoms. In the presence of ECM scaffolding, muscle regeneration with inhibitors, especially marimastat can be achieved.

TNF $\alpha$  is one of the essential regulators in myogenesis. It acts as a critical activator of p38, a mitogen-activated protein kinase (MAPK), a fundamentally important protein for myogenesis [32]. TNF $\alpha$  upregulates cytokines such as IL-1 $\beta$  and IL-6. IL-1 $\beta$  inhibits the differentiation of satellite cells to enhance the proliferation [33, 34]. IL-6 also increases myoblast proliferation. This can be related to the continuous myoblast formation in the muscle tissues. Cytokine analysis performed on day five showed elevated TNF $\alpha$ , IL-1 $\beta$ , and IL-6 levels without any inhibitors. However, when the inhibitors were added, these levels were significantly reduced, indicating the progress towards resolving inflammation. The muscle regeneration also depends on the adequate blood supply to the damaged tissue. SVMPs cause damage and reduce the number of blood capillaries around damaged muscle fibres and microcapillary networks. Furthermore, vascular endothelial growth factor (VEGF) promotes angiogenesis after injury [35, 36]. We observed no significant change in VEGF levels with treatment and poor blood vessel reconstruction in muscle sections. INF- $\gamma$  is associated with trauma-induced muscle wasting [37]. It facilitates neutrophil migration from the site of the injury. The presence of this marker in a higher percentage suggests delayed removal of neutrophils from the injury site [38]. With marimastat treatment, it is possible to reduce muscle wasting, as treatment with it showed lower levels of INF- $\gamma$ .

Overall, marimastat and varespladib help control the muscle damage caused by SVMPs and PLA<sub>2</sub> *in vivo* by neutralising these venom toxins. They restored the balance between anti-inflammatory and pro-inflammatory responses, supporting muscle regeneration. During the initial

stages of muscle repair, these inhibitors neutralised the venom in the tissue, reflecting the reduction of tissue necrosis, intramuscular bleeding, and muscle fibrosis. As a result, the progress in the growth of newly formed muscle fibres was prominent with treatment. In addition, ECM reconstruction was effective, especially with marimastat. Anti-snake venom cannot reach the site of local tissue and has significant limitations [39, 40]. However, these inhibitors can overcome the limitations of antivenom by reaching the site of damage and effectively neutralising the venom toxins. The inhibitors being specific for toxins and not the whole venom frees them from the limitation of geographical variation in the snake venom. From these data, we establish that these small molecule inhibitors can be viable options for treating snake venom-induced muscle damage.

## References

1. Harrison, R.A., et al., *Snake envenoming: a disease of poverty*. PLoS Negl Trop Dis, 2009. **3**(12): p. e569.
2. Williams, H.F., et al., *Challenges in diagnosing and treating snakebites in a rural population of Tamil Nadu, India: The views of clinicians*. Toxicon, 2017. **130**: p. 44-46.
3. Vaiyapuri, S., et al., *Snakebite and its socio-economic impact on the rural population of Tamil Nadu, India*. PLoS One, 2013. **8**(11): p. e80090.
4. Alirol, E., et al., *Snake bite in South Asia: a review*. PLoS Negl Trop Dis, 2010. **4**(1): p. e603.
5. Williams, D.J., et al., *Strategy for a globally coordinated response to a priority neglected tropical disease: Snakebite envenoming*. PLoS Negl Trop Dis, 2019. **13**(2): p. e0007059.
6. Chippaux, J.P., *Estimate of the burden of snakebites in sub-Saharan Africa: a meta-analytic approach*. Toxicon, 2011. **57**(4): p. 586-99.
7. Tasoulis, T. and G.K. Isbister, *A Review and Database of Snake Venom Proteomes*. Toxins (Basel), 2017. **9**(9).
8. Markland, F.S., *Snake venoms and the hemostatic system*. Toxicon, 1998. **36**(12): p. 1749-800.
9. Gomes, A.A.S., et al., *The allosteric activation mechanism of a phospholipase A2-like toxin from Bothrops jararacussu venom: a dynamic description*. Sci Rep, 2020. **10**(1): p. 16252.
10. Gutierrez, J.M. and A. Rucavado, *Snake venom metalloproteinases: their role in the pathogenesis of local tissue damage*. Biochimie, 2000. **82**(9-10): p. 841-50.
11. Williams, H.F., et al., *Mechanisms underpinning the permanent muscle damage induced by snake venom metalloprotease*. PLoS Negl Trop Dis, 2019. **13**(1): p. e0007041.

12. Bartlett, K.E., et al., *Dermonecrosis caused by spitting cobra snakebite results from toxin potentiation and is prevented by the repurposed drug varespladib*. bioRxiv, 2023: p. 2023.07.20.549878.
13. Xie, C., et al., *Neutralizing Effects of Small Molecule Inhibitors and Metal Chelators on Coagulopathic Viperinae Snake Venom Toxins*. Biomedicines, 2020. **8**(9).
14. Underwood, C.K., et al., *The interaction of metal ions and Marimastat with matrix metalloproteinase 9*. J Inorg Biochem, 2003. **95**(2-3): p. 165-70.
15. Abraham, E., et al., *Efficacy and safety of LY315920Na/S-5920, a selective inhibitor of 14-kDa group IIA secretory phospholipase A2, in patients with suspected sepsis and organ failure*. Crit Care Med, 2003. **31**(3): p. 718-28.
16. Albulescu, L.O., et al., *A therapeutic combination of two small molecule toxin inhibitors provides broad preclinical efficacy against viper snakebite*. Nat Commun, 2020. **11**(1): p. 6094.
17. Calvete, J.J., et al., *Exploring the venom proteome of the western diamondback rattlesnake, Crotalus atrox, via snake venomomics and combinatorial peptide ligand library approaches*. J Proteome Res, 2009. **8**(6): p. 3055-67.
18. Alqallaf, A., et al., *The therapeutic potential of soluble activin type IIB receptor treatment in a limb girdle muscular dystrophy type 2D mouse model*. Neuromuscul Disord, 2022. **32**(5): p. 419-435.
19. Charge, S.B. and M.A. Rudnicki, *Cellular and molecular regulation of muscle regeneration*. Physiol Rev, 2004. **84**(1): p. 209-38.
20. Lin Shiau, S.Y., M.C. Huang, and C.Y. Lee, *Mechanism of action of cobra cardiotoxin in the skeletal muscle*. J Pharmacol Exp Ther, 1976. **196**(3): p. 758-70.
21. Roldan-Padron, O., et al., *Snake Venom Hemotoxic Enzymes: Biochemical Comparison between Crotalus Species from Central Mexico*. Molecules, 2019. **24**(8).
22. Herrera, C., et al., *Tissue localization and extracellular matrix degradation by PI, PII and PIII snake venom metalloproteinases: clues on the mechanisms of venom-induced hemorrhage*. PLoS Negl Trop Dis, 2015. **9**(4): p. e0003731.
23. Frantz, C., K.M. Stewart, and V.M. Weaver, *The extracellular matrix at a glance*. J Cell Sci, 2010. **123**(Pt 24): p. 4195-200.
24. Arias, A.S., A. Rucavado, and J.M. Gutierrez, *Peptidomimetic hydroxamate metalloproteinase inhibitors abrogate local and systemic toxicity induced by Echis ocellatus (saw-scaled) snake venom*. Toxicon, 2017. **132**: p. 40-49.
25. Escalante, T., et al., *Effectiveness of batimastat, a synthetic inhibitor of matrix metalloproteinases, in neutralizing local tissue damage induced by BaP1, a hemorrhagic metalloproteinase from the venom of the snake bothrops asper*. Biochem Pharmacol, 2000. **60**(2): p. 269-74.
26. Salvador, G.H.M., et al., *Structural basis for phospholipase A2-like toxin inhibition by the synthetic compound Varespladib (LY315920)*. Sci Rep, 2019. **9**(1): p. 17203.
27. Sonavane, M., et al., *Intramuscular Bleeding and Formation of Microthrombi during Skeletal Muscle Damage Caused by a Snake Venom Metalloprotease and a Cardiotoxin*. Toxins (Basel), 2023. **15**(9).

28. Gutierrez, J.M., et al., *Why is Skeletal Muscle Regeneration Impaired after Myonecrosis Induced by Viperid Snake Venoms?* *Toxins* (Basel), 2018. **10**(5).
29. Xiao, H., et al., *Inactivation of Venom PLA(2) Alleviates Myonecrosis and Facilitates Muscle Regeneration in Envenomed Mice: A Time Course Observation.* *Molecules*, 2018. **23**(8).
30. Cholok, D., et al., *Traumatic muscle fibrosis: From pathway to prevention.* *J Trauma Acute Care Surg*, 2017. **82**(1): p. 174-184.
31. Caldwell, C.J., D.L. Matthey, and R.O. Weller, *Role of the basement membrane in the regeneration of skeletal muscle.* *Neuropathol Appl Neurobiol*, 1990. **16**(3): p. 225-38.
32. Chen, S.E., B. Jin, and Y.P. Li, *TNF-alpha regulates myogenesis and muscle regeneration by activating p38 MAPK.* *Am J Physiol Cell Physiol*, 2007. **292**(5): p. C1660-71.
33. Gallucci, S., et al., *Myoblasts produce IL-6 in response to inflammatory stimuli.* *Int Immunol*, 1998. **10**(3): p. 267-73.
34. Panzer, S., M. Madden, and K. Matsuki, *Interaction of IL-1 beta, IL-6 and tumour necrosis factor-alpha (TNF-alpha) in human T cells activated by murine antigens.* *Clin Exp Immunol*, 1993. **93**(3): p. 471-8.
35. Becker, C., et al., *Skeletal muscle cells expressing VEGF induce capillary formation and reduce cardiac injury in rats.* *Int J Cardiol*, 2006. **113**(3): p. 348-54.
36. Ochoa, O., et al., *Delayed angiogenesis and VEGF production in CCR2-/- mice during impaired skeletal muscle regeneration.* *Am J Physiol Regul Integr Comp Physiol*, 2007. **293**(2): p. R651-61.
37. Madihally, S.V., et al., *Interferon gamma modulates trauma-induced muscle wasting and immune dysfunction.* *Ann Surg*, 2002. **236**(5): p. 649-57.
38. Olsson, T., et al., *Neuronal interferon-gamma immunoreactive molecule: bioactivities and purification.* *Eur J Immunol*, 1994. **24**(2): p. 308-14.
39. Williams, H.F., et al., *The Urgent Need to Develop Novel Strategies for the Diagnosis and Treatment of Snakebites.* *Toxins* (Basel), 2019. **11**(6).
40. Alangode, A., K. Rajan, and B.G. Nair, *Snake antivenom: Challenges and alternate approaches.* *Biochem Pharmacol*, 2020. **181**: p. 114135.





## **2.2 Soluble activin receptor type IIB-mediated inhibition improves muscle regeneration following *Crotalus atrox* venom-induced damage**

### **Authors**

**Medha Sonavane<sup>1</sup>, Ali Alqallaf<sup>2,3</sup>, Robert D. Mitchel<sup>4</sup>, José R. Almeida<sup>1</sup>, Jarred Williams<sup>1</sup>, Olli Ritvos<sup>5</sup>, Ketan Patel<sup>2\*</sup>, and Sakthivel Vaiyapuri<sup>1\*</sup>**

<sup>1</sup>School of Pharmacy, University of Reading, Reading, RG6 6UB, United Kingdom

<sup>2</sup>School of Biological Sciences, University of Reading, Reading, RG6 6UB, United Kingdom

<sup>3</sup>Medical Services Authority, Ministry of Defence, Kuwait

<sup>4</sup>Micregen Ltd, Thames Valley Science Park, Reading, RG2 9LH, United Kingdom

<sup>5</sup>Department of Biochemistry and Developmental Biology, HiLIFE, Meilahti Clinical Proteomics Core Facility, University of Helsinki, Helsinki, Finland

\*Corresponding authors

*In preparation for publication*

### **Contribution to this chapter**

#### **Experimental contribution**

- Study design
- Animal work: dosing, dissections
- Tissue preparation: Muscle blocking, cryo-sectioning
- Staining and imaging- Staining muscle for histology and immunohistochemistry using various antibodies, imaging the sections

#### **General contribution**

- Data collection and analysis
- Preparing original figures
- Writing original manuscript

## Abstract

Viper bite envenomation often results in prominent skeletal muscle damage. According to our previous studies, the prolonged presence of *C. atrox* venom toxins and extensive muscle damage were observed in muscle tissue which mimicked chronic muscle damage often seen in various muscular dystrophies. In the case of chronic muscle damage, two critical processes occur: muscle regeneration is impaired, and fibroblasts are activated, leading to fibrosis. Myostatin/Activin signalling is a key regulator of both of these processes. Myostatin and its closely related molecules in particular activin inhibit myocyte proliferation and differentiation while promoting fibroblast proliferation and expression of extracellular matrix proteins. Thus, attenuating myostatin/activin signalling offers an attractive means of promoting muscle development while decreasing fibrosis. Hence, we have used the soluble activin type IIb receptor, which acts as a ligand trap for both myostatin and activin to dampen signalling and assessed whether this intervention can alter the pathological trajectory of *C. atrox* venom-induced muscle damage. We report that soluble activin type IIb receptor treatment increased the size of regenerating fibres while at the same time reducing the level of fibrotic tissue in muscle damaged with *C. atrox* venom.

## 1. Introduction

Muscle damage is one of the most severe consequences of snakebite envenomation (SBE), specifically following viper bites. The annual global burden of SBE-mediated disabilities is around 500,000 [1, 2]. Despite that, treatment options for SBE-induced muscle damage are limited. Viper snakes are primarily responsible for SBE-mediated skeletal muscle damage [3, 4]. Viper venoms contain numerous enzymatic and non-enzymatic proteins [5]. This potent mixture can cause severe systemic and local envenomation effects. The systemic effects are mostly haemotoxic and are typically managed by the administration of antivenoms. However, local effects such as ischemia, tissue damage, necrosis, and muscle fibrosis, are often treated with surgical procedures such as tissue debridement, fasciotomy, or amputations [6-8]. Rattlesnakes are part of the Crotalinae subfamily and are found throughout the Americas [9]. In the US, about 9000 people are affected by snakebites every year. The Western Diamondback rattlesnake (*Crotalus atrox*) is prominent in southwestern USA and Mexico and is responsible for most fatalities in northern Mexico [10]. *C. atrox*

venom contains a cocktail of proteins including snake venom metalloproteases (SVMP), snake venom serine proteinases (SVSP), phospholipase A<sub>2</sub> (PLA<sub>2</sub>), L-amino acid oxidase (LAAO) and C-type lectin-like proteins [11]. We have previously shown that one component termed, CAMP, a P-III SVMP from the venom of *C. atrox* is capable of inducing permanent muscle damage when injected into the tibialis anterior muscle of mice [12]. Our investigations showed that this toxin persists for days in the damaged muscle and suggested that it continually interferes with the innate muscle regeneration which it ultimately deregulates. The resultant outcome of continued degeneration/regeneration mimics chronic muscle damage often seen in a spectrum of human muscle diseases including Duchenne Muscular Dystrophy, which manifests in the formation of fibrotic tissues and poorly developed myofibres [12].

Skeletal muscle has a truly remarkable ability to regenerate, as demonstrated in mouse models where the destruction of a muscle can be reconstituted in a matter of a few weeks. The whole process is underpinned by the presence of a resident population of stem cells called 'satellite cells' (SC) [13]. Nevertheless, several other key factors are required for muscle regeneration. The entire process can be divided into two components: the clearance of damaged tissues and the reconstitution of lost cells. Acute muscle damage results in the infiltration of neutrophils and activation of monocytes which develop an 'inflammatory environment' that not only clears cell debris but also promotes the activation of two important cell types: SC and fibro-adipogenic progenitors (FAPs). FAPs act to promote expansion and self-renewal of SC as well as remodelling the extracellular matrix (ECM), a key step towards muscle regeneration. Importantly, the proinflammatory environment controls the development of FAPs to maintain them as precursors as well as limiting their number through the induction of apoptosis [14]. As the regeneration process continues, the environment becomes anti-inflammatory due to the activity of M2 macrophages. These cells secrete various factors that promote differentiation of SC to reconstitute lost myofibres but can also lead to the differentiation of any active FAPs into either fibroblasts or adipocytes [15]. In normal regeneration, SC numbers are expanded, and they differentiate into myoblasts which then fuse to form myofibres. The FAPs are eliminated resulting in the absence of fibrosis or fat deposition. However, in chronic muscle damage, the different phases of regeneration become entangled so that

they are no longer occurring in an orderly sequence, rather, they might be happening simultaneously and so interfere with each other. Two consequences of this degeneration process are the differentiation of FAPs into fibroblasts as well as poorly developed myofibres [14].

Signalling mediated by myostatin and its closely related family members especially activin is important for muscle regeneration. Myostatin and activin, members of the transforming growth factor (TGF)  $\beta$ -superfamily of secreted proteins, signal by binding to the extracellular portion of the activin type II receptor. This leads to a series of intracellular events mediated by a signalling protein, Smad2/3. In muscle cells, this signalling inhibits proliferation, and differentiation of myoblasts and in muscle fibres it leads to decreased protein synthesis [16, 17]. However, it promotes fibroblast proliferation which then can differentiate into myofibroblasts which are responsible for the formation of fibrotic tissues [18]. Hence the inhibition of myostatin/activin signalling has become an attractive proposition to overcome some of the issues associated with chronic muscle damage (poor muscle formation and fibrosis). Numerous strategies have been developed to attenuate myostatin/activin signalling. We have developed a soluble ligand trap, based on the extracellular portion of the activin type IIB receptor (sActRIIB), which acts to sequester myostatin and activin thus rendering them incapable of binding to their normal receptor [19].

In this study, we demonstrate that sActRIIB treatment following *C. atrox* venom-induced muscle damage promotes fibre regeneration and decreases the fibrosis.

## **2. Materials and methods**

### *Materials*

Lyophilised *C. atrox* venom and all other chemicals were purchased from Sigma Aldrich, UK unless otherwise stated.

### *2.1 Ethical statement*

All animal experiments were conducted following the regulations and principles of the British Home Office for the Animals (Scientific Procedures) Act 1986. All procedures used in this study were reviewed and approved by the University of Reading Animal Welfare and Ethics Review Board and British Home Office (PPLIEC1C0382).

## 2.2 Enzymatic assays

The metalloprotease activity of *C. atrox* venom was determined using DQ-gelatin (ThermoFisher Scientific, UK), a fluorogenic substrate. DQ-gelatin is a substrate for collagenolytic enzymes. Briefly, the whole venom (10 µg/mL) in phosphate-buffered saline (PBS, pH 7.4) was mixed with DQ-gelatin (20 µg/mL) and incubated at 37°C. The fluorescence levels were then measured by spectrofluorimetry continuously for 90 minutes (FLUOstar OPTIMA, BMG Labtech, Germany) with an excitation wavelength of 485 nm and an emission wavelength of 520 nm.

## 2.3 TA muscle damage in mice

A murine model of muscle damage was used to test the effects of *C. atrox* venom on skeletal muscle and the impact of subsequent treatment. C57BL/6 male mice (10 weeks old) were obtained from Charles River, UK. The male mice were used as they have bigger muscle fibres than female mice which might help with the analysis of individual markers. The animals were anaesthetised using 3.5% (v/v) isoflurane in oxygen and maintained at 2% during the intra-muscular injection procedure. The right tibialis anterior (TA) muscle of mice was injected intramuscularly at a venom dose of 5 µg per 20g (0.25µg/g) of animal weight. The venom dose was selected based on the enzymatic activity. Thereafter, specific cohorts of the mice were given sActRIIB 10 mg/kg (200 µg/20 g animal) through the intraperitoneal route one hour after the venom injection and every third day after that. The mice were sacrificed by carbon dioxide inhalation and death was confirmed by cervical dislocation. Muscles were collected from mice on days 5, 10 and 15 to examine the level of damage at different time points.

## 2.4 Dissection and tissue processing

TA muscles of mice were dissected intact and immediately frozen on isopentane cooled with liquid nitrogen. Dissected muscles were placed in pre-cooled tubes and stored at -80°C. Muscles were blocked in an Optimal Cutting Temperature (OCT) compound and cut into 15µm thick transverse sections using a cryo-microtome for further analysis.

## 2.5 H&E staining

TA muscle sections were removed from the -80°C freezer and kept at room temperature for 15 minutes. Muscle sections were then rehydrated with PBS after which immersed in Harris haematoxylin for 2 minutes before washing under tap water for 2 minutes. Next, the sections were immersed twice in 70% acidic alcohol [70% (v/v) ethanol and 0.1% (v/v) HCl] to remove any background stain. After this, the slides were washed under running tap water for 5 minutes. Thereafter, the sections were immersed in 1% (w/w) eosin for 2 minutes before being dehydrated through an ethanol series (70%, 90%, and 100%). Finally, the slides were immersed twice in Xylene for 3 minutes to displace the ethanol. The slides were mounted using the DPX (Dystertine, Plastisizer and Xylene) mounting media. The size of regenerated fibres was calculated by taking the area of 50 fibres that displayed centrally located nuclei from each section which were then averaged.

### *2.6 Picrosirius red staining*

Picrosirius red was used to identify fibrotic tissues by immersing sections in heated Bouin solution (56°C) for 15 minutes. Afterwards, the slides were rinsed with distilled water for 15 minutes at room temperature. The slides were then transferred to a jar containing picrosirius red stain and incubated for 1 hour in the dark. The slides were then rinsed in two separate jars containing acidified water [0.5% (v/v) glacial acetic acid] and dehydrated three times in 100% ethanol for 5 minutes. Finally, the slides were cleaned by immersion in Xylene for 5 minutes and then mounted with DPX mounting media. The fibrosis analysis was carried out using threshold analysis. A set area (200  $\mu\text{m}^2$ ) was selected from the undamaged muscle and a baseline set using the ImageJ (version 1.52a) threshold analysis tool. This value was compared to that from a 200  $\mu\text{m}^2$  area of a damaged muscle region to give a relative value (%) of picrosirius red coverage.

### *2.7 Immunohistochemistry*

The sections were rehydrated by washing with PBS, followed by 15 minutes of incubation with a permeabilisation buffer [20 mM HEPES, 3 mM  $\text{MgCl}_2$ , 50 mM NaCl, 0.05% (w/v) sodium azide, 300 mM sucrose and 0.5% (v/v) Triton X-100]. After washing with PBS, non-specific binding of antibodies was prevented using a blocking wash buffer [PBS with 5% (v/v) foetal bovine serum and 0.05% (v/v) Triton X-100] and incubating for 30 minutes at room temperature. Premade primary antibodies (details are provided in supplementary information) in blocking wash buffer were

incubated with the sections overnight at 4°C. Unbound primary antibodies were then removed by washing the sections with a blocking wash buffer three times. Next, the sections were incubated with secondary antibodies (diluted in blocking wash buffer) for 1 hour in the dark at room temperature. The slides were then mounted with a fluorescent mounting medium containing 4,6-diamidino-2-phenylindole (DAPI) (Fisher Scientific, UK) with Dako fluorescence mounting medium (Dako, UK). The muscle sections were visualised using a Zeiss AxioImager fluorescence microscope.

Analysis of immuno-stained sections was carried out as follows. The size of IgG infiltrated or embryonic myosin MYHIII expressing fibres was determined by measuring the area of 30 fibres from one section of each animal using ImageJ. The measured area was compared between treated and untreated muscle fibres at same time point to analyse the effect of the given treatment. To measure the thickness of collagen IV and laminin, fibres with centrally located nuclei were first selected from the damaged region of the muscle. The thickness of collagen IV and laminin was measured and compared with the thickness of the undamaged. Dystrophin circularity was assessed by determining the percentage of a fibre circumference that expressed dystrophin in muscle fibres with centrally located nuclei. 30 centrally located fibres from one section of each animal were measured using ImageJ. The intramuscular bleeding was calculated using threshold analysis sections stained for fibrinogen using ImageJ. An area of 200  $\mu\text{m}^2$  was selected from the damaged region of the muscles and compared to the baseline threshold value from undamaged muscle.

## 2.8 Statistical analysis

The collected images were processed and analysed using ImageJ and Zeiss AxioImager (4.9.1) software. Statistical analysis was performed using either an unpaired t-test to compare the treated and untreated groups at various time points and one-way ANOVA multiple comparison followed by Tukey's test to compare all treated and untreated groups at various time point, with undamaged muscle. The statistical analysis was performed using GraphPad Prism (version 7).

## 3. Results

### 3.1 *sActRIIB* treatment increases the weight of *C. atrox* venom-damaged TA muscles



*C. atrox* venom showed high levels of collagenolytic activity (**Figure 1A & 1B**). We developed two cohorts (4 in each) of mice to assess the impact of inhibiting myostatin/activin signalling on *C. atrox* venom-damaged muscle. First group, the control group was only treated with *C. atrox* venom (CA), whereas the second group had both *C. atrox* venom and sActRIIB treatment (CA/sAct). The contralateral muscle from the CA group was used as an undamaged (UD) muscle for analysis and comparison. TA muscles were injected with venom and then treated with sActRIIB intraperitoneally. The muscles were collected at different time points and weighed after dissections to determine the overall impact of the treatments. On day 5, there were no significant differences in TA weights between the three cohorts (**Figure 1D**). However, on day 10, CA muscles showed a significant decrease in weight compared to UD, whereas CA/sAct showed a significant increase compared to UD. Furthermore, CA/sAct TA muscles were significantly heavier what do you mean than those of CA mice. On day 15, CA muscles were still significantly lighter than those of UD, whereas CA/sAct muscles showed significant weight increases compared to the other two groups (**Figure 1D**).

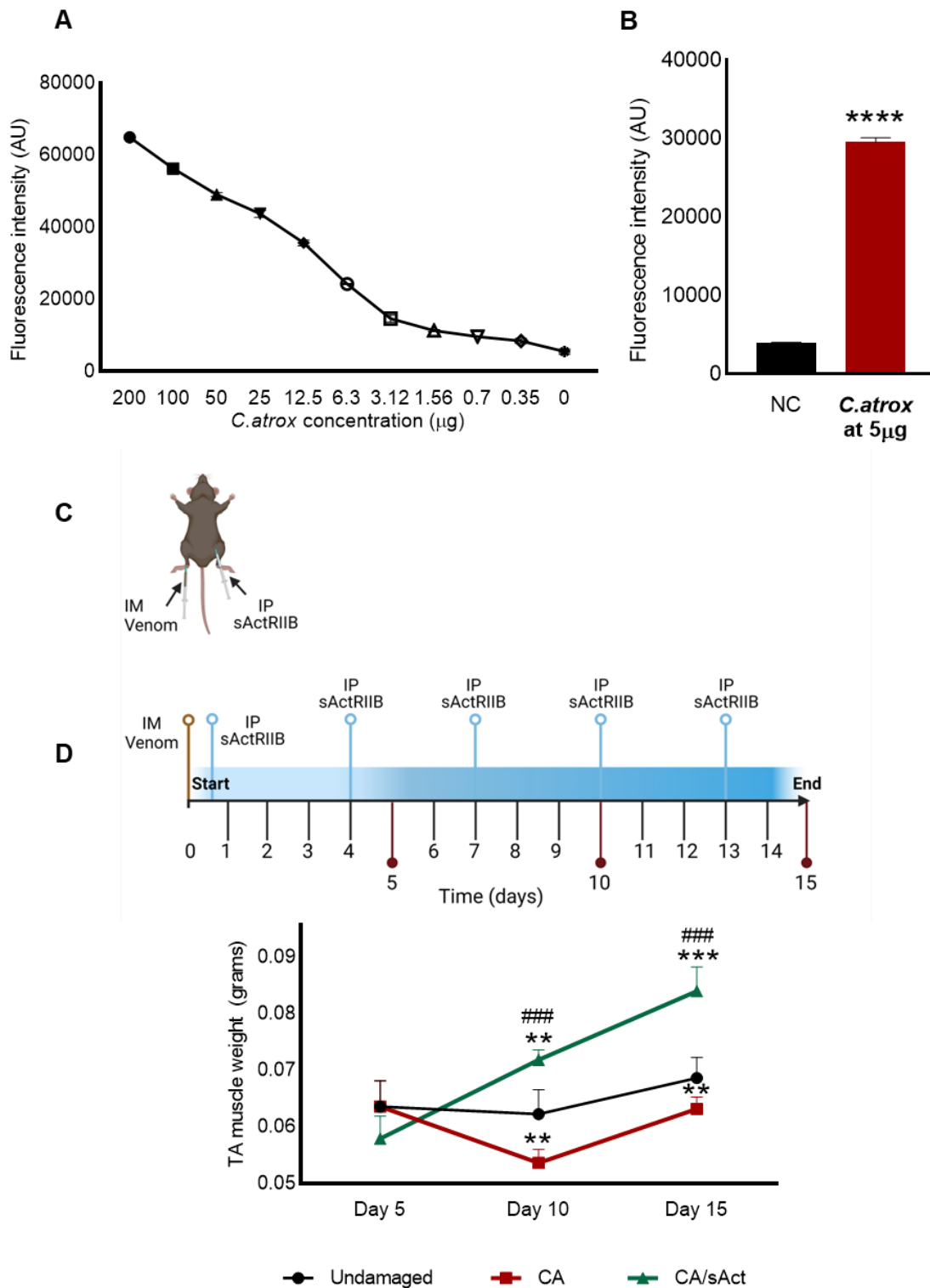


**Figure 1: *C. atrox* venom profiling for metalloprotease activity and its deployment *in vivo*.** **A&B)** Quantification of metalloprotease activity in *C. atrox* venom using DQ-gelatin as a substrate – highlight the concentration of venom used. **C)** Graphical representation of *in vivo* muscle damage protocol. **D)** Tibialis anterior muscle weights in three cohorts over time (n=4). The \* represents the comparison between undamaged muscle with either CA or CA/sAct cohorts, and # represents the comparison between CA and CA/sAct cohorts at the same time point. Statistical analysis in B was performed using Student’s t-test. One-way ANOVA followed by Tukey’s post-hoc test was used in C. \*\*  $p < 0.01$  and \*\*\* or ###  $p < 0.001$ .

### 3.2 sActRIIB treatment promotes muscle regeneration and attenuates fibrosis

The presence of centrally located nuclei is a marker for newly formed muscle fibres. As expected, there were no such fibres in the UD muscles in H&E-stained sections (Figure 2A). We therefore compared the size of muscle fibres displaying centrally located nuclei between the CA and CA/sAct groups at the same time point. The results showed that newly formed fibres were larger in the CA/sAct cohort compared to CA at day 15 (**Figure 2A and C**). Interestingly even though the sActRIIB induced fibre enlargement, they were still smaller than undamaged fibres (black bar in **Figure 2C**).

Next, we analysed whether sActRIIB played any role in modifying the development of fibrotic tissues after *C. atrox* venom injection. The degree of picosirius red staining was used to visualise collagen fibres (at early time point) or total fibrosis (at later time points). Picosirius red staining was present in UD muscle which marks the connective tissue in healthy muscle which accounts for approximately 4% of the area (**Figure 2B and D**). Significantly elevated levels of picosirius red staining were observed in all muscle samples compared to the UD at all time points from both experimental cohorts except the CA/sActRIIB muscle at day 15 (**Figure 2B and 2D**). At this time point, there was no significant difference in picosirius red staining coverage between the CA/sActRIIB muscle and UD. When compared between CA and CA/sActRIIB at same time point, there was significantly lower picosirius staining in CA/sActRIIB muscle on days 10 and 15. Hence we observed that with persistent dosing of sActRIIB, venom induced muscle fibrosis significantly reduced. Hence, the enlargement of newly generated fibres and decrease in fibrosis are induced by sActRIIB treatment at later time points.

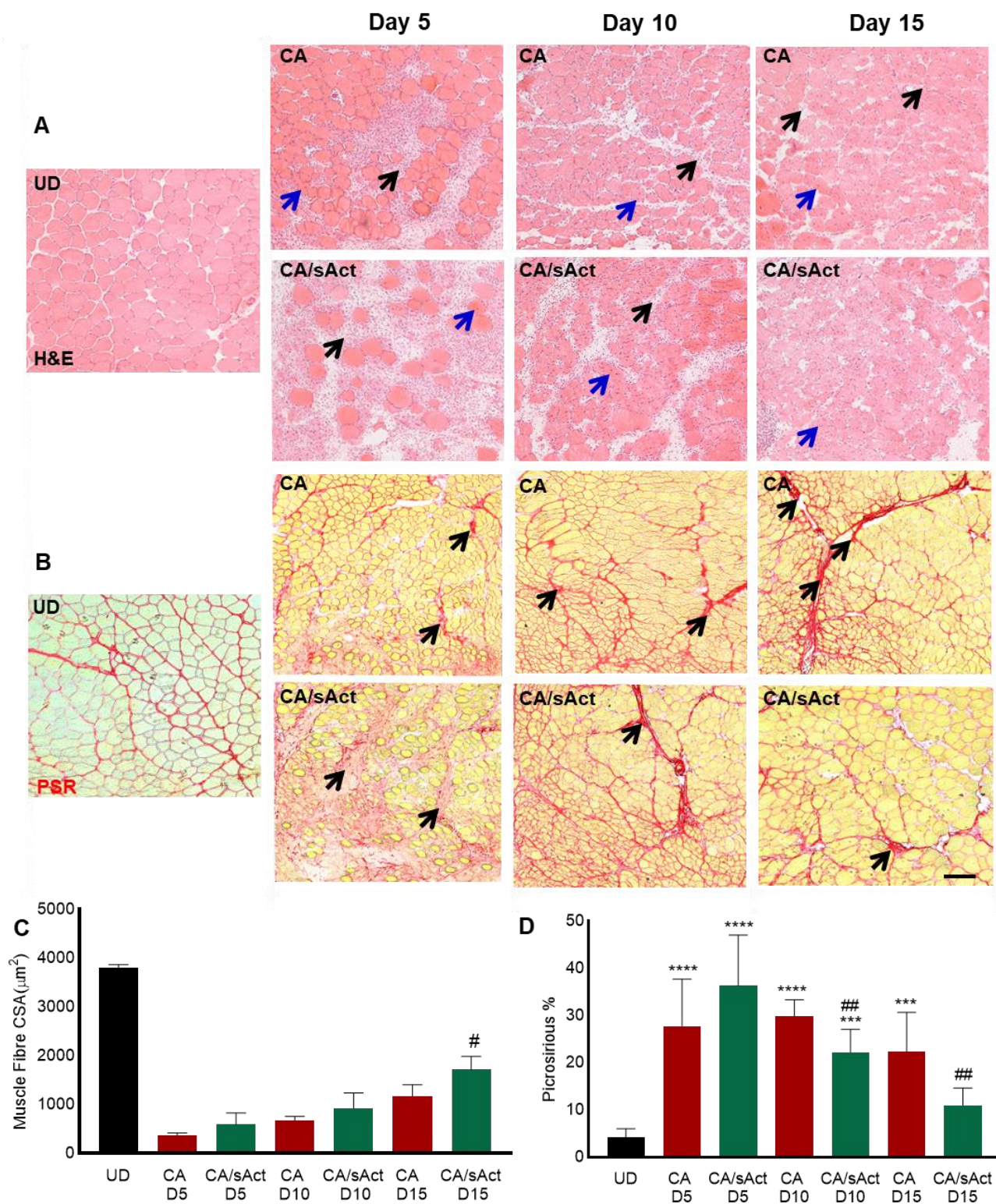


**Figure 2: Analysis of muscle regeneration and fibrosis. A)** H&E staining for TA muscle section on UD and CA and CA with sActRIIB at days 5, 10 and 15. Blue arrows show fibres with centrally located nuclei. Black arrows show infiltration of immune cells. **B)** Picrosirius red staining for TA muscle section on UD and venom-treated samples at days 5, 10 and 15. The black arrows show fibrotic tissues. **C)** Area of fibres with centrally located nuclei at three-time points using ImageJ **D)** Quantification of picosirius red staining area in the damaged region. n=4 mice per cohort. The \* represents a comparison between undamaged (UD) muscle with either venom injected (CA) or venom + sActRIIB (CA/sAct), and # represents a comparison between CA and CA/sAct cohorts at identical times post-venom injection. Statistical analysis in C was performed using pair-wise

comparison for individual variables. One-way ANOVA followed by Tukey's post-hoc test was used in D. # $p < 0.01$ , \*\*\* $p < 0.001$  or \*\*\*\* $p < 0.0001$ . The scale bar represents 100 $\mu$ M.

### *3.3 sActRIIB reduced tissue necrosis but did not affect the early stages of muscle fibre development*

Viper venom is known to induce muscle necrosis and attenuate regeneration. Dying/necrotising fibres facilitate the infiltration of circulating immunoglobulins (IgG) and newly regenerating fibres express embryonic myosin heavy chain (MYHIII). Hence, we analysed muscle necrosis and the formation of new fibres by staining for IgG and MYHIII as markers, respectively. The UD samples had no muscle fibres infiltrated with IgG (**Figure 3A & 3C**). Examination of the necrotic fibre profile in the treated cohorts showed approximately a 50% reduction with sActRIIB treatment on day 5. Thereafter no evidence of necrosis was detected across all the cohorts (**Figure 3A and C**). Next, we examined the early stages of fibre development. There were no MYHIII-positive fibres in the UD samples (**Figure 3B**). CA muscles had MYHIII expression only on day 5 CA/sAct muscles had robust MYHIII expression at day 5 and a few fibres showing positivity at day 10 (**Figure 3B**). However, treatment with sActRIIB did not increase the size of the regenerating fibres expressing embryonic myosin (**Figure 3B and D**). Therefore, sActRIIB acts to modify the degeneration programme but not the early stages of muscle fibre regeneration.

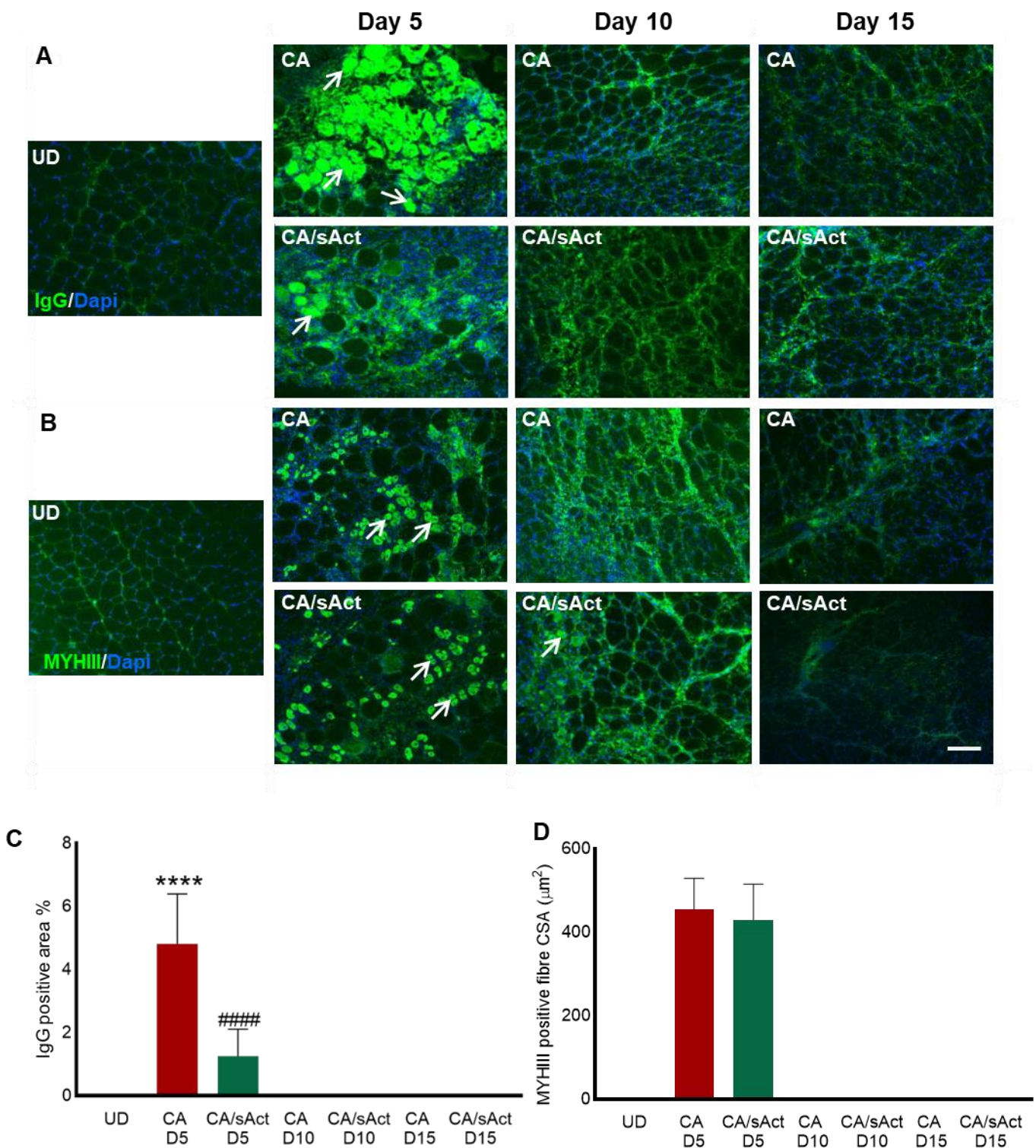


**Figure 3: Profiling dying and newly regenerated muscle fibres. A)** IgG infiltration in the muscle fibres in undamaged (UD), venom injected (CA) and venom+ sActRIIB treatment (CA/sAct) muscle on days 5, 10 and 15. White arrows indicate infiltrated fibres. **B)** Myofibres expressing embryonic myosin (MYHIII). White arrows indicate newly formed fibres. **C)** Quantification of IgG positive area %. **D)** Quantification of fibre size showing MYHIII expression. n=4 mice per cohort. # represents a comparison between values from CA and CA/sAct cohorts at the same time point, Statistical analysis

in C and D was performed using pair-wise comparison for individual variables. \*\*\*\* or ####  $p < 0.0001$ . The scale bar represents 100 $\mu$ M.

### 3.4 *sActRIIB* promoted the remodelling of ECM proteins and accelerated dystrophin expression

A thin layer of ECM protein represents a mature and normal muscle fibre condition (UD panels in **Figures 4A** and **B**). We profiled the distribution of ECM in the three cohorts of mice by examining two major components in skeletal muscle: collagen IV and laminin. Following muscle damage, we detected an abnormal distribution of both markers in the CA samples on day 5. Here they are manifested by abnormal thickness (as compared to UD) as well as a disruption in its expression domain, evident by lack of synthesis of certain ECM protein (**Figure 4A-E**). We noted the presence of many fibres where both collagen IV and laminin did not fully surround the muscle fibre (indicated by arrows) (**Figure 4A** and **B**). These features did not manifest in the CA/*sAct* cohort. At later time points, both the CA and CA/*sAct* cohorts displayed similar collagen IV and laminin profiles.

Next, we examined the distribution of dystrophin, a key protein required to maintain muscle fibre integrity. Following muscle damage, dystrophin is lost and then returned to its normal profile (a thin layer around the inner surface of the sarcolemma) following successful regeneration (UD panels in **Figure 4C**). Measuring the extent of dystrophin expression on the inner surface (circularity) was used as a measure of fibre maturation. On day 5, CA muscles showed no regenerating fibres with the presence of dystrophin – say what the arrows are indicating. However, CA/*sAct* contained many newly formed fibres expressing dystrophin. Nevertheless, they did not display an expression domain around the entire inner surface (only approximately 55%). By days 10 and 15 both the CA and CA/*sAct* cohorts showed 100% dystrophin circularity in newly formed fibres (**Figure 4C** and **F**).

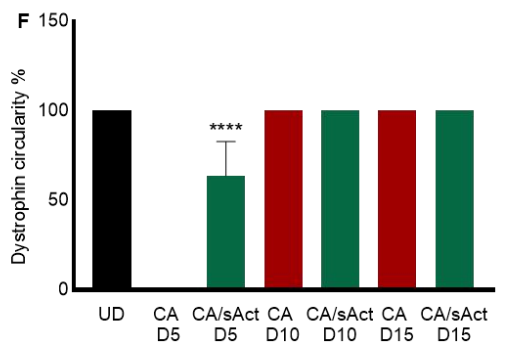
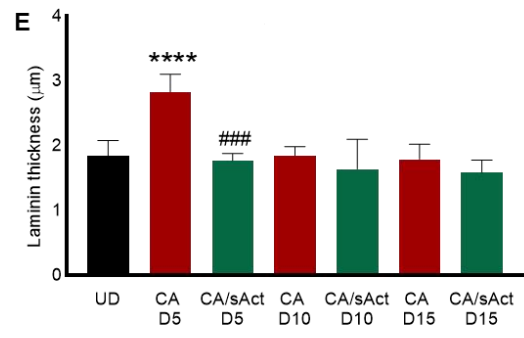
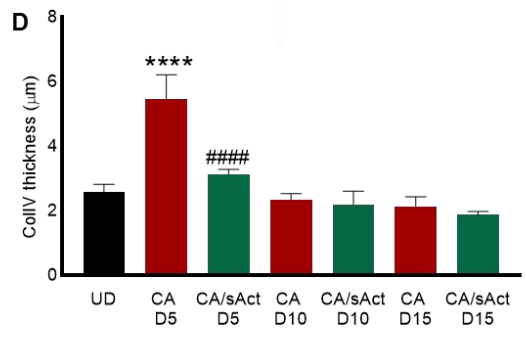
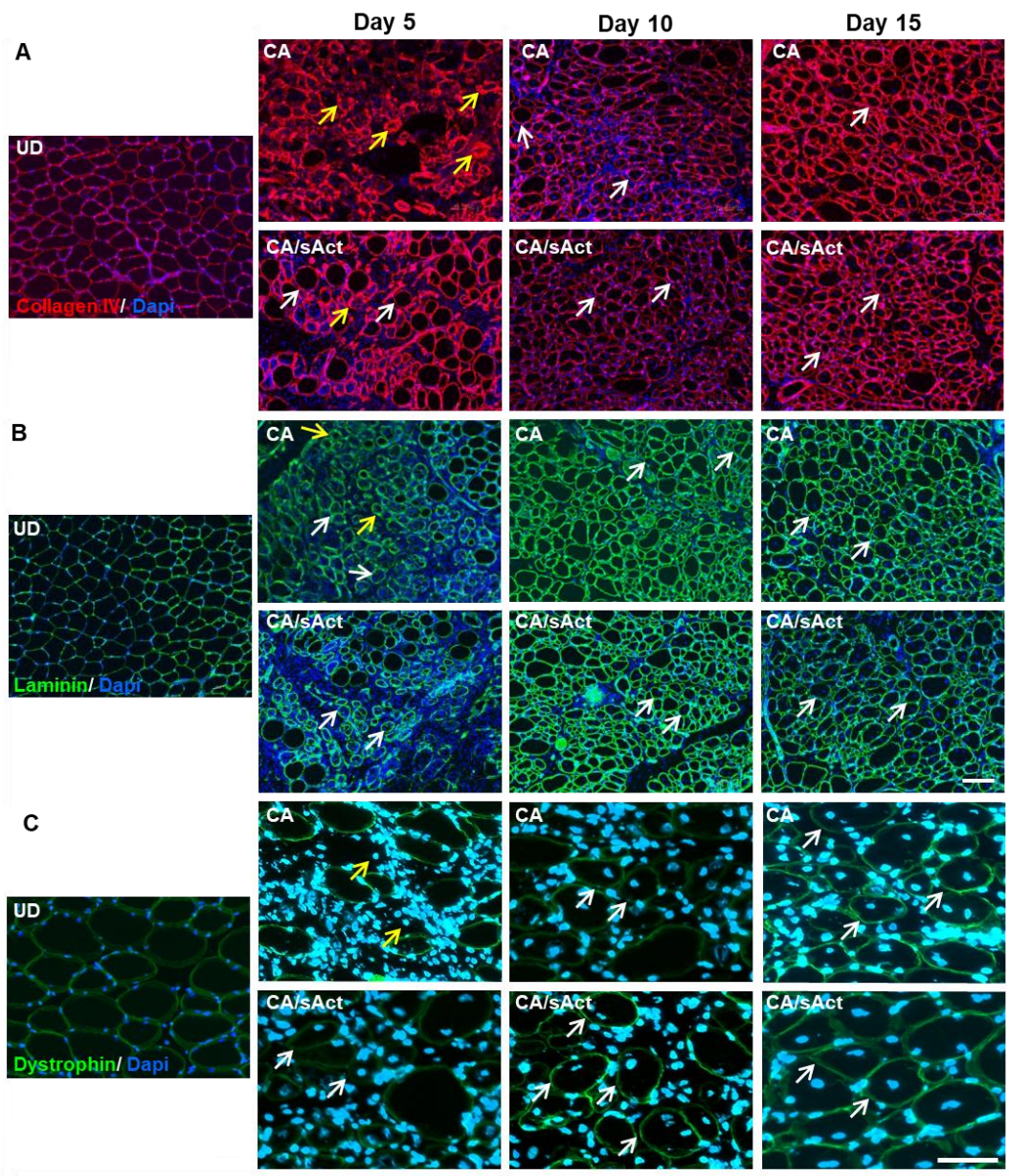




**Figure 4: Profiling extracellular matrix organisation and dystrophin expression in regenerating fibres.** **A)** Collagen IV in the muscle fibres in undamaged (UD), venom injected (CA) and venom with sActRIIB treatment (CA/sAct) muscle on days 5, 10 and 15. Yellow arrows indicate uneven collagen IV expression around fibres, and white arrows show even expression of this protein. **B)** Laminin expression in muscle sections at various time points. Yellow arrows indicate uneven laminin expression around fibres, and white arrows show even expression of protein. **C)** Dystrophin expression around regenerating fibres. Yellow arrows indicate fibres lacking dystrophin expression, and white arrows show fibres with dystrophin around the entire fibre. **D)** Quantification of collagen IV thickness domain using ImageJ. **E)** Quantification of Laminin thickness domain using ImageJ. **F)** Quantification of dystrophin circularity. n=4 mice per cohort. The \* represents a comparison between undamaged (UD) muscle with either CA) or CA/sAct, and # represents a comparison between CA and CA/sAct cohorts at identical times. Statistical analysis in C and D was performed using pair-wise comparison and one-way ANOVA followed by Tukey's post-hoc test. \*\*\*\* or #####  $p < 0.0001$ . The scale bar in A and B represents 100 $\mu$ M. The scale bar in C represents 50 $\mu$ M.

### 3.5 sActRIIB reduced intramuscular bleeding

Excessive fibrinogen in the intramuscular space indicates bleeding in the muscles. The CA muscles showed high levels of fibrinogen (covering approximately 40% of damaged regions) on day 5. However, the sActRIIB treatment significantly reduced fibrinogen levels, to account for 10% coverage on day 5, indicating a potential decrease in bleeding (**Figure 5A and 5C**). The levels of fibrinogen were largely reduced in both cohorts at days 10 and 15. Muscle sections were also stained with CD31 to identify the capillaries surrounding the muscle fibres, as adequate blood supply is crucial for muscle regeneration. We found that treatment with sActRIIB did not appear to impact angiogenesis during muscle repair (**Figure 5B**)

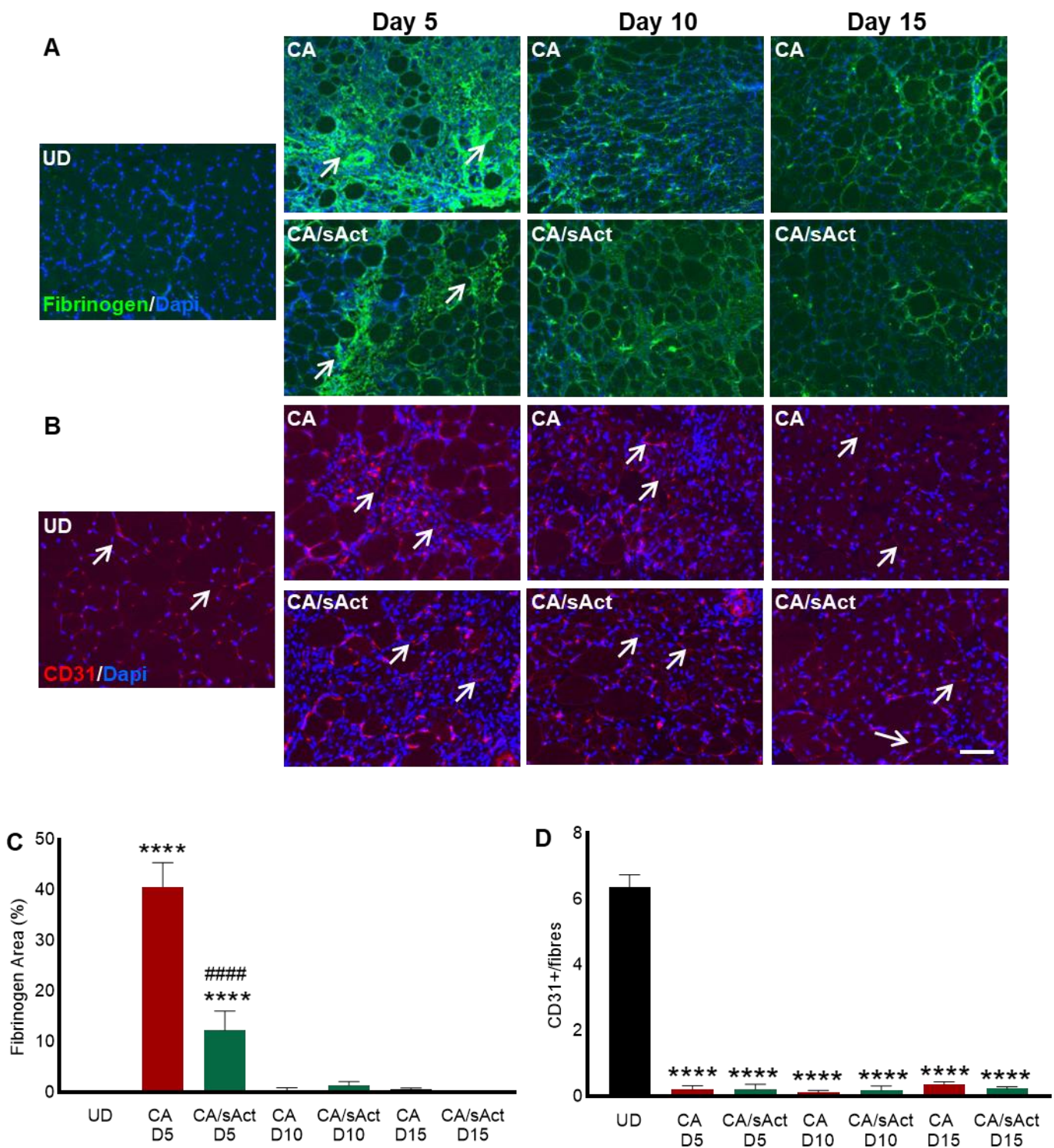


**Figure 5: Intramuscular bleeding and angiogenesis in damaged muscle. A)** Intramuscular bleeding profiled by fibrinogen distribution in undamaged muscle (UD) and venom (CA) and venom+ treatment (CA/sAct) injected and muscle on days 5, 10 and 15. White arrows show prominent fibrinogen deposition. **B)** Profiling capillaries in damaged muscle. White arrows show the expression of CD31 around regenerating fibres. **C)** Quantification of Fibrinogen coverage in damaged regions. N=4. The \* represents a comparison between undamaged (UD) muscle with either CA) or CA/sAct, and # represents a comparison between CA and CA/sAct cohorts at identical times. Statistical analysis in C was performed using pairwise comparison and for D one-way ANOVA followed by Tukey's post-hoc test was used. ### $p < 0.001$ . The scale bar represents 100 $\mu$ M.

#### 4. Discussion

We used the whole *C. atrox* venom in contrast to our previous study which only utilised a specific PIII metalloprotease (CAMP) [12]. Another notable difference between the two studies is the duration of the investigations, here we examined muscle for 15 days whereas previously the research was limited to 10 days. Nevertheless, we have noted similar effects at comparable time points between the two studies. Notably, we report that damage was evident in both studies at day 10 which persisted in this study to day 15. Therefore, in both studies, the innate regeneration mechanisms were unable to resolve damage induced by CAMP alone or whole *C. atrox* venom. Hence, decreasing the relative amount of CAMP to total protein (as in this study) is still a very injurious reagent. Using whole venom may give better idea about the pathological conditions seen in *C. atrox* envenomation [21].

In the present study, sActRIIB treatment had the following effects on skeletal muscle after damage induced by *C. atrox* venom: 1. Muscles showed significant weight gain. 2. Regenerating fibre enlargement. 3. Decreased levels of fibrosis. 4. Decreased levels of early necrosis but newly formed fibre size was unaffected. 5. Collagen and laminin structures were better preserved. 6. Dystrophin expression was restored early. 7. Intramuscular bleeding was significantly reduced. Despite these positive changes, the muscle was not fully protected from the damaging influence of *C. atrox* venom by sActRIIB treatment evident ongoing remodelling of ECM markers and absence of angiogenesis in both treated and untreated muscles. One of the striking features of sActRIIB treatment was that on muscle weights following *C. atrox* venom injection. We noted that the TA muscles in the CA/sAct cohorts were heavier than CA muscles, an effect that was independent of the size of regeneration muscle fibres, which are with centrally located nuclei or those that expressed the developmental form of MYHIII. We postulate that the weight increase in muscle is due to the hypertrophic action of attenuating activin/myostatin signalling in the undamaged muscle fibres. Myostatin/activin-mediated signalling is known to induce catabolic pathways while at the same time inhibiting those responsible for fibre enlargement, mediated through the inhibition of Akt activity [22]. Hence, we suggest that at the stage of intervention, normal fibre growth was being held back and that this inhibition was lifted by sActRIIB treatment. This line of thinking agrees with a huge body of

work that shows that myostatin/activin inhibition is at play during the entire lifespan of animal models [23, 24]. Although the regenerating fibres at day 15 were larger in the CA/sAct cohorts compared to CA treatment alone, this change was minor and unlikely to account for the massive change in total TA weights. Interestingly, the newly formed muscle fibres (expressing MYHIII) did not respond to sActRIIB treatment suggesting that although myostatin and activin may be in circulation, these fibres develop through programmes that were not regulated by them. Future studies to examine the AKT pathway in *C. atrox venom-damaged* fibres are required to develop a greater understanding of the early phases of regeneration following envenomation.

We propose that the beneficial effects of attenuating myostatin/activin following *C. atrox* venom injection is imparted in two phases, early and late. In the early phase the intervention protects muscle fibres from damage as evidenced by the smaller IgG infiltrated fibres and the less severe impact on laminin/collagen IV expression as well as the early appearance of dystrophin in regenerating fibres. One possible means by which sActRIIB attenuates fibre damage could be through its inhibition of pathways that lead to the stimulation of IL-6 expression, a potent mediator of muscle protein breakdown [25]. A large number of clinically approved anti-IL6 therapies have already been developed which could be repurposed to control inflammatory pathways following SBE [26].

One of the most striking features of the sActRIIB intervention is the histologically improved structure of muscle which takes place at the last time point. In particular, we note that there was considerably less fibrosis in the CA/sAct cohort compared to CA. Additionally, there was a small albeit significant increase in the size of regenerating fibres. Importantly the improvement in fibrosis was not evident until the later time points. We propose that the results related to fibrosis can be explained by focusing on the fate of FAPs and how this is controlled by myostatin/activin. Recent research has shed light on these processes in the context of chronic muscle damage as seen in several muscular dystrophies [27]. FAPs are present to support perfect regeneration by promoting a cell activities including myoblast expansion and fate [28]. However, the number of FAPs is carefully controlled so that only basal levels survive after damage resolution, in readiness for the next round of muscle damage. However, the meticulous control of FAPs becomes deregulated in scenarios of chronic muscle damage, leading to their survival and allowing them to differentiate into either

fibroblasts or adipocytes [29]. Thereafter, fibroblast number can be expanded by signalling pathways activated by activin/myostatin [18]. Indeed, there seems to be a positive feedback loop that leads to the eventual formation of fibrosis. Herein, circulating myostatin may initiate fibroblast proliferation. These then go on to express the myokines, leading to ever-increasing proliferation and subsequent differentiation into myofibroblasts (marked by the expression of  $\alpha$  smooth muscle actin) [18]. sActRIIB could limit fibrosis after *C. atrox* venom damage by simply attenuating Myostatin signalling so that fibroblast expansion is limited. However, our data shows that fibrosis actually develops but is then subsequently decreased. We propose a new role for Activin/Myostatin in the development of fibrosis. We suggest that Activin/Myostatin are continually required for the formation of myofibroblasts and that in their absence, fibroblasts lose their ability to form aberrant ECM. Instead, they revert to fibroblasts that remodel ECM back towards a normal state. Indeed, the ability of fibroblasts to remodel ECM has been extensively studied, especially in the context of lung fibrosis [30]. This line of investigation requires future studies in the context of muscle to determine how fibrosis can be eliminated through the inhibition of Activin/Myostatin. All of these are valid points but we haven't tested any of these.

Muscle fibrosis is primarily caused by the action of SVMPs present in the snake venom. *C. atrox* venom was selected because of high SVMP percentage in the venom. In summary, we show that attenuating myostatin/activin signalling improves muscle regeneration after *C. atrox* venom damage. However, the muscle was by no means completely regenerated as evident by ongoing remodelling of dystrophin and lack of effective angiogenesis in the damaged muscle. As previously stated, this could be due to the presence of long-acting metalloprotease activity, which continually induces injury. Hence, we propose that as well as using reagents that promote regeneration (here sActRIIB), a second line of intervention based on inhibiting key harmful molecules in venom would be advisable. The latter could involve antivenom or small molecule inhibitors [31]. We note that there are presently several approved antivenoms being used in cases of rattlesnake envenomation including ANAVIP and CroFab [32]. Although these are very effective, there are reports of persistent cellular damage even after their use [33]. Hence it would be intriguing to test their efficacy in

preventing muscle damage when anti-venom therapy is combined with regeneration-promoting agents like sActRIIB.

## References

1. Longbottom, J., et al., *Vulnerability to snakebite envenoming: a global mapping of hotspots*. *Lancet*, 2018. **392**(10148): p. 673-684.
2. Williams, D.J., et al., *Strategy for a globally coordinated response to a priority neglected tropical disease: Snakebite envenoming*. *PLoS Negl Trop Dis*, 2019. **13**(2): p. e0007059.
3. Lomonte, B. and J.M. Gutierrez, *Phospholipases A2 from viperidae snake venoms: how do they induce skeletal muscle damage?* *Acta Chim Slov*, 2011. **58**(4): p. 647-59.
4. Gutierrez, J.M. and A. Rucavado, *Snake venom metalloproteinases: their role in the pathogenesis of local tissue damage*. *Biochimie*, 2000. **82**(9-10): p. 841-50.
5. Markland, F.S., *Snake venoms and the hemostatic system*. *Toxicon*, 1998. **36**(12): p. 1749-800.
6. Severyns, M., et al., *Case Report: Bothrops lanceolatus Snakebite Surgical Management-Relevance of Fasciotomy*. *Am J Trop Med Hyg*, 2018. **99**(5): p. 1350-1353.
7. Silva, A., et al., *Clinical and Pharmacological Investigation of Myotoxicity in Sri Lankan Russell's Viper (Daboia russelii) Envenoming*. *PLoS Negl Trop Dis*, 2016. **10**(12): p. e0005172.
8. Gutierrez, J.M., et al., *Why is Skeletal Muscle Regeneration Impaired after Myonecrosis Induced by Viperid Snake Venoms?* *Toxins (Basel)*, 2018. **10**(5).
9. Ruha, A.M., et al., *The Epidemiology, Clinical Course, and Management of Snakebites in the North American Snakebite Registry*. *J Med Toxicol*, 2017. **13**(4): p. 309-320.
10. Jia, Y., I. Lopez, and P. Kowalski, *Toxin transcripts in Crotalus atrox venom and in silico structures of toxins*. *J Venom Res*, 2020. **10**: p. 18-22.
11. Calvete, J.J., et al., *Exploring the venom proteome of the western diamondback rattlesnake, Crotalus atrox, via snake venomomics and combinatorial peptide ligand library approaches*. *J Proteome Res*, 2009. **8**(6): p. 3055-67.
12. Williams, H.F., et al., *Mechanisms underpinning the permanent muscle damage induced by snake venom metalloprotease*. *PLoS Negl Trop Dis*, 2019. **13**(1): p. e0007041.
13. Collins, C.A., et al., *Stem cell function, self-renewal, and behavioral heterogeneity of cells from the adult muscle satellite cell niche*. *Cell*, 2005. **122**(2): p. 289-301.
14. Theret, M., F.M.V. Rossi, and O. Contreras, *Evolving Roles of Muscle-Resident Fibro-Adipogenic Progenitors in Health, Regeneration, Neuromuscular Disorders, and Aging*. *Front Physiol*, 2021. **12**: p. 673404.
15. Yang, W. and P. Hu, *Skeletal muscle regeneration is modulated by inflammation*. *J Orthop Translat*, 2018. **13**: p. 25-32.
16. Langley, B., et al., *Myostatin inhibits myoblast differentiation by down-regulating MyoD expression*. *J Biol Chem*, 2002. **277**(51): p. 49831-40.
17. Amthor, H., et al., *Muscle hypertrophy driven by myostatin blockade does not require stem/precursor-cell activity*. *Proc Natl Acad Sci U S A*, 2009. **106**(18): p. 7479-84.
18. Li, Z.B., H.D. Kollias, and K.R. Wagner, *Myostatin directly regulates skeletal muscle fibrosis*. *J Biol Chem*, 2008. **283**(28): p. 19371-8.

19. Relizani, K., et al., *Blockade of ActRIIB signaling triggers muscle fatigability and metabolic myopathy*. Mol Ther, 2014. **22**(8): p. 1423-1433.
20. van Putten, M., et al., *Natural disease history of the D2-mdx mouse model for Duchenne muscular dystrophy*. FASEB J, 2019. **33**(7): p. 8110-8124.
21. Ownby, C.L., *Pathogenesis of Hemorrhage Induced by Rattlesnake Venoms and Their Purified Hemorrhagic Toxins*, in *Vascular Endothelium: Physiological Basis of Clinical Problems*, J.D. Catravas, et al., Editors. 1991, Springer US: Boston, MA. p. 276-276.
22. Han, H.Q., et al., *Myostatin/activin pathway antagonism: molecular basis and therapeutic potential*. Int J Biochem Cell Biol, 2013. **45**(10): p. 2333-47.
23. Collins-Hooper, H., et al., *Propeptide-mediated inhibition of myostatin increases muscle mass through inhibiting proteolytic pathways in aged mice*. J Gerontol A Biol Sci Med Sci, 2014. **69**(9): p. 1049-59.
24. Chan, A.S.M., et al., *Bone Geometry Is Altered by Follistatin-Induced Muscle Growth in Young Adult Male Mice*. JBMR Plus, 2021. **5**(4): p. e10477.
25. Zhang, L., et al., *Pharmacological inhibition of myostatin suppresses systemic inflammation and muscle atrophy in mice with chronic kidney disease*. FASEB J, 2011. **25**(5): p. 1653-63.
26. Rossi, J.F., et al., *Interleukin-6 as a therapeutic target*. Clin Cancer Res, 2015. **21**(6): p. 1248-57.
27. Wang, X., et al., *Diverse effector and regulatory functions of fibro/adipogenic progenitors during skeletal muscle fibrosis in muscular dystrophy*. iScience, 2023. **26**(1): p. 105775.
28. Giuliani, G., M. Rosina, and A. Reggio, *Signaling pathways regulating the fate of fibro/adipogenic progenitors (FAPs) in skeletal muscle regeneration and disease*. FEBS J, 2022. **289**(21): p. 6484-6517.
29. Fiore, D., et al., *Pharmacological blockage of fibro/adipogenic progenitor expansion and suppression of regenerative fibrogenesis is associated with impaired skeletal muscle regeneration*. Stem Cell Res, 2016. **17**(1): p. 161-9.
30. McKleroy, W., T.H. Lee, and K. Atabai, *Always cleave up your mess: targeting collagen degradation to treat tissue fibrosis*. Am J Physiol Lung Cell Mol Physiol, 2013. **304**(11): p. L709-21.
31. Puzari, U., P.A. Fernandes, and A.K. Mukherjee, *Advances in the Therapeutic Application of Small-Molecule Inhibitors and Repurposed Drugs against Snakebite*. J Med Chem, 2021. **64**(19): p. 13938-13979.
32. Brandehoff, N., et al., *Total CroFab and Anavip Antivenom Vial Administration in US Rattlesnake Envenomations: 2019-2021*. J Med Toxicol, 2023. **19**(3): p. 248-254.
33. Trautman, W. and A. Pizon, *Severe, persistent thrombocytopenia in Crotalus horridus envenomation despite antivenom: A retrospective review*. Toxicol, 2023. **224**: p. 107029.

**Funding** The authors would like to thank the Medical Research Council, UK (reference: MR/W019353/1 & Integrative Toxicology Training Partnership–PhD studentship) for their funding support.

## Primary Antibodies

<b>Antigen</b>	<b>Type</b>	<b>Immunoglobulin</b>	<b>Host Species</b>	<b>Dilution Ratio</b>	<b>Supplier</b>
MYHIII	Monoclonal	IgG	Mouse	1:200	DSHB
Collagen IV	Polyclonal	IgG	Rabbit	1:200	Abcam
Dystrophin	Polyclonal	IgG	Rabbit	1:200	Santa Cruz Biotechnology
Laminin	Polyclonal	IgG	Mouse	1:200	Sigma L9393
CD31	Monoclonal	IgG2a	Rat	1:200	AbD serctec

## Secondary antibodies

<b>Antibody</b>	<b>Immunoglobulin</b>	<b>Host Species</b>	<b>Dilution Ratio</b>	<b>Supplier</b>
Alexa flour 488 anti-mouse	IgG	Goat	1:200	Invitrogen
Alexa flour 594 anti-rabbit	IgM	Goat	1:200	Invitrogen
Alexa flour 594 anti-rat	IgG	Goat	1:200	Invitrogen
Fibrinogen-FITC anti-human	IgG	Rabbit	1:50	Dako

**Supplementary Materials:** Table S1: Primary and secondary antibodies used in this study.



**Data Availability Statement:** All data from this study are included within this manuscript.

**Conflicts of Interest:** The authors declare no conflict of interest.



## **2.3 Mesenchymal stem cells-derived secretome improves skeletal muscle regeneration following Russell's Viper-induced muscle damage**

### **Authors**

**Medha Sonavane<sup>1</sup>, Ali Alqallaf<sup>2,3</sup>, Robert D. Mitchel<sup>4</sup>, Ketan Patel<sup>2\*</sup>, and Sakthivel Vaiyapuri<sup>1\*</sup>**

<sup>1</sup>School of Pharmacy, University of Reading, Reading, RG6 6UB, United Kingdom

<sup>2</sup>School of Biological Sciences, University of Reading, Reading, RG6 6UB, United Kingdom

<sup>3</sup>Medical Services Authority, Ministry of Defence, Kuwait

<sup>4</sup>Micregen Ltd, Thames Valley Science Park, Reading, RG2 9LH, United Kingdom

\*Corresponding authors

*In preparation for publication*

### **Contribution to this chapter**

#### **Experimental contribution**

- Study design
- Animal work: dosing, dissections
- Tissue preparation: Muscle blocking, cryo-sectioning
- Staining and imaging- Staining muscle for histology and immunohistochemistry using various antibodies, imaging the sections

#### **General contribution**

- Data collection and analysis
- Preparing original figures
- Writing original manuscript

## **Abstract**

India is termed the 'snakebite capital' of the world, with around 58,000 annual deaths. Moreover, the number of snakebite-induced permanent disabilities is much higher in India. The medically important species in India are often called the 'Big Four' snakes (Russell's viper, cobra, krait, and saw-scaled viper). The Russell's viper (*Daboia russelii*) is alone responsible for around 60% of the total envenomation cases and most of the disabilities and morbidities are associated with this species. The venom of Russell's viper is rich in phospholipase A<sub>2</sub> and snake venom metalloproteases. These toxins can cause severe tissue necrosis and permanent muscle damage by affecting the skeletal muscle's innate regeneration ability and immune responses. A favourable microenvironment is essential for effective muscle regeneration following damage. Stem cells secrete a plethora of cytokines and growth factors that are essential for effective muscle regeneration. Recent studies have shown that the regenerative effects of stem cells are mainly due to the paracrine activities of these secretory molecules. Therefore, we determined the effects of secretome derived from adipose-derived mesenchymal stem cells on the skeletal muscle damage induced by Russell's viper venom. The secretome had a positive influence on overall muscle regeneration. The secretome showed improved proliferation and fusion of muscle stem cells, induced hypertrophy in the regenerating muscle fibres, and promoted muscle fibre differentiation and maturation following venom-induced damage. Moreover, the secretome improved the synthesis and remodelling of extracellular matrix proteins which are critical for muscle regeneration. Overall, this study demonstrates that this cell-free secretome can be an attractive regenerative medicine to treat/prevent viper venom-induced muscle damage.

## **1. Introduction**

Snakebite envenoming (SBE) is a high-priority neglected tropical disease that predominantly affects rural communities living in developing countries [1]. SBE-induced deaths and disabilities are largely reported in South Asian countries, sub-Saharan Africa and Central and South America [2, 3]. The global burden of SBE is around 138,000 deaths and approximately 400,000 permanent disabilities [4]. India is termed the 'snakebite capital' of the world, as it suffers around 58,000 SBE-induced

deaths annually [2]. In India, most mortalities and morbidities are mainly due to four medically important snakes: Russell's viper (*Daboia russelii*), the Indian cobra (*Naja naja*), the common krait (*Bungarus caeruleus*), and saw-scaled viper (*Echis carinatus*), which are often called as the 'Big Four' snakes [5]. Indian cobra and common krait belong to the Elapidae family, and Russell's and saw-scaled vipers belong to the Viperidae family. SBE-related morbidities and permanent disabilities are often associated with viper envenomation. Amongst the Big Four snakes, Russell's viper (RV) is one of the widely distributed snake species and is responsible for around 60% of total incidents [2] and around 80% of SBE-induced deaths and disabilities [6]. RV envenomation is clinically complex and can affect several tissues and organs in the body. The pathological symptoms of RV envenomation include systemic effects such as coagulopathies, haemorrhage, neurotoxicity, and acute kidney injury and local effects including necrosis and muscle damage, which often lead to permanent disabilities [6-8].

RV venom is rich in phospholipase A<sub>2</sub> (PLA<sub>2</sub>) and snake venom metalloproteases (SVMPs). These toxins are associated with skeletal muscle damage and cause permanent disabilities. PLA<sub>2</sub> can damage the phospholipid bilayer of the cells leading to tissue necrosis. Whereas SVMPs induce intra-muscular bleeding, destroy microcapillary networks, damage the extracellular matrix (ECM), impact proliferation and migration of satellite cells, affect angiogenesis and alter immune responses [9-11]. The leading cause of permanent muscle damage is impaired muscle regeneration although skeletal muscle has innate regenerative capacity. The regeneration of skeletal muscle involves the removal of cell debris and necrotic tissues, activation of satellite cells, myogenesis and then maturation of regenerated myofibers. This process is managed by immune cells, inflammatory responses, and satellite cells along with other cell types. Numerous cytokines and growth factors released from these cells facilitate effective muscle regeneration [12]. They promote activation, proliferation, and differentiation of satellite cells (SC), reconstruction and remodelling of ECM and angiogenesis [13, 14]. The impact of developing a favourable microenvironment on muscle regeneration following acute damage has been studied for several years. The favourable microenvironment supports the migration, activation, and differentiation of SCs by altering their signalling pathways. Additionally, the microenvironment facilitates the reconstruction of damaged

ECM, which provides structural support to SCs [15]. The microenvironment also promotes communications between immune cells, fibroblasts, and SCs [16]. Microenvironments also play an essential role in influencing the metabolism and availability of nutrients for SCs [19]. Therefore, it is critical to provide a favourable microenvironment to support muscle regeneration following muscle damage.

Mesenchymal stem cells are adult multipotent stem cells originally identified in bone marrow, but thereafter, they have been isolated from various tissues in the body. The adipose-derived mesenchymal stem cells (ADMSC) were first isolated in 2001 and since then they have become an attractive tool for tissue engineering and regenerative medicine due to their self-renewal ability and multipotency [20, 21]. ADMSCs were initially thought to influence muscle regeneration through their ability to recognise damaged tissues and differentiate into required cell types [22]. However, recent studies have shown that the paracrine activity of the molecules secreted (secretome) by these cells is more responsible for tissue repair than the cells themselves [23]. Indeed, the secretome from ADMSC has been shown to influence skeletal muscle regeneration in acute and chronic skeletal muscle injuries [24].

The primary impact of snake venom is often acute; however, the venom is active in the tissue causing persistent and prolonged tissue damage like chronic muscle damage [10]. In viper venom-induced muscle damage, the coordination between immune and myogenic cells is disrupted, and the venom destroys the microcapillary network which prevents the infiltration of immune cells [25]. Hence, we hypothesise that the presence of ADMSC-derived secretome will promote effective muscle regeneration following viper venom-induced muscle damage by creating a favourable microenvironment for the coordinated actions of muscle regeneration. Therefore, here we evaluated the impact of ADMSC secretome on skeletal muscle regeneration following RV-venom-induced damage.

## **2 Material and Methods**

### *Materials*

RV venom in lyophilised form was sourced from Kentucky Reptiles Zoo (USA). The venom was obtained from multiple specimens bred and maintained in captivity. Sources of all the other chemicals are specified where necessary.

### *2.1 Ethical statement*

The experiments conducted in this study were carried out following the regulations and principles of the British Home Office (Project license number: PPL70/7516) and the Animals (Scientific Procedures) Act 1986. All the procedures used in this study were reviewed and approved by the University Research Ethics Committee.

### *2.2 Enzymatic assays*

The metalloprotease activity of RV venom was assessed using DQ-gelatin, a fluorogenic substrate (ThermoFisher Scientific, UK). Briefly, RV venom (50 µg/mL) and DQ-gelatin (10 µg/mL) were mixed with phosphate buffer saline (PBS, pH 7.4) in 100 µL of total reaction volume and incubated at 37°C. The level of fluorescence was measured using spectrofluorimetry (FLUOstar OPTIMA, Germany) at an excitation wavelength of 485 nm and 520 nm emission wavelength. Similarly, the PLA<sub>2</sub> activity of the RV venom was assessed using the EnzChek™ Phospholipase A<sub>2</sub> Assay Kit. The level of fluorescence was measured with excitation at 460 nm and emission at 515/575 nm by spectrofluorimetry.

### *2.3 Production of ADMSC secretome*

Human ADMSCs [Life Technologies, UK (Cat-510070)] were cultured in MesenPro RS media (Life Technologies, UK). The media was supplemented with 1% (w/v) L-glutamine (Life Technologies, UK) and 1% (w/v) penicillin/streptomycin (Life Technologies, UK). The experiments were carried out with the cells at passage 6 or below to maintain consistency of the generated secretome. To collect ADMSC secretome, the adherent cells were harvested using enzymatic dissociation and centrifuged at 300 g for 5 minutes at room temperature. The cells were washed in sterile PBS and repeated the centrifugation step three times. The cells were then divided into small aliquots of 1x10<sup>6</sup> cells per tube. The aliquots were pelleted down, covered with 400 µL of fresh sterile PBS, and kept at room temperature for 24 hours. The supernatant was then collected without disturbing the pellet by

centrifuging the cells, filtered through a 0.2 µm syringe filter and centrifuged at 2000 g for 20 min at room temperature.

#### *2.4 Administration of venom and ADMSC secretome in mice*

The CD1 mice (5 – 6 weeks old) were obtained from Charles River, UK. The mice were divided into two cohorts (n=3). One cohort received a dose of ADMSC secretome (100 µL) via intraperitoneal route 24 hours and again 2 hours before venom injection. For intramuscular injections, the mice were anaesthetised using 3.5% (v/v) isoflurane in oxygen. Then, the mice received an intramuscular injection of RV venom 66 ng/g (i.e., 5 times lower than the reported LD<sub>50</sub> value for RV venom) animal weight and injection volume of 30 µL into the left tibialis anterior (TA) muscle. On day 5, mice were euthanised using CO<sub>2</sub> inhalation followed by cervical dislocation. The TA muscle was dissected, weighed and immediately frozen using liquid nitrogen-cooled isopentane. Muscles were then stored at -80°C until further use. The frozen TA muscles were mounted using Tissue-TEK® OCT medium, and sections of 13 µm thickness were obtained using cryo-microtome.

#### *2.5 Haematoxylin and Eosin (H&E) staining*

H&E staining is a routine histology method that helps visualise cellular organisation and tissue morphology. H&E stain the nuclei of the cells blue and cytoplasm pink. Briefly, the muscle slides were taken out from a -80°C freezer and brought to room temperature (left for 15 minutes). The muscle sections were washed three times (10 min each) with PBS to rehydrate and remove any debris. Next, the sections were immersed in Harris haematoxylin for 1 minute and then washed under tap water for 2 minutes to remove the excess dye. Then, the sections were immersed twice in 70% acidic alcohol (70% ethanol, 0.1% HCl) to remove any background stain. After this, the slides were washed under running tap water for 5 minutes. Next, the sections were counterstained in 1% (w/v) eosin for 2 minutes. Then, subsequent dehydration steps were carried out by immersing the slides in different ethanol concentrations, including 70%, 90%, and 100%. Finally, the slides were immersed twice in Xylene for 3 minutes to displace the ethanol. The slides were mounted using the DPX (Dyestine, Plastisizer and Xylene) mounting media. The area of the fibres with centrally located nuclei (CLN) was measured using ImageJ (1.52a). 50 fibres were measured from each muscle and then averaged to calculate the cumulative values.



## 2.6 Immunohistochemistry

The hydrophobic barrier was created around the muscle sections using a pap pen. After washing three times with PBS, the slides were incubated in permeabilisation buffer [20 mM HEPES, 3 mM MgCl<sub>2</sub>, 50 mM NaCl, 0.05% (w/v) sodium azide, 300 mM sucrose and 0.5% (v/v) Triton X-100]. After 15 minutes, the sections were washed with PBS to remove the permeabilisation buffer and then blocked using a blocking-wash buffer solution [PBS with 5% (v/v) foetal bovine serum, 0.05% (v/v) Triton X-100] for 30 minutes at room temperature. Primary antibodies were prepared in the blocking-wash buffer at a dilution of 1:200 and then incubated with the sections overnight at 4°C. The next day, the unbound primary antibodies were washed using blocking-wash buffer three times and incubated with secondary antibodies conjugated with different fluorophores at a dilution of 1:200 (in blocking-wash buffer) for 1 hour in the dark at room temperature. The slides were then mounted with a Dako (Agilent Technologies, UK) fluorescent mounting medium containing 4,6-diamidino-2-phenylindole (DAPI) to visualise nuclei. The muscle sections were visualised and imaged using a Zeiss AxioImager fluorescence microscope. To measure the structural maturity of collagen IV, laminin and dystrophin, fluorescence intensity was used as a relative measure [10]. The intensity was measured using ImageJ (1.52a). 50 fibres with CLN from each mouse were measured for each marker. The data for individual markers was then averaged for statistical analysis.

## 2.7 Statistical analysis

The sections were imaged in parts and then merged using the ImageJ mosaic tool. Different tools in ImageJ were used for measuring the area or intensity of different markers. Zeiss AxioImager (4.9.1) software was used to select different channels or filters during imaging. GraphPad Prism 7 was used for statistical analysis, and the P values were calculated using the student t-test or one-way ANOVA for multiple comparisons.

## 3 Results

### 3.1 RV venom shows high SVMP and PLA<sub>2</sub> activity

The local tissue damage occurs mainly because of two toxin families found in viper venoms, SVMPs and PLA<sub>2</sub>. The SVMP activity of different concentrations of RV venom was measured using DQ-

gelatin. RV venom showed a dose-dependent increase in SVMP activity (**Figure 1A**). The PLA<sub>2</sub> activity was analysed using a commercially available kit. The RV venom showed significant PLA<sub>2</sub> activity at 25 µg/mL compared to the negative control (**Figure 1B**).

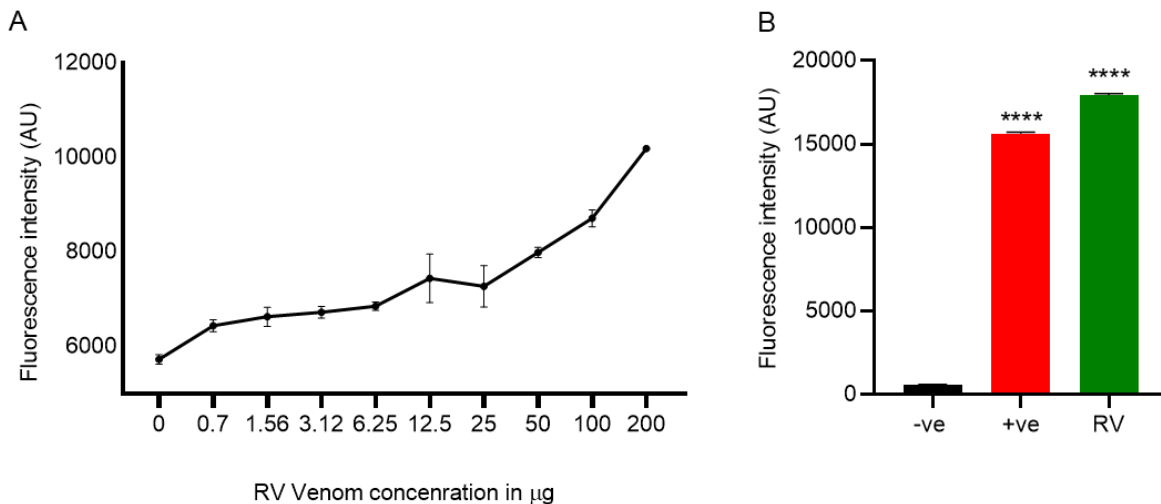


**Figure 1: SVMP and PLA<sub>2</sub> activity of RV venom.** SVMP activity of RV venom was measured by a DQ-gelatin assay using different concentrations of venom (**A**). PLA<sub>2</sub> activity of RV venom at 50 µg was measured using a commercially available kit (**B**). The negative control (-ve) contains the assay buffer with the substrate. The positive control (+ve) is purified PLA<sub>2</sub> from bee venom provided with the assay kit. Data represent mean ± S.D. (n=3). The p-value shown is calculated by one-way ANOVA with multiple comparison tests for independent variables using GraphPad Prism. (\*\*\*\*p<0.0001).

### 3.2 ADMSC secretome promotes muscle regeneration following RV-venom-induced damage

The ADMSC secretome was injected via intraperitoneal route 24 and again 2 hours before intramuscular injection of venom and muscles were collected on day 5 (**Figure 2A**). During the dissection, we observed that the skin around the site of venom injection developed scar tissues. The venom-injected muscles were necrotic, and even the tendons were loosely attached to the other exterior muscles (**Figure 2B**). The data suggests that the venom-induced TA muscle weight is around 10 µg less than the undamaged muscle. However, there was no significant difference between the secretome treated and the undamaged muscle (**Figure 2C**). These data suggest that the secretome has improved venom-induced muscle loss.

The characteristic feature of the regenerating fibres is CLN. Therefore, the regeneration progress was analysed by measuring the cross-section areas of the fibres with CLN. In the presence of secretome, the muscle has shown significant improvement in regeneration. Due to the administration of secretome, the regenerating fibres are one-fold bigger than the regenerating fibres from control muscles (**Figure 3A-3B**).

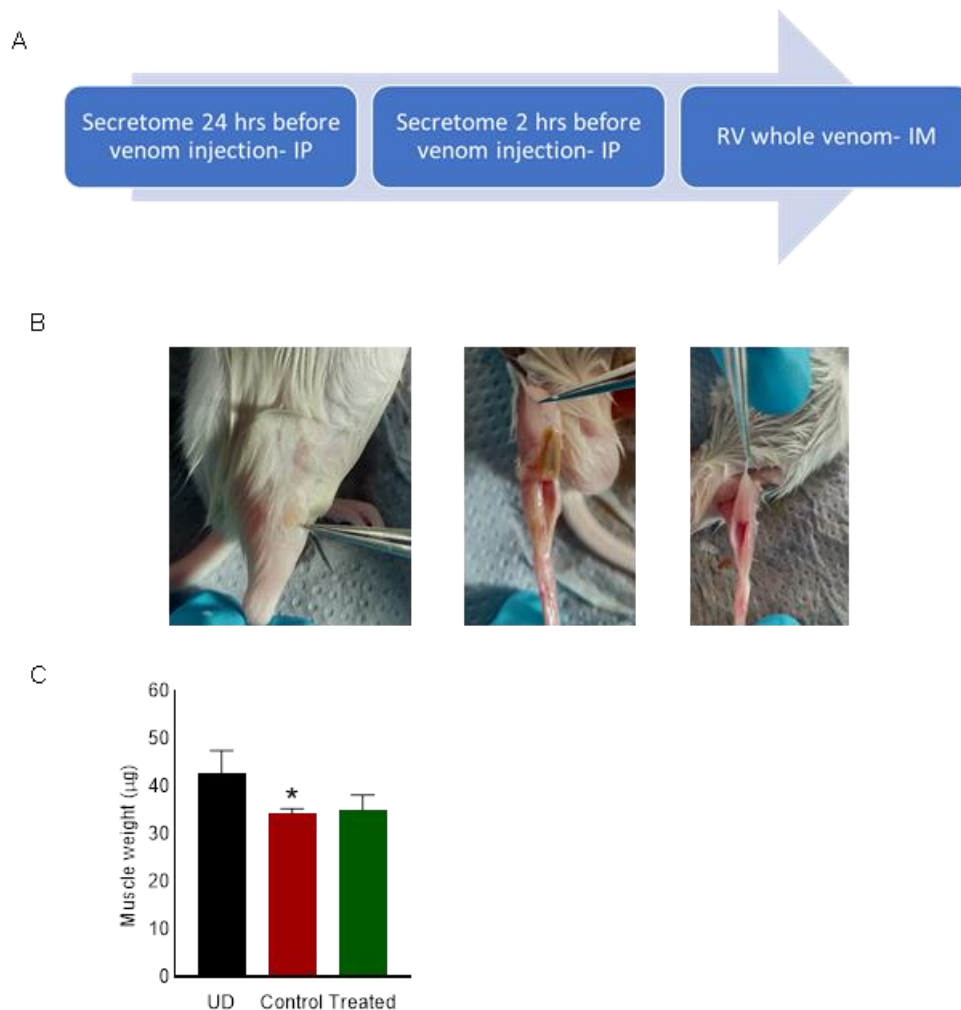


**Figure 2: Injection time points, tissue necrosis by RV venom and the effect of secretome on TA muscle mass.** The secretome was injected at two different time points before the administration of RV venom and muscle samples were obtained on day 5 (**A**). During dissection, scar tissue was observed on the skin, near the site of RV venom injection and extensive tissue necrosis was evident in the RV-injected muscle (**B**). The TA muscle weights of different cohorts of mice were compared with the undamaged (UD) TA muscle. Data represent mean  $\pm$  S.D. (n=3 mice). The *p* value shown is calculated by one-way ANOVA using GraphPad Prism. (\**p*<0.05).

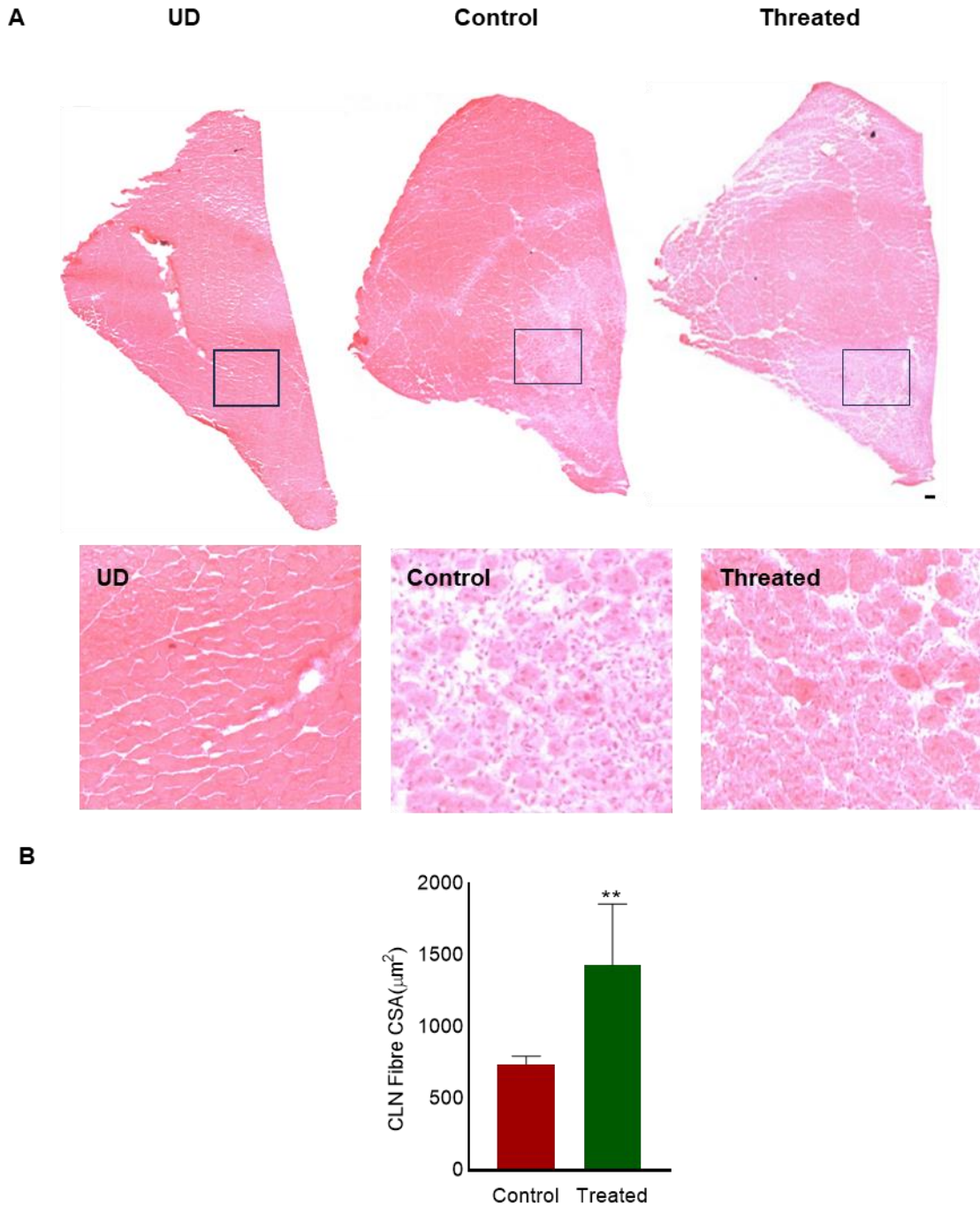


**Figure 3: ADMSC secretome resulted in larger regenerating fibres.** H&E staining was performed on TA muscle sections and the presented images are representative of whole muscle and magnified region of undamaged (UD), control (RV venom injection) and treated (secretome +RV venom injections) (**A-B**) muscles on day 5. The cross-section area of regenerating fibres was calculated by measuring the area of fibres with CLN. 50 regenerating fibres were measured from each muscle using ImageJ. The p-value shown is as calculated by the student T-test followed using GraphPad Prism (\*\* $p < 0.01$ ). The scale bar represents 100 µM.

### 3.3 ADMSC secretome enhances the proliferation and maturation of myoblasts

The embryonic myosin heavy chain (MYHIII) is a contractile protein expressed during the early stage of muscle regeneration. To determine the impact of secretome on MYHIII expression, the cross-section area of the fibres with CLN expressing MYHIII was measured. The cross-section area of the fibres from secretome-treated cohorts was around one-fold higher than the control muscles (**Figure 4A**). The regenerating muscle fibres were also analysed for the presence of 2a and 2b myosin chains, which are the isoforms of the fast myosin heavy chain. The 2a expression was not observed in the fibres with CLN (**Figure 4B**). Whereas CLN fibres with 2b expression were significantly larger in secretome-treated muscle samples (**Figure 4C**).

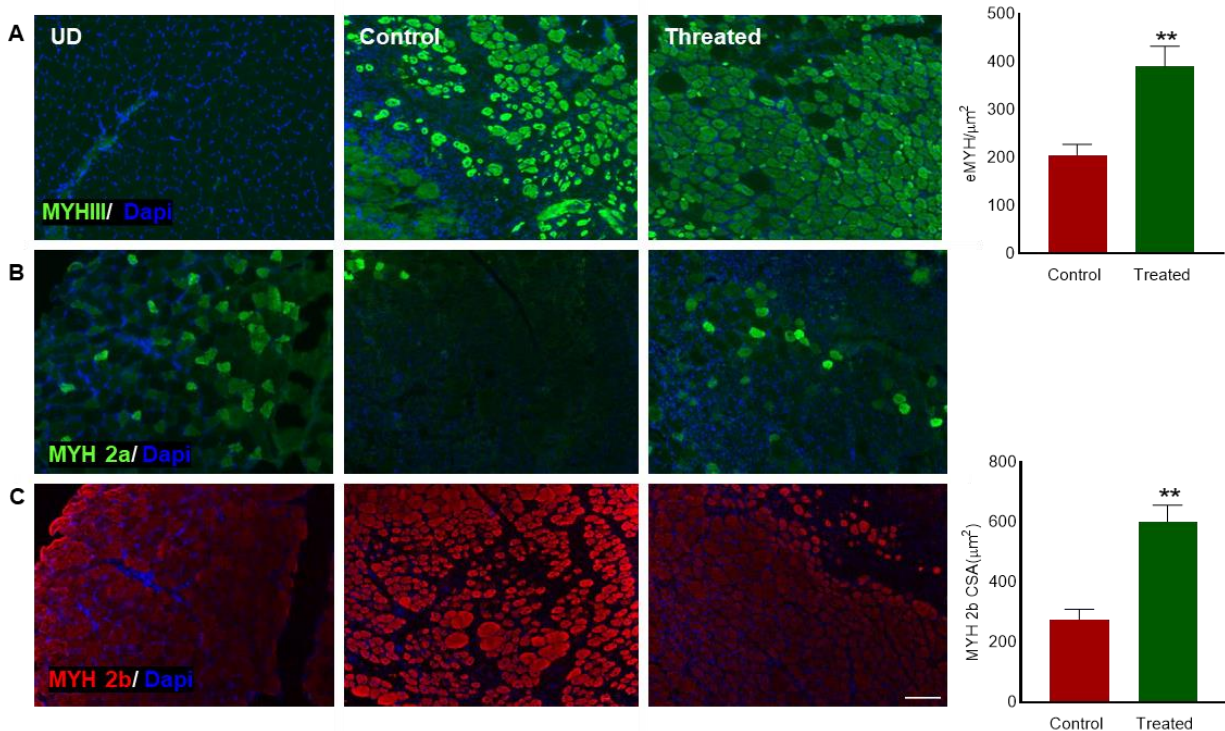


**Figure 4: Effect of secretome on myogenesis.** The muscle sections were stained with fluorescently-tagged MYHIII (A), MYH-2a (B) and 2b (C) antibodies. DAPI was used to stain the nuclei. The cross-section area of newly regenerating fibres was calculated by measuring MYHIII positive fibres with CLN. No 2a stained fibres with CLN were observed on day 5. The cross-section area of differentiated fibres was calculated using 2b positive fibres with CLN. We analysed the damaged area from the TA muscle obtained from each animal cohort (n=3), and 30 muscle fibres were measured from each mouse muscle. The cross-section area was measured using ImageJ (1.52a). The *p* value shown is as calculated by the student T-test using GraphPad Prism (\*\**p*<0.01). The scale bar represents 100 µM.

### 3.4 ADMSC secretome improved the reconstruction and remodelling of the ECM

To determine the impact of secretome on the construction and remodelling of the ECM, proteins such as collagen IV and dystrophin were analysed in TA muscle sections. Collagen IV and dystrophin are important structural proteins in the ECM and are essential to maintaining the structural integrity of the ECM. Compared to the undamaged muscles, the fluorescence intensity of collagen IV (**Figure 5A**) or dystrophin (**Figure 5B**) in CLN fibres in venom-treated muscles was 20% lower indicating the impact of venom on the ECM. In contrast, there was no significant difference in the intensity of the secretome-treated muscle fibres for collagen IV and dystrophin compared to the undamaged muscle. There was no statistical difference in the levels of laminin compared to any cohorts (**Figure 5C**). This lack of significance is most likely due to the high variability in the measured intensities.

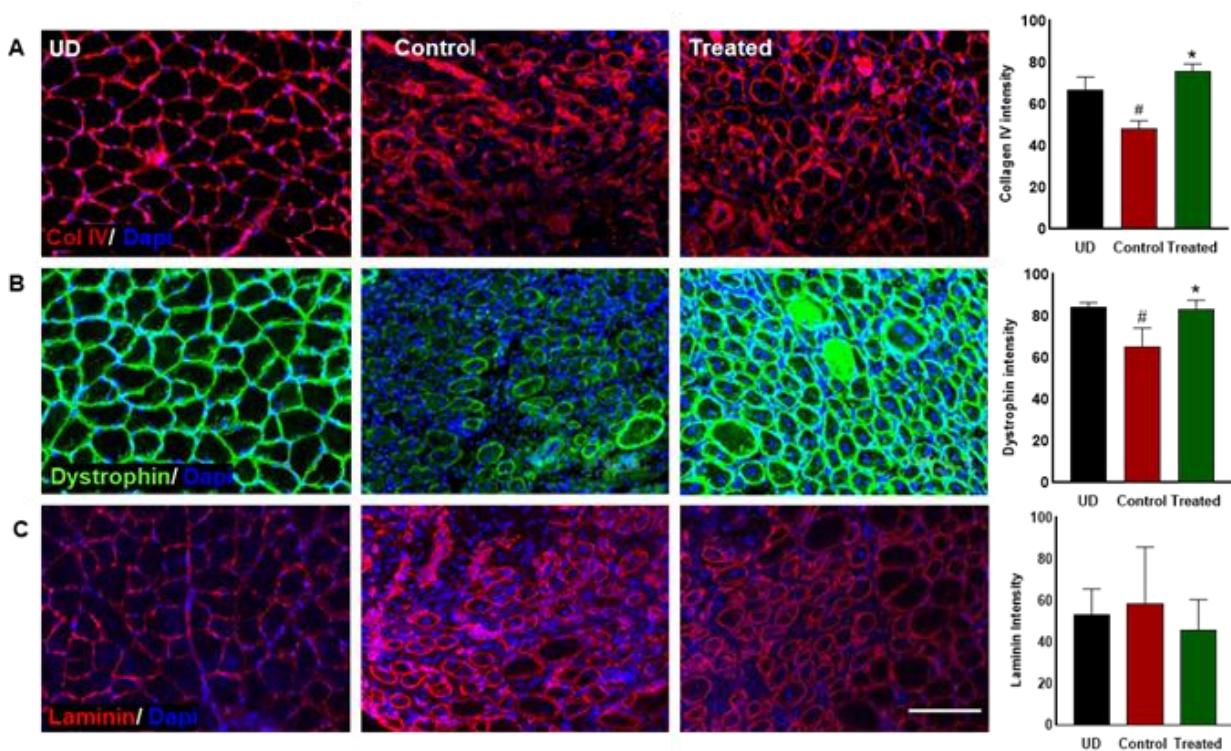


**Figure 5: Effect of secretome on ECM remodelling.** The muscle sections were stained by fluorescently tagged collagen IV, laminin, and dystrophin antibodies. Nuclei were stained using DAPI. The images shown are representative of undamaged muscle (UD), control (RV venom injected) and treated (secretome + RV venom injected) muscles on day 5. The maturity of the structure of collagen IV (**A**), dystrophin (**B**) and laminin (**C**) was measured by their representative intensity using ImageJ (1.52a). The  $p$  values shown are as calculated by the student T-test using GraphPad Prism ( $*p < 0.05$ ). The \* represents a comparison between the control and treated cohorts and # represents the comparison between the UD and either control or treated cohorts. The scale bar represents 100  $\mu\text{m}$ . We analysed the damaged area from the TA muscle obtained from each animal cohort ( $n=3$ ), and 50 muscle fibres were measured from the Ach muscle. The scale bar represents 100  $\mu\text{m}$

## 4 Discussion

Viper venoms can cause extensive damage to skeletal muscles, often leading to permanent disabilities. In SBE victims, bites mostly occur on the upper or lower limbs [26] and they can affect their mobility and productivity. In India, where RV envenomation is a prominent issue [2], the most vulnerable populations are agricultural workers. For them, mobility restriction or permanent disabilities can have extensive socioeconomic impacts as they may not be able to perform their occupations [27, 28]. Viper venoms are rich in toxins such as SVMPs, snake venom serine proteases and PLA<sub>2</sub>, along with other toxic and non-toxic components [29]. Viper envenomation can cause systemic haemotoxic effects and severe local myotoxic effects. Viper venoms affect natural muscle regeneration following damage through the actions of SVMPs and PLA<sub>2</sub>. These toxins cause severe damage to critical components such as the basement membrane, ECM, and satellite cells involved in effective muscle regeneration. PLA<sub>2</sub> affects the phospholipid bilayer of the cells which results in tissue necrosis. In contrast, SVMPs destroy collagen, a major component of the ECM, and have direct and indirect impacts on the proliferation of SCs. In addition, SVMPs damage the microvascular network and affect the angiogenesis [10]. RV venom composition is well studied, and it has significant variations in the biochemical composition, which results in diverse pathological outcomes and potency. The venom of RV present in eastern India has been reported to be the most potent compared to the specimens found in other regions [30]. The most abundant toxins in RV venom are PLA<sub>2</sub> and SVMPs [31]. The effect of these toxins along with other low abundant toxic and non-toxic families can induce severe muscle necrosis in RV envenomation victims. The most common local manifestations of RV envenomation include pain, swelling, blister formation, compartment syndrome, haemorrhage and necrosis [32]. Currently, surgical methods such as fasciotomy, tissue debridement and amputations are used to treat these local pathological effects, but they may result in permanent disabilities. Hence, developing an alternative, effective treatment solution is critical to improving the pathological outcome of viper envenomation-mediated muscle damage.

The skeletal muscle comprises myofibers, a vascular network, nerves, and connective tissues. The basic structural and functional unit of skeletal muscle is myofiber [33, 34]. The skeletal muscle can

regenerate after injury, and the regeneration is a robust process coordinated by immune and satellite cells. The satellite cells are quiescent in the adult muscles but can quickly get activated upon muscle injury. Skeletal muscle regeneration is achieved through an overlapping response of immune cells, and activation, differentiation, and fusion of SCs and maturation and remodelling of the newly regenerated myofibers. To complete this process, a favourable microenvironment is essential. The skeletal muscle is a very adaptive tissue, and its regenerative potential is altered during acute and chronic muscle degeneration. In muscle regeneration post viper venom-induced muscle damage, the immune cell response is dysregulated, and the activation, proliferation, and fusion capacity of SCs are affected [10, 35]. The infiltration of immune cells is often absent around the damaged muscle [25]. Hence, enrichment of this microenvironment can promote the regeneration of damaged skeletal muscle as stem cells actively communicate and interact with their surrounding environment [36]. The use of secretomes of various stem cell populations is one of the emerging methods of tissue engineering and regenerative medicine. Due to their inherent potency, ADMSCs have become an exciting target in regenerative medicine. ADMSCs are easily accessible and are known to modulate endogenous regulation of muscle regeneration [37, 38]. Recent studies suggest that the regenerative effects of stem cells are mainly due to the factors secreted by the stem cells rather than the cells themselves. The paracrine effects of secretome regulate essential processes like proliferation of SCs, angiogenesis, ECM remodelling and immune responses through secretion of cytokines and growth factors including but not limited to interleukins, insulin-like growth factor-1, hepatocyte growth factors, vascular endothelial growth factors [39-41]. Therefore, in the present study, the ADMSC-derived secretome was administered into an experimental mouse model before the intramuscular injections of the RV venom and the impact of the secretome on the venom-induced muscle damage was analysed. The results demonstrate that the secretome improved the regeneration of muscle fibres. Indeed, it improved the early stage of muscle regeneration as observed through the expression of myosin 2B on day 5. Moreover, the reconstruction and remodelling of the ECM were also improved by the secretome.

The paracrine signalling of secretome increases cell-cell communication and facilitates the proliferation and fusion of SCs [42, 43]. The secretome contains several factors like interleukins (IL-



6 and IL10), tumour necrotic factor- $\alpha$  (TNF- $\alpha$ ), and transforming growth factor- $\beta$  (TGF- $\beta$ ), which modulate the immune responses, reduce inflammation and promote tissue repair [44]. The insulin-like growth factors, fibroblast growth factors, and hepatocyte growth factors present in ADMSC secretome stimulate the activation and proliferation of SCs [45]. Extracellular vesicles are another important component of the secretome, packed with miRNA. Several studies suggest that this miRNA package can promote the proliferation and differentiation of SCs [46]. We observed in this study that the regenerating muscle fibres in the damaged area were significantly larger when treated with secretome. This finding supports the fact that the proliferation and fusion of SCs were enhanced by secretome treatment. To evaluate the effects of ADMSC secretome on newly formed regenerating fibres, we measured the cross-section area of the fibres expressing MYH-III. It is expressed during the early stage of muscle regeneration and significantly larger fibres in the secretome-treated animals suggesting that in the presence of secretome, the regeneration process was expedited [47]. The skeletal muscle contains different isoforms of muscle fibres. During the regeneration process, myoblasts express MYHIII, and these myoblasts fuse to form mature muscle fibres. In the murine model, isoforms 2a, 2x and 2b muscle fibres are observed, typically termed as fast twitch muscle fibres. In post-injury, the muscle needs high force, and fast contracting fibres, and these characteristics are associated with 2b fibres. In the present study, 2b fibres with CLN were analysed. The CSA of the fibres in the secretome-treated animals was larger than in the control animals. The cytokines and growth factors in the secretome promote fusion and maturation of the muscle fibres, and the increase in CSA suggests that the secretome induced hypertrophy in the muscle fibres, which is an indication of progress in regeneration. In RV-mediated muscle damage, lack of oxygen is an important factor for impaired muscle regeneration due to damage to the microcapillaries [48, 49]. The 2b fibres use anaerobic glycolysis as their ATP source, which might be why 2b fibres are observed in regenerated muscle following RV venom-induced muscle damage [50].

ADMSC secretome can promote the synthesis of ECM proteins. The extracellular vesicles carry numerous bioactive molecules including miRNAs and proteins that modulate cellular responses that are essential for remodelling the ECM [51]. Along with cytokines and growth factors, the secretome can produce certain ECM components. The angiogenic factors and anti-fibrotic factors are

responsible for the homeostasis of the ECM. Secretome can also modulate the matrix metalloproteases and their tissue-derived inhibitors. TGF- $\beta$  is a critical player in ECM synthesis and remodelling present in ADMSC secretome. TGF- $\beta$  can stimulate ECM protein synthesis, including collagen and laminin. The modulated immune responses can affect the levels of IL-6, which is essential for ECM modulation [23, 52]. The secretome of ADMSC has been effective in enhancing the synthesis and modulation of dystrophin, another key component in the muscle [53]. Due to all these paracrine effects from numerous secretory factors, the ADMSC secretome could expedite the synthesis and remodelling of the ECM in RV venom-mediated skeletal muscle damage as demonstrated in this study.

Overall, we demonstrated the effects of ADMSC-derived secretome on promoting skeletal muscle regeneration following RV venom-induced muscle damage. The secretome enhances muscle regeneration, induces hypertrophy in regenerating fibres, facilitates muscle fibre differentiation, and effectively achieves ECM remodelling. However, to test this effect in a more realistic scenario, analysing the regeneration effects of secretome post-venom-induced muscle damage is essential. It is also important to analyse the long-term repercussions, such as muscle fibrosis, and whether the secretome effectively reduces it. From the current study, we can interpret that the presence of ADMSC secretome positively impacts tissue regeneration in case of RV-induced muscle damage. These data reveal an exciting new opportunity to test regenerative medicine approaches for venom-induced skeletal muscle damage. However, there could be a few difficulties in using stem cell secretome as a treatment for SBE. The countries or the part of the countries where SBE is prevalent lack well-equipped medical facilities. The secretome must be stored and maintained at an ultralow temperature ( $-80^{\circ}\text{C}$ ) to maintain its functional integrity. The SBE victims are often from low-income backgrounds and the cost of treatment is critical for these victims. The cost of production, scalability, and storage of secretome may potentially increase the cost of treatment for SBE victims. However, these obstacles can be overcome by further research.

## References

1. Chippaux, J.P., *Snakebite envenomation turns again into a neglected tropical disease!* J Venom Anim Toxins Incl Trop Dis, 2017. **23**: p. 38.
2. Suraweera, W., et al., *Trends in snakebite deaths in India from 2000 to 2019 in a nationally representative mortality study.* Elife, 2020. **9**.
3. Chippaux, J.P., *Estimate of the burden of snakebites in sub-Saharan Africa: a meta-analytic approach.* Toxicon, 2011. **57**(4): p. 586-99.
4. Gutierrez, J.M., et al., *Snakebite envenoming.* Nat Rev Dis Primers, 2017. **3**: p. 17079.
5. Simpson, I.D. and R.L. Norris, *Snakes of medical importance in India: is the concept of the "Big 4" still relevant and useful?* Wilderness Environ Med, 2007. **18**(1): p. 2-9.
6. Ghosh, R., et al., *A retrospective study of clinico-epidemiological profile of snakebite related deaths at a Tertiary care hospital in Midnapore, West Bengal, India.* Toxicol Rep, 2018. **5**: p. 1-5.
7. Gopalakrishnan, M., et al., *A simple mortality risk prediction score for viper envenoming in India (VENOMS): A model development and validation study.* PLoS Negl Trop Dis, 2022. **16**(2): p. e0010183.
8. Senthikumar, S., et al., *Peripheral Arterial Thrombosis following Russell's Viper Bites.* TH Open, 2023. **7**(2): p. e168-e183.
9. Xiao, H., et al., *Snake Venom PLA(2), a Promising Target for Broad-Spectrum Antivenom Drug Development.* Biomed Res Int, 2017. **2017**: p. 6592820.
10. Williams, H.F., et al., *Mechanisms underpinning the permanent muscle damage induced by snake venom metalloprotease.* PLoS Negl Trop Dis, 2019. **13**(1): p. e0007041.
11. Sonavane, M., et al., *Intramuscular Bleeding and Formation of Microthrombi during Skeletal Muscle Damage Caused by a Snake Venom Metalloprotease and a Cardiotoxin.* Toxins (Basel), 2023. **15**(9).
12. Yang, W. and P. Hu, *Skeletal muscle regeneration is modulated by inflammation.* J Orthop Translat, 2018. **13**: p. 25-32.
13. Ceafalan, L.C., B.O. Popescu, and M.E. Hinescu, *Cellular players in skeletal muscle regeneration.* Biomed Res Int, 2014. **2014**: p. 957014.
14. Fu, X., H. Wang, and P. Hu, *Stem cell activation in skeletal muscle regeneration.* Cell Mol Life Sci, 2015. **72**(9): p. 1663-77.
15. Bloom, A.B. and M.H. Zaman, *Influence of the microenvironment on cell fate determination and migration.* Physiol Genomics, 2014. **46**(9): p. 309-14.
16. VanderVeen, B.N., E.A. Murphy, and J.A. Carson, *The Impact of Immune Cells on the Skeletal Muscle Microenvironment During Cancer Cachexia.* Front Physiol, 2020. **11**: p. 1037.

17. Chazaud, B., *Inflammation and Skeletal Muscle Regeneration: Leave It to the Macrophages!* Trends Immunol, 2020. **41**(6): p. 481-492.
18. Chen, Y.F., et al., *Immunometabolism of macrophages regulates skeletal muscle regeneration.* Front Cell Dev Biol, 2022. **10**: p. 948819.
19. Nguyen, J.H., et al., *The Microenvironment Is a Critical Regulator of Muscle Stem Cell Activation and Proliferation.* Front Cell Dev Biol, 2019. **7**: p. 254.
20. Zuk, P.A., et al., *Human adipose tissue is a source of multipotent stem cells.* Mol Biol Cell, 2002. **13**(12): p. 4279-95.
21. Tsuji, W., J.P. Rubin, and K.G. Marra, *Adipose-derived stem cells: Implications in tissue regeneration.* World J Stem Cells, 2014. **6**(3): p. 312-21.
22. Torres-Torrillas, M., et al., *Adipose-Derived Mesenchymal Stem Cells: A Promising Tool in the Treatment of Musculoskeletal Diseases.* Int J Mol Sci, 2019. **20**(12).
23. Baraniak, P.R. and T.C. McDevitt, *Stem cell paracrine actions and tissue regeneration.* Regen Med, 2010. **5**(1): p. 121-43.
24. Mitchell, R., et al., *Secretome of adipose-derived mesenchymal stem cells promotes skeletal muscle regeneration through synergistic action of extracellular vesicle cargo and soluble proteins.* Stem Cell Res Ther, 2019. **10**(1): p. 116.
25. Gutierrez, J.M., C.L. Ownby, and G.V. Odell, *Skeletal muscle regeneration after myonecrosis induced by crude venom and a myotoxin from the snake Bothrops asper (Fer-de-Lance).* Toxicon, 1984. **22**(5): p. 719-31.
26. Evers, L.H., et al., *Adder bite: an uncommon cause of compartment syndrome in northern hemisphere.* Scand J Trauma Resusc Emerg Med, 2010. **18**: p. 50.
27. Vaiyapuri, S., et al., *Snakebite and its socio-economic impact on the rural population of Tamil Nadu, India.* PLoS One, 2013. **8**(11): p. e80090.
28. Babo Martins, S., et al., *Assessment of the effect of snakebite on health and socioeconomic factors using a One Health perspective in the Terai region of Nepal: a cross-sectional study.* Lancet Glob Health, 2022. **10**(3): p. e409-e415.
29. Tasoulis, T. and G.K. Isbister, *A current perspective on snake venom composition and constituent protein families.* Arch Toxicol, 2023. **97**(1): p. 133-153.
30. Senji Laxme, R.R., et al., *Biogeographic venom variation in Russell's viper (Daboia russelii) and the preclinical inefficacy of antivenom therapy in snakebite hotspots.* PLoS Negl Trop Dis, 2021. **15**(3): p. e0009247.
31. Faisal, T., et al., *Proteomics, toxicity and antivenom neutralization of Sri Lankan and Indian Russell's viper (Daboia russelii) venoms.* J Venom Anim Toxins Incl Trop Dis, 2021. **27**: p. e20200177.
32. Mehta, S.R. and V.K. Sashindran, *Clinical Features And Management Of Snake Bite.* Med J Armed Forces India, 2002. **58**(3): p. 247-9.

33. Krauss, R.S. and A.P. Kann, *Muscle stem cells get a new look: Dynamic cellular projections as sensors of the stem cell niche*. *Bioessays*, 2023. **45**(5): p. e2200249.
34. Snow, M.H., *Myogenic cell formation in regenerating rat skeletal muscle injured by mincing. II. An autoradiographic study*. *Anat Rec*, 1977. **188**(2): p. 201-17.
35. Ryan, R.Y.M., et al., *Immunological Responses to Envenomation*. *Front Immunol*, 2021. **12**: p. 661082.
36. Morash, T., et al., *Mammalian Skeletal Muscle Fibres Promote Non-Muscle Stem Cells and Non-Stem Cells to Adopt Myogenic Characteristics*. *Fibers*, 2017. **5**(1): p. 5.
37. Forcales, S.V., *Potential of adipose-derived stem cells in muscular regenerative therapies*. *Front Aging Neurosci*, 2015. **7**: p. 123.
38. Kim, M., et al., *Muscle regeneration by adipose tissue-derived adult stem cells attached to injectable PLGA spheres*. *Biochem Biophys Res Commun*, 2006. **348**(2): p. 386-92.
39. Takahashi, M., et al., *Cytokines produced by bone marrow cells can contribute to functional improvement of the infarcted heart by protecting cardiomyocytes from ischemic injury*. *Am J Physiol Heart Circ Physiol*, 2006. **291**(2): p. H886-93.
40. Corti, S., et al., *Neural stem cells LewisX+ CXCR4+ modify disease progression in an amyotrophic lateral sclerosis model*. *Brain*, 2007. **130**(Pt 5): p. 1289-305.
41. Xu, L., et al., *Human neural stem cell grafts ameliorate motor neuron disease in SOD-1 transgenic rats*. *Transplantation*, 2006. **82**(7): p. 865-75.
42. Qazi, T.H., et al., *Biomaterials that promote cell-cell interactions enhance the paracrine function of MSCs*. *Biomaterials*, 2017. **140**: p. 103-114.
43. Kusuma, G.D., et al., *Effect of the microenvironment on mesenchymal stem cell paracrine signaling: opportunities to engineer the therapeutic effect*. *Stem cells and development*, 2017. **26**(9): p. 617-631.
44. Kyurkchiev, D., et al., *Secretion of immunoregulatory cytokines by mesenchymal stem cells*. *World J Stem Cells*, 2014. **6**(5): p. 552-70.
45. Daneshmandi, L., et al., *Emergence of the Stem Cell Secretome in Regenerative Engineering*. *Trends Biotechnol*, 2020. **38**(12): p. 1373-1384.
46. Shirazi, S., et al., *The importance of cellular and exosomal miRNAs in mesenchymal stem cell osteoblastic differentiation*. *Sci Rep*, 2021. **11**(1): p. 5953.
47. Lo Sicco, C., et al., *Mesenchymal Stem Cell-Derived Extracellular Vesicles as Mediators of Anti-Inflammatory Effects: Endorsement of Macrophage Polarization*. *Stem Cells Transl Med*, 2017. **6**(3): p. 1018-1028.
48. Escalante, T., et al., *Key events in microvascular damage induced by snake venom hemorrhagic metalloproteinases*. *J Proteomics*, 2011. **74**(9): p. 1781-94.
49. Chaillou, T., et al., *Effect of hypoxia exposure on the recovery of skeletal muscle phenotype during regeneration*. *Mol Cell Biochem*, 2014. **390**(1-2): p. 31-40.

50. Talbot, J. and L. Maves, *Skeletal muscle fiber type: using insights from muscle developmental biology to dissect targets for susceptibility and resistance to muscle disease*. Wiley Interdiscip Rev Dev Biol, 2016. **5**(4): p. 518-34.
51. Sheta, M., et al., *Extracellular Vesicles: New Classification and Tumor Immunosuppression*. Biology (Basel), 2023. **12**(1).
52. Xu, X., et al., *Effects of mesenchymal stem cell transplantation on extracellular matrix after myocardial infarction in rats*. Coron Artery Dis, 2005. **16**(4): p. 245-55.
53. Sandonà, M., et al., *Mesenchymal stromal cells and their secretome: new therapeutic perspectives for skeletal muscle regeneration*. Frontiers in Bioengineering and Biotechnology, 2021. **9**: p. 652970.



## **2.4 Intramuscular bleeding and formation of microthrombi during skeletal muscle damage caused by a snake venom metalloprotease and a cardiotoxin**

**Medha Sonavane<sup>1</sup>, José R. Almeida<sup>1</sup>, Elanchezhian Rajan<sup>1</sup>, Harry F. Williams<sup>2</sup>, Felix Townsend<sup>3</sup>, Ellie Cornish<sup>3</sup>, Robert D. Mitchell<sup>4</sup>, Ketan Patel<sup>3</sup> and Sakthivel Vaiyapuri<sup>1\*</sup>**

<sup>1</sup>School of Pharmacy, University of Reading, Reading, RG6 6UB, United Kingdom

<sup>2</sup>Toxiven Biotech Private Limited, Coimbatore-641042, Tamil Nadu, India

<sup>3</sup>School of Biological Sciences, University of Reading, Reading, RG6 6UB, United Kingdom

<sup>4</sup>Micregen Ltd, Thames Valley Science Park, Reading, RG2 9LH, United Kingdom

\*Corresponding author

*Published article*

### **Contribution to this chapter**

#### **Experimental contribution**

- Study design
- Tissue preparation: cryo-sectioning
- Staining and imaging- Staining muscle for histology and immunohistochemistry using various antibodies, imaging the sections

#### **General contribution**

- Data collection and analysis
- Preparing original figures
- Writing original manuscript



## **Abstract:**

The interactions between specific snake venom toxins and muscle constituents are the major cause of severe muscle damage that often results in amputations and subsequent socioeconomic ramifications for victims and/or their families. Therefore, improving our understanding of venom-induced muscle damage and determining the underlying mechanisms of muscle degeneration/regeneration following snakebites is critical to developing better strategies to tackle this issue. Here, we analysed the intramuscular bleeding and thrombosis in two different snake venom toxins [CAMP - *Crotalus atrox* metalloprotease (a PIII metalloprotease from the venom of this snake) and a three-finger toxin (CTX, cardiotoxin from the venom of *Naja pallida*)]-mediated muscle injuries in mice. Classically, these toxins represent diverse scenarios characterised by persistent muscle damage (CAMP) and successful regeneration (CTX) following acute damage, as normally observed in envenomation by most vipers and some elapid snakes of Asian, Australasian, and African origin, respectively. Our immunohistochemical analysis confirmed that both CAMP and CTX induced extensive muscle destruction on day 5, although, the effects of CTX were reversed over time. We identified the presence of fibrinogen and P-selectin exposure inside the damaged muscle sections, suggesting the signs of bleeding and the formation of platelet aggregates/microthrombi in tissues, respectively. Intriguingly, CAMP causes integrin shedding but does not affect any blood clotting parameters, whereas, CTX significantly extends the clotting time and has no impact on integrin shedding. The rates of fibrinogen clearance and reduction in microthrombi were greater in CTX-treated muscle compared to CAMP-treated. Together, these findings reveal novel aspects of venom-induced muscle damage and highlight the relevance of haemostatic events such as bleeding and thrombosis for muscle regeneration and provide useful mechanistic insights for developing better therapeutic interventions.

## **1. Introduction**

Snakebite envenoming (SBE) is one of the leading causes of mortality and morbidity among rural agricultural communities in many tropical countries [1,2]. SBE has been classified as a high

priority neglected tropical disease by the World Health Organisation (WHO) and causes around 150,000 deaths and 500,000 permanent disabilities worldwide every year [3]. Venom-induced skeletal muscle damage is a key factor for SBE-induced permanent disabilities [4]. Antivenoms are generally not beneficial in treating and preventing SBE-induced muscle damage as the large immunoglobulin molecules are unable to penetrate the damaged local tissues [5,6]. Moreover, the damaged blood vessels and blood clots (thrombi) in capillaries will restrict the blood flow to the affected tissues resulting in ischaemia further preventing the antivenom from reaching the damaged regions [7]. Extensive tissue damage can necessitate surgical procedures such as fasciotomy (to release the compartment pressure), debridement (to remove the affected tissues), and amputation (to completely remove the affected region/limb to prevent further damage and infection) to manage this condition [8]. Hence, improving our fundamental understanding of how venom toxins affect skeletal muscle and induce permanent muscle damage is critical for developing effective treatments for SBE-induced muscle damage. Venoms include both enzymatic and non-enzymatic proteins and small peptides [9,10]. Specific venom toxins such as three-finger toxins (3FTx), phospholipase A<sub>2</sub>, and snake venom metalloproteases (SVMP) are the main components responsible for causing local tissue damage [7]. An earlier study from our group reported the mechanisms of action involved in skeletal muscle damage induced by a P-III SVMP (named CAMP) from the venom of *Crotalus atrox* in comparison to a 3FTx (cardiotoxin, CTX) from the venom of *Naja pallida* [11]. CAMP induced extensive damage to the extracellular matrix and affected the functions of satellite cells and angiogenesis, impairing muscle regeneration. In contrast, CTX caused muscle necrosis although it did not affect satellite cells or the extracellular matrix (ECM), with full recovery from the damage achieved through the innate muscle regeneration process [11]. However, the ability of these venom toxins to induce bleeding and thrombosis while causing muscle damage was not compared simultaneously in the previous study. The circulatory system and continuous blood supply play a vital role in tissue repair and muscle regeneration [12]. However, damage to vasculature results in excessive bleeding, subsequent thrombus formation and inflammatory responses in the affected muscle [7,13,14]. Moreover, thrombus formation will rapidly consume circulating platelets and/or coagulation factors leading to venom-induced consumption coagulopathy, which further augments bleeding [15,16]. Therefore, it is critical to establish the mechanisms of action of muscle-damaging

enzymatic and non-enzymatic venom components in inducing intramuscular bleeding and thrombosis. In this study, we determined the ability of CAMP and CTX in inducing bleeding and microthrombi formation in locally damaged skeletal muscle. The outcomes of this study provide evidence to demonstrate the impact of enzymatic (CAMP) and non-enzymatic (CTX) venom toxins in inducing bleeding and thrombosis in muscle tissues.

## **2. Materials and Methods**

### *2.1. Materials used*

Purified CTX from the venom of the Red-spitting Cobra (*Naja pallida*) was purchased from Latoxan (France). Lyophilised *Crotalus atrox* (*C. atrox*) venom was purchased from Sigma Aldrich (UK). CAMP was purified from the venom of *C. atrox* using a combination of ion exchange and gel filtration chromatography, as reported previously [11].

### *2.2. Injection of venom toxins in TA muscles of mice*

All mice were anaesthetised using 3.5% (v/v) isoflurane in oxygen and then kept at 2% (v/v) isoflurane throughout the procedure. 1 µg of purified CAMP or CTX in 30 µL volume was injected into the left TA muscle. The right TA muscle was given a control injection of 30 µL of PBS. PBS injections were given to test if there is any tissue damage caused due to insertion of the injection needles. The mice were monitored for either 5 or 10 days before being sacrificed by CO<sub>2</sub> inhalation and muscles collected.

### *2.3. Dissection and processing of tissues*

The tissue samples were collected on either day 5 or 10 following the injection of toxins. Animals were dissected, and the TA muscles were carefully removed by the tendon to avoid mechanical damage. The muscle samples were frozen in liquid nitrogen-cooled isopentane and kept at -80°C. The muscle tissue was then embedded in Tissue-TEK<sup>®</sup> OCT (Optimal Cutting Temperature) medium and sliced into 13 µm thick transverse sections using a cryo-microtome. These sections were placed onto glass slides and stored at -80°C until required for further use.

### *2.4. H & E staining of muscle sections*

The muscle sections on glass slides were removed from the -80°C freezer and left at room temperature for 15 minutes, and later, the sections were soaked in PBS to rehydrate them. The slides were then submerged in Harris haematoxylin stain for two minutes. After rinsing the slides in water for two minutes, they were dipped twice in 70% acidic alcohol [70% ethanol (v/v) and 0.1% (v/v) HCl] and then rinsed again in water for five minutes. The slides were then placed into a container with a 1% (w/v) eosin solution for two minutes and then transferred into a slide container containing 70% ethanol. The slides were dehydrated by soaking them in 70%, 90%, and 100% ethanol. Finally, the slides were transferred into xylene for two rounds of three minutes. The sections were fixed using distyrene, plasticiser and xylene (DPX) mounting media. The muscle sections were observed and imaged using a Zeiss AxioImager light microscope (five sections per mouse, 5 mice for each cohort).

### *2.5. Immunohistochemistry of TA muscle sections*

Using a wash buffer solution [PBS with 5% (v/v) foetal bovine serum and 0.05% (v/v) Triton X-100], FITC-conjugated primary antibodies were diluted at 1:50 dilution. The slides were cleaned and hydrated three times with PBS for 5 minutes each. Next, permeabilisation buffer [20 mM HEPES, 3 mM MgCl<sub>2</sub>, 50 mM NaCl, 0.05% (w/v) sodium azide, 300 mM sucrose and 0.5% (v/v) Triton X-100] was added and allowed to incubate for 15 minutes. A blocking wash buffer was added and incubated for 30 minutes. The pre-made primary antibodies were added, and the slides were incubated for 1 hour at room temperature. Unbound antibodies were washed off, and the slides were mounted in 6-diamino-2-phenylindole (DAPI) containing mounting media. The sections (five sections per mouse and five mice for each cohort) were visualised, and the images were obtained using a Zeiss AxioImager fluorescence microscope. For fibrinogen, the whole muscle image which was made using multiple images of that muscle at 10x objective, was analysed using threshold analysis. The baseline threshold was set using the muscle image of an undamaged mouse. For P-selectin and integrin, multiple images for each muscle section from each mouse were taken using a 40x objective. Using the Image J 3D analysis tool, the baselines were set using undamaged contralateral muscle and then quantified the number and area of thrombi. For each mouse, the values were calculated as mean and then analysed together with the data obtained from all animals.

## 2.6. ROTEM analysis

The ROTEM Delta analyser by Werfen, UK was used to study the effects of CAMP and CTX on human whole blood clotting. Intem and extem analyses were conducted to determine the impact of venom toxins on intrinsic and extrinsic pathways of blood clotting, respectively. Fitem analysis was carried out to determine the effects of toxins on clotting in the absence of platelets, while aptem analysis was completed to assess the impact of venom toxins on blood clotting in the lack of fibrinolysis. The blood was collected from healthy human volunteers after informed consent. 5 mL blood was collected from each individual in an EDTA tube. In each assay, 8  $\mu$ M of CAMP or 50  $\mu$ M of CTX was mixed with 300  $\mu$ l of citrated whole human blood and pre-set volumes of respective reagents for different assays according to the manufacturer's instructions. The blood samples were recalcified using a startem reagent (0.2 M  $\text{CaCl}_2$  in HEPES buffer, pH 7.4), and clotting was initiated using intrinsic (partial thromboplastin phospholipid from rabbit brain and ellagic acid) and extrinsic clotting activators (recombinant tissue factor, phospholipids, and heparin). The fitem (cytochalasin D and 0.2 M  $\text{CaCl}_2$  in HEPES buffer, pH 7.4) and aptem (aprotinin and 0.2M  $\text{CaCl}_2$  in HEPES buffer, pH 7.4) assays were performed using specific reagents before the initiation of clotting using the extem activation reagent. Various parameters of whole blood coagulation were analysed using ROTEM assays.

## 2.7. Statistical analysis

All statistical analyses were performed using GraphPad Prism 8. Based on the data type, an unpaired student t-test or one-way ANOVA was used to calculate the  $p$  values to determine the statistical significance. All the staining and analysis were performed blindly by individuals who were not involved in experimental procedures in mice.

## 3. Results

### 3.1. CAMP and CTX induce damage to the tibialis anterior (TA) muscle in mice

To determine the impact of CAMP and CTX in inducing bleeding and thrombosis in skeletal muscle, they [1  $\mu$ g of CAMP or CTX in 30  $\mu$ L of phosphate-buffered saline (PBS)] were intramuscularly injected into the TA muscles of mice. The muscles were collected on days 5 and 10 and used for

further analysis. The histological analysis of the muscles using haematoxylin & eosin (H&E) staining confirmed the quality of muscle sections. The undamaged control muscle (injected with the same volume of PBS) displayed a normal morphology (**Figure 1A**), whereas CTX and CAMP-treated muscles showed clear signs of damage (**Figure 1B and 1C**). The infiltration of immune cells was evident in the damaged areas of the muscles treated with CTX and CAMP on day 5. However, on day 10, the muscles showed signs of recovery (presence of centrally located nuclei in myofibres with reduced spaces between them, reduced infiltrated immune cells and clusters of small fibres), especially in CTX-damaged tissues. This data confirms that both CTX and CAMP damaged the TA muscle as previously reported [11].

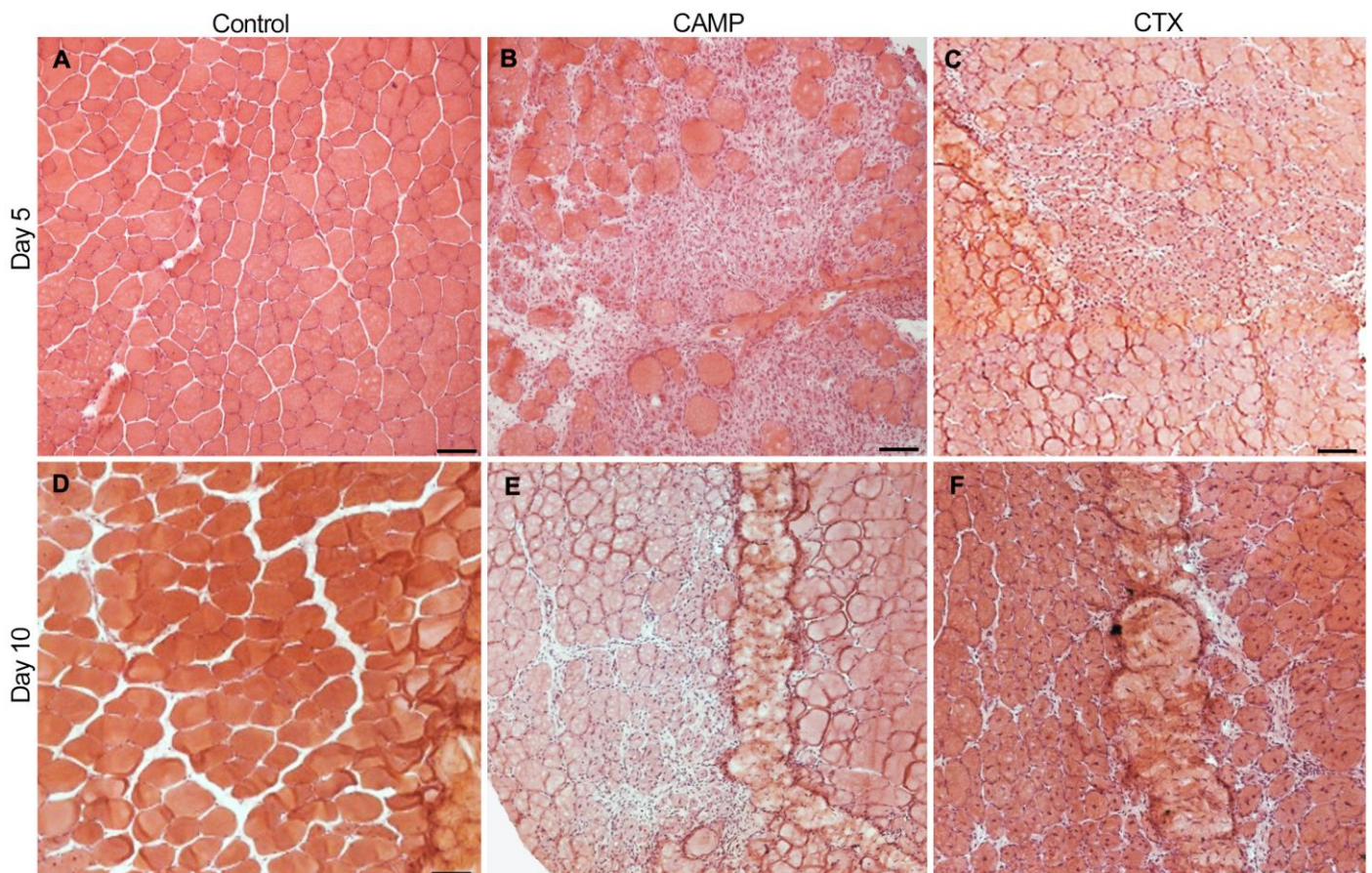


**Figure 1. H and E staining of TA muscles treated with CAMP or CTX on days 5 and 10.** The TA muscles of mice that were treated with PBS (**A, D**), CAMP (**B, E**) and CTX (**C, F**) were collected on days 5 and 10 following the injection of toxins, and their sections were analysed by H and E staining. The thickness of the muscle sections was 13  $\mu\text{m}$ . The scale bar represents 100  $\mu\text{m}$ . The images shown are representative of experiments performed using five mice in each cohort.

### *3.2. CAMP and CTX induce bleeding in damaged muscle*

Fibrinogen is a highly abundant clotting protein in the blood, and it acts as a scaffold for platelet aggregation and thrombus formation. Therefore, the presence of fibrinogen was measured as a marker for bleeding in the muscle sections. CTX- and CAMP-treated muscle sections on days 5 and 10 along with control muscles were stained using FITC-labelled anti-fibrinogen antibodies. The control muscle showed no fibrinogen, indicating that there was no bleeding in the undamaged tissues (**Figure 2A**). However, CAMP-treated muscle sections showed the presence of fibrinogen on day 5 (on average 25% fluorescence intensity) although it was significantly reduced by day 10 to roughly 12-13% (**Figure 2B**). Similarly, the administration of CTX induced bleeding in the muscle on day 5, with a significant reduction on day 10. The percentage of fibrinogen was largely reduced by day 10 compared to day 5 in CTX-treated sections. Although CTX-treated muscle presented significantly higher fibrinogen in the muscle sections than CAMP on day 5, the clearance rate was greater with a reduction from an initial 50% to 3% by day 10 in CTX-treated muscle. The presence of fibrinogen in both toxin-treated muscles indicated intramuscular bleeding, although we cannot rule out the staining of thrombi as they also contain fibrinogen.

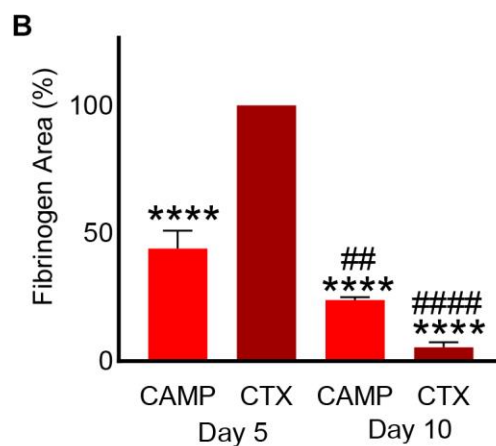
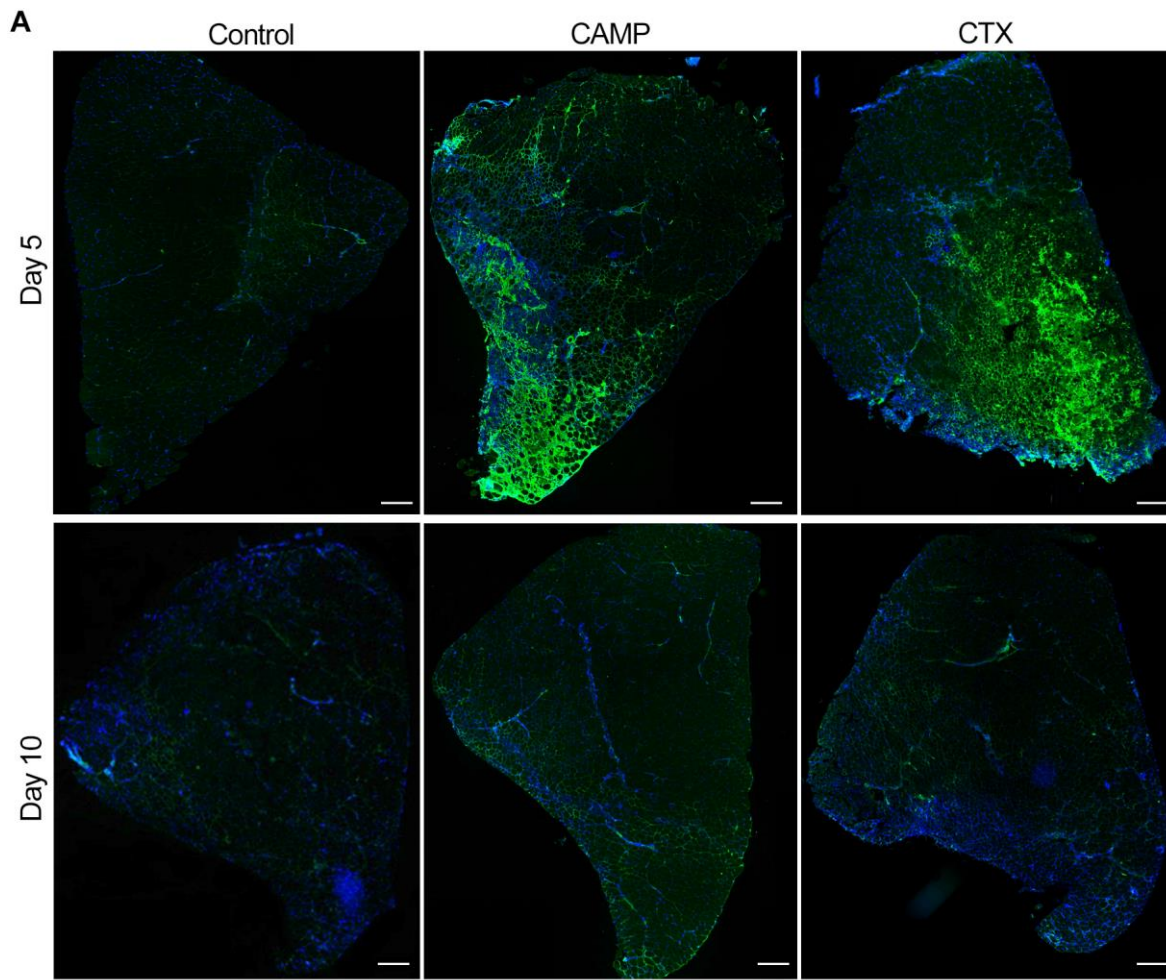


**Figure 2. Intramuscular bleeding in muscles treated with CAMP and CTX.** FITC-labelled anti-fibrinogen antibodies were used to stain CAMP and CTX-treated muscle sections along with controls and analyse the extent of bleeding in the muscle at 5- and 10-day post-injection of toxins. DAPI was used to stain the nuclei. **A**) Representative images of control, CAMP and CTX-treated TA muscles at days 5 and 10. The bar diagram (**B**) shows the level of fluorescence at days 5 and 10 in CAMP and CTX-treated muscles, and their comparisons. The percentage of fibrinogen area was calculated by dividing the fibrinogen-stained area by the total muscle area. The columns represent mean  $\pm$  S.D. ( $n = 5$  mice for each cohort, five sections per mouse). \*\*\*\* $p < 0.0001$  when compared to the level of fluorescence obtained at day 5 in CTX-treated muscle, which was taken as 100% to



calculate the relative difference in others. ## $p < 0.01$  and #### $p < 0.0001$  when comparing CAMP and CTX-treated muscle at day 10 with their corresponding values at day 5. Student's two-tailed t-test was used for independent variables. The scale bars represent 100  $\mu\text{m}$ .

### 3.3. *Microthrombi formation in CTX and CAMP-damaged muscles*

Microthrombi are small blood clots or aggregates of platelets and fibrin formed in capillaries and/or tissues. Upon stimulation of platelets, the inside-out signalling to the integrin  $\alpha\text{IIb}\beta\text{3}$  switches its conformation from a low-affinity state to a high-affinity state for fibrinogen binding, which causes aggregation of platelets by using fibrinogen as a scaffold [17]. Similarly, P-selectin is secreted from  $\alpha$ -granules upon activation. Both of these factors play a critical role in the formation of platelet-mediated blood clots [17]. Therefore, the presence of integrin  $\alpha\text{IIb}\beta\text{3}$  and P-selectin exposure on the surface of platelets confirms the existence of platelet aggregates/thrombi. The muscle sections obtained from CTX and CAMP-treated mice were stained with FITC-labelled anti-integrin  $\alpha\text{IIb}\beta\text{3}$  and anti-P-selectin antibodies.

In CAMP-treated muscle, there was no detectable level of fluorescence observed for integrin  $\alpha\text{IIb}\beta\text{3}$  on either day 5 or 10 (**Figure 3**). However, CTX-treated muscle on days 5 and 10 displayed the presence of microthrombi as measured through the level of fluorescence for integrin  $\alpha\text{IIb}\beta\text{3}$ . Moreover, in CTX-treated muscles, the frequency of microthrombi was significantly reduced by day 10 compared to day 5, although the area of the microthrombi within the muscle remains the same.

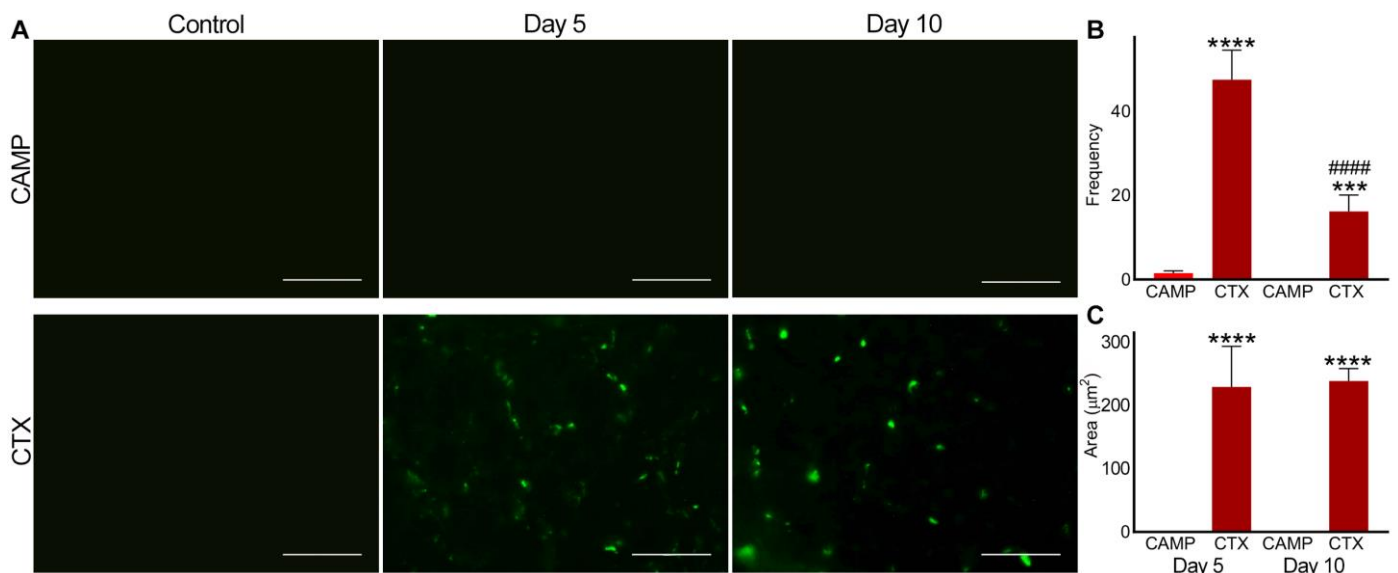
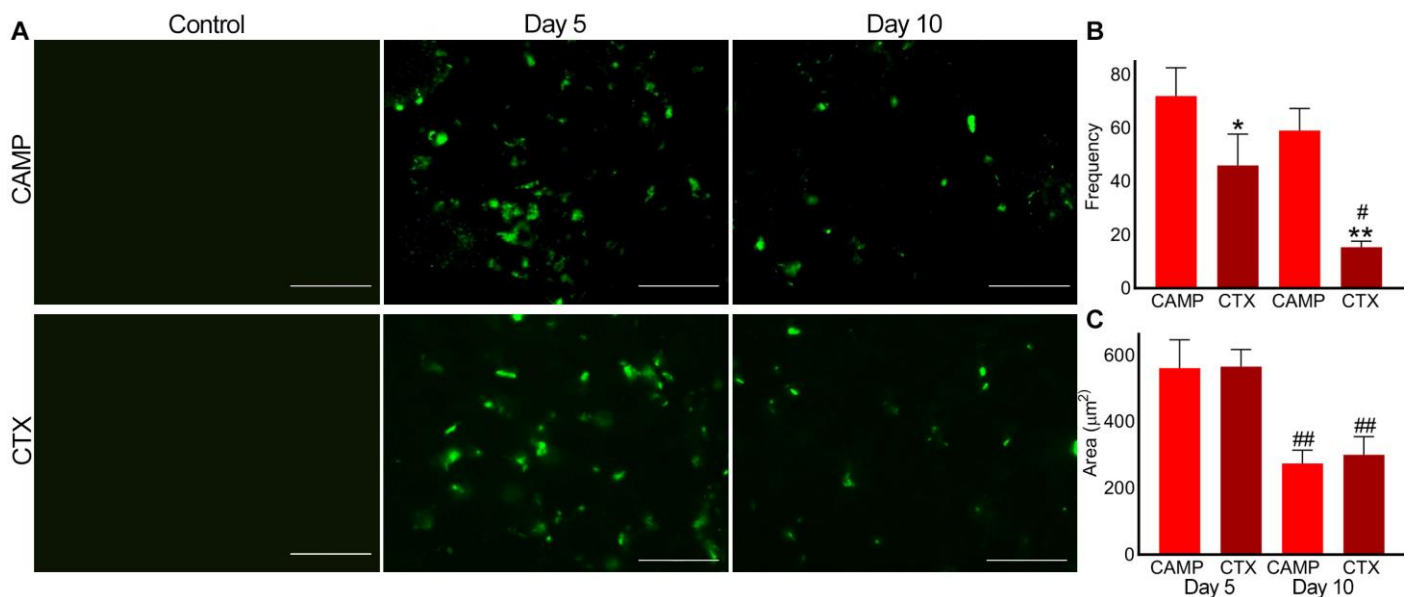


Figure 3. Microthrombi formation in CAMP and CTX-damaged muscle by staining integrin  $\alpha\text{IIb}\beta_3$ . FITC-conjugated anti-integrin  $\alpha\text{IIb}\beta_3$  antibodies were used to stain and analyse microthrombi formation in TA muscles injected with PBS (control), CAMP or CTX on days 5 and 10 post-injection of toxins. A) the images shown are representative of experiments performed with five mice in each cohort. Muscle sections were imaged at 40x magnification. Images were analysed using ImageJ 3D object counter to obtain the frequency (B) and area (C) of the microthrombi in CAMP and CTX-treated muscles. The columns represent the mean  $\pm$  S.D. ( $n=5$  mice for each cohort, five sections per mouse). \*\*\*\* $p<0.0001$  when comparing CTX with CAMP on the corresponding day. ##### $p<0.0001$  when compared to CTX at day 5. One-way ANOVA followed by Tukey's test was used to analyse the data. The scale bars represent 50  $\mu\text{m}$ .

Similarly, P-selectin was absent in the control muscle sections (**Figure 4**). However, it was evident in CAMP and CTX-treated muscle sections on days 5 and 10 confirming the presence of microthrombi. On day 5, the frequency of microthrombi was around 20% higher in CAMP-treated muscles compared to CTX-treated muscles, although there was no difference in the size of the thrombi. Even on day 10, the frequency of the microthrombi was around 40% higher in CAMP-damaged muscles compared to CTX-treated muscles. However, CTX-treated muscles showed a significant reduction in microthrombi frequency of around 50% on day 10. The area of microthrombi was reduced by almost 50% on day 10 in both CAMP- and CTX-treated muscles compared to day 5.



**Figure 4. Microthrombi formation in CAMP and CTX-induced muscle damage using P-selectin as a marker.** FITC-conjugated mouse anti-P-selectin antibodies were used to stain and analyse microthrombi formation in mouse TA muscle injected with PBS (control), CAMP or CTX. **A)** the images shown are representative of experiments performed with five mice. The muscle sections were imaged at 40x magnification. Images were analysed using ImageJ 3D object counter to obtain the frequency (**B)** and area (**C)** of the microthrombi in CAMP and CTX-treated muscles. The columns represent mean  $\pm$  S.D. (n=5 mice for each cohort, five sections per mouse). \* $p < 0.05$ , and \*\* $p < 0.01$  when compared with CAMP on the corresponding day. # $p < 0.05$  and ## $p < 0.01$  when compared with the same toxin on day 5. One-way ANOVA followed by Tukey's test was used to analyse the data. The scale bars represent 50  $\mu\text{m}$ .

### 3.4. CTX extends clotting time

To determine the direct effects of CAMP and CTX on blood clotting in human blood under *in vitro* settings, a rotational thromboelastometry (ROTEM) analysis was performed using human-citrated whole blood. The data of the intem analysis, which evaluates the intrinsic and common pathways, confirmed that clotting was delayed when CTX was added to whole blood (**Figure 5A**). Moreover, it reduced the fibrinolysis by around 30% compared to the controls. However, there was no significant difference in the size (area under the curve) or clot firmness (data not shown) between the control and CTX-induced clots. Similarly, the extem analysis, which evaluates the extrinsic and common pathways, showed a delay in clotting time and reduced fibrinolysis in CTX-treated blood (**Figure 5B**). The impact of CTX on clotting, independently of platelets, was determined by fibtem analysis. This assay confirmed that clotting time was delayed, although clot firmness and size remained unchanged (**Figure 5C**). The aptem analysis (in the absence of fibrinolysis) suggested that CTX delayed blood clotting but slightly accelerated clot formation time compared to CAMP

**(Figure 5D).** These results indicate that CTX affects blood clotting through multiple coagulation pathways independently of platelets and fibrinolysis. When similar experiments were performed using CAMP, it showed no major changes in clotting time, clot formation time, clot firmness or lysis compared to the controls in any analysis. Only in extem analysis, CAMP delayed the clot formation time by around 10%.

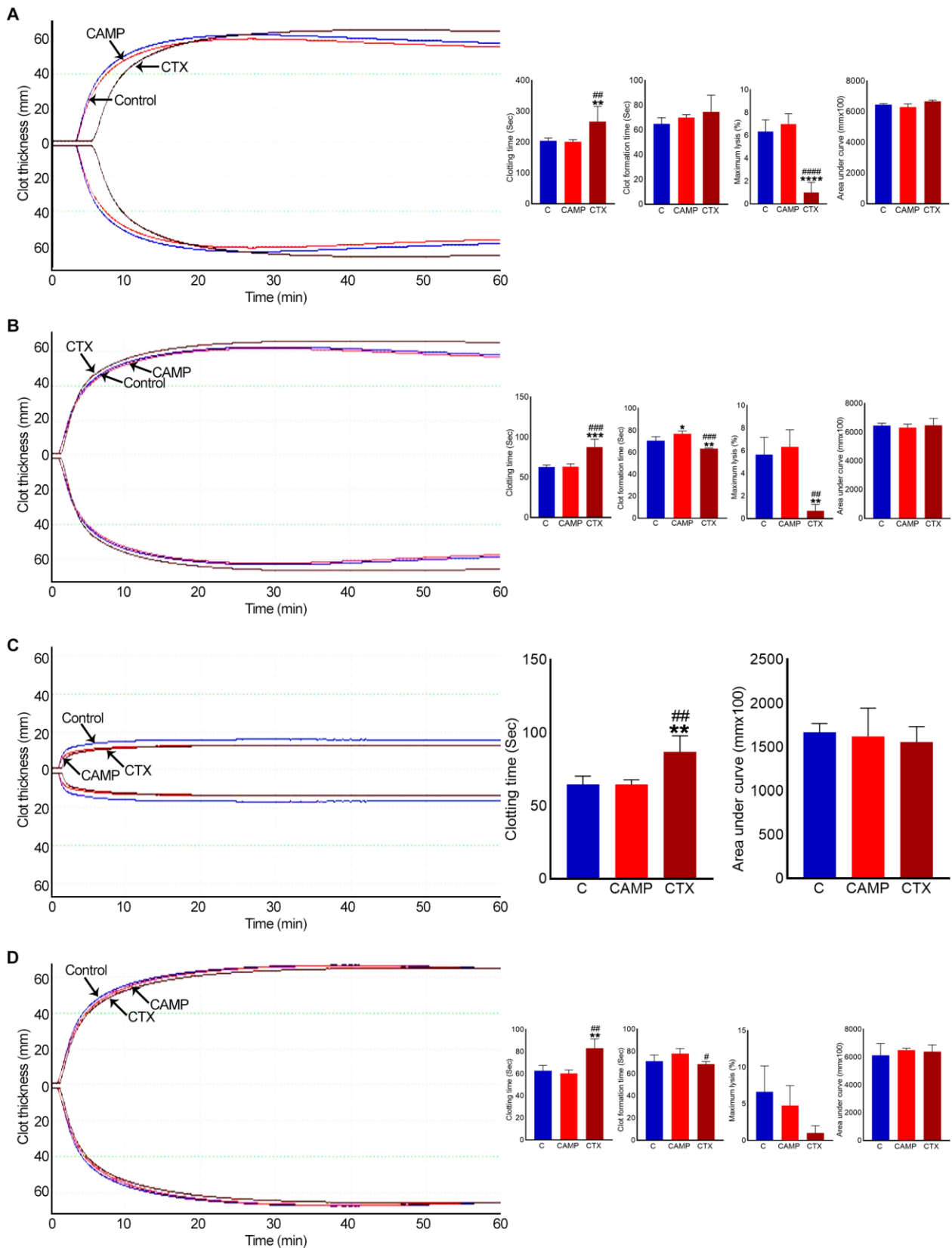


**Figure 5. ROTEM analysis in whole human blood with CAMP and CTX.** A) Intem, B) Extem, C) Fibtem and D) Aptem data show the impact of 50  $\mu$ M CAMP or CTX in human whole blood clotting via different pathways. Graphs represent clotting time, clot formation time, maximum lysis, and area under the curve. The columns represent the mean  $\pm$  S.D. (n=4 independent donors from whom the blood samples were obtained for these

experiments). \* $p < 0.05$ , \*\* $p < 0.01$ , \*\*\* $p < 0.001$  and \*\*\*\* $p < 0.0001$  when compared to the control group (C). # $p < 0.05$ , ## $p < 0.01$ , ### $p < 0.001$  and #### $p < 0.0001$  when compared to CAMP. One-way ANOVA followed by Tukey's test was used to analyse these data.

#### 4. Discussion

The life-threatening pathophysiology of SBE is driven by the individual and synergistic actions of biologically active venom toxins with different molecular targets, which can lead to various effects in the body including haemostatic disturbances and muscle damage [18,19]. At the clinical level, venom-induced consumption coagulopathy (VICC) with diverse manifestations triggered by different toxins is a serious issue, and the resulting haemostatic effects may vary depending on the consumed factor in the coagulation cascade [20,21]. This systemic and potentially lethal phenomenon following SBE in patients is recognised by activation of the clotting cascade and/or elevated degradation of the fibrinogen [22]. At a molecular level, toxins can affect thrombi formation via varied targets and/or due to their thrombolytic properties, resulting in thrombotic/bleeding complications [14]. However, the coordination and regulation of haemostatic responses following skeletal muscle injury, including intramuscular bleeding and thrombosis have not been fully understood. Determining the differences that contribute to these haemostatic events by clinically relevant venom toxins is key to elucidating the general impacts on muscle damage and subsequent regeneration. Due to the role that the circulatory system plays in wound healing and tissue regeneration, it is vital to study its state during venom-induced muscle damage. The circulatory system delivers leukocytes to damaged areas to enable the clearing of cell debris and to prevent infections [23]. Additionally, the limited effectiveness of currently used antivenom treatment for managing local tissue injury and mitigating its long-standing consequences [5,24] reiterates the importance of a comprehensive investigation of venom-induced muscle damage including the haemostatic elements to allow the development of better management strategies for this condition. Therefore, we analysed a parallel comparison of haemotoxicity induced by enzymatic (CAMP) and non-enzymatic (CTX) muscle-damaging venom components during skeletal muscle damage to establish their diverse effects.

SVMPs are crucial components in viper venom-induced myotoxicity due to its ability to hinder adequate muscle regeneration and complete functional recovery following acute damage [25]. The proteolytic activity of these toxins causes important alterations to different components of the muscle

architecture especially the ECM, which is essential for muscle regeneration [4,11]. CAMP was previously reported to damage the ECM in skeletal muscle [11]. As shown here, during the CAMP-induced muscle injury, there was extensive local damage with significant bleeding, as evidenced by fibrinogen in the injured muscles. *In vitro* studies have previously demonstrated that some P-III SVMPs have a fibrinolytic effect on human plasma fibrinogen [26]. Therefore, CAMP might be directly cleaving plasma fibrinogen as well as affecting the ECM in blood capillaries during muscle damage to induce bleeding. Earlier research has established that viper venoms contain procoagulant toxins that can induce VICC due to the consumption of clotting factors [27]. These proteolytic enzymes often cause rapid clot formation *in vitro* but can induce bleeding complications due to the rapid consumption of several factors. Fibrinogen, the common point of the clotting pathway, is the most consistently consumed factor in VICC [15]. Notably, some studies have revealed that SVMPs could cleave integrins and fibrin clots, leading to further bleeding [28,29]. As a P-III SVMP, CAMP has a disintegrin-like functional domain in its structure but a possible reason for the lack of integrin  $\alpha\text{IIb}\beta\text{3}$  signal in the muscle tissues is likely to be due to its direct effect on this integrin shedding. Integrin  $\alpha\text{IIb}\beta\text{3}$  plays a crucial role in platelet aggregation and adhesion [30]. Therefore, lack of integrin  $\alpha\text{IIb}\beta\text{3}$  might be one of the main causes of extensive and prolonged bleeding in CAMP-damaged muscle. Treatment with CAMP enhanced the detection of P-selectin in the microthrombi of damaged tissue. CAMP treatment showed a high frequency of P-selectin microthrombi within the muscle even at a later time point, indicating ongoing muscle damage. Moreover, CAMP may possess thrombolytic properties, and the reduction in the microthrombi area could be due to thrombolysis. Interestingly, CAMP exhibited an insignificant effect on Intem and Extem analysis. The intrinsic pathway is initiated by activators like collagen, which is a substrate for CAMP. Hence, the lack of collagen in the blood due to CAMP activity could indicate indirect effects of CAMP on Intem analysis. These findings highlight the mechanistic action of a purified toxin, CAMP on inducing bleeding and thrombotic complications during muscle damage. However, this cannot be generalized to all SVMPs in diverse venoms as they possess variable potencies, substrate specificities and a diverse range of pharmacological properties, which can also interact with other families of toxins to exert synergistic activities. Similarly, when the whole venom is used, the level of haemotoxic effects may vary compared to the purified toxin.

In the CTX-induced injury model, we observed acute muscle damage accompanied by bleeding and thrombosis. CTX extended the clotting time in ROTEM analysis, which suggests its ability to cause bleeding. The likely mechanisms of CTX-induced bleeding may include the necrosis of endothelial cells in microcapillaries that perfuse the damaged muscle and/or anticoagulant properties of these non-enzymatic molecules. In the first scenario, lysis or necrosis of the cell membrane leads to capillary permeation, causing blood to leak into the interstitial space of muscle tissue. This event could also be related to the activation of native matrix metalloproteases, which regulate vascular ECM and homeostasis [31]. This increases blood flow to the damaged site and aids the perpetuation of the haemorrhagic effect [32,33]. In the second case, some 3FTXs can bind and inhibit specific coagulation factors or complexes [34]. For example, members of this toxin family, such as hemextin A, ringhalexin and exactin have been proposed as potential anticoagulant lead molecules for the development of therapeutics, research tools and diagnostic probes due to their selective effects on specific coagulation factors [35,36]. The first wave of haemostasis is due to the accumulation of platelets at the site of the injury [37]. Platelet activation and thrombus formation are achieved by modulating and binding of various receptors on the platelet surface to their ligands. Platelet integrins and their ligands initiate stable adhesion, and inside-out signalling to integrin  $\alpha\text{IIb}\beta\text{3}$  recruits more platelets for aggregation. The integrin  $\alpha\text{IIb}\beta\text{3}$  enhances platelet activation through cytoskeleton rearrangement and granule secretion, thereby facilitating haemostatic plug or thrombus formation. The lack of integrin  $\alpha\text{IIb}\beta\text{3}$  reduces platelet aggregation and impairs thrombus growth. In CTX-injured muscle sections, integrin staining revealed clots, which may be one of the reasons why CTX-induced bleeding gradually improves. P-selectin plays a crucial role in thrombus formation and wound healing pathways by recruiting white blood cells to the injured site. The frequency of P-selectin-stained thrombi decreased in CTX-mediated damage with the progression of tissue repair, suggesting that the muscle damage is advancing towards resolution. Similar results were reported in a recent study exploring the contribution of platelet-released chemokines to successful muscle regeneration [38]. In this study, platelet thrombi were monitored using anti-GP1b $\beta$  antibodies, which showed the presence of these aggregates in early stages (on days 1 and 7), with considerable reduction at day 14 in the CTX-induced muscle injury model [38]. Our CTX-induced muscle injury model corroborated these previous findings. Additionally, the same study showed how platelet-



derived signals modulate neutrophil recruitment and coordinate a favourable niche for immune infiltration and myogenesis that precede the restoration of muscle structure and function [38]. The use of neutrophils-depleted mice has revealed the active involvement of neutrophils in the regenerative phase following the damage caused by *Bothrops asper* [39]. Imbalances in these events can establish a persistent inflammatory state with a predominance of atrophic mediators that culminate in unresolved damage, as observed in the CAMP-induced muscle injury model. The ROTEM analysis showed that CTX may affect intrinsic and extrinsic pathways as well as the common pathway as it delayed clotting time in all analyses. This suggests the need for further investigations to establish the exact contribution of CTX to clotting cascades and thereby, intramuscular bleeding and thrombosis.

The paradigm of successful or poor muscle regeneration following elapid and viper envenomation respectively, has been mainly discussed in relevance to the impact of the protagonist toxins and their effects on essential components for myogenesis, such as the ECM, inflammation, and blood supply [11, 40, 41]. Figure 6 summarises the current knowledge of venom toxins-mediated muscle damage with key features/events that affect the regenerative process. The results of this study are also included in this scheme and highlighted in red. Earlier studies have shown that CAMP damages the capillaries and hinders angiogenesis in damaged muscles [42, 43]. On the other hand, degradation of the ECM in skeletal muscle leads to a lack of scaffolding for myogenesis and angiogenesis [44]. Hence, muscle tissue struggles with regeneration when P-III metalloproteases are administered. In a previous study from our group, CTX caused no change in the number of capillaries per muscle fibre [11]. This observation suggested that CTX does not have direct haemotoxic properties through affecting ECM and angiogenesis. The current results based on different biomarkers show that haemorrhage occurs in CTX-damaged muscle. The actions of matrix metalloproteases in vasculature remodelling and tissue regeneration after muscle injury may also contribute to bleeding and subsequent thrombosis [45]. Interestingly, the level of fibrinogen was significantly reduced with the progression of muscle regeneration. This reduction in fibrinogen aligns with the fact that intact blood capillaries facilitated muscle repair. Since fibrinogen deposition can promote a profibrotic environment, the reduction of fibrinogen levels in CTX-induced muscle injury is consistent with reduced fibrosis and better functional outcomes during the elapid snake envenomation [46].

However, a lower clearance rate was detected in CAMP-damaged muscle sections. As discussed earlier and supported by previous studies [47, 48, 49], neutrophils are fundamental players in muscle repair progress and they help to orchestrate a pro-reparative scenario dictated by macrophage phenotype transition [50]. Neutrophil recruitment to damaged tissue in turn can be modulated by platelet-derived chemokines and microthrombi formation, which may account for differences in the removal rates of fibrinogen and intramuscular microthrombi [38, 51]. The action and temporal presence of these myotoxins must also be considered in this speculative view. Previous studies have shown the long-lasting presence of SVMP which leads to continuous ECM degradation and haemorrhagic effects [11, 52]. The temporal action of cardiotoxin is in line with the restoration of muscle architecture and complete removal of the signs of intramuscular bleeding [53,54]. In summary, the combination of these evidences supports the current concept of poor muscle regeneration in viperid envenomation due to direct damage to the vasculature with the dysregulated responses, subsequent poor repair, and severe tissue destruction [55]. As a result, this reduced remodelling in the CAMP-induced muscle injury model leads to extensive collagen deposition seen as the excessive muscle accumulation of fibrous connective tissue that affects the motile and contractile functions of SBE victims [56].

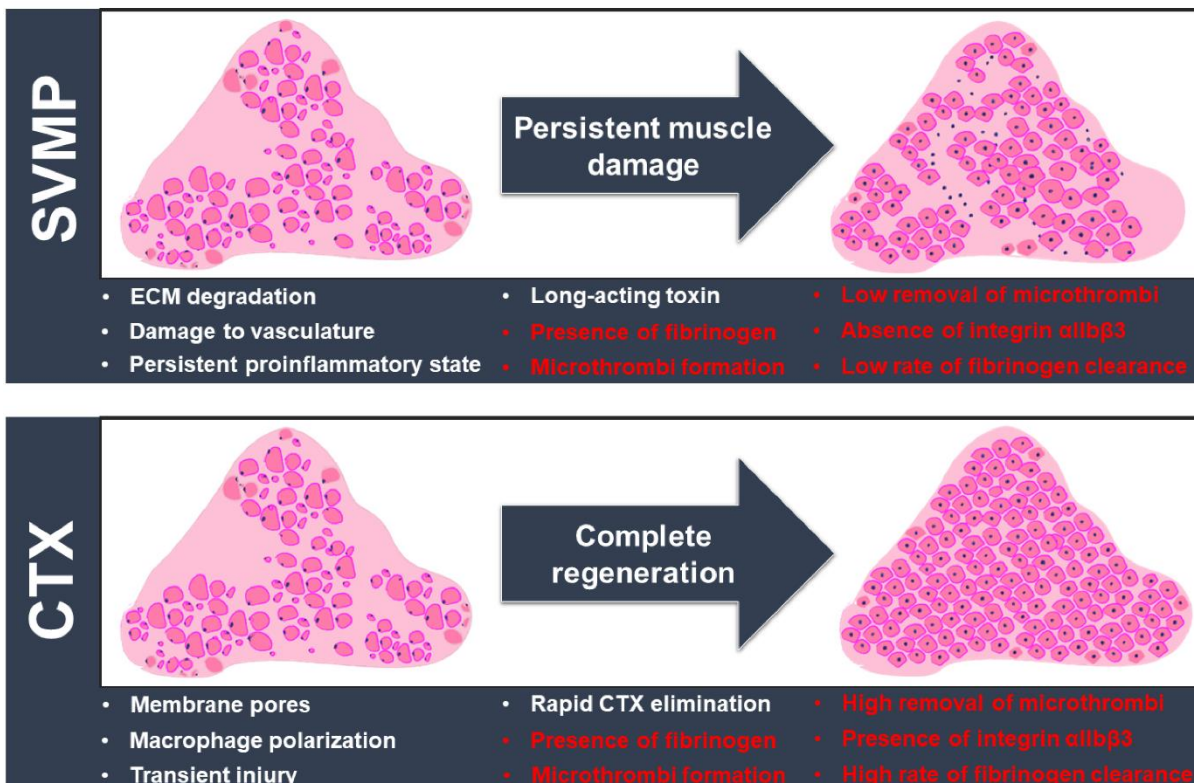


**Figure 6. The landscape of venom-induced muscle damage by SVMPs and CTX.** SVMP (specifically CAMP) and CTX induce extensive muscle damage, but their different mechanisms of action lead to divergent outcomes. Key factors influencing the muscle regeneration process are highlighted here. The contributions of this to the understanding of venom-induced muscle damage are shown in red. SVMP hydrolyses the ECM components and causes vascular alterations, with a significant impact on the influx of inflammatory cells. A persistent proinflammatory environment drives the excessive deposition of fibrous connective tissue with alterations of the muscle architecture and functional implications. On the other hand, CTX triggers an acute, transient injury through a membranolytic action without compromising the ECM and vasculature. A spatiotemporal transition of inflammatory cells promotes a myogenic program resulting in complete regeneration. The normal architecture of the muscle is then re-established with a homogenous distribution of fibre sizes and morphology. We evidenced the intramuscular presence of fibrinogen and microthrombi formation in both toxins-induced muscle damage. However, significant differences in terms of the clearance rate of fibrinogen, removal of microthrombi and levels of integrin  $\alpha 11\beta 3$  were detected. They may be related to the two contrasting muscle regeneration profiles. Another important aspect to be considered is the kinetic action and removal of the myotoxins. The long-term presence of SVMPs is likely to drive repetitive degradative/regenerative cycles that hamper the complete elimination of fibrinogen and microthrombi and exacerbates the inflammatory state that impairs tissue repair. In contrast, cardiotoxin has a transient activity that culminates in the successful removal of fibrinogen and microthrombi, which should result in a favourable outcome for regeneration.

In summary, this comparative study demonstrates intramuscular bleeding and microthrombi formation following SVMPs or 3FTX-induced myotoxicity. Overall, it offers valuable insights into the homeostasis of muscle tissue and their rearrangements induced by catalytically active and non-enzymatic venom molecules with their specific actions on haemostatic processes. This highlights the importance of studying overlooked toxins-mediated disturbances that may contribute to the severe pathological sequelae observed in skeletal muscle. Our observational study raises a series of hypotheses that deserve deeper analysis. For example, the presence of fibrinogen and potential intramuscular bleeding in CTX-induced muscle injury needs further investigation. Additionally, research focused on pharmacological interventions is important to identify the extent and the role of these alterations and underlying mechanisms that impede muscle regeneration. By integrating their mechanism of action in haemostatic effects, we provide a better picture of the toxins' impacts on thrombus formation, bleeding, and vascular damage in venom-induced muscle injury. These will pave the way to a comprehensive understanding of the processes involved in muscle damage and its possible implications for the development of life-changing solutions to treat venom-induced muscle injury, facilitate tissue regeneration, and prevent long-term physical sequelae. In practical terms, the multidimensional nature of muscle damage and the diversity of underlying factors require more detailed investigations that may culminate in therapeutic benefits and clinical translation. Future studies should explore whether variations in toxins would influence the pattern of haemostatic

responses during muscle damage described here and evaluate the neutralisation of these muscle-perturbing venom proteins by current and next-generation of antivenom therapies.

## References

1. Williams, D.J.; Faiz, M.A.; Abela-Ridder, B.; Ainsworth, S.; Bulfone, T.C.; Nickerson, A.D.; Habib, A.G.; Junghanss, T.; Fan, H.W.; Turner, M.; et al. Strategy for a globally coordinated response to a priority neglected tropical disease: Snakebite envenoming. *PLoS Negl. Trop. Dis.* **2019**, *13*, e0007059, doi:10.1371/journal.pntd.0007059.
2. Samuel, S.P.; Chinnaraju, S.; Williams, H.F.; Pichamuthu, E.; Subharao, M.; Vaiyapuri, M.; Arumugam, S.; Vaiyapuri, R.; Baksh, M.F.; Patel, K.; et al. Venomous snakebites: Rapid action saves lives-A multifaceted community education programme increases awareness about snakes and snakebites among the rural population of Tamil Nadu, India. *PLoS Negl. Trop. Dis.* **2020**, *14*, e0008911, doi:10.1371/journal.pntd.0008911.
3. Gutiérrez, J.M.; Calvete, J.J.; Habib, A.G.; Harrison, R.A.; Williams, D.J.; Warrell, D.A. Snakebite envenoming. *Nat. Rev. Dis. Primers* **2017**, *3*, 17063, doi:10.1038/nrdp.2017.63.
4. Sanchez-Castro, E.E.; Pajuelo-Reyes, C.; Tejedo, R.; Soria-Juan, B.; Tapia-Limonchi, R.; Andreu, E.; Hitos, A.B.; Martin, F.; Cahuana, G.M.; Guerra-Duarte, C.; et al. Mesenchymal stromal cell-based therapies as promising treatments for muscle regeneration after snakebite envenoming. *Front. Immunol.* **2021**, *11*, 609961., doi:10.3389/fimmu.2020.609961.
5. Williams, H.F.; Layfield, H.J.; Vallance, T.; Patel, K.; Bicknell, A.B.; Trim, S.A.; Vaiyapuri, S. The urgent need to develop novel strategies for the diagnosis and treatment of snakebites. *Toxins* **2019**, *11*(6), 363, doi:10.3390/toxins11060363.
6. Knudsen, C.; Laustsen, A.H. Recent advances in next generation snakebite antivenoms. *Trop. Med. Infect. Dis.* **2018**, *3*(2), 42, doi:10.3390/tropicalmed3020042.
7. Gutiérrez, J.M.; Escalante, T.; Hernández, R.; Gastaldello, S.; Saravia-Otten, P.; Rucavado, A. Why is skeletal muscle regeneration impaired after myonecrosis induced by viperid snake venoms? *Toxins* **2018**, *10*(5), 182 doi:10.3390/toxins10050182.
8. Russell, J.J.; Schoenbrunner, A.; Janis, J.E. Snake Bite management: a scoping review of the literature. *Plast. Reconstr. Surg. Glob. Open* **2021**, *9*, e3506, doi:10.1097/gox.0000000000003506.
9. Ferraz, C.R.; Arrahman, A.; Xie, C.; Casewell, N.R.; Lewis, R.J.; Kool, J.; Cardoso, F.C. Multifunctional toxins in snake venoms and therapeutic implications: from pain to hemorrhage and necrosis. *Front. Ecol. Evol.* **2019**, *7*, doi:10.3389/fevo.2019.00218.
10. Almeida, J.R.; Gomes, A.; Mendes, B.; Aguiar, L.; Ferreira, M.; Brioschi, M.B.C.; Duarte, D.; Nogueira, F.; Cortes, S.; Salazar-Valenzuela, D.; et al. Unlocking the potential of snake venom-

- based molecules against the malaria, Chagas disease, and leishmaniasis triad. *Int. J. Biol. Macromol.* **2023**, *242*, 124745, doi:10.1016/j.ijbiomac.2023.124745.
11. Williams, H.F.; Mellows, B.A.; Mitchell, R.; Sfyri, P.; Layfield, H.J.; Salamah, M.; Vaiyapuri, R.; Collins-Hooper, H.; Bicknell, A.B.; Matsakas, A.; et al. Mechanisms underpinning the permanent muscle damage induced by snake venom metalloprotease. *PLoS Negl. Trop. Dis.* **2019**, *13*, e0007041, doi:10.1371/journal.pntd.0007041.
  12. Laumonier, T.; Menetrey, J. Muscle injuries and strategies for improving their repair. *J. Exp. Orthop.* **2016**, *3*, 15, doi:10.1186/s40634-016-0051-7.
  13. Stark, K.; Massberg, S. Interplay between inflammation and thrombosis in cardiovascular pathology. *Nat. Rev. Cardiol.* **2021**, *18*, 666-682, doi:10.1038/s41569-021-00552-1.
  14. Larréché, S.; Chippaux, J.P.; Chevillard, L.; Mathé, S.; Résière, D.; Siguret, V.; Mégarbane, B. Bleeding and thrombosis: insights into pathophysiology of *Bothrops* venom-related hemostasis disorders. *Int. J. Mol. Sci.* **2021**, *22*, doi:10.3390/ijms22179643.
  15. Berling, I.; Isbister, G.K. Hematologic effects and complications of snake envenoming. *Transf. Med. Rev.* **2015**, *29*, 82-89, doi:https://doi.org/10.1016/j.tmr.2014.09.005.
  16. Slagboom, J.; Kool, J.; Harrison, R.A.; Casewell, N.R. Haemotoxic snake venoms: their functional activity, impact on snakebite victims and pharmaceutical promise. *Br. J. Haemat.* **2017**, *177*, 947-959, doi:https://doi.org/10.1111/bjh.14591.
  17. Durrant, T.N.; van den Bosch, M.T.; Hers, I. Integrin  $\alpha(\text{IIb})\beta(3)$  outside-in signaling. *Blood* **2017**, *130*, 1607-1619, doi:10.1182/blood-2017-03-773614.
  18. Almeida, J.R.; Resende, L.M.; Watanabe, R.K.; Carregari, V.C.; Huancahuire-Vega, S.; Caldeira, C.A.S.; Coutinho-Neto, A.; Soares, A.M.; Vale, N.; Gomes, P.A.C.; et al. Snake venom peptides and low mass proteins: molecular tools and therapeutic Agents. *Curr. Med. Chem.* **2017**, *24*, 3254-3282, doi:10.2174/0929867323666161028155611.
  19. Silva, L.M.; Silva, C.A.; Silva, A.; Vieira, R.P.; Mesquita-Ferrari, R.A.; Cogo, J.C.; Zamuner, S.R. Photobiomodulation protects and promotes differentiation of C2C12 myoblast cells exposed to snake venom. *PLoS One* **2016**, *11*, e0152890, doi:10.1371/journal.pone.0152890.
  20. Senthilkumaran, S.; Patel, K.; Rajan, E.; Vijayakumar, P.; Miller, S.W.; Rucavado, A.; Gilabadi, S.; Sonavane, M.; Richards, N.J.; Williams, J.; et al. Peripheral arterial thrombosis following Russell's viper bites. *TH Open* **2023**, *7*, e168-e183, doi:10.1055/s-0043-1769625.
  21. Senthilkumaran, S.; Almeida, J.R.; Williams, J.; Williams, H.F.; Thirumalaikolundusubramanian, P.; Patel, K.; Vaiyapuri, S. Rapid identification of bilateral adrenal and pituitary haemorrhages induced by Russell's viper envenomation results in positive patient outcome. *Toxicon* **2023**, *225*, 107068, doi:https://doi.org/10.1016/j.toxicon.2023.107068.
  22. Maduwage, K.; Isbister, G.K. Current treatment for venom-induced consumption coagulopathy resulting from snakebite. *PLoS Negl. Trop. Dis.* **2014**, *8*, e3220, doi:10.1371/journal.pntd.0003220.

23. Forcina, L.; Cosentino, M.; Musarò, A. Mechanisms regulating muscle regeneration: insights into the interrelated and time-dependent phases of tissue healing. *Cells* **2020**, *9*(5), 1297, doi:10.3390/cells9051297.
24. Vera-Palacios, A.L.; Sacoto-Torres, J.D.; Hernández-Altamirano, J.A.; Moreno, A.; Peñuela-Mora, M.C.; Salazar-Valenzuela, D.; Mogollón, N.G.S.; Almeida, J.R. A first look at the inhibitory potential of *Urospatha sagittifolia* (Araceae) ethanolic extract for *Bothrops atrox* snakebite envenomation. *Toxins* **2022**, *14*(7), 496, doi:10.3390/toxins14070496.
25. Gutiérrez, J.M.; Rucavado, A. Snake venom metalloproteinases: their role in the pathogenesis of local tissue damage. *Biochimie* **2000**, *82*, 841-850, doi:10.1016/s0300-9084(00)01163-9.
26. Olaoba, O.T.; Karina Dos Santos, P.; Selistre-de-Araujo, H.S.; Ferreira de Souza, D.H. Snake venom metalloproteinases (SVMPs): a structure-function update. *Toxicon X* **2020**, *7*, 100052, doi:10.1016/j.toxcx.2020.100052.
27. Park, E.J.; Choi, S.; Kim, H.H.; Jung, Y.S. Novel treatment strategy for patients with venom-induced consumptive coagulopathy from a pit viper bite. *Toxins* **2020**, *12*(5), 295, doi:10.3390/toxins12050295.
28. Kini, R.M.; Koh, C.Y. Metalloproteases affecting blood coagulation, fibrinolysis, and platelet aggregation from snake venoms: definition and nomenclature of interaction sites. *Toxins* **2016**, *8*(10), 284, doi:10.3390/toxins8100284.
29. Sanchez, E.F.; Richardson, M.; Gremski, L.H.; Veiga, S.S.; Yarleque, A.; Niland, S.; Lima, A.M.; Estevao-Costa, M.I.; Eble, J.A. A novel fibrinolytic metalloproteinase, barnettlysin-I from *Bothrops barnetti* (barnett's pitviper) snake venom with anti-platelet properties. *Biochim. Biophys. Acta – Gen. Subj.* **2016**, *1860*, 542-556, doi:https://doi.org/10.1016/j.bbagen.2015.12.021.
30. Huang, J.; Li, X.; Shi, X.; Zhu, M.; Wang, J.; Huang, S.; Huang, X.; Wang, H.; Li, L.; Deng, H.; et al. Platelet integrin  $\alpha\text{IIb}\beta\text{3}$ : signal transduction, regulation, and its therapeutic targeting. *J. Hematol. Oncol.* **2019**, *12*, 26, doi:10.1186/s13045-019-0709-6.
31. Wang, X.; Khalil, R.A. Matrix metalloproteinases, vascular remodeling, and vascular disease. *Adv. Pharmacol.* **2018**, *81*, 241-330, doi:10.1016/bs.apha.2017.08.002.
32. Yang, W.; Hu, P. Skeletal muscle regeneration is modulated by inflammation. *J. Orthop. Translat.* **2018**, *13*, 25-32, doi:10.1016/j.jot.2018.01.002.
33. Megha, K.B.; Joseph, X.; Akhil, V.; Mohanan, P.V. Cascade of immune mechanism and consequences of inflammatory disorders. *Phytomed.* **2021**, *91*, 153712, doi:10.1016/j.phymed.2021.153712.
34. Kini, R.M.; Koh, C.Y. Snake venom three-finger toxins and their potential in drug development targeting cardiovascular diseases. *Biochem. Pharmacol.* **2020**, *181*, 114105, doi:10.1016/j.bcp.2020.114105.

35. Girish, V.M.; Kini, R.M. Exactin: A specific inhibitor of Factor X activation by extrinsic tenase complex from the venom of *Hemachatus haemachatus*. *Sci. Rep.* **2016**, *6*, 32036, doi:10.1038/srep32036.
36. Barnwal, B.; Jobichen, C.; Girish, V.M.; Foo, C.S.; Sivaraman, J.; Kini, R.M. Ringhalexin from *Hemachatus haemachatus*: A novel inhibitor of extrinsic tenase complex. *Sci. Rep.* **2016**, *6*, 25935, doi:10.1038/srep25935.
37. Hou, Y.; Carrim, N.; Wang, Y.; Gallant, R.C.; Marshall, A.; Ni, H. Platelets in hemostasis and thrombosis: Novel mechanisms of fibrinogen-independent platelet aggregation and fibronectin-mediated protein wave of hemostasis. *J. Biomed. Res.* **2015**, *29*, 437-444, doi:10.7555/jbr.29.20150121.
38. Graca, F.A.; Stephan, A.; Minden-Birkenmaier, B.A.; Shirinifard, A.; Wang, Y.D.; Demontis, F.; Labelle, M. Platelet-derived chemokines promote skeletal muscle regeneration by guiding neutrophil recruitment to injured muscles. *Nat. Commun.* **2023**, *14*, 2900, doi:10.1038/s41467-023-38624-0.
39. Teixeira, C.F.; Zamunér, S.R.; Zuliani, J.P.; Fernandes, C.M.; Cruz-Hofling, M.A.; Fernandes, I.; Chaves, F.; Gutiérrez, J.M. Neutrophils do not contribute to local tissue damage, but play a key role in skeletal muscle regeneration, in mice injected with *Bothrops asper* snake venom. *Muscle Nerve.* **2003**, *28*(4), 449-59, doi: 10.1002/mus.10453.
40. Escalante, T.; Saravia-Otten, P.; Gastaldello, S.; Hernández, R.; Marín, A.; García, G.; García, L.; Estrada, E.; Rucavado, A.; Gutiérrez, J.M. Changes in basement membrane components in an experimental model of skeletal muscle degeneration and regeneration induced by snake venom and myotoxic phospholipase A<sub>2</sub>. *Toxicon.* **2021**, *192*, 46-56, doi: 10.1016/j.toxicon.2021.01.003.
41. Masuda, H.; Sato, A.; Shizuno, T.; Yokoyama, K.; Suzuki, Y.; Tokunaga, M., Asahara T. Batroxobin accelerated tissue repair via neutrophil extracellular trap regulation and defibrinogenation in a murine ischemic hindlimb model. *PLoS ONE.* **2019**, *14*(8), e0220898.
42. Escalante, T.; Shannon, J.; Moura-da-Silva, A.M.; Gutiérrez, J.M.; Fox, J.W. Novel insights into capillary vessel basement membrane damage by snake venom hemorrhagic metalloproteinases: a biochemical and immunohistochemical study. *Arch. Biochem. Biophys.* **2006**, *455*, 144-153, doi:10.1016/j.abb.2006.09.018.
43. Escalante T.; Rucavado A.; Fox J.W.; Gutiérrez J.M. Key events in microvascular damage induced by snake venom hemorrhagic metalloproteinases. *J. Proteomics.* **2011**, *24*, 74(9), 1781-94, doi: 10.1016/j.jprot.2011.03.026.
44. Zhang, W.; Liu, Y.; Zhang, H. Extracellular matrix: an important regulator of cell functions and skeletal muscle development. *Cell & Biosci.* **2021**, *11*, 65, doi:10.1186/s13578-021-00579-4.
45. Chen, X.; Li, Y. Role of matrix metalloproteinases in skeletal muscle: migration, differentiation, regeneration and fibrosis. *Cell Adh. Migr.* **2009**, *3*, 337-341, doi:10.4161/cam.3.4.9338.

46. Vidal, B.; Serrano, A.L.; Tjwa, M.; Suelves, M.; Ardite, E.; De Mori, R.; Baeza-Raja, B.; Martínez de Lagrán, M.; Lafuste, P.; Ruiz-Bonilla, V.; et al. Fibrinogen drives dystrophic muscle fibrosis via a TGFbeta/alternative macrophage activation pathway. *Genes Dev.* **2008**, *22*, 1747-1752, doi:10.1101/gad.465908.
47. Ranéia e Silva, P.A.; da Costa Neves, A.; da Rocha, C.B.; da Rocha, C.B.; Moura-da-Silva, A.M.; Faquim-Mauro, E.L. Differential macrophage subsets in muscle damage induced by a K49-PLA<sub>2</sub> from *Bothrops jararacussu* venom modulate the time course of the regeneration process. *Inflammation.* **2019**, *42*, 1542–1554.
48. Zuliani J.P.; Soares A.M.; Gutiérrez J.M. Polymorphonuclear neutrophil leukocytes in snakebite envenoming. *Toxicon.* **2020**, *187*, 188-197. doi: 10.1016/j.toxicon.2020.09.006.
49. Garcia Denegri, M.E.; Teibler, G.P.; Maruñak, S.L.; Hernández D.R.; Acosta O.C.; Leiva L.C. Efficient muscle regeneration after highly haemorrhagic *Bothrops alternatus* venom injection. *Toxicon.* **2016**, *122*, 167-175. doi: 10.1016/j.toxicon.2016.10.005.
50. Paiva-Oliveira, E.L.; da Silva, R.F.; Bellio, M.; Quirico-Santos, T., Lagrota-Candido, J. Pattern of cardiotoxin-induced muscle remodeling in distinct TLR-4 deficient mouse strains. *Histochem. Cell. Biol.* **2017**, *148*, 49–60.
51. Ulloa-Fernández, A.; Escalante, T.; Gutiérrez, J.M.; Rucavado A. Platelet depletion enhances lethal, hemorrhagic and myotoxic activities of *Bothrops asper* snake venom in a murine model. *Toxicon.* **2022**, *219*, 106936, doi: 10.1016/j.toxicon.2022.106936.
52. Van de Velde, A.C.; Fusco, L.S.; Echeverría, S.M.; Sasovsky, D.J., Leiva, L.C.; Gutiérrez, J.M.; Bustillo S. Traces of *Bothrops* snake venoms in necrotic muscle preclude myotube formation in vitro. *Toxicon.* **2022**, *211*, 36-43, doi: 10.1016/j.toxicon.2022.03.008.
53. Wang, Y.; Lu, J., Liu, Y. Skeletal muscle regeneration in cardiotoxin-induced muscle injury models. *Int. J. Mol. Sci.* **2022**, *23*,13380, doi: 10.3390/ijms232113380.
54. Yan, Z.; Choi, S.; Liu, X.; Zhang, M.; Schageman, J.J.; Lee, S.Y.; Hart, R.; Lin, L.; Thurmond F.A.; Williams, R.S. Highly coordinated gene regulation in mouse skeletal muscle regeneration. *J. Biol. Chem.* **2003**, *278*, 8826-8836, doi: 10.1074/jbc.M209879200
55. Hernández, R.; Cabalceta, C.; Saravia-Otten, P.; Chaves, A.; Gutiérrez, J.M.; Rucavado, A. Poor regenerative outcome after skeletal muscle necrosis induced by *Bothrops asper* venom: alterations in microvasculature and nerves. *PLoS One* **2011**, *6*, e19834, doi:10.1371/journal.pone.0019834. Waidyanatha, S.; Silva, A.; Siribaddana, S.; Isbister, G.K. Long-term effects of snake envenoming. *Toxins* **2019**, *11*, doi:10.3390/t





## 3. Conclusions

### 3. Conclusions

Snakebite envenoming (SBE) is a major occupational health hazard for the large population residing in the world. Permanent tissue damage and disabilities are one of the dire consequences of SBE, claiming around 500,000 SBE victims annually. The most SBE-prone population belongs to agricultural workers, and permanent disability affects the physical, psychological, and economic status of not only the snakebite victims but also has a cumulative impact on society. Anti-venom is the only treatment for SBE, and it helps treat the systemic effects of envenomation. Recently, substantial efforts have been made to improve anti-venom efficacy and potency to treat SBE. However, studies on snake venom-induced muscle damage and the therapeutic options are still limited. The primary aim of this thesis was to study the effects of individual proteins and whole venom from the Viperidae family on skeletal muscles and explore potential therapeutic molecules to improve muscle regeneration. Viper venom is rich in snake venom metalloproteases (SVMPs), snake venom serine proteases (SVSPs) and phospholipase A<sub>2</sub> (PLA<sub>2</sub>) toxin families. SVMPs and PLA<sub>2</sub> have been studied for their systemic and local effects. SVMPs directly and indirectly impact critical cells and molecules involved in tissue regeneration, including muscle stem cells, extracellular matrix (ECM) components, and microcapillary networks. They can alter immune response, impairing muscle regeneration and leading to fibrosis. PLA<sub>2</sub>, on the other hand, acts on the phospholipid bilayer of the cells, leading to tissue necrosis. The pathological changes caused by SVMP activity often led to the formation of fibrotic tissue in the snakebite victims. Due to direct and indirect impacts on satellite cells (SC) and immune response, viper venom does have a significant impact on the innate mechanism of muscle regeneration. The lack of a microcapillary network further worsens the situation, as immune cells and blood supply cannot reach the site of damage. Hence, it is essential to identify issues related to muscle regeneration in viper envenoming, impact on blood coagulation and microthrombi formation, and mitigate the impact of long-lasting venom proteins in the muscle tissue and its long-term repercussions.

In this study, we narrow down potential target areas to improve snake venom-induced muscle damage. The focus areas are to neutralise the long-lasting venom proteins, reduce muscle fibrosis to contain permanent tissue damage, and boost innate muscle regeneration. We have used three

approaches: 1. Neutralise venom proteins in the muscle tissue using small molecule inhibitors, marimastat and varespladib. 2. Use anti-fibrotic molecule soluble activin receptor IIB (sActRIIB) to reduce muscle fibrosis or scar tissue formation in the regenerated muscle post-venom-induced damage. 3. Use Adipose-derived mesenchymal stem cell (ADMSC) secretome to improve the innate regeneration capacity of the damaged tissue. We also observed and analysed the effects of purified venom toxins on intramuscular bleeding and thrombus formation in the tissue.

*Conclusion 1. Effective muscle regeneration can be achieved by neutralising venom proteins in the muscle tissue using small molecule inhibitors (SMI), marimastat and varespladib.*

The long-term presence of venoms in the tissue is a major reason for persistent muscle damage. SVMPs are a main contributing toxin family in *C. atrox* venom. In the presence of marimastat, there was a significant reduction in the venom in the damaged muscle. This effect was evident in marimastat, and the muscle treated with marimastat and varespladib combination but not in the tissue treated with varespladib alone. Tissue necrosis was reduced with individual SMI treatment. Blocking the action of SVMPs also reduced tissue necrosis, intramuscular bleeding, and muscle fibrosis. The effect of inhibitors was evident in the reconstruction and remodelling of ECM proteins such as collagen, laminin, and dystrophin. However, none of the inhibitors, individually or in combination, improved angiogenesis. The SMI treatment also regulated cytokine response. TNF $\alpha$ , IL-1 $\beta$ , and IL-6 levels were elevated in the untreated samples from early time points; this can be tied down to the continuous myoblast formation in the muscle tissue. TNF $\alpha$  upregulates IL-1 $\beta$ , IL-6. IL-1 $\beta$  inhibits the differentiation of SC to enhance the proliferation. IL-6 increases myoblast proliferation. With treatment, these levels were significantly low, indicating the progress towards resolving inflammation. With the given SMI treatment, we did not observe any improvement in vessel reconstruction. VEGF promotes angiogenesis after injury. We observed no significant change in VEGF levels with treatment, and poor blood vessel reconstruction. INF- $\gamma$  is associated with trauma-induced muscle wasting. With marimastat treatment, it is possible to reduce muscle wasting, as treatment with this SMI showed lower levels of INF- $\gamma$ .

Anti-snake venom cannot reach the site of local tissue and has significant limitations for being produced against the whole venom. However, SMI can overcome anti-snake venom's limitations by

reaching the site of damage and effectively neutralising the venom toxins *in vivo*. Furthermore, SMI being specific for a single toxin and not the whole venom frees them from the limitation of geographical variation in the snake venom. From all this data, we can establish that these SMI can be viable options for treating snake venom-induced muscle damage. However, further investigation is needed to observe the effect on angiogenesis through the venom inhibitions achieved by these inhibitors.

*Conclusion 2. The use of the anti-fibrotic molecule sActRIIB can reduce muscle fibrosis or scar tissue formation in the regenerated muscle after vein-induced damage.*

Further in this study, we examined whether reduction in muscle fibrosis can promote regeneration after viper venom-induced muscle damage. We used an anti-fibrotic molecule, sActRIIB, to reduce fibrosis and improve muscle regeneration. sActRIIB molecule targets the activin/myostatin pathway. Activin/myostatin is a known promotor of muscle fibrosis and can reduce muscle mass. In the present study, sActRIIB treatment improved muscle regeneration following damage induced by *C. atrox* venom.

With the sActRIIB treatment, we observed that the damaged muscles significantly increased their weight. However, this effect was independent of the size of regeneration muscle fibres, be they with centrally located nuclei or those that expressed the developmental form of Myosin Heavy Chain, MYHIII. We postulate that the weight increase in muscle is due to the hypertrophic action of attenuating activin/myostatin signalling in the undamaged muscle fibres. One of the most striking features of the sActRIIB intervention is the histologically improved muscle structure, which occurs at the later time point. We note that there was considerably less fibrosis with the given treatment. Additionally, there was a small but significant increase in the size of regenerating fibres. We propose that the results related to fibrosis can be explained by focusing on the fate of FAPS and how this is controlled by activin/myostatin. sActRIIB could limit fibrosis after *C. atrox* venom damage by simply attenuating myostatin signalling to limit fibroblast expansion. Our data showed that fibrosis develops but is then subsequently decreased. We suggest that activin/myostatin are continually required to form myofibroblasts and that in their absence, fibroblasts lose their ability to form aberrant ECM. Instead, they revert to fibroblasts that restore ECM to a normal state. This line of investigation

requires future studies in the context of muscle to determine how fibrosis can be eliminated by inhibiting activin/myostatin.

In summary, attenuating activin/myostatin signalling improves muscle regeneration after *C. atrox* venom damage. However, the muscle was by no means completely regenerated. As previously stated, this could be due to long-acting metalloprotease activity, which continually induces injury. Hence, we propose that, as well as using reagents that promote regeneration (here sActRIIB), a second line of intervention based on inhibiting key harmful molecules in venom would be advisable. The latter could involve anti-venom antibodies or small molecule inhibitors. Hence, it would be intriguing to test their efficacy in preventing muscle damage when anti-venom therapy is combined with regeneration-promoting agents like sActRIIB.

*Conclusion 3. The use of ADMSC secretome can improve the innate regeneration capacity of the damaged tissue in viper envenomation-mediated skeletal muscle damage.*

Next, we studied the effect of ADMSC condition media on the damage caused by Russell's viper (RV) venom. The study suggests that the ADMSC secretome can provide a favourable nourishing environment for skeletal muscle regeneration in case of damage caused by RV venom. Skeletal muscle regeneration is achieved through an overlapping response of inflammatory cells, activation-differentiation and fusion of SC and maturation and remodelling of the newly regenerated myofiber. ADMSC secretome is packed with essential secretory factors that play a critical role in promoting SC activation, proliferation, differentiation, and maturation of myofibres. The secretome also contains factors which can modulate ECM reconstruction and remodelling.

In summary, the use of ADMSC secretome revealed a range of paracrine effects that play a critical role in different aspects of muscle regeneration and ECM remodelling. The enhancement in proliferation, differentiation, induction of hypertrophy of regenerating myofibers, and ECM reconstruction indicate the intricate ADMSC secretome response. The observed response could be due to the presence of key factors such as interleukins (IL-6, IL-10), tumour necrotic factor- $\alpha$  (TNF- $\alpha$ ) and transforming growth factor- $\beta$  (TGF- $\beta$ ), the involvement of insulin-like growth factors, fibroblast growth factors, and hepatocyte growth factors which modulate the immune response, reduce inflammation and promote tissue repair. Packed with miRNA, extracellular vesicles are crucial

players in promoting satellite cell proliferation and differentiation and ECM reconstruction and remodelling. Notably, TGF- $\beta$  within the ADMSC secretome emerges as a critical regulator in ECM synthesis and remodelling that can influence the levels of IL-6, a vascular endothelial growth factor essential for ECM modulation. The ADMSC secretome, through its diverse paracrine effects, emerges as a promising candidate for expediting the synthesis and remodelling of ECM proteins in the context of RV-mediated skeletal muscle damage. This data opens an exciting new opportunity to test this hypothesis as a potential therapeutic option to reduce pathological complications and improve muscle regeneration in case of RV-mediated skeletal muscle damage. However, to test this effect in a more realistic scenario, observing the regenerative effect secretome post venom-induced muscle damage is essential. It is also important to analyse the long-term repercussions, such as muscle fibrosis, and whether the secretome effectively reduces it.

There could be a few difficulties in using stem cell secretome as a treatment for SBE, such as scaling up secretome production and maintaining proper storage conditions, which can be costly. The SBE victims are often from low-income backgrounds, and the cost of treatment is critical for these victims. The production cost, scalability, and storage of secretome may potentially increase the cost of treatment for SBE victims.

*Conclusion 4. It is essential to study the effects of venom proteins on intramuscular bleeding and thrombus formation in case of snake venom-induced muscle damage.*

Cardiotoxins from the Elapidae family have also been reported to have myotoxic effects. This study examined the effects of SVMP (CAMP) from *C. atrox* and a cardiotoxin (CTX) from *N. pallida* on intramuscular bleeding and thrombus formation. We have studied the effect of CAMP (P-III SVMP) and CTX concerning intramuscular bleeding, thrombus formation and potential impact on blood clotting. CAMP exhibited strong haemotoxic and cytotoxic properties, whereas CTX-induced muscle damage gradually progressed towards damage resolution. The snake venom proteins can affect thrombus formation by targeting various molecules involved in the blood coagulation cascade, resulting in bleeding complications. Venom-induced consumption coagulopathy (VICC) is a significant pathological manifestation reported by viper envenomation. In this study, we observed significant bleeding in the tissue damaged by CAMP, evidenced by the presence of fibrinogen in the

muscle tissue, which was reduced later. CAMP has been reported to have fibrinolytic effects on human plasma fibrinogen, which might be the reason behind the reduction in fibrinogen levels in the muscle. CAMP is P-III SVMP and has a disintegrin-like functional domain. The lack of integrin  $\alpha\text{IIb}\beta\text{3}$  might be a direct effect of integrin shedding. Integrin  $\alpha\text{IIb}\beta\text{3}$  plays an important role in platelet adhesion and aggregation; hence, the lack of this signal in CAMP treated muscle indicated a possible reason for prolonging bleeding in camp-damaged muscle. The P-selectin signal was present in the CAMP treated muscle at early and later times. The size of the thrombi was reduced at a later time point; however, it is possible that the reduction in thrombus size is a result of the thrombolytic property of CAMP. A high frequency of P-selectin thrombi indicates ongoing damage. The intrinsic pathway of blood clotting is initiated by factors such as collagen. This mechanism was confirmed by analysis of the CAMP effect on intrinsic and extrinsic pathways. Due to a lack of collagen in the blood, CAMP did not show any effect on blood clotting. These findings are specific to the CAMP, and the effect of different metalloprotease or whole venom may be different.

CTX treatment induced significant intramuscular bleeding, evidenced by the presence of fibrinogen in the tissue. However, at a later point, the bleeding was significantly reduced. In the CTX-treated muscles, integrin  $\alpha\text{IIb}\beta\text{3}$  and P-selectin signals were observed in the microthrombi. The size and frequency of the microthrombi were reduced considerably with the progress of muscle healing. This data suggests that CTX has haemotoxic properties; however, the damage caused can lead to self-resolution. A very interesting finding from this study was the observation of the effect of CTX on extrinsic and intrinsic pathways, ultimately acting on the common pathway of the blood clotting cascade. CTX extended clotting time, which suggests its ability to cause bleeding.

The findings included in this thesis have given extensive insights into skeletal muscle pathologies induced by SVMP rich snake venom and opened up new exciting opportunities to explore different treatment molecules to overcome these challenges. The different approaches used in these studies target different aspects of impaired muscle regeneration arising due to viper envenomation. The therapeutic options being targeted towards specialised areas of muscle regeneration give an advantage over geographic and species-wise variability in snake venom. These are all primary studies on animal models, with massive potential in translation research.



## **4. PUBLICATIONS AND PRESENTATIONS**

## 4. PUBLICATIONS AND PRESENTATIONS

### Research article

#### **Intramuscular Bleeding and Formation of Microthrombi during Skeletal Muscle Damage Caused by a Snake Venom Metalloprotease and a Cardiotoxin**

**Medha Sonavane**, José R Almeida, Elanchezhian Rajan, Harry F Williams, Felix Townsend, Elizabeth Cornish, Robert D Mitchell, Ketan Patel, Sakthivel Vaiyapuri

Toxins 2023 Aug 28

### Paper not related to this work:

#### **Peripheral Arterial Thrombosis following Russell's Viper Bites**

Subramanian Senthilkumaran, Ketan Patel, Elanchezhian Rajan, Pradeep Vijaykumar, Stephen W. Miller, Alexandra Rucavado, Soheil Gilabadi, **Medha Sonavane**, Nicholas J. Richards, Jarred Williams, Harry F. Williams, Steven A. Trim, Ponniah Thirumalaikolunusubramanian, José María Gutiérrez, and Sakthivel Vaiyapuri.

TH Open.2023 Jun17

#### **Repurposing Cancer Drugs Batimastat and Marimastat to Inhibit the Activity of a Group I Metalloprotease from the Venom of the Western Diamondback Rattlesnake, *Crotalus atrox***

Harry J. Layfield, Harry F. Williams, Divyashree Ravishankar, Amita Mehmi, **Medha Sonavane**, Anika Salim, Rajendra Vaiyapuri, Karthik Lakshminarayan, Thomas M Vallance, Andrew B. Bicknell, Steven A. Trim, Ketan Patel, Sakthivel Vaiyapuri

Toxins 2020 May 9.

### Poster:

#### **Novel strategies for the treatment of snakebite-induced tissue damage**

Pharmacy showcases 2019.

### Presentations:

#### **Multifaceted approaches to treated snake venom-induced muscle damage**

Pharmacy showcases 2021

#### **ADMSC-derived condition media for Russell's viper envenomation-mediated skeletal muscle damage**

Oxford Venoms and Toxins Conference 2021

## Article

# Intramuscular Bleeding and Formation of Microthrombi during Skeletal Muscle Damage Caused by a Snake Venom Metalloprotease and a Cardiotoxin

Medha Sonavane <sup>1</sup>, José R. Almeida <sup>1</sup> , Elanchezian Rajan <sup>1</sup> , Harry F. Williams <sup>2</sup> , Felix Townsend <sup>3</sup>, Elizabeth Cornish <sup>3</sup>, Robert D. Mitchell <sup>4</sup>, Ketan Patel <sup>3</sup> and Sakthivel Vaiyapuri <sup>1,\*</sup> 

<sup>1</sup> School of Pharmacy, University of Reading, Reading RG6 6UB, UK; m.sonavane@pgr.reading.ac.uk (M.S.); j.r.dealmeida@reading.ac.uk (J.R.A.); e.rajan@reading.ac.uk (E.R.)

<sup>2</sup> Toxiven Biotech Private Limited, Coimbatore 641042, Tamil Nadu, India; harryfonsecawilliams@gmail.com

<sup>3</sup> School of Biological Sciences, University of Reading, Reading RG6 6UB, UK; fet7@aber.ac.uk (F.T.); ecornish352@hotmail.co.uk (E.C.); ketan.patel@reading.ac.uk (K.P.)

<sup>4</sup> Micregen Ltd., Thames Valley Science Park, Reading RG2 9LH, UK; robertmitchell@micregen.com

\* Correspondence: to.svaiyapuri@reading.ac.uk

**Abstract:** The interactions between specific snake venom toxins and muscle constituents are the major cause of severe muscle damage that often result in amputations and subsequent socioeconomic ramifications for snakebite victims and/or their families. Therefore, improving our understanding of venom-induced muscle damage and determining the underlying mechanisms of muscle degeneration/regeneration following snakebites is critical to developing better strategies to tackle this issue. Here, we analysed intramuscular bleeding and thrombosis in muscle injuries induced by two different snake venom toxins (CAMP—*Crotalus atrox* metalloprotease (a PIII metalloprotease from the venom of this snake) and a three-finger toxin (CTX, a cardiotoxin from the venom of *Naja pallida*). Classically, these toxins represent diverse scenarios characterised by persistent muscle damage (CAMP) and successful regeneration (CTX) following acute damage, as normally observed in envenomation by most vipers and some elapid snakes of Asian, Australasian, and African origin, respectively. Our immunohistochemical analysis confirmed that both CAMP and CTX induced extensive muscle destruction on day 5, although the effects of CTX were reversed over time. We identified the presence of fibrinogen and P-selectin exposure inside the damaged muscle sections, suggesting signs of bleeding and the formation of platelet aggregates/microthrombi in tissues, respectively. Intriguingly, CAMP causes integrin shedding but does not affect any blood clotting parameters, whereas CTX significantly extends the clotting time and has no impact on integrin shedding. The rates of fibrinogen clearance and reduction in microthrombi were greater in CTX-treated muscle compared to CAMP-treated muscle. Together, these findings reveal novel aspects of venom-induced muscle damage and highlight the relevance of haemostatic events such as bleeding and thrombosis for muscle regeneration and provide useful mechanistic insights for developing better therapeutic interventions.

**Keywords:** bleeding; cardiotoxin; metalloprotease; muscle damage; thrombosis; microthrombi

**Key Contribution:** This study examined haemostatic events during snake venom cardiotoxin- and metalloprotease-induced muscle damage in mice. Both catalytically active (CAMP) and non-enzymatic (CTX) toxins induced bleeding and thrombus formation in murine skeletal muscles; but different clearance rates for fibrinogen and microthrombi were observed. These data for CAMP and CTX to induce haemostatic responses in locally damaged skeletal muscle will help broaden their use as research tools and guide the development of better therapies to aid muscle regeneration following snakebite envenoming.



**Citation:** Sonavane, M.; Almeida, J.R.; Rajan, E.; Williams, H.F.; Townsend, F.; Cornish, E.; Mitchell, R.D.; Patel, K.; Vaiyapuri, S. Intramuscular Bleeding and Formation of Microthrombi during Skeletal Muscle Damage Caused by a Snake Venom Metalloprotease and a Cardiotoxin. *Toxins* **2023**, *15*, 530. <https://doi.org/10.3390/toxins15090530>

Received: 26 June 2023

Revised: 1 August 2023

Accepted: 21 August 2023

Published: 28 August 2023



**Copyright:** © 2023 by the authors. Licensee MDPI, Basel, Switzerland. This article is an open access article distributed under the terms and conditions of the Creative Commons Attribution (CC BY) license (<https://creativecommons.org/licenses/by/4.0/>).

## 1. Introduction

Snakebite envenoming (SBE) is one of the leading causes of mortality and morbidity among rural agricultural communities in many tropical countries [1,2]. SBE has been classified as a high-priority neglected tropical disease by the World Health Organisation (WHO) and causes around 150,000 deaths and 500,000 permanent disabilities worldwide every year [3]. Venom-induced skeletal muscle damage is a key factor of SBE-induced permanent disabilities [4]. Antivenoms are generally not beneficial in treating and preventing SBE-induced muscle damage as the large immunoglobulin molecules are unable to penetrate the damaged local tissues [5,6]. Moreover, the damaged blood vessels and blood clots (thrombi) in capillaries will restrict the blood flow to the affected tissues resulting in ischaemia, further preventing the antivenom from reaching the damaged regions [7]. Extensive tissue damage can necessitate surgical procedures such as fasciotomy (to release the compartment pressure), debridement (to remove the affected tissues), and amputation (to completely remove the affected region/limb to prevent further damage and infection) to manage this condition [8]. Hence, improving our fundamental understanding of how venom toxins affect skeletal muscle and induce permanent muscle damage is critical for developing effective treatments for SBE-induced muscle damage.

Venoms include both enzymatic and non-enzymatic proteins and small peptides [9,10]. Specific venom toxins such as three-finger toxins (3FTX), phospholipase A<sub>2</sub> (PLA<sub>2</sub>), and snake venom metalloproteases (SVMP) are the main components responsible for causing local tissue damage [7]. An earlier study from our group reported the mechanisms of action involved in skeletal muscle damage induced by a P-III SVMP (named CAMP) from the venom of *Crotalus atrox* in comparison to a 3FTX (cardiotoxin, CTX) from the venom of *Naja pallida* [11]. CAMP induced extensive damage to the extracellular matrix (ECM) and affected the functions of satellite cells and angiogenesis, impairing muscle regeneration. In contrast, CTX caused muscle necrosis although it did not affect satellite cells or the ECM, with full recovery from the damage being achieved through the innate muscle regeneration process [11]. However, the ability of these venom toxins to induce bleeding and thrombosis while causing muscle damage was not compared simultaneously in the previous study. The circulatory system and a continuous blood supply play a vital role in tissue repair and muscle regeneration [12]. However, damage to vasculature results in excessive bleeding, subsequent thrombus formation and inflammatory responses in the affected muscle [7,13,14]. Moreover, thrombus formation will rapidly consume circulating platelets and/or coagulation factors leading to venom-induced consumption coagulopathy, which further augments bleeding [15,16]. Therefore, it is critical to establish the mechanisms of action of muscle-damaging enzymatic and non-enzymatic venom components in inducing intramuscular bleeding and thrombosis. In this study, we determined the ability of CAMP and CTX in inducing bleeding and microthrombus formation in locally damaged skeletal muscle. The outcomes of this study provide evidence to demonstrate the impact of enzymatic (CAMP) and non-enzymatic (CTX) venom toxins in inducing bleeding and thrombosis in muscle tissues.

## 2. Results

### 2.1. CAMP and CTX Induce Damage to the Tibialis Anterior (TA) Muscle in Mice

To determine the impact of CAMP and CTX in inducing bleeding and thrombosis in skeletal muscle, they were intramuscularly injected (1 µg of CAMP or CTX in 30 µL of phosphate-buffered saline (PBS)) into the TA muscles of mice. The muscles were collected on days 5 and 10 and used for further analysis. The histological analysis of the muscles using haematoxylin and eosin (H&E) staining confirmed the quality of muscle sections. The undamaged control muscle (injected with the same volume of PBS) displayed a normal morphology (Figure 1A), whereas CTX and CAMP-treated muscles showed clear signs of damage (Figure 1B,C). The infiltration of immune cells was evident in the damaged areas of the muscles treated with CTX and CAMP on day 5. However, on day 10, the muscles showed signs of recovery (the presence of centrally located nuclei in myofibres

with reduced spaces between them, a reduced number of infiltrated immune cells and clusters of small fibres), especially in CTX-damaged tissues. These data confirm that both CTX and CAMP damaged the TA muscle as previously reported [11].

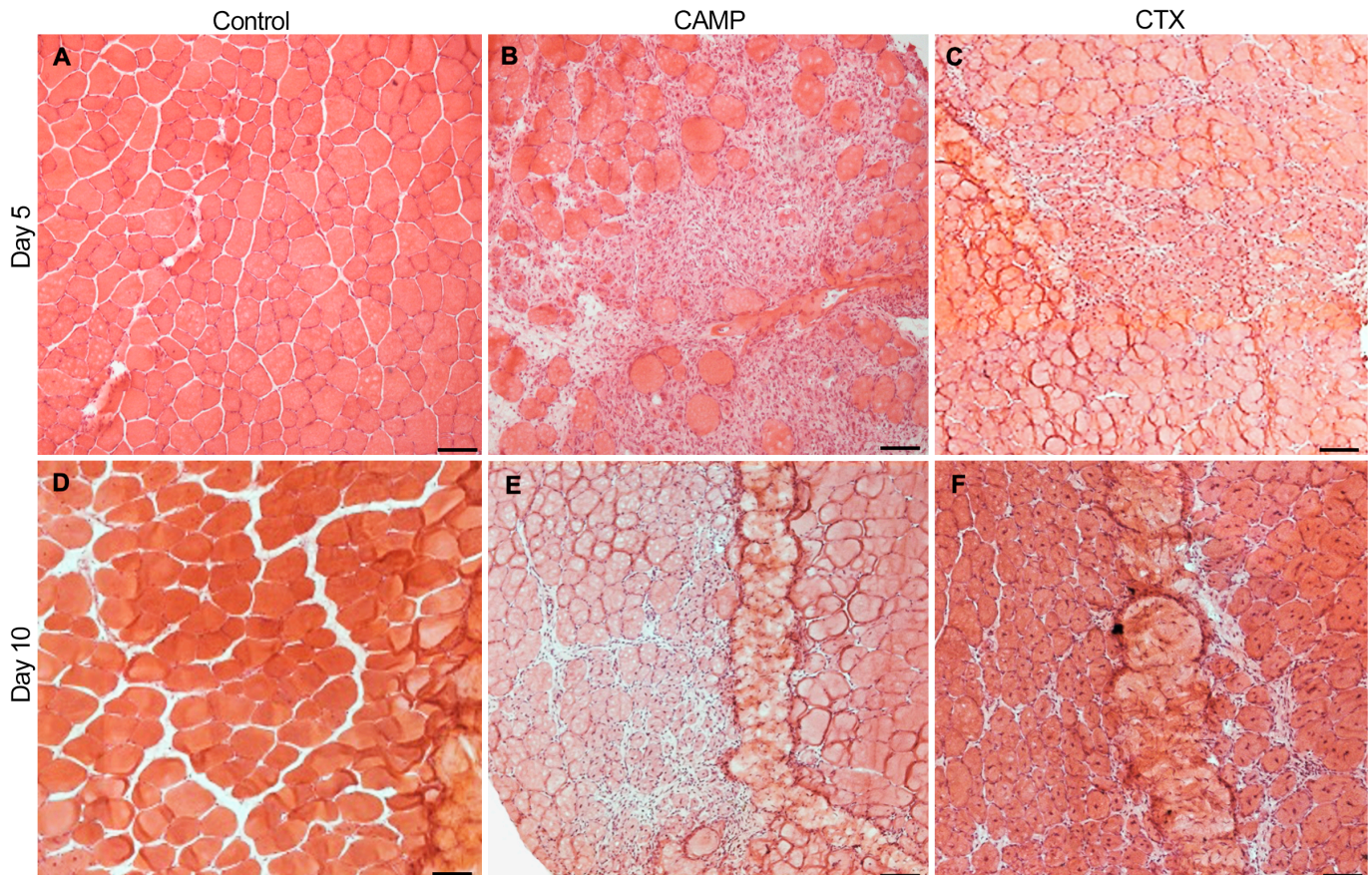


**Figure 1.** H & E staining of TA muscles treated with CAMP or CTX on days 5 and 10. The TA muscles of mice that were treated with PBS (A,D), CAMP (B,E) and CTX (C,F) were collected on days 5 and 10 following the injection of toxins, and their sections were analysed via H&E staining. The thickness of the muscle sections was 13  $\mu\text{m}$ . The scale bar represents 100  $\mu\text{m}$ . The images shown are representative of experiments performed using five mice in each cohort.

## 2.2. CAMP and CTX Induce Bleeding in Damaged Muscle

Fibrinogen is a highly abundant clotting protein in the blood, and it acts as a scaffold for platelet aggregation and thrombus formation. Therefore, the presence of fibrinogen was measured as a marker of bleeding in the muscle sections. CTX- and CAMP-treated muscle sections on days 5 and 10 along with control muscles were stained using FITC-labelled anti-fibrinogen antibodies. The control muscle showed no fibrinogen, indicating that there was no bleeding in the undamaged tissues (Figure 2A). However, CAMP-treated muscle sections showed the presence of fibrinogen on day 5 (with around 25% fluorescence intensity on average) although it was significantly reduced by day 10 to roughly 12% (Figure 2B). Similarly, the administration of CTX induced bleeding in the muscle on day 5, with a significant reduction on day 10. The percentage of fibrinogen was largely reduced by day 10 compared to day 5 in CTX-treated sections. Although CTX-treated muscle presented significantly higher fibrinogen in the muscle sections than CAMP-treated muscle on day 5, the clearance rate was greater with a reduction from an initial fluorescence intensity of 50% to 3% by day 10 in CTX-treated muscle. The presence of fibrinogen in both toxin-treated muscles indicated intramuscular bleeding, although we cannot rule out the staining of thrombi as they also contain fibrinogen.

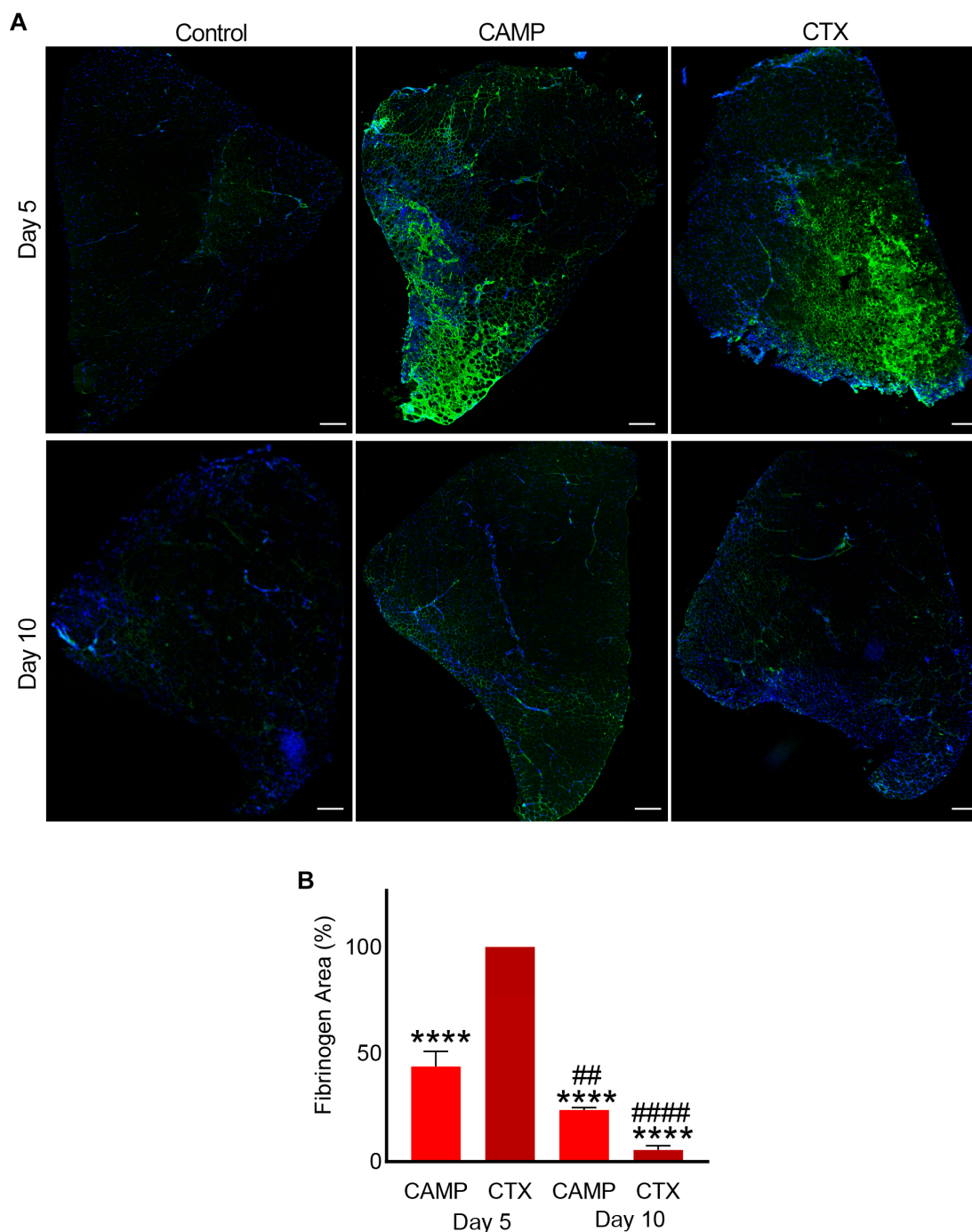


**Figure 2.** Intramuscular bleeding in muscles treated with CAMP and CTX. FITC-labelled anti-fibrinogen antibodies were used to stain CAMP- and CTX-treated muscle sections along with controls and analyse the extent of bleeding in the muscle at days 5 and 10 post-injection of the toxins. DAPI was used to stain the nuclei. **(A)** Representative images of control, CAMP- and CTX-treated TA muscles at days 5 and 10. **(B)** A bar diagram showing the level of fluorescence at days 5 and 10 in CAMP- and CTX-treated muscles, and their comparisons. The percentage of the fibrinogen area was calculated by dividing the fibrinogen-stained area by the total muscle area. The columns represent mean  $\pm$  SD (n = 5 mice for each cohort, five sections per mouse). \*\*\*\*  $p < 0.0001$  when compared to the level of fluorescence obtained at day 5 in CTX-treated muscle, which was taken as 100% to calculate the relative differences in others. ##  $p < 0.01$  and #####  $p < 0.0001$  when comparing CAMP- and CTX-treated muscle at day 10 with their corresponding values at day 5. Student’s t-test was used for independent variables. The scale bars represent 100  $\mu$ m.

### 2.3. Microthrombus Formation in CTX- and CAMP-Damaged Muscles

Microthrombi are small blood clots or aggregates of platelets and fibrin formed in capillaries and/or tissues. Upon stimulation of platelets, the inside-out signalling to the integrin  $\alpha\text{IIb}\beta\text{3}$  switches its conformation from a low-affinity state to a high-affinity state for fibrinogen binding, which causes the aggregation of platelets via the use of fibrinogen as a scaffold [17]. Similarly, P-selectin is secreted from  $\alpha$ -granules upon platelet activation. Both of these factors play a critical role in the formation of platelet-mediated blood clots [17]. Therefore, the presence of integrin  $\alpha\text{IIb}\beta\text{3}$  and P-selectin exposure on the surface of platelets confirms the existence of platelet aggregates/thrombi. The muscle sections obtained from CTX- and CAMP-treated mice were stained with FITC-labelled anti-integrin  $\alpha\text{IIb}\beta\text{3}$  and anti-P-selectin antibodies.

In CAMP-treated muscle, there was no detectable level of fluorescence observed for integrin  $\alpha\text{IIb}\beta\text{3}$  on either day 5 or 10 (Figure 3). However, CTX-treated muscle on days 5 and 10 displayed the presence of microthrombi as measured through the level of fluorescence for integrin  $\alpha\text{IIb}\beta\text{3}$ . Moreover, in CTX-treated muscles, the frequency of microthrombi was significantly reduced by day 10 compared to that on day 5, although the area of the microthrombi within the muscle remained the same.

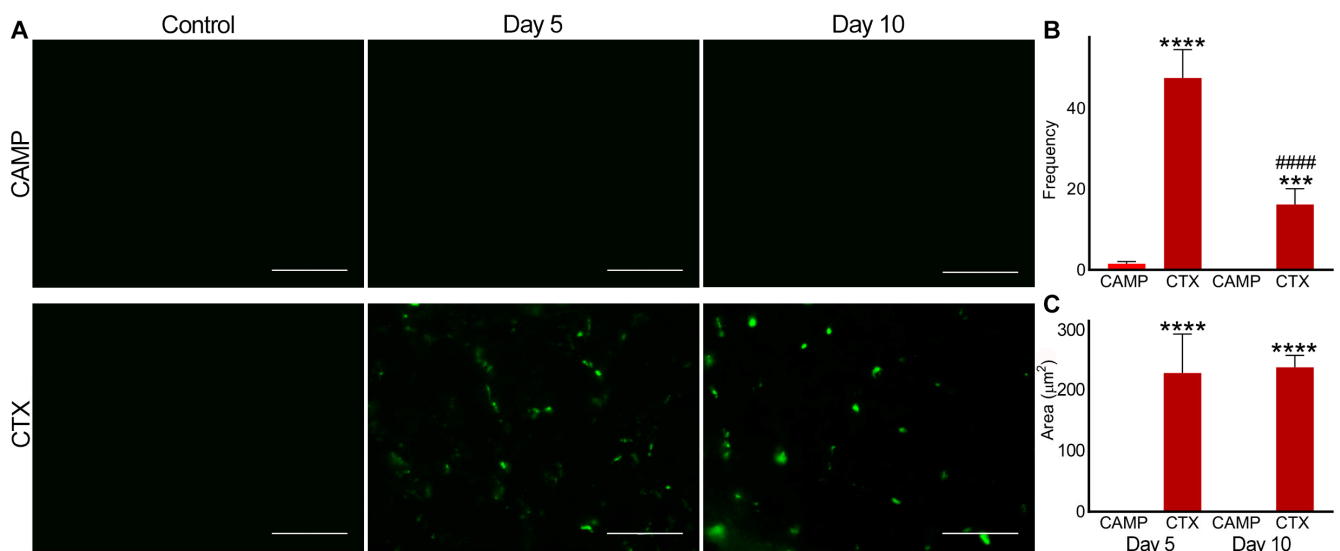


**Figure 3.** Analysis of microthrombus formation in CAMP- and CTX-damaged muscle by staining integrin  $\alpha\text{IIb}\beta\text{3}$ . FITC-conjugated anti-integrin  $\alpha\text{IIb}\beta\text{3}$  antibodies were used to stain and analyse microthrombus formation in TA muscles injected with PBS (control), CAMP or CTX on days 5 and 10 post-injection of the toxins. (A) Representative images of experiments performed with five mice in each cohort. Muscle sections were imaged at a  $40\times$  magnification. Images were analysed using the ImageJ 3D object counter to obtain the frequency (B) and area (C) of the microthrombi in CAMP- and CTX-treated muscles. The columns represent the mean  $\pm$  SD ( $n = 5$  mice for each cohort, five sections per mouse). \*\*\*  $p < 0.001$  and \*\*\*\*  $p < 0.0001$  when comparing CTX with CAMP on the corresponding day. #####  $p < 0.0001$  when comparing CTX day 10 to CTX at day 5. A one-way ANOVA followed by Tukey's test was used to analyse the data. The scale bars represent  $50\ \mu\text{m}$ .

Similarly, P-selectin was absent in the control muscle sections (Figure 4). However, it was evident in CAMP- and CTX-treated muscle sections on days 5 and 10, confirming the presence of microthrombi. On day 5, the frequency of microthrombi was around 20% higher in CAMP-treated muscles compared to that in CTX-treated muscles, although there was no difference in the size of the thrombi. Even on day 10, the frequency of the microthrombi was around 40% higher in CAMP-damaged muscles compared to that in CTX-treated muscles. However, CTX-treated muscles showed a significant reduction in microthrombus frequency of around 50% on day 10. The area of microthrombi was reduced by almost 50% on day 10 in both CAMP- and CTX-treated muscles compared to that on day 5.

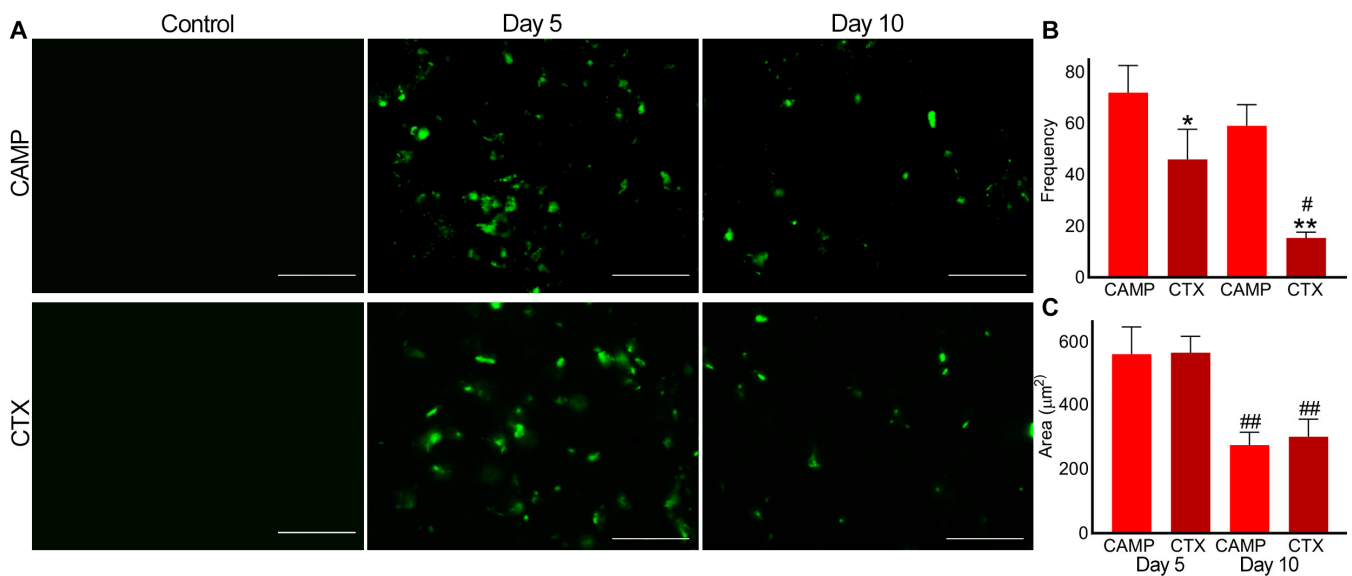


**Figure 4.** Analysis of microthrombus formation in CAMP- and CTX-induced muscle damage using P-selectin as a marker. FITC-conjugated mouse anti-P-selectin antibodies were used to stain and analyse microthrombus formation in mouse TA muscles injected with PBS (control), CAMP or CTX. (A) Representative images of experiments performed with five mice. The muscle sections were imaged at a 40× magnification. Images were analysed using an ImageJ 3D object counter to obtain the frequency (B) and area (C) of the microthrombi in CAMP- and CTX-treated muscles. The columns represent the mean ± SD (n = 5 mice for each cohort, five sections per mouse). \*  $p < 0.05$ , and \*\*  $p < 0.01$  when compared with CAMP on the corresponding day. #  $p < 0.05$  and ##  $p < 0.01$  when compared with the same toxin on day 5. A one-way ANOVA followed by Tukey’s test was used to analyse the data. The scale bars represent 50 µm.

#### 2.4. CTX Extends Clotting Time

To determine the direct effects of CAMP and CTX on blood clotting in human blood under in vitro settings, a rotational thromboelastometry (ROTEM) analysis was performed using human-citrated whole blood. The data of the intem analysis, which evaluates the intrinsic and common pathways, confirmed that clotting was delayed when CTX was added to the whole blood (Figure 5A). Moreover, it reduced fibrinolysis by around 30% compared to the controls. However, there was no significant difference in the clot size (area under the curve) or in clot firmness (data not shown) between the control and CTX-induced clots. Similarly, the extem analysis, which evaluated the extrinsic and common pathways, showed a delay in clotting time and reduced fibrinolysis in CTX-treated blood (Figure 5B). The impact of CTX on clotting, independently of platelets, was determined via fibtem analysis. This assay confirmed that clotting time was delayed, although clot firmness and size remained unchanged (Figure 5C). The aptem analysis (in the absence of fibrinolysis) suggested that CTX delayed blood clotting but slightly accelerated the clot formation time compared to that with CAMP (Figure 5D). These results indicate that CTX affects blood clotting through multiple coagulation pathways independently of platelets and fibrinolysis.

When similar experiments were performed using CAMP, it showed no major changes in clotting time, clot formation time, clot firmness or lysis compared to the controls in any analysis. Only in extem analysis did CAMP delay the clot formation time by around 10%.



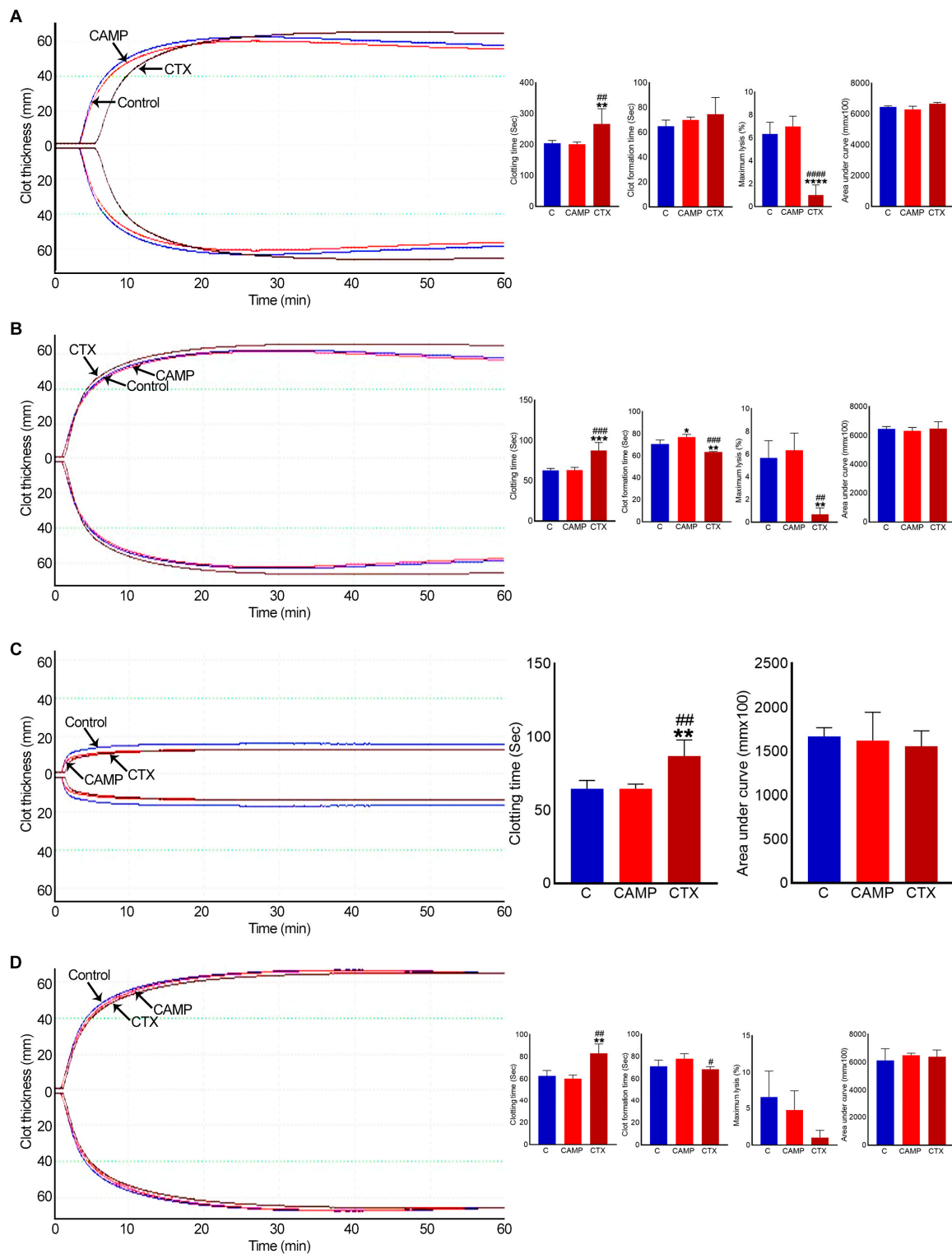


**Figure 5.** ROTEM analysis in whole human blood with CAMP and CTX. (A) Intem, (B) extm, (C) fibtem and (D) aptem data showing the impact of 10  $\mu$ M CAMP or CTX in human whole blood clotting via different pathways. Graphs represent clotting time, clot formation time, maximum lysis, and area under the curve. The columns represent the mean  $\pm$  SD (n = 4 independent donors from whom the blood samples were obtained for these experiments). \*  $p < 0.05$ , \*\*  $p < 0.01$ , \*\*\*  $p < 0.01$  and \*\*\*\*  $p < 0.0001$  when compared to the control group (C). #  $p < 0.05$ , ##  $p < 0.01$ , ###  $p < 0.001$  and ####  $p < 0.0001$  when compared to CAMP. A one-way ANOVA followed by Tukey’s test was used to analyse these data.

### 3. Discussion

The life-threatening pathophysiology of SBE is driven by the individual and synergistic actions of biologically active venom toxins with different molecular targets, which can lead to various effects in the body including haemostatic disturbances and muscle damage [18,19]. At the clinical level, venom-induced consumption coagulopathy (VICC) with diverse manifestations triggered by different toxins is a serious issue, and the resulting haemostatic effects may vary depending on the consumed factor in the coagulation cascade [20,21]. This systemic and potentially lethal phenomenon following SBE in patients is recognised via the activation of the clotting cascade and/or elevated degradation of the fibrinogen [22]. At a molecular level, toxins can affect thrombus formation via varied targets and/or due to their thrombolytic properties, resulting in thrombotic/bleeding complications [14]. However, the coordination and regulation of haemostatic responses following skeletal muscle injury including intramuscular bleeding and thrombosis have not been fully understood. Determining the differences that contribute to these haemostatic events by studying clinically relevant venom toxins is key to elucidating the general impacts on muscle damage and subsequent regeneration. Due to the role that the circulatory system plays in wound healing and tissue regeneration, it is vital to study its state during venom-induced muscle damage. The circulatory system delivers leukocytes to damaged areas to enable the clearing of cell debris and to prevent infections [23]. Additionally, the limited effectiveness of currently used antivenom treatment for managing local tissue injury and mitigating its long-standing consequences [5,24] reiterates the importance of a comprehensive investigation of venom-induced muscle damage including haemostatic elements to allow the development of better management strategies for this condition. Therefore, we analysed a parallel comparison of haemotoxicity induced by enzymatic (CAMP) and non-enzymatic (CTX) muscle-damaging venom components during skeletal muscle damage to establish their diverse effects.

SVMPs are crucial components in viper venom-induced myotoxicity due to their ability to hinder adequate muscle regeneration and complete functional recovery following acute damage [25]. The proteolytic activity of these toxins causes important alterations to different components of the muscle architecture, especially the ECM, which is essential for muscle regeneration [4,11]. CAMP was previously reported to damage the ECM in skeletal muscle [11]. As shown here, during CAMP-induced muscle injury, there was extensive local damage with significant bleeding, as evidenced by fibrinogen in the injured muscles. In vitro studies have previously demonstrated that some P-III SVMPs have a fibrinogenolytic effect on human plasma fibrinogen [26]. Therefore, CAMP might directly cleave plasma fibrinogen as well as affecting the ECM in blood capillaries during muscle damage to induce bleeding. Earlier research has established that viper venoms contain procoagulant toxins that can induce VICC due to the consumption of clotting factors [27]. These proteolytic enzymes often cause rapid clot formation in vitro but can induce bleeding complications due to the rapid consumption of several factors. Fibrinogen, the common point of the clotting pathway, is the most consistently consumed factor in VICC [15]. Notably, some studies have revealed that SVMPs could cleave integrins and fibrin clots, leading to further bleeding [28,29]. As a P-III SVMP, CAMP has a disintegrin-like functional domain in its structure but a possible reason for the lack of the integrin  $\alpha\text{IIb}\beta\text{3}$  signal in the muscle tissues is likely due to its direct effect on this integrin shedding. Integrin  $\alpha\text{IIb}\beta\text{3}$  plays a crucial role in platelet aggregation and adhesion [30]. Therefore, a lack of integrin  $\alpha\text{IIb}\beta\text{3}$  might be one of the main causes of extensive and prolonged bleeding in CAMP-damaged muscle. Treatment with CAMP enhanced the detection of P-selectin in the microthrombi of damaged tissue. CAMP treatment showed a high frequency of P-selectin microthrombi within the muscle even at a later time point, indicating ongoing muscle damage. Moreover, CAMP may possess thrombolytic properties, and the reduction in the microthrombi area could be due to thrombolysis. Interestingly, CAMP exhibited an insignificant effect on intem and extem analysis. The intrinsic pathway is initiated by activators such as collagen, which is a substrate for CAMP. Hence, the lack of collagen in the

blood due to CAMP activity could indicate the indirect effects of CAMP on item analysis. These findings highlight the mechanistic action of a purified toxin, CAMP, on inducing bleeding and thrombotic complications during muscle damage. However, this cannot be generalized to all SVMPs in diverse venoms as they possess variable potencies, substrate specificities and a diverse range of pharmacological properties, which can also interact with other families of toxins to exert synergistic activities. Similarly, when whole venom is used, the level of haemotoxic effects may vary compared to those of the purified toxin.

In the CTX-induced injury model, we observed acute muscle damage accompanied by bleeding and thrombosis. CTX extended the clotting time in ROTEM analysis, which suggests its ability to cause bleeding. The likely mechanisms of CTX-induced bleeding may include the necrosis of endothelial cells in microcapillaries that perfuse the damaged muscle and/or anticoagulant properties of these non-enzymatic molecules. In the first scenario, lysis or necrosis of the cell membrane leads to capillary permeation, causing blood to leak into the interstitial space of muscle tissue. This event could also be related to the activation of native matrix metalloproteases, which regulate vascular ECM and homeostasis [31]. This increases blood flow to the damaged site and aids the perpetuation of the haemorrhagic effect [32,33]. In the second case, some 3FTXs can bind and inhibit specific coagulation factors or complexes [34]. For example, members of this toxin family, such as hemextin A, ringhalexin and exactin have been proposed as potential anticoagulant lead molecules for the development of therapeutics, research tools and diagnostic probes due to their selective effects on specific coagulation factors [35,36]. The first wave of haemostasis is due to the accumulation of platelets at the site of the injury [37]. Platelet activation and thrombus formation are achieved by the modulation and binding of various receptors on the platelet surface to their ligands. Platelet integrins and their ligands initiate stable adhesion, and inside-out signalling to integrin  $\alpha\text{IIb}\beta\text{3}$  recruits more platelets for aggregation. The integrin  $\alpha\text{IIb}\beta\text{3}$  enhances platelet activation through cytoskeleton rearrangement and granule secretion, thereby facilitating haemostatic plug or thrombus formation. The lack of integrin  $\alpha\text{IIb}\beta\text{3}$  reduces platelet aggregation and impairs thrombus growth. In CTX-injured muscle sections, integrin staining revealed clots, which may be one of the reasons why CTX-induced bleeding gradually improves. P-selectin plays a crucial role in thrombus formation and wound healing pathways by recruiting white blood cells to the injured site. The frequency of P-selectin-stained thrombi decreased in CTX-mediated damage with the progression of tissue repair, suggesting that the muscle damage was advancing towards a resolution. Similar results were reported in a recent study exploring the contribution of platelet-released chemokines to successful muscle regeneration [38]. In this study, platelet thrombi were monitored using anti-GP1b $\beta$  antibodies, which showed the presence of these aggregates in early stages (on days 1 and 7), with a considerable reduction at day 14 in the CTX-induced muscle injury model [38]. Our CTX-induced muscle injury model corroborated these previous findings. Additionally, the same study showed how platelet-derived signals modulate neutrophil recruitment and coordinate a favourable niche for immune infiltration and myogenesis that precede the restoration of muscle structure and function [38]. The use of neutrophil-depleted mice has revealed the active involvement of neutrophils in the regenerative phase following the damage caused by *Bothrops asper* [39]. Imbalances in these events can establish a persistent inflammatory state with a predominance of atrophic mediators that culminate in unresolved damage, as observed in the CAMP-induced muscle injury model. The ROTEM analysis showed that CTX may affect intrinsic and extrinsic pathways as well as the common pathway as it delayed clotting time in all analyses. This suggests the need for further investigations to establish the exact contribution of CTX to clotting cascades and thereby, intramuscular bleeding and thrombosis.

The paradigm of successful or poor muscle regeneration following elapid and viperid envenomation has been mainly discussed with relevance to the impact of the protagonist toxins and their effects on essential components for myogenesis, such as the ECM, inflammation, and blood supply [11,40,41]. Figure 6 summarises the current knowledge of venom toxin-mediated muscle damage with key features/events that affect the regenerative process. The results of this study are also included in this scheme and highlighted in red. Earlier studies have shown that CAMP damages the capillaries and hinders angiogenesis in damaged muscles [42,43]. On the other hand, the degradation of the ECM in skeletal muscle leads to a lack of scaffolding for myogenesis and angiogenesis [44]. Hence, muscle tissue struggles with regeneration when P-III metalloproteases are administered. In a previous study from our group, CTX caused no change in the number of capillaries per muscle fibre [11]. This observation suggested that CTX does not have direct haemotoxic properties through affecting ECM and angiogenesis. The current results based on different biomarkers show that haemorrhage occurs in CTX-damaged muscle. The actions of matrix metalloproteases in vasculature remodelling and tissue regeneration after muscle injury may also contribute to bleeding and subsequent thrombosis [45]. Interestingly, the level of fibrinogen was significantly reduced with the progression of muscle regeneration. This reduction in fibrinogen aligns with the fact that intact blood capillaries facilitated muscle repair. Since fibrinogen deposition can promote a profibrotic environment, the reduction in fibrinogen levels in CTX-induced muscle injury is consistent with reduced fibrosis and better functional outcomes during elapid snake envenomation [46]. However, a lower clearance rate was detected in CAMP-damaged muscle sections. As discussed earlier and supported by previous studies [47–49], neutrophils are fundamental players in muscle repair progress and they help to orchestrate a pro-reparative scenario dictated by macrophage phenotype transition [50]. Neutrophil recruitment to damaged tissue in turn can be modulated by platelet-derived chemokines and microthrombus formation, which may account for differences in the removal rates of fibrinogen and intramuscular microthrombi [38,51]. The action and temporal presence of these myotoxins must also be considered in this speculative view. Previous studies have shown the long-lasting presence of SVMP, which leads to continuous ECM degradation and haemorrhagic effects [11,52]. The temporal action of cardiotoxin is in line with the restoration of muscle architecture and complete removal of the signs of intramuscular bleeding [53,54]. In summary, the accumulation of this evidence supports the current concept of poor muscle regeneration in viperid envenomation due to direct damage to vasculature with dysregulated responses, subsequent poor repair, and severe tissue destruction [55]. As a result, this reduced remodelling in the CAMP-induced muscle injury model leads to extensive collagen deposition, seen as the excessive muscle accumulation of fibrous connective tissue that affects the motile and contractile functions of SBE victims [56].

In summary, this comparative study demonstrates intramuscular bleeding and microthrombus formation following SVMP- or 3FTX-induced myotoxicity. Overall, it offers valuable insights into the homeostasis of muscle tissue and their rearrangements induced by catalytically active and non-enzymatic venom molecules with their specific actions on haemostatic processes. This highlights the importance of studying disturbances induced by overlooked toxins that may contribute to the severe pathological sequelae observed in skeletal muscle. Our observational study raises a series of hypotheses that deserve deeper analysis. For example, the presence of fibrinogen and potential intramuscular bleeding in CTX-induced muscle injury needs further investigation. Additionally, research focused on pharmacological interventions is important to identify the extent and the role of these alterations and the underlying mechanisms that impede muscle regeneration. By integrating their mechanism of action in haemostatic effects, we provide a better picture of the toxins' impacts on thrombus formation, bleeding, and vascular damage in venom-induced muscle injury. These will pave the way to a comprehensive understanding of the processes involved in muscle damage and its possible implications for the development of life-changing solutions to treat venom-induced muscle injury, facilitate tissue regeneration,

and prevent long-term physical sequelae. In practical terms, the multidimensional nature of muscle damage and the diversity of underlying factors require more detailed investigations that may culminate in therapeutic benefits and clinical translation. Future studies should explore whether or not variations in toxins would influence the pattern of haemostatic responses during muscle damage described here and evaluate the neutralisation of these muscle-perturbing venom proteins using current and next-generation antivenom therapies.

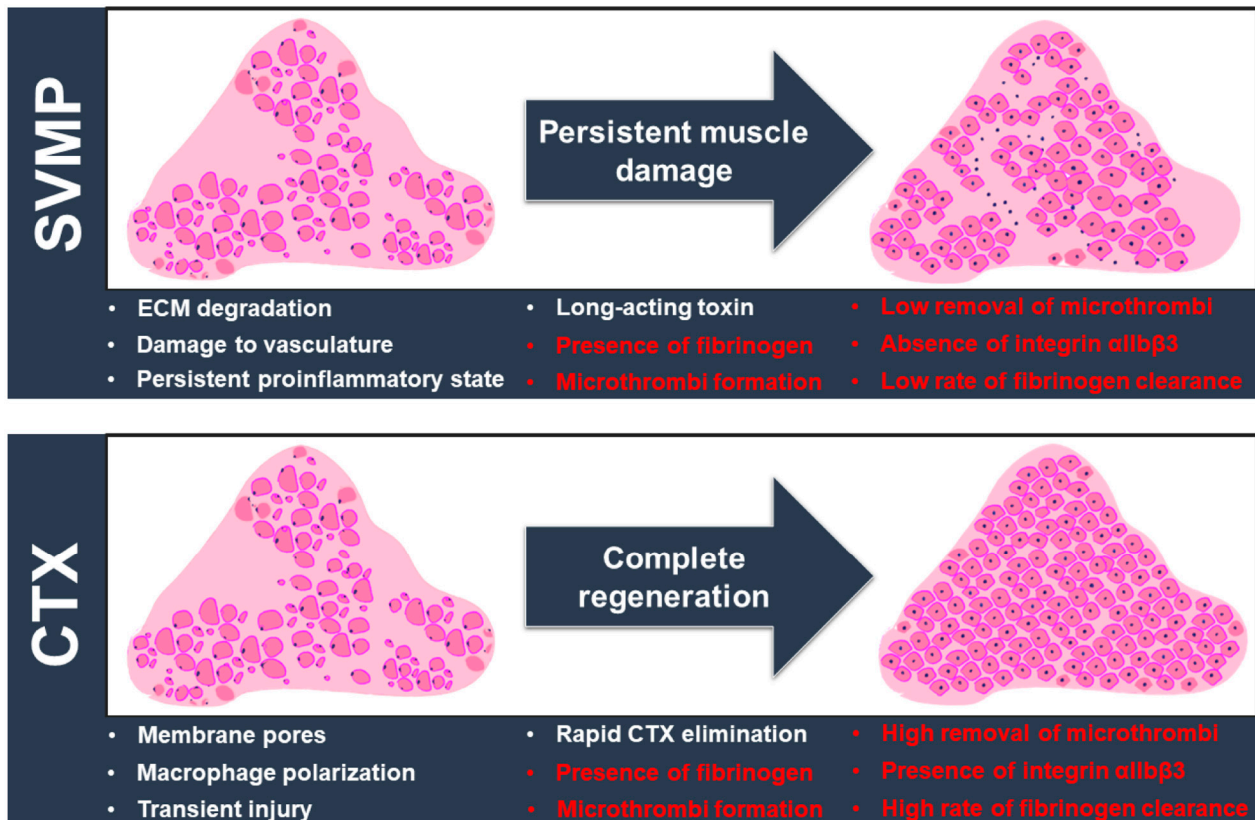


**Figure 6.** The landscape of venom-induced muscle damage by SVMPs and CTX. SVMP (specifically CAMP) and CTX induce extensive muscle damage through different actions (as shown in white), but their different mechanisms of action lead to divergent outcomes. Key factors influencing the muscle regeneration process are highlighted here. The different outcomes developed following SVMP/CTX-induced muscle damage are shown in red. SVMP hydrolyses the ECM components and causes vascular alterations, with a significant impact on the influx of inflammatory cells. A persistent proinflammatory environment drives the excessive deposition of fibrous connective tissues with alterations in muscle architecture and functional implications. On the other hand, CTX triggers an acute, transient injury through a membranolytic action without compromising the ECM and vasculature. A spatiotemporal transition of inflammatory cells promotes a myogenic program resulting in complete regeneration. The normal architecture of the muscle is then re-established with a homogenous distribution of fibre sizes and morphology. We evidenced the intramuscular presence of fibrinogen and microthrombus formation in muscle damage induced by both toxins. However, significant differences in terms of the clearance rate of fibrinogen, removal of microthrombi and levels of integrin  $\alpha\text{IIb}\beta\text{3}$  were detected. They may be related to the two contrasting muscle regeneration profiles. Another important aspect to be considered is the kinetic action and removal of myotoxins. The long-term presence of SVMPs is likely to drive repetitive degradative/regenerative cycles that hamper the complete elimination of fibrinogen and microthrombi and exacerbate the inflammatory state that impairs tissue repair. In contrast, CTX has a transient activity that culminates in the successful removal of fibrinogen and microthrombi, which should result in a favourable outcome for regeneration.

## 4. Materials and Methods

### 4.1. Materials Used

Purified CTX from the venom of the red-spitting cobra (*Naja pallida*) was purchased from Latoxan (Valence, France). Lyophilised *Crotalus atrox* (*C. atrox*) venom was purchased from Sigma Aldrich (Gillingham, UK). CAMP was purified from the venom of *C. atrox* using a combination of ion exchange and gel filtration chromatography, as reported previously [11].

### 4.2. Injection of Venom Toxins in TA Muscles of Mice

All mice were anaesthetised using 3.5% (*v/v*) isoflurane in oxygen and then kept at 2% (*v/v*) isoflurane throughout the procedure. An amount of 1 µg of purified CAMP or CTX in a 30 µL volume was injected into the left TA muscle. The right TA muscle was given a control injection of 30 µL of PBS. The mice were monitored for either 5 or 10 days before being sacrificed via CO<sub>2</sub> inhalation and muscle collection.

### 4.3. Dissection and Processing of Tissues

The tissue samples were collected on either day 5 or 10 following the injection of toxins. Animals were dissected, and the TA muscles were carefully removed from the tendon to avoid mechanical damage. The muscle samples were frozen in liquid nitrogen-cooled isopentane and kept at −80 °C. The muscle tissue was then embedded in Tissue-TEK<sup>®</sup> OCT (Optimal Cutting Temperature) medium and sliced into 13 µm thick transverse sections using a cryo-microtome. These sections were placed onto glass slides and stored at −80 °C until required for further use.

### 4.4. H&E Staining of Muscle Sections

The muscle sections on glass slides were removed from the −80 °C freezer and left at room temperature for 15 min, and later, the sections were soaked in PBS to rehydrate them. The slides were then submerged in Harris haematoxylin stain for two minutes. After rinsing the slides in water for two minutes, they were dipped twice in 70% acidic alcohol (70% ethanol (*v/v*) and 0.1% (*v/v*) HCl) and then rinsed again in water for five minutes. The slides were then placed into a container with a 1% (*w/v*) eosin solution for two minutes and then transferred into a slide container containing 70% ethanol. The slides were dehydrated by soaking them in 70%, 90%, and 100% ethanol. Finally, the slides were transferred into xylene for two rounds of three minutes. The sections were fixed using distyrene, plasticiser and xylene (DPX) mounting media. The muscle sections were observed and imaged using a Zeiss AxioImager light microscope (five sections per mouse, 5 mice for each cohort).

### 4.5. Immunohistochemistry of TA Muscle Sections

Using a wash buffer solution (PBS with 5% (*v/v*) foetal bovine serum and 0.05% (*v/v*) Triton X-100), FITC-conjugated primary antibodies (anti-human fibrinogen antibodies from Agilent Technologies, Stockport, UK and anti-integrin αIIbβ3 and anti-P-selectin antibodies were from Emfret Analytics, Eibelstadt, Germany) were diluted at 1:50 dilution. The slides were cleaned and hydrated three times with PBS for 5 min each. Next, a permeabilisation buffer (20 mM HEPES, 3 mM MgCl<sub>2</sub>, 50 mM NaCl, 0.05% (*w/v*) sodium azide, 300 mM sucrose and 0.5% (*v/v*) Triton X-100) was added and allowed to incubate for 15 min. A blocking wash buffer was added and incubated for 30 min. The pre-made primary antibodies were added, and the slides were incubated for 1 h at room temperature. Unbound antibodies were washed off, and the slides were mounted in 6-diamino-2-phenylindole (DAPI) containing mounting media. The sections (five sections per mouse and five mice for each cohort) were visualised, and the images were obtained using a Zeiss AxioImager fluorescence microscope (Zeiss Microscopy Ltd., Cambridge, UK). For fibrinogen, the whole-muscle image which was made using multiple images of that muscle at a 10× objective, was analysed using threshold analysis. The baseline threshold was set using the muscle image of an undamaged mouse. For P-selectin and

integrin  $\alpha$ IIb $\beta$ 3, multiple images for each muscle section from each mouse were taken using a 40 $\times$  objective. Using the Image J (version 1.53k, NIH, Bethesda, MD, USA) 3D analysis tool, the baselines were set using undamaged contralateral muscle and then the number and area of thrombi were quantified. For each mouse, the values were calculated as means and then analysed together with the data obtained from all animals.

#### 4.6. ROTEM Analysis

The ROTEM Delta analyser (Werfen, UK), was used to study the effects of CAMP and CTX on human whole blood clotting. Intem and extem analyses were conducted to determine the impact of venom toxins on intrinsic and extrinsic as well as common pathways of blood clotting, respectively. Fibtem analysis was carried out to determine the effects of toxins on clotting in the absence of platelets, while aptem analysis was completed to assess the impact of venom toxins on blood clotting in the lack of fibrinolysis. In each assay, 10  $\mu$ M of CAMP or CTX was mixed with 300  $\mu$ L of citrated whole human blood and pre-set volumes of the respective reagents for different assays in accordance with the manufacturer's instructions. The blood samples were recalcified using a startem reagent (0.2 M CaCl<sub>2</sub> in a HEPES buffer, pH 7.4), and clotting was initiated using intrinsic (partial thromboplastin phospholipid from rabbit brain and ellagic acid) and extrinsic clotting activators (recombinant tissue factor, phospholipids, and heparin). The fibtem (cytochalasin D and 0.2 M CaCl<sub>2</sub> in the HEPES buffer, pH 7.4) and aptem (aprotinin and 0.2 M CaCl<sub>2</sub> in the HEPES buffer, pH 7.4) assays were performed using specific reagents before the initiation of clotting using the extem activation reagent. Various parameters of whole blood coagulation were analysed using ROTEM assays.

#### 4.7. Statistical Analysis

All statistical analyses were performed using GraphPad Prism 8. Based on the data type, a student t-test or one-way ANOVA was used to calculate the *p* values to determine statistical significance. All the staining procedures and analyses were performed blindly by individuals who were not involved in experimental procedures on mice.

**Author Contributions:** Conceptualisation, M.S., K.P. and S.V.; methodology, M.S., K.P. and S.V.; software, K.P. and S.V.; validation, M.S. and S.V.; formal analysis, M.S., K.P. and S.V.; investigation, M.S., K.P., H.F.W., E.R., F.T., E.C. and S.V.; resources, K.P. and S.V.; data curation, M.S., J.R.A., H.F.W., E.R., F.T., E.C., R.D.M. and S.V.; writing—original draft preparation, M.S., K.P. and S.V.; writing—review and editing, M.S., J.R.A., and S.V.; visualisation, M.S., J.R.A. and S.V.; supervision, K.P. and S.V.; project administration, S.V.; funding acquisition, M.S., K.P. and S.V. All authors have read and agreed to the published version of the manuscript.

**Funding:** This research was funded by the Medical Research Council, UK (reference: MR/W019353/1).

**Institutional Review Board Statement:** The animal experiments were performed in line with the principles and guidelines of the British Home Office (PPL70/7516) and the Animals Scientific Procedures Act 1986 and approved by the University of Reading Research Ethics Committee. The blood collection from healthy humans for ROTEM analysis was also approved by the University of Reading Research Ethics Committee on 10th May 2017 (reference number: UREC 17/17).

**Informed Consent Statement:** Informed consent was obtained from all subjects involved in this study for blood collection, and they consented for publishing the results in this article.

**Data Availability Statement:** All data from this study are included within this manuscript.

**Acknowledgments:** We would like to thank Jarred Williams for proofreading this manuscript.

**Conflicts of Interest:** The authors declare no conflict of interest.

## References

1. Williams, D.J.; Faiz, M.A.; Abela-Ridder, B.; Ainsworth, S.; Bulfone, T.C.; Nickerson, A.D.; Habib, A.G.; Junghanss, T.; Fan, H.W.; Turner, M.; et al. Strategy for a globally coordinated response to a priority neglected tropical disease: Snakebite envenoming. *PLoS Neglected Trop. Dis.* **2019**, *13*, e0007059. [[CrossRef](#)] [[PubMed](#)]
2. Samuel, S.P.; Chinnaraju, S.; Williams, H.F.; Pichamuthu, E.; Subharao, M.; Vaiyapuri, M.; Arumugam, S.; Vaiyapuri, R.; Baksh, M.F.; Patel, K.; et al. Venomous snakebites: Rapid action saves lives—A multifaceted community education programme increases awareness about snakes and snakebites among the rural population of Tamil Nadu, India. *PLoS Neglected Trop. Dis.* **2020**, *14*, e0008911. [[CrossRef](#)]
3. Gutiérrez, J.M.; Calvete, J.J.; Habib, A.G.; Harrison, R.A.; Williams, D.J.; Warrell, D.A. Snakebite envenoming. *Nat. Rev. Dis. Primers* **2017**, *3*, 17063. [[CrossRef](#)] [[PubMed](#)]
4. Sanchez-Castro, E.E.; Pajuelo-Reyes, C.; Tejedó, R.; Soria-Juan, B.; Tapia-Limonchi, R.; Andreu, E.; Hitos, A.B.; Martín, F.; Cahuana, G.M.; Guerra-Duarte, C.; et al. Mesenchymal stromal cell-based therapies as promising treatments for muscle regeneration after snakebite envenoming. *Front. Immunol.* **2021**, *11*, 609961. [[CrossRef](#)]
5. Williams, H.F.; Layfield, H.J.; Vallance, T.; Patel, K.; Bicknell, A.B.; Trim, S.A.; Vaiyapuri, S. The urgent need to develop novel strategies for the diagnosis and treatment of snakebites. *Toxins* **2019**, *11*, 363. [[CrossRef](#)] [[PubMed](#)]
6. Knudsen, C.; Laustsen, A.H. Recent advances in next generation snakebite antivenoms. *Trop. Med. Infect. Dis.* **2018**, *3*, 42. [[CrossRef](#)]
7. Gutiérrez, J.M.; Escalante, T.; Hernández, R.; Gastaldello, S.; Saravia-Otten, P.; Rucavado, A. Why is skeletal muscle regeneration impaired after myonecrosis induced by viperid snake venoms? *Toxins* **2018**, *10*, 182. [[CrossRef](#)]
8. Russell, J.J.; Schoenbrunner, A.; Janis, J.E. Snake Bite management: A scoping review of the literature. *Plast. Reconstr. Surg. Glob. Open* **2021**, *9*, e3506. [[CrossRef](#)]
9. Ferraz, C.R.; Arrahman, A.; Xie, C.; Casewell, N.R.; Lewis, R.J.; Kool, J.; Cardoso, F.C. Multifunctional toxins in snake venoms and therapeutic implications: From pain to hemorrhage and necrosis. *Front. Ecol. Evol.* **2019**, *7*, 218. [[CrossRef](#)]
10. Almeida, J.R.; Gomes, A.; Mendes, B.; Aguiar, L.; Ferreira, M.; Brioschi, M.B.C.; Duarte, D.; Nogueira, F.; Cortes, S.; Salazar-Valenzuela, D.; et al. Unlocking the potential of snake venom-based molecules against the malaria, Chagas disease, and leishmaniasis triad. *Int. J. Biol. Macromol.* **2023**, *242*, 124745. [[CrossRef](#)]
11. Williams, H.F.; Mellows, B.A.; Mitchell, R.; Sfyri, P.; Layfield, H.J.; Salamah, M.; Vaiyapuri, R.; Collins-Hooper, H.; Bicknell, A.B.; Matsakas, A.; et al. Mechanisms underpinning the permanent muscle damage induced by snake venom metalloprotease. *PLoS Neglected Trop. Dis.* **2019**, *13*, e0007041. [[CrossRef](#)]
12. Laumonier, T.; Menetrey, J. Muscle injuries and strategies for improving their repair. *J. Exp. Orthop.* **2016**, *3*, 15. [[CrossRef](#)]
13. Stark, K.; Massberg, S. Interplay between inflammation and thrombosis in cardiovascular pathology. *Nat. Rev. Cardiol.* **2021**, *18*, 666–682. [[CrossRef](#)]
14. Larréché, S.; Chippaux, J.P.; Chevillard, L.; Mathé, S.; Résière, D.; Siguret, V.; Mégarbane, B. Bleeding and thrombosis: Insights into pathophysiology of *Bothrops* venom-related hemostasis disorders. *Int. J. Mol. Sci.* **2021**, *22*, 9643. [[CrossRef](#)]
15. Berling, I.; Isbister, G.K. Hematologic effects and complications of snake envenoming. *Transf. Med. Rev.* **2015**, *29*, 82–89. [[CrossRef](#)]
16. Slagboom, J.; Kool, J.; Harrison, R.A.; Casewell, N.R. Haemotoxic snake venoms: Their functional activity, impact on snakebite victims and pharmaceutical promise. *Br. J. Haematol.* **2017**, *177*, 947–959. [[CrossRef](#)] [[PubMed](#)]
17. Durrant, T.N.; van den Bosch, M.T.; Hers, I. Integrin  $\alpha(\text{IIb})\beta(3)$  outside-in signaling. *Blood* **2017**, *130*, 1607–1619. [[CrossRef](#)]
18. Almeida, J.R.; Resende, L.M.; Watanabe, R.K.; Carregari, V.C.; Huanchuire-Vega, S.; Caldeira, C.A.S.; Coutinho-Neto, A.; Soares, A.M.; Vale, N.; Gomes, P.A.C.; et al. Snake venom peptides and low mass proteins: Molecular tools and therapeutic Agents. *Curr. Med. Chem.* **2017**, *24*, 3254–3282. [[CrossRef](#)] [[PubMed](#)]
19. Silva, L.M.; Silva, C.A.; Silva, A.; Vieira, R.P.; Mesquita-Ferrari, R.A.; Cogo, J.C.; Zamuner, S.R. Photobiomodulation protects and promotes differentiation of C2C12 myoblast cells exposed to snake venom. *PLoS ONE* **2016**, *11*, e0152890. [[CrossRef](#)]
20. Senthilkumaran, S.; Patel, K.; Rajan, E.; Vijayakumar, P.; Miller, S.W.; Rucavado, A.; Gilabadi, S.; Sonavane, M.; Richards, N.J.; Williams, J.; et al. Peripheral arterial thrombosis following Russell’s viper bites. *TH Open* **2023**, *7*, e168–e183. [[CrossRef](#)] [[PubMed](#)]
21. Senthilkumaran, S.; Almeida, J.R.; Williams, J.; Williams, H.F.; Thirumalaikolundusubramanian, P.; Patel, K.; Vaiyapuri, S. Rapid identification of bilateral adrenal and pituitary haemorrhages induced by Russell’s viper envenomation results in positive patient outcome. *Toxicon* **2023**, *225*, 107068. [[CrossRef](#)]
22. Maduwage, K.; Isbister, G.K. Current treatment for venom-induced consumption coagulopathy resulting from snakebite. *PLoS Neglected Trop. Dis.* **2014**, *8*, e3220. [[CrossRef](#)] [[PubMed](#)]
23. Forcina, L.; Cosentino, M.; Musarò, A. Mechanisms regulating muscle regeneration: Insights into the interrelated and time-dependent phases of tissue healing. *Cells* **2020**, *9*, 1297. [[CrossRef](#)] [[PubMed](#)]
24. Vera-Palacios, A.L.; Sacoto-Torres, J.D.; Hernández-Altamirano, J.A.; Moreno, A.; Peñuela-Mora, M.C.; Salazar-Valenzuela, D.; Mogollón, N.G.S.; Almeida, J.R. A first look at the inhibitory potential of *Urospatha sagittifolia* (Araceae) ethanolic extract for *Bothrops atrox* snakebite envenomation. *Toxins* **2022**, *14*, 496. [[CrossRef](#)]
25. Gutiérrez, J.M.; Rucavado, A. Snake venom metalloproteinases: Their role in the pathogenesis of local tissue damage. *Biochimie* **2000**, *82*, 841–850. [[CrossRef](#)]
26. Olaoba, O.T.; Karina Dos Santos, P.; Selistre-de-Araujo, H.S.; Ferreira de Souza, D.H. Snake venom metalloproteinases (SVMPs): A structure-function update. *Toxicon X* **2020**, *7*, 100052. [[CrossRef](#)]




27. Park, E.J.; Choi, S.; Kim, H.H.; Jung, Y.S. Novel treatment strategy for patients with venom-induced consumptive coagulopathy from a pit viper bite. *Toxins* **2020**, *12*, 295. [[CrossRef](#)] [[PubMed](#)]
28. Kini, R.M.; Koh, C.Y. Metalloproteases affecting blood coagulation, fibrinolysis, and platelet aggregation from snake venoms: Definition and nomenclature of interaction sites. *Toxins* **2016**, *8*, 284. [[CrossRef](#)]
29. Sanchez, E.F.; Richardson, M.; Gremski, L.H.; Veiga, S.S.; Yarleque, A.; Niland, S.; Lima, A.M.; Estevao-Costa, M.I.; Eble, J.A. A novel fibrinolytic metalloproteinase, barnettlysin-I from *Bothrops barnetti* (barnett's pitviper) snake venom with anti-platelet properties. *Biochim. Biophys. Acta—Gen. Subj.* **2016**, *1860*, 542–556. [[CrossRef](#)]
30. Huang, J.; Li, X.; Shi, X.; Zhu, M.; Wang, J.; Huang, S.; Huang, X.; Wang, H.; Li, L.; Deng, H.; et al. Platelet integrin  $\alpha\text{IIb}\beta\text{3}$ : Signal transduction, regulation, and its therapeutic targeting. *J. Hematol. Oncol.* **2019**, *12*, 26. [[CrossRef](#)]
31. Wang, X.; Khalil, R.A. Matrix metalloproteinases, vascular remodeling, and vascular disease. *Adv. Pharmacol.* **2018**, *81*, 241–330. [[CrossRef](#)]
32. Yang, W.; Hu, P. Skeletal muscle regeneration is modulated by inflammation. *J. Orthop. Translat.* **2018**, *13*, 25–32. [[CrossRef](#)]
33. Megha, K.B.; Joseph, X.; Akhil, V.; Mohanan, P.V. Cascade of immune mechanism and consequences of inflammatory disorders. *Phytomedicine* **2021**, *91*, 153712. [[CrossRef](#)]
34. Kini, R.M.; Koh, C.Y. Snake venom three-finger toxins and their potential in drug development targeting cardiovascular diseases. *Biochem. Pharmacol.* **2020**, *181*, 114105. [[CrossRef](#)]
35. Girish, V.M.; Kini, R.M. Exactin: A specific inhibitor of Factor X activation by extrinsic tenase complex from the venom of *Hemachatus haemachatus*. *Sci. Rep.* **2016**, *6*, 32036. [[CrossRef](#)]
36. Barnwal, B.; Jobichen, C.; Girish, V.M.; Foo, C.S.; Sivaraman, J.; Kini, R.M. Ringhalexin from *Hemachatus haemachatus*: A novel inhibitor of extrinsic tenase complex. *Sci. Rep.* **2016**, *6*, 25935. [[CrossRef](#)]
37. Hou, Y.; Carrim, N.; Wang, Y.; Gallant, R.C.; Marshall, A.; Ni, H. Platelets in hemostasis and thrombosis: Novel mechanisms of fibrinogen-independent platelet aggregation and fibronectin-mediated protein wave of hemostasis. *J. Biomed. Res.* **2015**, *29*, 437–444. [[CrossRef](#)]
38. Graca, F.A.; Stephan, A.; Minden-Birkenmaier, B.A.; Shirinifard, A.; Wang, Y.D.; Demontis, F.; Labelle, M. Platelet-derived chemokines promote skeletal muscle regeneration by guiding neutrophil recruitment to injured muscles. *Nat. Commun.* **2023**, *14*, 2900. [[CrossRef](#)] [[PubMed](#)]
39. Teixeira, C.F.; Zamunér, S.R.; Zuliani, J.P.; Fernandes, C.M.; Cruz-Hofling, M.A.; Fernandes, I.; Chaves, F.; Gutiérrez, J.M. Neutrophils do not contribute to local tissue damage, but play a key role in skeletal muscle regeneration, in mice injected with *Bothrops asper* snake venom. *Muscle Nerve* **2003**, *28*, 449–459. [[CrossRef](#)] [[PubMed](#)]
40. Escalante, T.; Saravia-Otten, P.; Gastaldello, S.; Hernández, R.; Marín, A.; García, G.; García, L.; Estrada, E.; Rucavado, A.; Gutiérrez, J.M. Changes in basement membrane components in an experimental model of skeletal muscle degeneration and regeneration induced by snake venom and myotoxic phospholipase A<sub>2</sub>. *Toxicon* **2021**, *192*, 46–56. [[CrossRef](#)] [[PubMed](#)]
41. Masuda, H.; Sato, A.; Shizuno, T.; Yokoyama, K.; Suzuki, Y.; Tokunaga, M.; Asahara, T. Batroxobin accelerated tissue repair via neutrophil extracellular trap regulation and defibrinogenation in a murine ischemic hindlimb model. *PLoS ONE* **2019**, *14*, e0220898. [[CrossRef](#)] [[PubMed](#)]
42. Escalante, T.; Shannon, J.; Moura-da-Silva, A.M.; Gutiérrez, J.M.; Fox, J.W. Novel insights into capillary vessel basement membrane damage by snake venom hemorrhagic metalloproteinases: A biochemical and immunohistochemical study. *Arch. Biochem. Biophys.* **2006**, *455*, 144–153. [[CrossRef](#)] [[PubMed](#)]
43. Escalante, T.; Rucavado, A.; Fox, J.W.; Gutiérrez, J.M. Key events in microvascular damage induced by snake venom hemorrhagic metalloproteinases. *J. Proteomics.* **2011**, *74*, 1781–1794. [[CrossRef](#)] [[PubMed](#)]
44. Zhang, W.; Liu, Y.; Zhang, H. Extracellular matrix: An important regulator of cell functions and skeletal muscle development. *Cell Biosci.* **2021**, *11*, 65. [[CrossRef](#)]
45. Chen, X.; Li, Y. Role of matrix metalloproteinases in skeletal muscle: Migration, differentiation, regeneration and fibrosis. *Cell Adhes. Migr.* **2009**, *3*, 337–341. [[CrossRef](#)]
46. Vidal, B.; Serrano, A.L.; Tjwa, M.; Suelves, M.; Ardite, E.; De Mori, R.; Baeza-Raja, B.; Martínez de Lagrán, M.; Lafuste, P.; Ruiz-Bonilla, V.; et al. Fibrinogen drives dystrophic muscle fibrosis via a TGFbeta/alternative macrophage activation pathway. *Genes Dev.* **2008**, *22*, 1747–1752. [[CrossRef](#)]
47. Ranéia e Silva, P.A.; da Costa Neves, A.; da Rocha, C.B.; da Rocha, C.B.; Moura-da-Silva, A.M.; Faquim-Mauro, E.L. Differential macrophage subsets in muscle damage induced by a K49-PLA<sub>2</sub> from *Bothrops jararacussu* venom modulate the time course of the regeneration process. *Inflammation* **2019**, *42*, 1542–1554. [[CrossRef](#)]
48. Zuliani, J.P.; Soares, A.M.; Gutiérrez, J.M. Polymorphonuclear neutrophil leukocytes in snakebite envenoming. *Toxicon* **2020**, *187*, 188–197. [[CrossRef](#)]
49. Garcia Denegri, M.E.; Teibler, G.P.; Maruñak, S.L.; Hernández, D.R.; Acosta, O.C.; Leiva, L.C. Efficient muscle regeneration after highly haemorrhagic *Bothrops alternatus* venom injection. *Toxicon* **2016**, *122*, 167–175. [[CrossRef](#)]
50. Paiva-Oliveira, E.L.; da Silva, R.F.; Bellio, M.; Quirico-Santos, T.; Lagrota-Candido, J. Pattern of cardiotoxin-induced muscle remodeling in distinct TLR-4 deficient mouse strains. *Histochem. Cell Biol.* **2017**, *148*, 49–60. [[CrossRef](#)]
51. Ulloa-Fernández, A.; Escalante, T.; Gutiérrez, J.M.; Rucavado, A. Platelet depletion enhances lethal, hemorrhagic and myotoxic activities of *Bothrops asper* snake venom in a murine model. *Toxicon* **2022**, *219*, 106936. [[CrossRef](#)]

52. Van de Velde, A.C.; Fusco, L.S.; Echeverría, S.M.; Sasovsky, D.J.; Leiva, L.C.; Gutiérrez, J.M.; Bustillo, S. Traces of *Bothrops* snake venoms in necrotic muscle preclude myotube formation in vitro. *Toxicon* **2022**, *211*, 36–43. [[CrossRef](#)] [[PubMed](#)]
53. Wang, Y.; Lu, J.; Liu, Y. Skeletal muscle regeneration in cardiotoxin-induced muscle injury models. *Int. J. Mol. Sci.* **2022**, *23*, 13380. [[CrossRef](#)]
54. Yan, Z.; Choi, S.; Liu, X.; Zhang, M.; Schageman, J.J.; Lee, S.Y.; Hart, R.; Lin, L.; Thurmond, F.A.; Williams, R.S. Highly coordinated gene regulation in mouse skeletal muscle regeneration. *J. Biol. Chem.* **2003**, *278*, 8826–8836. [[CrossRef](#)]
55. Hernández, R.; Cabalceta, C.; Saravia-Otten, P.; Chaves, A.; Gutiérrez, J.M.; Rucavado, A. Poor regenerative outcome after skeletal muscle necrosis induced by *Bothrops asper* venom: Alterations in microvasculature and nerves. *PLoS ONE* **2011**, *6*, e19834. [[CrossRef](#)]
56. Waidyanatha, S.; Silva, A.; Siribaddana, S.; Isbister, G.K. Long-term effects of snake envenoming. *Toxins* **2019**, *11*, 193. [[CrossRef](#)] [[PubMed](#)]

**Disclaimer/Publisher’s Note:** The statements, opinions and data contained in all publications are solely those of the individual author(s) and contributor(s) and not of MDPI and/or the editor(s). MDPI and/or the editor(s) disclaim responsibility for any injury to people or property resulting from any ideas, methods, instructions or products referred to in the content.



# Peripheral Arterial Thrombosis following Russell's Viper Bites

Subramanian Senthilkumaran<sup>1,\*</sup> Ketan Patel<sup>2,\*</sup> Elanchezhian Rajan<sup>3,\*</sup> Pradeep Vijayakumar<sup>3</sup> Stephen W. Miller<sup>4</sup> Alexandra Rucavado<sup>5</sup> Soheil Gilabadi<sup>3</sup> Medha Sonavane<sup>3</sup> Nicholas J. Richards<sup>2</sup> Jarred Williams<sup>3</sup>  Harry F. Williams<sup>6</sup> Steven A. Trim<sup>7</sup> Ponniah Thirumalaikolundusubramanian<sup>8</sup> José María Gutiérrez<sup>5</sup> Sakthivel Vaiyapuri<sup>3</sup>

<sup>1</sup> Department of Emergency Medicine, Manian Medical Centre, Erode, Tamil Nadu, India

<sup>2</sup> School of Biological Sciences, University of Reading, Reading, United Kingdom

<sup>3</sup> School of Pharmacy, University of Reading, Reading, United Kingdom

<sup>4</sup> The Poison Control Center, Children's Hospital of Philadelphia, Philadelphia, Pennsylvania, United States

<sup>5</sup> Instituto Clodomiro Picado, Facultad de Microbiología, Universidad de Costa Rica, San José, Costa Rica

**Address for correspondence** Sakthivel Vaiyapuri, MSc, PhD, School of Pharmacy, University of Reading, Reading, RG6 6UB, United Kingdom (e-mail: s.vaiyapuri@reading.ac.uk).

<sup>6</sup> Toxiven Biotech Private Limited, Coimbatore, Tamil Nadu, India

<sup>7</sup> Venomtech Limited, Sandwich, United Kingdom

<sup>8</sup> The Tamil Nadu Dr M.G.R. Medical University, Chennai, Tamil Nadu, India

TH Open 2023;7:e168–e183.

## Abstract

Envenomings by Russell's viper (*Daboia russelii*), a species of high medical importance in India and other Asian countries, commonly result in hemorrhage, coagulopathies, necrosis, and acute kidney injury. Although bleeding complications are frequently reported following viper envenomings, thrombotic events occur rarely (reported only in coronary and carotid arteries) with serious consequences. For the first time, we report three serious cases of peripheral arterial thrombosis following Russell's viper bites and their diagnostic, clinical management, and mechanistic insights. These patients developed occlusive thrombi in their peripheral arteries and symptoms despite antivenom treatment. In addition to clinical features, computed tomography angiography was used to diagnose arterial thrombosis and ascertain its precise locations. They were treated using thrombectomy or amputation in one case that presented with gangrenous digits. Mechanistic insights into the pathology through investigations revealed the procoagulant actions of Russell's viper venom in standard clotting tests as well as in rotational thromboelastometry analysis. Notably, Russell's viper venom inhibited agonist-induced platelet activation. The procoagulant effects of Russell's viper venom were inhibited by a matrix metalloprotease inhibitor, marimastat, although a phospholipase A<sub>2</sub> inhibitor (varespladib) did not show any inhibitory effects. Russell's viper venom induced pulmonary thrombosis when injected intravenously in mice and thrombi in the microvasculature and affected skeletal muscle when administered locally. These data emphasize the significance of peripheral arterial thrombosis in snakebite victims and provide awareness, mechanisms, and robust strategies for clinicians to tackle this issue in patients.

## Keywords

- ▶ Russell's viper
- ▶ snakebite envenomation
- ▶ thrombosis
- ▶ peripheral arteries
- ▶ venom

\* These authors contributed equally to this study.

received  
November 30, 2022  
accepted after revision  
April 5, 2023

DOI <https://doi.org/10.1055/s-0043-1769625>  
ISSN 2512-9465.

© 2023. The Author(s).

This is an open access article published by Thieme under the terms of the Creative Commons Attribution License, permitting unrestricted use, distribution, and reproduction so long as the original work is properly cited. (<https://creativecommons.org/licenses/by/4.0/>)  
Georg Thieme Verlag KG, Rüdigerstraße 14, 70469 Stuttgart, Germany

## Introduction

Snakebite envenoming (SBE) has been classified as a high-priority neglected tropical disease by the World Health Organization. SBE results in around 140,000 deaths and 500,000 permanent disabilities annually worldwide.<sup>1,2</sup> Around 58,000 deaths occur every year in India alone, resulting in it being regarded as the “snakebite capital of the world.”<sup>3</sup> Russell's viper (*Daboia russelii*) is one of the “big four” venomous snakes (together with the Indian cobra [*Naja naja*], common krait [*Bungarus caeruleus*], and saw-scaled viper [*Echis carinatus*]) in India and is responsible for a majority of venomous bites resulting in deaths and disabilities.<sup>4–7</sup> The consequences of Russell's viper bites typically range from mild local effects to severe local necrosis and muscle damage as well as systemic effects such as hemorrhage, coagulopathies, neurotoxicity, and acute kidney injury.<sup>8</sup> Most SBE victims reside in rural, impoverished areas that lack adequate resources to handle these medical emergencies.<sup>9</sup> Moreover, victims who lack essential awareness of SBE often seek traditional treatments and other unproven methods thus delaying proven, time-sensitive treatments.<sup>6,7</sup> Delay in seeking appropriate treatment exacerbates envenoming effects resulting in serious consequences including death or loss of limbs.<sup>7</sup>

Snake venoms contain a range of toxins which can affect multiple organs, tissues, and the blood coagulation system.<sup>10,11</sup> Due to the nature of toxins present in its venom, Russell's viper bites may lead to transient, asymptomatic coagulopathies or overt hemorrhage in the bite site as well as in internal organs including the kidneys, brain, lungs, and spleen, often with poor prognosis.<sup>12–14</sup> Russell's viper bite-induced bleeding complications are commonly observed, and they often lead to fatalities or permanent disabilities.<sup>14–16</sup> Similar to many other viper venoms,<sup>12,13</sup> Russell's viper venom induces consumption coagulopathy which results in rapid depletion of coagulation factors owing to the action of procoagulant enzymes, and this contributes to excessive bleeding.<sup>14,17</sup> Venom procoagulant activities may also result in thrombosis in the microvasculature and less commonly in large blood vessels which can lead to ischemic stroke.<sup>18–20</sup> SBE-induced ischemic stroke has been reported to cause bilateral blindness with permanent disabilities in rare cases.<sup>21</sup> Sudden cardiac arrest following SBE including Russell's viper envenoming has also been reported.<sup>22,23</sup> While bleeding complications are often reported for Russell's viper as well as other viper bites, peripheral arterial thrombosis (specifically in limbs) following SBE has never been reported. Even the envenomings by the Caribbean endemic species, *Bothrops lanceolatus*, which often induce pulmonary embolism, myocardial infarction, and cerebral ischemia did not cause peripheral arterial thrombosis in limbs.<sup>24,25</sup> Here, we report three serious cases of peripheral arterial thrombosis in upper limbs following Russell's viper bite envenomings and discuss their underlying molecular mechanisms and clinical management strategies. This study provides essential awareness of the life-threatening impacts of SBE, which is urgently needed and adds to our growing understanding of the pathophysiology of envenomings by Russell's viper.

## Results

### Clinical Presentation of Patients

The first patient was a 21-year-old male auto-rickshaw driver who was bitten by a snake on a finger in his right hand while cleaning his vehicle near a pond in Sathyamagan within the Erode district of Tamil Nadu (South India). The offending snake was identified as Russell's viper by an experienced herpetologist (►Fig. 1A). The patient presented at a local hospital 75 minutes after the bite with symptoms of fever, vomiting, pain, bleeding at the bite site, and swelling of the right upper arm. He was treated with 18 vials (i.e., 180 mL) of equine polyvalent antivenom (Biological E Limited, India) raised against the Indian “big four” venomous snakes 100 minutes after the bite occurred. There was no history of oliguria, hematuria, ptosis, neck or limb weakness, or myalgia. The initial diffuse pain became localized to the fingers of his right hand and increased in intensity. He was subsequently referred to our emergency department (Manian Medical Centre, Erode, Tamil Nadu, India) 22 hours after the bite for further management. On examination, there was severe tenderness up to the axilla and limb swelling (►Fig. 1B). The entire limb was discolored, cold and clammy, and movement of the affected limb and fingers caused severe pain. Transthoracic echocardiography showed an ejection fraction of 70%, an absence of valvular pathology, and normal systolic and diastolic function. Laboratory investigations indicated normal values of D-dimer, fibrinogen, hemoglobin, platelet count, prothrombin time (PT), and activated partial thromboplastin time (aPTT), along with other parameters (►Table 1). His chest and neck X-ray as well as a chest computed tomography (CT) scan failed to reveal any thoracic outlet syndrome.

The second patient was a 35-year-old female housewife who was bitten on the right index finger by a snake while cleaning her cattle shed near Perundurai in the Erode district of Tamil Nadu. The snake was identified as Russell's viper (►Fig. 1C) by a herpetologist. The patient had no history of underlying diseases such as cancer, pregnancy, oral contraceptives, or type 2 diabetes mellitus and was COVID-19 negative. No underlying conditions were observed that would result in increased levels of procoagulant zymogens, decreased levels of coagulation inhibitors, or fibrinolytic abnormalities. She presented to a local hospital 90 minutes after the bite with severe pain and bleeding at the bite site and was treated with 20 vials (i.e., 200 mL) of polyvalent antivenom (VINS Bioproducts Limited, India) around 2 hours after the bite and given intravenous administration of broad-spectrum antibiotics. During the next 48 hours, she developed sudden onset of pain and swelling of the right hand which extended up to the elbow and was accompanied by pain and discoloration of the thumb and index finger. These symptoms persisted and she was referred to our emergency department (Manian Medical Centre) 4 days after the bite as there was no improvement. Physical examination revealed absent pulses of her right radial artery and well-defined gangrene of the distal phalanges of the right thumb, ring finger, and little finger, as well as the entire index finger



**Fig. 1** The offending Russell's viper specimens and local envenoming effects in victims. (A) The offending snake species of the first patient was identified as Russell's viper by a herpetologist. (B) Russell's viper bite induced bleeding at the bite site and swelling and discoloration of the right arm of the first patient. (C) The offending snake species which was confirmed as Russell's viper for the second patient (D), who displayed gangrenous digits (including the index finger where the bite occurred) in their right hand. The specimen of Russell's viper (E), which bit the third patient at the nape of the neck and caused local bleeding (F).

(►Fig. 1D). The neurological assessment revealed a lack of nociception in the affected area. Patent foramen ovale was ruled out as a cause of paradoxical embolism with transthoracic echocardiography. Tests for lupus anticoagulant, factor V Leiden, and prothrombin allele mutations were all negative. The levels of antithrombin, proteins C and S, and all other parameters (►Table 1) were within the normal limits.

The third patient was a 32-year-old male farmer who, while picking fruits in his farmland near Gobichettipalayam (Erode district, Tamil Nadu) was bitten by a Russell's viper (as confirmed by a herpetologist; ►Fig. 1E) on the nape of his neck (►Fig. 1F). He was admitted to our emergency department (Manian Medical Centre) within 90 minutes of the bite with a painful and swollen right upper limb, oozing blood from the bite location, and bleeding gums. The patient had no history of underlying diseases/conditions such as cancer and type 2 diabetes mellitus and was negative for COVID-19. There were no other diagnosed conditions relating to clotting abnormalities. On examination, the limb was swollen up to the hand, clammy and discolored. A 20-minute whole blood clotting test (WBCT20) for coagulopathy was performed and found to be prolonged (►Table 1). Since the patient presented with both local and systemic signs and symptoms of

envenoming, he was treated with 10 vials of (i.e., 100 mL) polyvalent antivenom (Bharat Serums and Vaccines Limited, India) within 2 hours after the bite. Hematologic, metabolic, biochemical, and coagulation parameters were found to be within normal limits after 4 hours of antivenom administration. Despite antivenom treatment, the patient developed a painful, swollen area in the right retro clavicular, supraclavicular region and anterior side of the right upper arm. He subsequently developed wrist drop, inability to flex all fingers, and total loss of sensation in the right arm. Both active flexion and passive extension of the elbow produced severe pain. The examination discovered an absent brachial, ulnar, and radial pulse. He was found to have 60% oxygen saturation in his right middle finger; however, all other right-hand fingers had 0% saturation and no flow tracing. There was no evidence of intracardiac thrombus or shunt on the transthoracic echocardiogram. The patient's thrombophilic profile (factor V Leiden, prothrombin mutation, homocysteine, and deficiencies for protein C, protein S, and antithrombin III) was unremarkable.

The antivenom in all patients was administered in line with the standard protocols (i.e., 10 vials stat over 30 minutes and then 6 vials every 6 hours based on the symptoms)

**Table 1** Laboratory investigation results using clinical samples obtained from patients upon admission to our emergency department

Specimen	Investigation	Patient 1	Patient 2	Patient 3	Unit	Normal range
EDTA blood	Hemoglobin	13.2	11.3	13.8	g%	12.0–16.0
EDTA blood	Total RBC count	4.74	4.99	4.82	Millions/ $\mu$ L	4.00–5.50
EDTA blood	HCT	39.8	35.4	41.0	%	33.00–50.00
EDTA blood	MCV	84.0	70.9	85.1	fl	81.10–96.00
EDTA blood	MCH	27.8	22.6	28.6	pg	27.20–33.20
EDTA blood	MCHC	33.2	31.9	33.7	%	32–36
EDTA blood	Total WBC count	11.88	6.26	13.91	$\times 10^3$ cells/ $\mu$ L	4.00–11.00
EDTA blood	Neutrophils	8.09	3.62	11.71	$\times 10^3$ cells/ $\mu$ L	2.0–7.0
EDTA blood	Lymphocytes	2.34	2.1	0.98	$\times 10^3$ cells/ $\mu$ L	1.0–3.0
EDTA blood	Monocytes	1.03	0.42	1.21	$\times 10^3$ cells/ $\mu$ L	0.1–0.8
EDTA blood	Eosinophils	0.37	0.1	0.0	$\times 10^3$ cells/ $\mu$ L	0.02–0.5
EDTA blood	Basophils	0.05	0.02	0.01	$\times 10^3$ cells/ $\mu$ L	0.02–0.1
EDTA blood	Neutrophils	68.1	57.9	84.2	%	55–75
EDTA blood	Lymphocytes	19.7	33.5	7.0	%	15–30
EDTA blood	Eosinophils	3.1	1.6	0.0	%	1–5
EDTA blood	Monocytes	8.7	6.7	8.7	%	2–10
EDTA blood	Basophils	0.4	0.3	0.1	%	Up to 1
EDTA blood	Platelet count	240	336	319	$\times 10^3$ cells/ $\mu$ L	150–450
EDTA blood	MPV	11.0	9.4	9.4	fl	6.5–12.0
EDTA blood	PDW	13.5	9.6	9.8	fl	9.0–13.0
Serum	Urea	21.4	14.98	14.98	mg/dL	15–40
Serum	Creatinine	1.02	0.76	0.89	mg/dL	0.6–1.4
Serum	Uric acid	4.7	5.0	6.9	mg/dL	3.4–7.2
Citrated plasma	Prothrombin time	13.8	14.3	26.2	Seconds	11.6 (control)
Citrated plasma	INR	1.26	1.31	2.39	Ratio	
Citrated plasma	aPTT	35.2	34.1	34.3	Seconds	26–40
Serum	Bilirubin (total)	0.85	0.68	1.0	mg/dL	0.2–1.2
Serum	Bilirubin (direct)	0.32	0.28	0.38	mg/dL	0–0.2
Serum	Bilirubin (indirect)	0.53	0.4	0.62	mg/dL	0.2–0.9
Serum	SGOT	16	14	35	U/L	5–35
Serum	SGPT	14	15	27	U/L	5.0–45

Abbreviations: aPTT, activated partial thromboplastin time; HCT, hematocrit; INR, international normalized ratio of clotting; MCH, mean corpuscular hemoglobin; MCHC, mean corpuscular hemoglobin concentration; MCV, mean corpuscular volume; MPV, mean platelet volume; PDW, platelet distribution width; RBC, red blood cells; SGOT, serum glutamic oxaloacetic transaminase; SGPT, serum glutamic pyruvate transaminase; WBC, white blood cells.

provided by the Government of India for the management of snakebites ([https://nhm.gov.in/images/pdf/guidelines/nrhm-guidelines/stg/Snakebite\\_QRG.pdf](https://nhm.gov.in/images/pdf/guidelines/nrhm-guidelines/stg/Snakebite_QRG.pdf)).

### CT Angiography Revealed the Presence of Thrombi in Peripheral Arteries

The clinical features such as pain, numbness, change in skin color, absence of pulses, and limited range of motion in these patients suggested that thrombosis might have occurred in their peripheral blood vessels. Compartment syndrome was suspected in the first patient and therefore a preliminary

Doppler ultrasound was performed. This revealed impaired blood flow to the extreme forearm arteries indicating acute limb ischemia. Subsequently, he was evaluated with a peripheral CT angiogram which showed complete occlusion of the right brachial artery (**Fig. 2A**). Similarly, a peripheral CT angiogram in the second patient revealed distal radial artery occlusion and short-segment occlusion in the palmar arterial arch between the thumb and the index fingers (**Fig. 2B**). In addition, one of the two digital arteries of the thumb and both digital arteries of the index finger were occluded. For the third patient, a clinical diagnosis of

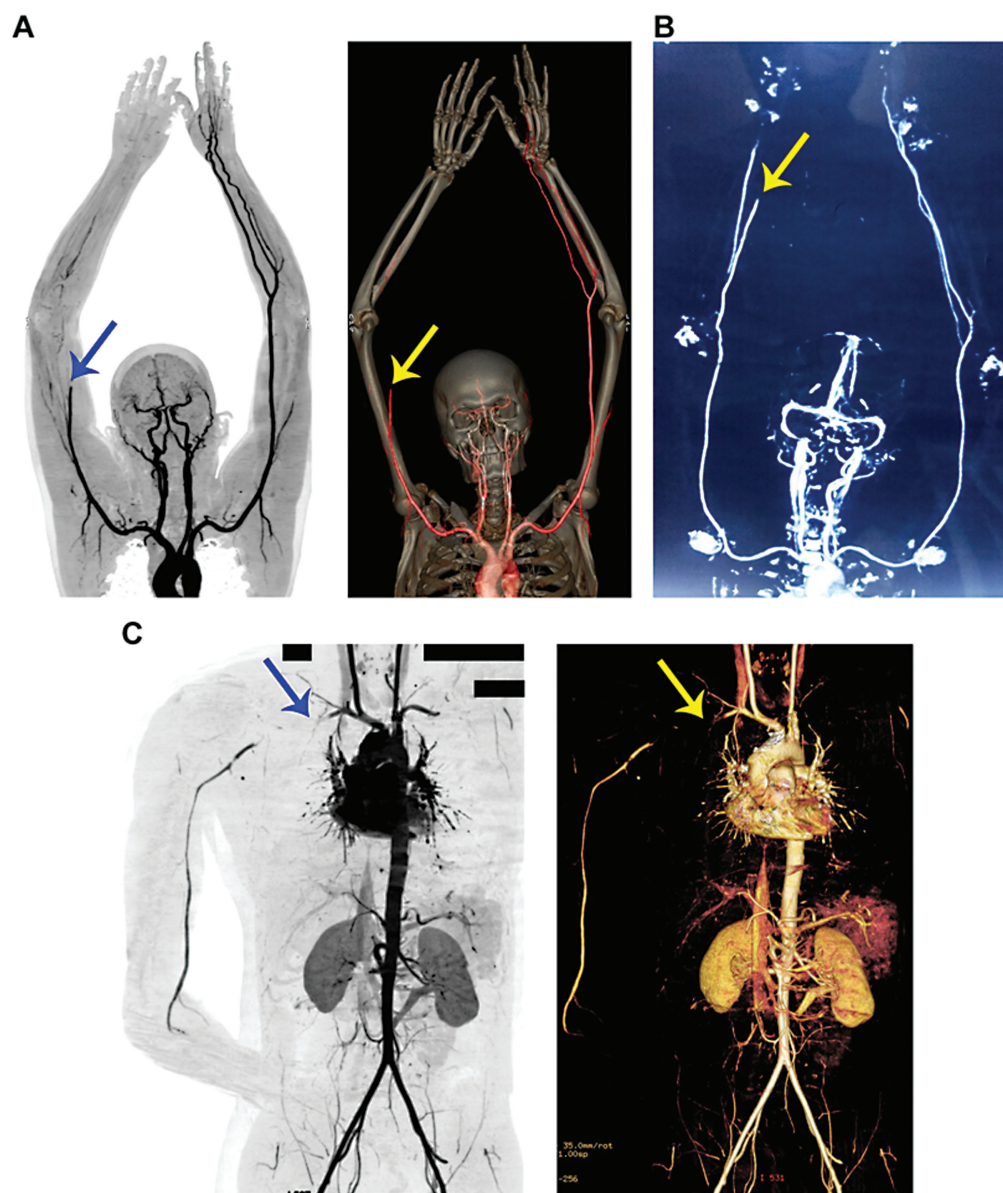


**Fig. 2** CT angiography reveals occluded peripheral arteries and a lack of downstream blood flow in Russell's bite victims. (A) The 2D contrasting and 3D constructed images of CT angiography confirm the occlusion of the right brachial artery and the lack of blood flow to downstream arteries in the first patient. (B) The 2D inverted contrasting image of CT angiography confirms the occlusion of the radial artery and blockade of blood flow downstream in the hand and fingers in the second patient. Similarly, 2D and 3D CT angiography (C) images confirm the occlusion of the right subclavian artery and the affected downstream blood flow in the third patient. The arrows indicate the site of occlusion. The black rectangle boxes are used to hide personal details on the image.

compartment syndrome with vascular compromise was assumed and, therefore, an urgent CT angiogram was performed. This revealed occlusive thrombi in the right mid-subclavian artery and subclavian vein, axillary, and brachial veins (► Fig. 2C). Arteries distal to the mid-subclavian artery showed minimal flow up to the wrist level. A large hematoma was seen in the right retro clavicular and supraclavicular region compressing the third part of the subclavian artery.

#### Clinical Management of Thrombosis in Patients

Following the confirmation of thrombosis, an emergency thrombectomy was performed in the first patient and successfully removed a thrombus measuring around 4 inches.

He was then treated with intravenous administration of low-molecular-weight heparin and oral warfarin. The patient also underwent two fasciotomies which reduced swelling and tenderness in the affected limb and improved movement. A Doppler ultrasound scan performed 3 days after the thrombectomy showed normal blood flow in the arteries of the affected limb. Upon discharge, he was prescribed warfarin for another 6 weeks and advised to follow up for regular monitoring of PT and the international normalized ratio (INR) of clotting. Since the second patient arrived with significant gangrenous tissues on the fingers, reperfusion therapy was not possible. Based on the occlusive thrombosis and resulting gangrene, the decision was made to amputate

the patient's entire thumb, index, and ring fingers, as well as the little finger at the middle phalanges. The thrombus (around 3–4 inches in size) at the distal radial artery was removed by thrombectomy and the patient was started on anticoagulant therapy similar to the first patient. Unlike the other two patients, in the third patient, an emergency subclavian thrombectomy was performed via transbronchial route using a Fogarty catheter (due to the location of the thrombus) which successfully removed a thrombus with the size of around 4 inches and rescued proximal flow. The patient was started on oral warfarin therapy and follow-up visits revealed that pulses were detectable in all distal vessels and the fingers had returned to normal function. The monthly regular check-ups were normal in all three patients. Follow-up blood tests including clotting factors such as V and X were performed 4 weeks after the discharge for all patients and we did not find any clotting or other relevant abnormalities.

### Russell's Viper Venom Exerts Procoagulant Effects

Since Russell's viper bites are frequently reported to cause bleeding complications associated with incoagulable blood due to venom-induced consumption coagulopathy, the development of occlusive thrombi in peripheral arteries is surprising. To determine the actions of Russell's viper venom (pooled venom from multiple specimens collected at the Kentucky Reptiles Zoo, United States) on various coagulation

parameters, in vitro coagulation experiments were performed. While Russell's viper venom displayed low metalloprotease (►Fig. 3A) and serine protease (►Fig. 3B) activities compared with the positive control (same concentration of the venom of *Crotalus atrox*), it exhibited high phospholipase A<sub>2</sub> (PLA<sub>2</sub>) activity (►Fig. 3C). In addition, the venom (50 µg/mL) significantly reduced PT (►Fig. 3D) and aPTT (►Fig. 3E) compared with the controls in citrated human plasma as a reflection of its procoagulant activity.

To further examine the effects of Russell's viper venom on blood clotting, rotational thromboelastometry (ROTEM) analysis was performed using human-citrated whole blood. The Intem (which evaluates the intrinsic and common pathways) analysis confirmed the accelerated clotting when Russell's viper venom (50 µg/mL) was added to whole blood in comparison to the control as demonstrated through reduced clotting time and maximum clot lysis (►Fig. 4A). However, there was no significant difference between the control and venom-induced clots in terms of size (area under the curve) and firmness. Similarly, the Extem (which evaluates the extrinsic and common pathways) analysis demonstrated accelerated clotting with reduced clot lysis, although the maximum size clot formation was significantly delayed (►Fig. 4B). To determine the impact of Russell's viper venom on clotting independently from platelets, the Fibtem analysis was performed. This analysis also confirmed the accelerated clotting, although the firmness of the clot was reduced (►Fig. 4C). Russell's viper

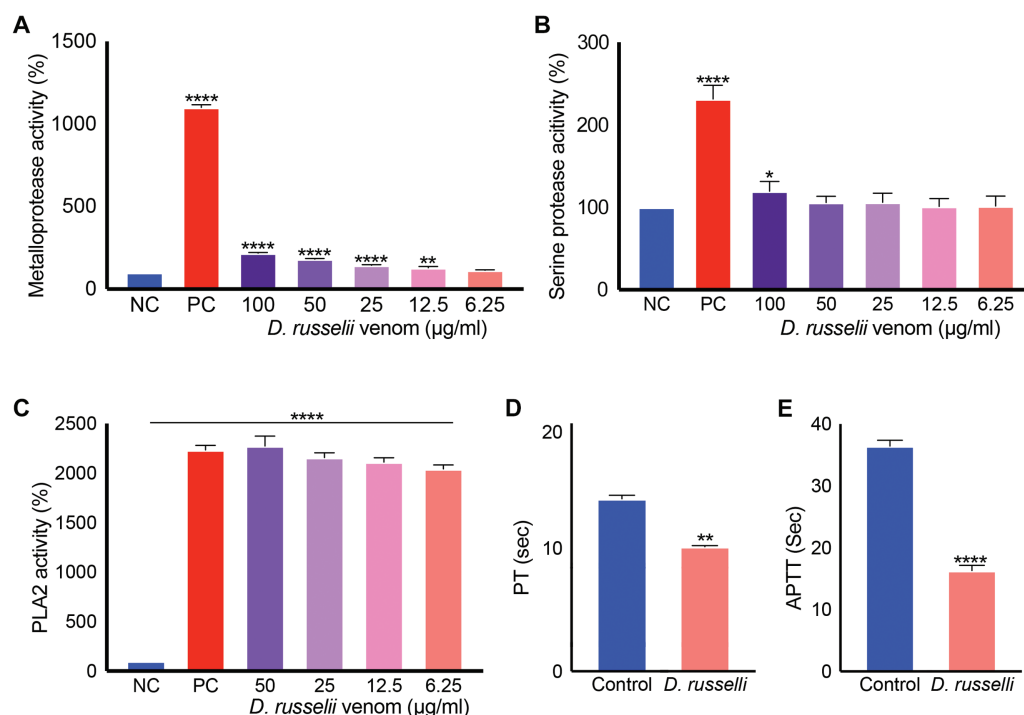


**Fig. 3** Enzymatic and clotting activities of Russell's viper venom. The metalloprotease (A), serine protease (B), and PLA<sub>2</sub> (C) activities of various concentrations of Russell's viper venom were measured using respective fluorogenic substrates by spectrofluorimetry. The base level fluorescence obtained with negative controls (NC; i.e., the substrate in the absence of venom) at 90 minutes was taken as 100% to calculate the enzyme activities in venom samples at the same time point. The venom of *Crotalus atrox* (50 µg/mL) was used as a positive control (PC) in all these assays. 50 µg/mL Russell's viper venom was mixed with plasma and relevant reagents to measure PT (D) and aPTT (E) using Ceveron T100 fully automated coagulation analyzer. Data represent mean ± S.D. (n = 4). The p-values (\*p < 0.05, \*\*p < 0.01, and \*\*\*\*p < 0.0001) shown were calculated by one-way ANOVA (A–C) or unpaired t-test (D and E) using GraphPad Prism.



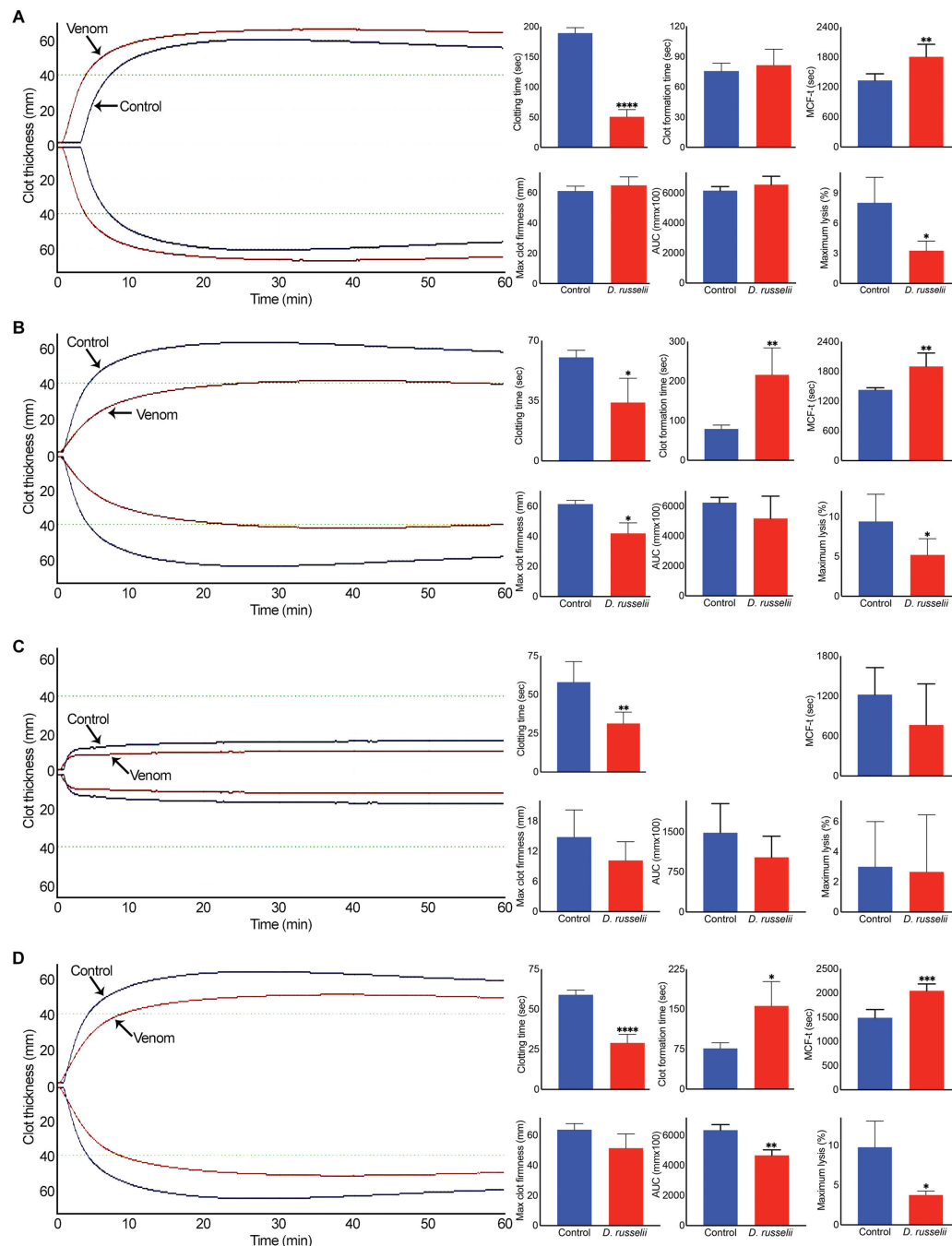


**Fig. 4** Effect of Russell's viper venom on ROTEM analysis. The impact of Russell's viper venom (50  $\mu\text{g}/\text{mL}$ ) on Intem (A), Extem (B), Fibtem (C), and Aptem (D) was analyzed by mixing the venom with citrated human whole blood and relevant reagents provided by the manufacturer and monitoring the clot formation over 60 minutes in a ROTEM Delta instrument. The curves shown are representative of four separate experiments performed using blood obtained from four individuals. Although various parameters were measured by ROTEM, here we demonstrate the impacts of venom on notable parameters such as clotting time (the time when clot formation was initiated), clot formation time (time to reach a 20-mm size clot), time to reach a maximum clot firmness (MCF-t), maximum clot firmness, area under the curve (AUC) of maximum clot formed, and maximum lysis. The cumulative data shown represent mean  $\pm$  SD ( $n = 4$ ). The  $p$ -values (\* $p < 0.05$ , \*\* $p < 0.01$ , \*\*\* $p < 0.001$ , and \*\*\*\* $p < 0.0001$ ) shown were calculated by an unpaired  $t$ -test using GraphPad Prism.

venom also displayed accelerated blood clotting and reduced lysis when fibrinolysis was prevented using the Aptem analysis (**Fig. 4D**). Together, these data demonstrate that Russell's viper venom induces blood clotting through common (or both intrinsic and extrinsic) coagulation pathways independently from platelets and fibrinolysis.

### Russell's Viper Venom Inhibits Agonist-Induced Platelet Activation

Since Russell's viper venom induced blood clotting even in the absence of platelets, its direct effects on human platelets were studied. Different concentrations of Russell's viper venom failed to induce platelet aggregation on their own

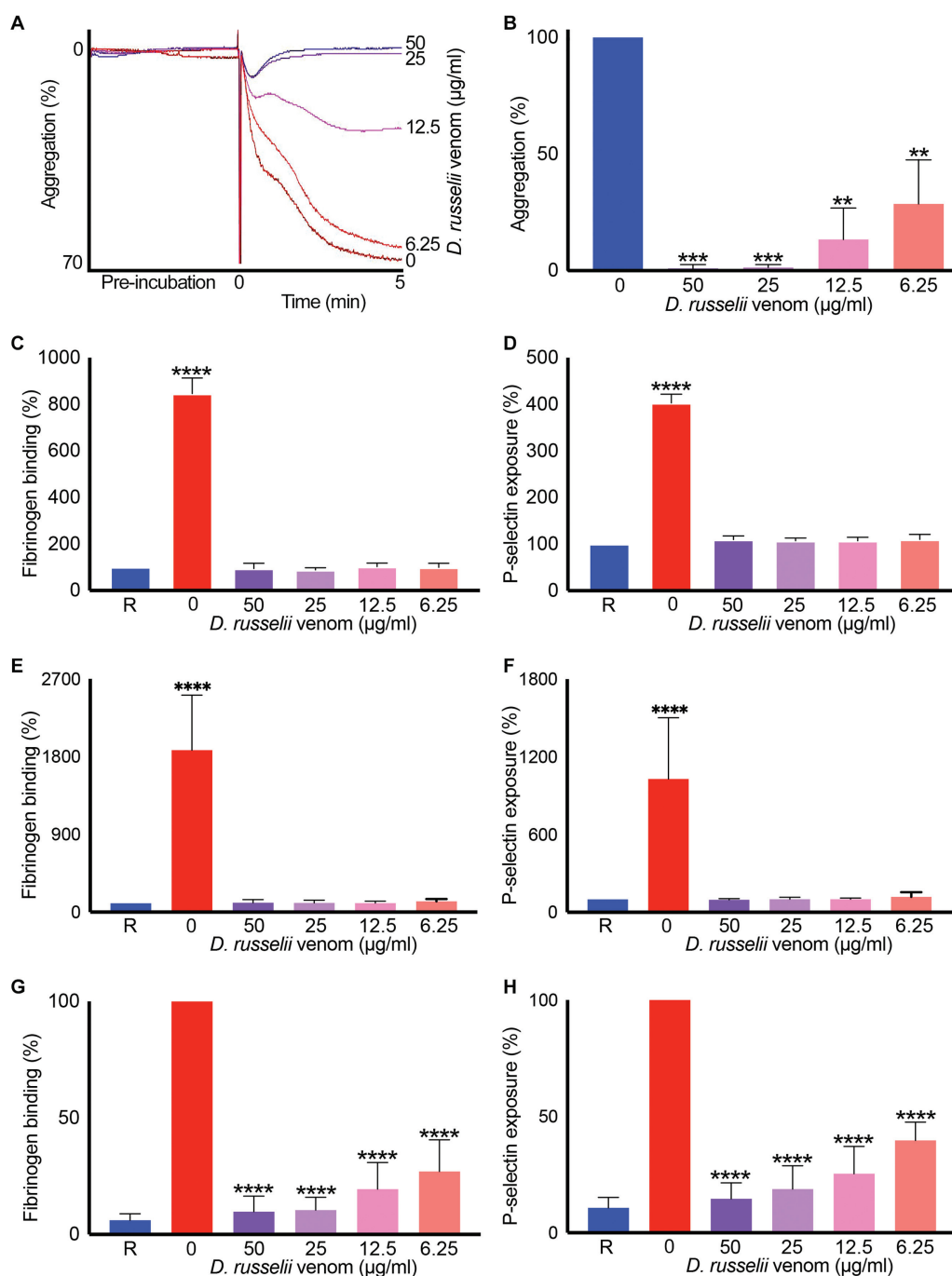


**Fig. 5** Impact of Russell's viper venom on human platelet activation. The human PRP was mixed with various concentrations of Russell's viper venom and incubated at 37 °C in an optical aggregometer while monitoring the level of aggregation for 5 minutes. Then the agonist, 5 µM ADP, was added, and the level of aggregation was monitored for another 5 minutes. The traces shown (A) are representative of four separate experiments. The level of aggregation obtained with the vehicle control (i.e., in the absence of venom) was taken as 100% to calculate the level of aggregation in venom-treated samples (B). The levels of fibrinogen binding and P-selectin exposure as markers for platelet activation were measured in the presence and absence of various concentrations of Russell's viper venom after 5 (C and D) and 20 (E and F) minutes of incubation without any platelet agonist. Similarly, the levels of fibrinogen binding (G) and P-selectin exposure (H) were measured following a 5-minute incubation with different concentrations of Russell's viper venom followed by 20-minute incubation with 5 µM ADP at 37 °C. The base level fluorescence obtained with relevant controls was taken as 100% to calculate the impact of venom in treated samples. Data represent mean  $\pm$  SD ( $n=4$ ). The  $p$ -values (\*\* $p < 0.01$ , \*\*\* $p < 0.0001$ , and \*\*\*\* $p < 0.0001$ ) shown were calculated by one-way ANOVA using GraphPad Prism. "R" represents the level of activation in resting platelets.

in human platelet-rich plasma (PRP), although they largely inhibited agonist (ADP)-induced platelet aggregation (**Fig. 5A, B**). To corroborate these effects, the levels of fibrinogen binding (as a marker for inside-out signaling

to integrin  $\alpha$ IIb $\beta$ 3) and P-selectin exposure (as a marker for  $\alpha$ -granule secretion) were quantified in the presence and absence of various concentrations of Russell's viper venom. Similar to the results obtained with aggregation, the various

concentrations of venom failed to induce platelet activation on their own either following incubation of 5 (►Fig. 5C, D) or 20 (►Fig. 5E, F) minutes. However, they largely inhibited ADP-induced fibrinogen binding (►Fig. 5G) and P-selectin exposure (►Fig. 5H) on human platelets. Taken together, these data demonstrate that Russell's viper venom-induced clotting in vitro, an activity known to be responsible for consumption coagulopathy in vivo, occurs mainly via activation of coagulation factors/cascades. Furthermore, the inhibition of platelet function may contribute to bleeding complications together with consumption coagulopathy.

### Marimastat Inhibits the Procoagulant Activity of Russell's Viper Venom

A matrix metalloprotease inhibitor, marimastat, has been demonstrated to possess broad-spectrum inhibitory effects on venom metalloproteases.<sup>26,27</sup> Hence, to determine its effects on Russell's viper venom-induced procoagulant effects, 10- $\mu$ M marimastat was incubated with 50  $\mu$ g/mL venom for 5 minutes before mixing with human citrated whole blood and analyzing (Extem) in ROTEM. As shown earlier, the venom has reduced clotting time, firmness, and clot size, while it increased clot formation time for a 20-mm clot in Extem analysis compared with the controls (►Fig. 6A).

Although marimastat did not affect any parameters of Extem on its own, it inhibited the procoagulant actions of Russell's viper venom. Similarly, varespladib is a PLA<sub>2</sub> inhibitor which has been shown to have significant impacts on venom PLA<sub>2</sub> of numerous snake species. To determine if PLA<sub>2</sub> in Russell's viper venom is involved in inducing clotting effects, 10- $\mu$ M varespladib was mixed with 50  $\mu$ g/mL venom before analyzing in Extem analysis. Varespladib on its own and with venom did not show any effects on Extem clotting parameters except a slight increase in clot formation time when mixed with the venom (►Fig. 6B). These data demonstrate that the procoagulant effects of Russell's viper venom are largely mediated through metalloproteases instead of PLA<sub>2</sub>, although we cannot rule out the possible contributions from other venom proteins.

### Histological Assessment of Thrombosis under In Vivo Settings in Mice

To determine if Russell's viper venom can acutely induce thrombosis in the vasculature, lung tissues obtained from mice injected intravenously with vehicle control (phosphate-buffered saline [PBS]) or Russell's viper venom were analyzed using hematoxylin and eosin staining. The tissues from control mice showed a normal histological appearance, and

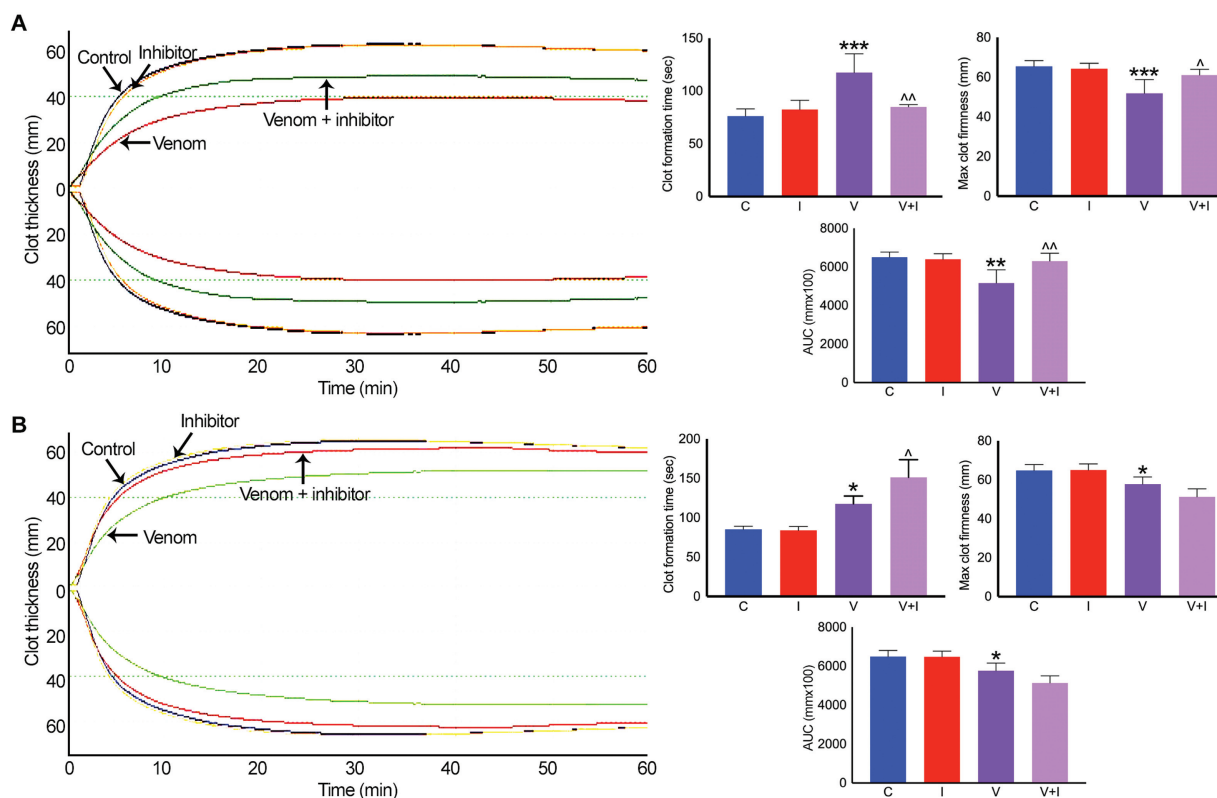


**Fig. 6** Effects of marimastat and varespladib on Russell's viper venom-induced clotting in ROTEM. 10  $\mu$ M marimastat (A) or varespladib (B) was mixed with 50  $\mu$ g/mL Russell's viper venom in citrated whole human blood before the addition of Extem reagents and monitoring the level of clot formation over 60 minutes in ROTEM. The traces shown are representative of four separate experiments performed using blood obtained from four donors. The cumulative data are shown for specific parameters such as clot formation time, maximum clot firmness, and area under the curve (AUC) for full clot formed. Data represent mean  $\pm$  SD ( $n=4$ ). The  $p$ -values (\* $p < 0.05$ , \*\* $p < 0.01$  and \*\*\* $p < 0.0001$ ) shown were calculated by one-way ANOVA using GraphPad Prism. C—vehicle control; I—inhibitor alone; V—venom alone; V+I—venom + inhibitor. ^Significance when venom-treated samples compared with the controls. ^^Significance when venom and inhibitor-treated samples compared with the venom-alone controls.

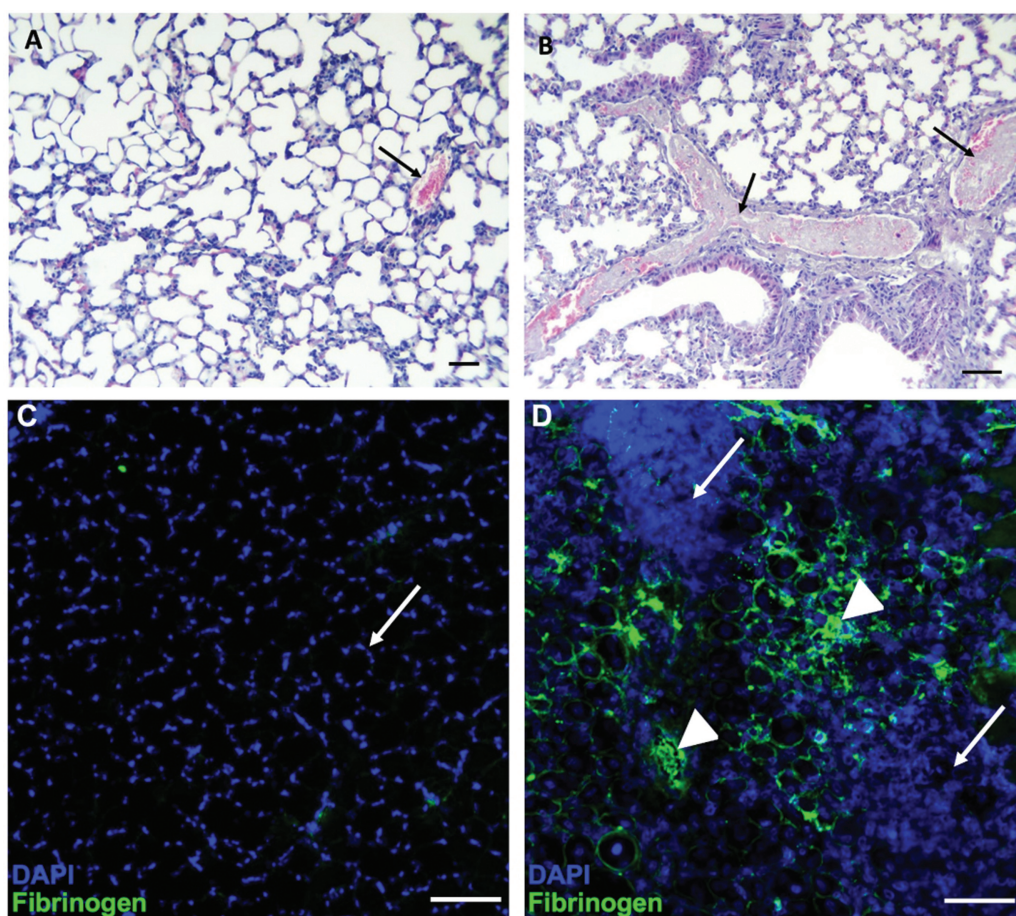


**Fig. 7** Russell's viper venom-induced thrombosis in mice. Light micrographs of lung tissues (stained with hematoxylin and eosin stain) of mice injected intravenously in the caudal vein, with PBS (A) or 12.5  $\mu\text{g}$  Russell's viper venom previously incubated with the PLA<sub>2</sub> inhibitor, varespladib (B) are shown. The tissue from control mice shows a normal histological pattern and a vein filled with erythrocytes (indicated by an arrow). In contrast, tissue from mice injected with Russell's viper venom shows two veins with prominent thrombi (indicated by arrows). Similarly, immunofluorescence images of the tibialis anterior muscle of mice injected with PBS or Russell's viper venom 5 days before dissection were obtained following staining with FITC-labeled anti-fibrinogen antibodies. (C) A section of the tibialis anterior muscle of control mice shows normal muscle architecture with nuclei at the periphery of muscle fibers (indicated by an arrow) and the lack of fibrinogen binding (no green signal). (D) The tibialis anterior muscle injected with Russell's viper venom (66 ng/g of mouse weight) shows extensive tissue damage with the destruction of muscle fibers as indicated by the presence of a large number of cells (arrow). Significant levels of fibrinogen found in the damaged regions (green color) demonstrate the presence of bleeding and thrombi (arrowheads). The bar represents 100  $\mu\text{m}$ .

blood vessels were filled with erythrocytes without any thrombi (**►Fig. 7A**). In contrast, mice that received Russell's viper venom inhibited with varespladib, to block the action of neurotoxic PLA<sub>2</sub>s, died within 15 minutes of injection. Tissues from these mice showed abundant thrombi in pulmonary veins and venules (**►Fig. 7B**). Noteworthy, edema, hemorrhage, and inflammatory infiltrate were absent in the lung tissue of envenomed mice. To further establish if Russell's viper venom induces thrombi in microvasculature and tissues, skeletal muscle (tibialis anterior) injected with vehicle control or Russell's viper venom was analyzed by immunohistochemistry using FITC-labeled anti-fibrinogen antibodies. The muscle sections from control mice showed normal tissue architecture 5 days after the injection. The nuclei were spaced at the periphery of muscle fibers giving the typical hollow fiber appearance. Notably, there was no binding of anti-fibrinogen antibodies to the control muscle sections (**►Fig. 7C**). However, muscle injected with Russell's

viper venom showed considerable disruption to tissue architecture evidenced by a massive invasion of cells leading to large areas covered by DAPI-positive nuclei, and a significant amount of fibrinogen deposition including large thrombi (**►Fig. 7D**). These data demonstrate that Russell's viper venom can induce thrombosis in the vasculature in affected tissues.

## Discussion

Bleeding complications (hemorrhage) from SBE inflicted by many viperid species are commonly reported and they can lead to cerebral hemorrhage,<sup>28,29</sup> pituitary failure,<sup>30</sup> pseudoaneurysm,<sup>15</sup> perinephric hematoma,<sup>31,32</sup> and acute kidney injury.<sup>33</sup> These complications can also contribute to the onset of cardiovascular shock and multiple organ failure. However, thrombosis, specifically peripheral arterial thrombosis, is a rare (but serious) phenomenon following SBE.

There have been scarce reports of cases with thrombosis as a consequence of viperid snakebites.<sup>34–36</sup> An exception to this trend of the low frequency of thrombotic phenomena in SBE is the envenoming by *Bothrops lanceolatus*, an endemic species in the Caribbean Island of Martinique. A significant proportion of patients bitten by this species develop thrombotic complications associated with infarctions in the lungs, heart, and brain<sup>24,37</sup>; however, no effects on limbs were reported in the literature. The mechanisms behind this effect were not established, although it has been proposed to be related to the actions of metalloproteases (which are abundant in this venom) on the vasculature.<sup>38,39</sup> Russell's viper is a foremost medically important venomous snake in India and other Asian countries. The bites from this species in India mostly lead to extensive bleeding, cardiovascular disturbances, muscle necrosis, acute kidney injury, neurotoxic effects, and multiple organ failure. These envenoming effects may result in permanent disabilities or death if not treated promptly. A few cases of cerebral thrombosis following envenomings by Russell's viper have been reported.<sup>40–44</sup> However, to the best of our knowledge, the peripheral arterial thrombosis resulting in loss of function of affected limbs has not been reported previously following Russell's viper bites. Hence, for the first time, we report three serious cases where the patients developed large (3–4 inches) occlusive thrombi in their peripheral arteries of upper limbs following Russell's viper bites despite antivenom treatment. While these patients were treated successfully using thrombectomy, one patient had to undergo amputation of their fingers. These thrombotic events are uncommon compared with the high prevalence of bleeding diatheses that accompany envenoming by Russell's vipers. Therefore, this condition needs significant scientific and medical attention to provide timely diagnosis and appropriate treatment for SBE victims, and thereby prevent permanent disabilities or deaths.

Russell's viper envenoming typically results in a pattern of local swelling and bleeding at the bite site, lymphadenopathy, hypotension, coagulopathy, and systemic bleeding,<sup>45</sup> although the severity of symptoms varies widely based on the amount of venom injected. Moreover, other complications such as acute kidney injury, systemic capillary leakage syndrome, vascular damage in the pituitary gland, and neurotoxicity also occur following Russell's viper bites.<sup>46</sup> In addition to clinical symptoms, simple coagulation tests such as a 20-minute whole blood clotting test, PT and aPTT, and the levels of fibrinogen and D-dimers are used to ascertain coagulopathy in SBE (including Russell's viper) victims.<sup>46</sup> Based on the severity of other complications, ultrasound, Doppler, CT, and magnetic resonance imaging (MRI) scans are utilized to establish bleeding and thrombotic conditions as well as organ damage/failure in Russell's viper and other SBE victims.<sup>15,32</sup> The patients described in this study were relatively young (aged 21–35 years) and had no significant previous medical conditions. However, they developed thrombi in their peripheral arteries and displayed symptoms at various time points following bites. The laboratory investigations demonstrated normal clotting and metabolic pro-

file in all patients indicating that the clotting might have occurred much earlier than their arrival at the emergency department. All of them were treated with polyvalent antivenom raised against the Indian “big four” venomous snakes. While in one case (the third patient who was admitted directly to the emergency department), the time between the bite and first antivenom administration was around 2 hours, in others these details were not available as they received treatments elsewhere before the admittance in the emergency department. Interestingly, antivenom treatment did not prevent the development of thrombi in these victims, possibly due to the rapid/transient actions of venom components in the circulation or to the fact that thrombosis might be the result of endogenous processes that, once established, cannot be reverted by antivenom. Thrombi were formed in the bitten limb of two victims who had bites on the hand or finger while the third patient bitten in the neck developed regional thrombi. CT angiography played a critical role in the diagnosis of thrombosis in these patients, and it allowed the evaluation of precise locations of thrombi. The patients were successfully treated with thrombectomy, although the second patient who presented 4 days after envenoming developed gangrene and thus the affected fingers and thumb had to be amputated. All these patients received anticoagulant therapy which aided in the prognosis postthrombectomy. The prognosis of the first and third patients demonstrates that the earlier intervention is critical in thrombotic conditions to restore adequate flow to the affected areas and prevent the loss of limbs.

Russell's viper venom largely contains serine proteases, metalloproteases, and PLA<sub>2</sub>s and all of these are known to interfere with the coagulation cascades, disrupt endothelial function, and cause tissue necrosis. Specifically, it comprises procoagulant factor V and X activators,<sup>47,48</sup> and prothrombin activating enzyme,<sup>49</sup> all of which induce blood clotting in vitro, while under in vivo settings, their action predominantly results in consumption coagulopathy with a rapid reduction in the concentrations of fibrinogen and other clotting factors, leading to bleeding. In some cases, thrombocytopenia as well as an increase in plasma fibrinolytic activity may occur, thus generating fibrin degradation products.<sup>50</sup> Our experimental observations using standard clotting tests and ROTEM corroborate the procoagulant activity of this venom. Such in vitro procoagulant activity is responsible for the consumption coagulopathy<sup>51</sup> that is usually observed in patients suffering envenomings by this species. The inhibitory effects displayed on agonist-induced platelet activation are likely to play a role in overall hemostatic disturbances and subsequent bleeding induced by this venom. In addition to direct hemostatic alterations, venom metalloproteases may promote hemorrhage by cleaving various components of the basement membrane such as type IV collagen in blood vessels,<sup>52</sup> which can be potentiated by coagulopathy. Indeed, the use of marimastat (a matrix metalloprotease inhibitor) in ROTEM experiments confirms the impact of Russell's viper venom metalloproteases in inducing procoagulant effects. It appears that the PLA<sub>2</sub>s present in this venom may not contribute to the procoagulant effects, as varespladib did

not reverse these actions. We cannot rule out the possible actions of other venom components in inducing blood clotting. Overall, the predominant hemotoxic actions of Russell's viper venom are associated with consumption coagulopathy, incoagulable nature of blood, and bleeding diathesis, although thrombosis was unusually observed in the patients reported in this study. In these sporadic cases, a portion of venom might have been injected directly into the blood vessels, thus causing the rapid formation of thrombi which can become immovable at junctions of arteries where continuous clotting can occur without embolization despite high arterial shear conditions. Indeed, our data demonstrate that the direct injection of Russell's viper venom in the caudal vein can induce the formation of large thrombi.

The continuous development of thrombi over several hours after envenoming resulted in delayed symptoms and loss of function of limbs until thrombi became occlusive. These patients might have experienced a high degree of endothelial damage secondary to the actions of venom metalloproteases in the vasculature, leading to an increase in exposed tissue factor, collagen, or von Willebrand factor with the resultant blood clotting. The experimental results presented in this study demonstrate that the clotting cascades played a major role independently from platelets, although this is unusual for arterial thrombosis. The activation of clotting factors and subsequent thrombosis with minimal inputs from platelets normally occurs under venous circulation often leading to pulmonary embolism.<sup>53</sup> Indeed, our experimental observations in mice indicate that prominent thrombi are observed in pulmonary veins within minutes of intravenous injection of the venom, thus suggesting that such venous thrombosis is the result of the rapid action of procoagulant enzymes in the venom in the circulation. Furthermore, our work shows that thrombi develop not only in the lungs in animal models but also in skeletal muscle (i.e., locally affected muscle around the bite/injection site). The skeletal muscle tissue has a very high capacity to regenerate, exemplified by the rapid formation of muscle fibers a few days after total muscle fiber necrosis induced by cardiotoxin. However, following Russell's viper venom-induced damage, there was considerable evidence for unresolved tissue necrosis as well as significant levels of fibrinogen deposition indicative of thrombi formation in the microvasculature and affected tissues. This is possibly due to the sustained action of venom components acting to continually damage the tissue as well as leading to thrombus formation. Russell's viper venom also induces prominent inflammatory responses,<sup>54</sup> and thus, the increase in a plethora of inflammatory mediators in the blood may also induce the acquisition of a proinflammatory and procoagulant phenotype in endothelial cells, thus favoring the formation of thrombi. Furthermore, the specific characteristics of individuals may affect the clinical features following SBE. It is possible that a certain subset of patients might possess increased levels of specific coagulation factors such as factors V and/or X which may create a hypercoagulable status during envenoming. Other endogenous factors such as undiagnosed atherosclerosis might also contribute to a condition that favors arterial thrombosis in

some patients. It is unknown if preexisting atherosclerosis (in blood vessels other than the ones imaged) in these patients may have played a role, although atherosclerotic risk increases with advanced age<sup>55</sup> and all of these patients were younger than 40 years. Therefore, it is likely that the thrombosis described in this study is multifactorial in its origin.

The regional variations of Russell's viper venom composition<sup>56-58</sup> and their impacts on clinical manifestations of envenomings were previously reported.<sup>46,59</sup> Indeed, we reported various unusual complications of Russell's viper envenomings in South India that could be attributable to the variations in venom composition. Hence, these three patients might have been bitten by Russell's vipers that might have had unusual quantities of procoagulant venom toxins resulting in stable occlusive thrombosis. Here, snake-related genetic factors could have also played a role in the development of thrombosis. For example, genetic variations in subpopulations of species might have increased the proportion of procoagulant enzymes. It is well known that venom composition varies geographically in Russell's vipers even within India, resulting in significant variations in antivenom efficacy.<sup>57,58</sup> Indeed, different subspecies of Russell's viper were identified across South Asia.<sup>60</sup> Hence, further studies with additional cases describing thromboembolic events would be required to determine if a geographic relationship exists. Although difficult to assess in the field, the variable amount of venom delivered in a single bite might also play a role. Thus, a combination of patient-specific and snake-specific features may also contribute to the likelihood of the development of occlusive thrombi in some cases.

In conclusion, the procoagulant actions of Russell's viper venom mostly result in consumption coagulopathy leading to the incoagulable nature of blood, which contributes to the local and systemic bleeding characteristic of these envenomings. Conversely, as shown in this study, in some victims, occlusive thrombosis may occur which may impair blood flow downstream of the clot and cause ischemia resulting in pain, numbness, and, if left untreated, excessive tissue necrosis leading to permanent disabilities. Therefore, robust diagnostic and management strategies are required to handle Russell's viper bite victims. In addition to the usual coagulation tests, CT angiography is required for the robust diagnosis of thrombosis. It should be performed early when patients complain of relevant symptoms following bites. If thrombosis is confirmed, prompt thrombectomy with minimal surgery or percutaneous catheterization should be performed to remove the thrombi and rescue blood flow. Moreover, anticoagulant therapy is necessary to prevent subsequent thrombosis postthrombectomy. The patients should be monitored for excessive bleeding phenotype while receiving anticoagulant therapy. Clinicians in areas endemic to SBE including Russell's viper should be aware of such serious complications.

## Methods

### Patients' Data Collection

The collection of data from snakebite victims for this study was approved by the Institutional Ethics Committee at

Toxiven Biotech Private Limited (ICMR-Toxiven Ethics 2019-001/002). Written informed consent was obtained from all patients. The patients were treated using standard protocols and specialized treatments as described in this article.

### CT Angiography

Helical CT angiography was performed using a fourth generation multidetector CT scanner (GE Optima CT660 128 Slice, UK) with a 0.6-second gantry rotation period. The angiography was achieved by acquiring four rows of 1.25-mm sections at a pitch of 1.5 following intravenous administration of 100 to 150 mL of iohexol (Omnipaque, 300 mg/mL iodine) with a power injector at a rate of 4 mL/second. When the arterial attenuation value (180–200 H) was reached following the injection of the contrasting agent, helical scanning was manually initiated. Around 150 to 300 axial images were obtained, and 2 to 10 reformatted images were constructed for the upper extremity in a CT 3D rendering workstation (Ultra 60, Sun Microsystems Inc, United States).

### Thrombectomy Procedure

In the first patient, a longitudinal medial incision was made at the right cubital fossa followed by dissection and isolation of the right brachial artery. Arteriotomy and subsequent thrombectomy using a 6-Fr Fogarty catheter (Edwards Lifesciences LLC, United States) was used to remove around 3- to 4-inch-long thrombus from the right brachial artery. To ensure adequate forward and backward blood flow following thrombectomy, 100,000 units of streptokinase and 500 units of heparin were infused. The incised artery was closed using Prolene 6/0 in a simple continuous fashion, and Nylon 3/0 was used for closing the skin. A similar procedure was used in the second patient to remove the thrombus from the right radial artery, and amputation of the entire thumb, index, and ring fingers, as well as the little finger at the middle phalanges level was performed. In the third patient, under general anesthesia, ultrasound-guided access to the right subclavian artery was achieved using a micropuncture technique. Subsequently, a thrombectomy was performed using a 3-Fr Fogarty catheter and the clot was removed.

### Enzymatic Assays

The venom metalloprotease activity was analyzed using DQ-gelatin (ThermoFisher Scientific, UK) as a fluorogenic substrate. Various concentrations of Russell's viper venom (Kentucky Reptile Zoo, United States) were mixed with 10 µg/mL DQ-gelatin in a total reaction volume of 100 µL (final volume was made up using PBS) in a 96-well microtiter plate. The plate was incubated at 37 °C, and the level of fluorescence was measured at various time points using an excitation wavelength of 485 nm and emission at 520 nm in a Fluostar Optima (BMG Labtech, Germany) spectrofluorometer. Similarly, the serine protease activity was measured using  $\alpha$ -benzoyl-L-arginine 7-amido-4-methyl coumarin HCl (Sigma Aldrich, UK) as a fluorogenic substrate. Following the mixing of the substrate (2 µM) with different concentrations of Russell's viper venom, the plate was incubated at 37 °C and the resulting fluorescence was measured at an

excitation wavelength of 366 nm and emission wavelength of 460 nm at various time points. The PLA<sub>2</sub> activity of Russell's viper venom was measured using an EnzCheck Phospholipase A<sub>2</sub> kit (ThermoFisher Scientific; dioleoyl phosphatidylcholine and dioleoyl phosphatidylglycerol as substrates) according to the manufacturer's instructions.

### Human Blood Collection and Preparation of Plasma/PRP

The blood samples from healthy human volunteers were collected in line with the procedures approved by the University of Reading Research Ethics Committee (UREC 17/17). Following written informed consent, blood was collected via venipuncture in vacutainers containing 3.2% (w/v) sodium citrate. To obtain PRP, blood was centrifuged at 100 g for 20 minutes at 20 °C in a benchtop centrifuge. The top layer of PRP was collected carefully without disturbing the white (opaque layer) or red blood cells and used in platelet aggregation assays. To obtain plasma, the whole blood was centrifuged at 1,400 g for 10 minutes at 20 °C. The top clear layer of plasma was carefully collected and used in clotting experiments. The citrated whole blood was used in ROTEM experiments without any modifications.

### Clotting Assays

PT and aPTT were measured using standard protocols in a Ceveron T100 fully automated coagulation analyzer (Technoclone, Austria). A concentration of 50 µg/mL of Russell's viper venom was mixed with a predetermined volume of plasma obtained from different donors and standard PT (thromboplastin and 25 mM CaCl<sub>2</sub>)/aPTT (silica/sulfatide phospholipids in 25 mM CaCl<sub>2</sub>) reagents provided by the manufacturer and analyzed in Ceveron T 100.

### ROTEM Analysis

The ROTEM analysis was performed using a ROTEM Delta instrument (Werfen, UK) to determine the impacts of Russell's viper venom on various parameters of whole blood clotting. The Intem and Extem analyses were performed to determine the impact of venom on intrinsic and extrinsic (as well as common) pathways of blood clotting, respectively. Fibtem was performed to determine the impact of fibrinogen and clotting factors in whole blood clotting in the absence of platelets. Aptem was completed to analyze the impact of venom on blood clotting in the absence of fibrinolysis. For each assay, 50 µg/mL of Russell's viper venom was mixed with 300 µL of citrated human whole blood and pre-set volumes of respective reagents in line with the manufacturer's instructions. For Intem and Extem, the blood samples were recalcified using a Startem reagent (0.2 M CaCl<sub>2</sub> in HEPES buffer, pH 7.4) and blood clotting was initiated using intrinsic (partial thromboplastin phospholipid from rabbit brain and ellagic acid) and extrinsic (recombinant tissue factor, phospholipids, and heparin) activators. For Fibtem, the blood was mixed with a Fibtem reagent (cytochalasin D and 0.2 M CaCl<sub>2</sub> in HEPES buffer, pH 7.4) prior to the initiation of clotting using the Extem activator. For Aptem, the blood was mixed with Aptem reagent (aprotinin and 0.2 M

CaCl<sub>2</sub> in HEPES buffer, pH 7.4) prior to the activation of clotting using Extem activation reagent. To determine the impacts of marimastat and varespladib on Russell's viper venom-induced effects in Extem, 10 µM of each inhibitor was added with and without 50 µg/mL venom. The clot formation and lysis were monitored for 60 minutes in all assays.

### Flow Cytometry and Aggregation Assays

The PRP was incubated with various concentrations of Russell's viper venom for 5 minutes in the presence of 2 µg/mL FITC-labeled antihuman fibrinogen antibodies (Dako, UK) and 2 µg/mL PECy5-labeled CD62P (P-selectin) antibodies (BD Biosciences, UK). The platelets were then added either with modified Tyrode's HEPES buffer (2.9 mM KCl, 134 mM NaCl, 0.34 mM Na<sub>2</sub>HPO<sub>4</sub>·12H<sub>2</sub>O, 1 mM MgCl<sub>2</sub>, 12 mM NaHCO<sub>3</sub>, 20 mM HEPES, pH 7.3) or 5 µM ADP (prepared in modified Tyrode's HEPES buffer), and further incubated for 5 or 20 minutes at 37 °C. Then 0.2% (v/v) formyl saline was used to fix the cells before analysis by flow cytometry (Accuri C6, BD Biosciences, UK). The median fluorescence intensity of each sample was collected by analyzing 5,000 cells within the gated region for platelets. The levels of median fluorescence intensity obtained with the relevant controls were taken as 100% to calculate the effects in venom-treated samples.

The aggregation assays were performed using an optical aggregometer (Chrono-Log, United States). The PRP was added with various concentrations of Russell's viper venom and incubated at 37 °C in an optimal aggregometer (Chrono-Log) while monitoring the level of aggregation for 5 minutes. Then ADP (5 µM) was added, and the baseline was set to 0, and the aggregation was monitored for another 5 minutes.

### In Vivo Thrombotic Assays in Mice

To assess whether Russell's viper venom induces intravascular thrombosis in vivo, experiments were performed in mice. Before injection, Russell's viper venom was incubated for 20 minutes at room temperature with a PLA<sub>2</sub> inhibitor, varespladib (500 µM), to inhibit the neurotoxic PLA<sub>2</sub>s of the venom. Then, a group of three CD-1 mice of both sexes (18–20 g) received an intravenous injection, in the caudal vein, of 12.5 µg venom, dissolved in a volume of 100 µL 0.12 M NaCl, 0.04 M phosphates, pH 7.2 (PBS). Another group of three control mice received 100 µL of PBS alone. Mice injected with varespladib-inhibited venom died within 15 minutes of injection, and control mice were sacrificed at the same time interval by an overdose of ketamine and xylazine. Immediately after death, the thoracic cavity of mice was opened, and tissue samples of lungs were collected and added to a formalin fixative solution. Tissues were processed for embedding in paraffin. Then, sections of 5 µm were obtained and stained with hematoxylin and eosin for histological observation. These experiments involving the use of mice were approved by the Institutional Committee for the Care and Use of Laboratory Animals (CICUA) of the University of Costa Rica (permission CICUA-025–15).

Similarly, to determine if Russell's viper venom can induce thrombosis in microvasculature and/or affected muscle tissues, the tibialis anterior muscle of mice (CD-1)

was injected with Russell's viper venom (66 ng/g of mouse weight) and thereafter left to recover. The control mice were injected with an equal volume of PBS. Five days after damage, the mice were sacrificed and the muscle was processed for immunohistology analysis following cryosection (used 15-µm sections). The sections were incubated with FITC-labeled antifibrinogen antibodies (Dako, UK) and counterstained with DAPI to identify nuclei. These experiments involving the use of mice were approved by the Ethics Committee of the University of Reading and the British Home Office.

### Statistical Analysis

All data analyses in this study were performed using Prism 7 (GraphPad Inc, United States). The data are represented as mean ± SD. The statistical significance between control and treated samples was calculated using an ordinary one-way ANOVA with Dunnett's (or Turkey's test for ROTEM data with inhibitors) multiple comparisons test. Where only one concentration of venom was used to compare its effects with controls, an unpaired *t*-test was used.

### Authors' Contributions

S.S.: study design, data collection, analysis, supervision; K.P.: experimental design, data analysis, writing manuscript; E.R.: data collection, analysis, making figures; P.V.: data collection, analysis, making figures; S.W.M.: data analysis, writing manuscript; A.R.: experimental design, data collection, analysis; S.G.: data collection, analysis; M.S.: data collection, analysis; N.J.R.: data collection, analysis; J.W.: experimental design, data collection, analysis, writing manuscript; H.F.W.: data analysis, writing manuscript; S.A.T.: data analysis, writing manuscript; P.T.: study design, data analysis, writing manuscript; J.M.G.: experimental design, data collection, analysis, writing manuscript, making figures; S.V.: study design, experimental design, data collection, analysis, supervision, writing manuscript.

### Funding

The authors would like to thank the British Heart Foundation (reference: PG/19/62/34593) and Medical Research Council (reference: MR/W019353/1 & Integrative Toxicology Training Partnership – PhD studentship), United Kingdom, for their funding support for this research.

### Conflict of Interest

None declared.

### Acknowledgments

The authors thank Daniela Solano for her support with the preparation of histology sections.

### References

- Longbottom J, Shearer FM, Devine M, et al. Vulnerability to snakebite envenoming: a global mapping of hotspots. *Lancet* 2018;392(10148):673–684
- Kasturiratne A, Wickremasinghe AR, de Silva N, et al. The global burden of snakebite: a literature analysis and modelling based on






- regional estimates of envenoming and deaths. *PLoS Med* 2008;5(11):e218
- 3 Suraweera W, Warrell D, Whitaker R, et al. Trends in snakebite deaths in India from 2000 to 2019 in a nationally representative mortality study. *eLife* 2020;9:e54076
  - 4 Simpson ID, Norris RL. Snakes of medical importance in India: is the concept of the "Big 4" still relevant and useful? *Wilderness Environ Med* 2007;18(01):2–9
  - 5 Menon JC, Joseph JK, Whitaker RE. Venomous snake bite in India - Why do 50,000 Indians die every year? *J Assoc Physicians India* 2017;65(08):78–81
  - 6 Vaiyapuri S, Vaiyapuri R, Ashokan R, et al. Snakebite and its socio-economic impact on the rural population of Tamil Nadu, India. *PLoS One* 2013;8(11):e80090
  - 7 Samuel SP, Chinnaraju S, Williams HF, et al. Venomous snakebites: rapid action saves lives - a multifaceted community education programme increases awareness about snakes and snakebites among the rural population of Tamil Nadu, India. *PLoS Negl Trop Dis* 2020;14(12):e0008911
  - 8 Kularatne SA. Epidemiology and clinical picture of the Russell's viper (*Daboia russelii russelii*) bite in Anuradhapura, Sri Lanka: a prospective study of 336 patients. *Southeast Asian J Trop Med Public Health* 2003;34(04):855–862
  - 9 Harrison RA, Hargreaves A, Wagstaff SC, Faragher B, Laloo DG. Snake envenoming: a disease of poverty. *PLoS Negl Trop Dis* 2009;3(12):e569
  - 10 McCleary RJ, Kini RM. Snake bites and hemostasis/thrombosis. *Thromb Res* 2013;132(06):642–646
  - 11 Gutiérrez JM, Calvete JJ, Habib AG, Harrison RA, Williams DJ, Warrell DA. Snakebite envenoming. *Nat Rev Dis Primers* 2017;3:17063
  - 12 Slagboom J, Kool J, Harrison RA, Casewell NR. Haemotoxic snake venoms: their functional activity, impact on snakebite victims and pharmaceutical promise. *Br J Haematol* 2017;177(06):947–959
  - 13 Berling I, Isbister GK. Hematologic effects and complications of snake envenoming. *Transfus Med Rev* 2015;29(02):82–89
  - 14 Senthilkumaran S, Vijayakumar P, Savania R, et al. Splenic rupture and subsequent splenectomy in a young healthy victim following Russell's viper bite. *Toxicon* 2021;204:9–13
  - 15 Senthilkumaran S, Miller SW, Williams HF, et al. Ultrasound-guided compression method effectively counteracts Russell's viper bite-induced pseudoaneurysm. *Toxins (Basel)* 2022;14(04):260
  - 16 Mahasandana S, Rungruxsirivorn Y, Chantarangkul V. Clinical manifestations of bleeding following Russell's viper and green pit viper bites in adults. *Southeast Asian J Trop Med Public Health* 1980;11(02):285–293
  - 17 Isbister GK, Maduwage K, Scorgie FE, et al. Venom concentrations and clotting factor levels in a prospective cohort of Russell's viper bites with coagulopathy. *PLoS Negl Trop Dis* 2015;9(08):e0003968
  - 18 Isbister GK. Snakebite doesn't cause disseminated intravascular coagulation: coagulopathy and thrombotic microangiopathy in snake envenoming. *Semin Thromb Hemost* 2010;36(04):444–451
  - 19 Pothukuchi VK, Kumar A, Teja C, Verma A. A rare case series of ischemic stroke following Russell's viper snake bite in India. *Acta Med Indones* 2017;49(04):343–346
  - 20 Kumar G, Nagender Y, Sneha T, Reddy S, Ahmed R. Successful conservative management of high output chylothorax in a case of polytrauma. *J Med Soc* 2015;29:51–53
  - 21 Subasinghe CJ, Sarathchandra C, Kandeepan T, Kulatunga A. Bilateral blindness following Russell's viper bite - a rare clinical presentation: a case report. *J Med Case Reports* 2014;8:99
  - 22 Ongprakobkul C, Jaigla P, Kositanurit W, Thanprasertsuk S. Sudden cardiac arrest and cerebral thrombosis due to bites by Russell's viper (*Daboia siamensis*). *Toxicol Commun* 2019;3:40–42
  - 23 Gaballa M, Taher T, Brodin LA, et al. Images in cardiovascular medicine. Myocardial infarction as a rare consequence of a snakebite: diagnosis with novel echocardiographic tissue Doppler techniques. *Circulation* 2005;112(11):e140–e142
  - 24 Thomas L, Tyburn B, Bucher B, et al; Research Group on Snake Bites in Martinique. Prevention of thromboses in human patients with *Bothrops lanceolatus* envenoming in Martinique: failure of anticoagulants and efficacy of a monospecific antivenom. *Am J Trop Med Hyg* 1995;52(05):419–426
  - 25 Malbranque S, Piercecchi-Marti MD, Thomas L, et al. Fatal diffuse thrombotic microangiopathy after a bite by the "Fer-de-Lance" pit viper (*Bothrops lanceolatus*) of Martinique. *Am J Trop Med Hyg* 2008;78(06):856–861
  - 26 Layfield HJ, Williams HF, Ravishankar D, et al. Repurposing cancer drugs batimastat and marimastat to inhibit the activity of a group I metalloprotease from the venom of the western diamondback rattlesnake, *Crotalus atrox*. *Toxins (Basel)* 2020;12(05):309
  - 27 Menzies SK, Clare RH, Xie C, et al. *In vitro* and *in vivo* preclinical venom inhibition assays identify metalloproteinase inhibiting drugs as potential future treatments for snakebite envenoming by *Dispholidus typus*. *Toxicon* 2022;14:100118
  - 28 Menon G, Kongwad LI, Nair RP, Gowda AN. Spontaneous intracerebral bleed post snake envenomation. *J Clin Diagn Res* 2017;11(04):PD03–PD04
  - 29 Aissaoui Y, Hammi S, Chkoura K, Ennafaia I, Boughalem M. Association of ischemic and hemorrhagic cerebral stroke due to severe envenomation by the Sahara horned viper (*Cerastes cerastes*). [in French]. *Bull Soc Pathol Exot* 2013;106(03):163–166
  - 30 Bhattacharya S, Krishnamurthy A, Gopalakrishnan M, et al. Endocrine and metabolic manifestations of snakebite envenoming. *Am J Trop Med Hyg* 2020;103(04):1388–1396
  - 31 Golay V, Roychowdhary A, Pandey R. Spontaneous peri-nephric hematoma in a patient with acute kidney injury following Russell's viper envenomation. *Saudi J Kidney Dis Transpl* 2015;26(02):335–338
  - 32 Senthilkumaran S, Miller SW, Williams HF, et al. Development of Wunderlich syndrome following a Russell's viper bite. *Toxicon* 2022;215:11–16
  - 33 Senthilkumaran S, Patel K, Salim A, et al. Neutrophil gelatinase-associated lipocalin acts as a robust early diagnostic marker for renal replacement therapy in patients with Russell's viper bite-induced acute kidney injuries. *Toxins (Basel)* 2021;13(11):797
  - 34 Chani M, Abouzahir A, Larréché S, Mion G. [Pulmonary embolism in the context of severe envenomation by a Moroccan viper. [in French]. *Bull Soc Pathol Exot* 2012;105(03):162–165
  - 35 Lu ZY, Wang XD, Yan J, Ni XL, Hu SP. Critical lower extremity ischemia after snakebite: a case report. *World J Clin Cases* 2021;9(26):7857–7862
  - 36 Bart G, Pineau S, Biron C, Connault J, Artifoni M. Bilateral pulmonary embolism following a viper envenomation in France: a case report and review. *Medicine (Baltimore)* 2016;95(19):e2798
  - 37 Resiere D, Mégarbane B, Valentino R, Mehdaoui H, Thomas L. *Bothrops lanceolatus* bites: guidelines for severity assessment and emergent management. *Toxins (Basel)* 2010;2(01):163–173
  - 38 Gutiérrez JM, Sanz L, Escolano J, et al. Snake venomics of the lesser Antillean pit vipers *Bothrops caribbaeus* and *Bothrops lanceolatus*: correlation with toxicological activities and immunoreactivity of a heterologous antivenom. *J Proteome Res* 2008;7(10):4396–4408
  - 39 Resiere D, Arias AS, Villalta M, et al. Preclinical evaluation of the neutralizing ability of a monospecific antivenom for the treatment of envenomings by *Bothrops lanceolatus* in Martinique. *Toxicon* 2018;148:50–55
  - 40 Das SK, Khaskil S, Mukhopadhyay S, Chakrabarti S. A patient of Russell's viper envenomation presenting with cortical venous thrombosis: an extremely uncommon presentation. *J Postgrad Med* 2013;59(03):235–236

- 41 Prasad UDN, Bandara J, Senanayake HMS. Multiple cerebral and cerebellar infarctions following Russell's viper (*Daboia russelii*) envenomation - a case report. *Clin Med Rev Case Rep* 2020; 7:313
- 42 Ameratunga B. Middle cerebral occlusion following Russell's viper bite. *J Trop Med Hyg* 1972;75(05):95–97
- 43 Hung DZ, Wu ML, Deng JF, Yang DY, Lin-Shiau SY. Multiple thrombotic occlusions of vessels after Russell's viper envenoming. *Pharmacol Toxicol* 2002;91(03):106–110
- 44 Gawarammana I, Mendis S, Jeganathan K. Acute ischemic strokes due to bites by *Daboia russelii* in Sri Lanka - first authenticated case series. *Toxicon* 2009;54(04):421–428
- 45 Chauhan V, Thakur S. The North-South divide in snake bite envenomation in India. *J Emerg Trauma Shock* 2016;9(04): 151–154
- 46 Warrell DA. Clinical toxicology of snake bites in Asia. In: *Handbook of Clinical Toxicology of Animal Venoms and Poisons*. Boca Raton: CRC Press; 1995:493–588
- 47 Kisiel W. Molecular properties of the factor V-activating enzyme from Russell's viper venom. *J Biol Chem* 1979;254(23): 12230–12234
- 48 Takeya H, Nishida S, Miyata T, et al. Coagulation factor X activating enzyme from Russell's viper venom (RVV-X). A novel metalloproteinase with disintegrin (platelet aggregation inhibitor)-like and C-type lectin-like domains. *J Biol Chem* 1992;267(20): 14109–14117
- 49 Op den Brouw B, Coimbra FCP, Casewell NR, Ali SA, Vonk FJ, Fry BG. A genus-wide bioactivity analysis of *Daboia* (Viperinae: Viperidae) viper venoms reveals widespread variation in haemotoxic properties. *Int J Mol Sci* 2021;22(24):13486
- 50 Aung-Khin M, Ma-Ma K, Zin T. Effects of Russell's viper venom on blood coagulation, platelets and the fibrinolytic enzyme system. *Jpn J Med Sci Biol* 1977;30(02):101–108
- 51 Silva A, Scorgie FE, Lincz LF, Maduwage K, Siribaddana S, Isbister GK. Indian polyvalent antivenom accelerates recovery from venom-induced consumption coagulopathy (VICC) in Sri Lankan Russell's viper (*Daboia russelii*) envenoming. *Front Med (Lausanne)* 2022;9:852651
- 52 Gutiérrez JM, Escalante T, Rucavado A, Herrera C. Hemorrhage caused by snake venom metalloproteinases: a journey of discovery and understanding. *Toxins (Basel)* 2016;8(04):93
- 53 Chernysh IN, Nagaswami C, Kosolapova S, et al. The distinctive structure and composition of arterial and venous thrombi and pulmonary emboli. *Sci Rep* 2020;10(01):5112
- 54 Rucavado A, Escalante T, Kalogeropoulos K, Camacho E, Gutiérrez JM, Fox JW. Analysis of wound exudates reveals differences in the patterns of tissue damage and inflammation induced by the venoms of *Daboia russelii* and *Bothrops asper* in mice. *Toxicon* 2020;186:94–104
- 55 Wang JC, Bennett M. Aging and atherosclerosis: mechanisms, functional consequences, and potential therapeutics for cellular senescence. *Circ Res* 2012;111(02):245–259
- 56 Kalita B, Mackessy SP, Mukherjee AK. Proteomic analysis reveals geographic variation in venom composition of Russell's Viper in the Indian subcontinent: implications for clinical manifestations post-envenomation and antivenom treatment. *Expert Rev Proteomics* 2018;15(10):837–849
- 57 Senji Laxme RR, Khochare S, Attarde S, et al. Biogeographic venom variation in Russell's viper (*Daboia russelii*) and the preclinical inefficacy of antivenom therapy in snakebite hotspots. *PLoS Negl Trop Dis* 2021;15(03):e0009247
- 58 Pla D, Sanz L, Quesada-Bernat S, et al. Phylovenomics of *Daboia russelii* across the Indian subcontinent. Bioactivities and comparative in vivo neutralization and in vitro third-generation antivenomics of antivenoms against venoms from India, Bangladesh and Sri Lanka. *J Proteomics* 2019;207:103443
- 59 Warrell DA. Snake venoms in science and clinical medicine. 1. Russell's viper: biology, venom and treatment of bites. *Trans R Soc Trop Med Hyg* 1989;83(06):732–740
- 60 Wüster W, Otsuka S, Malhotra A, Thorpe RS. Population systematics of Russell's viper: a multivariate study. *Biol J Linn Soc Lond* 1992;47(01):97–113

Article

# Repurposing Cancer Drugs Batimastat and Marimastat to Inhibit the Activity of a Group I Metalloprotease from the Venom of the Western Diamondback Rattlesnake, *Crotalus atrox*

Harry J. Layfield <sup>1,†</sup>, Harry F. Williams <sup>1,2,†</sup>, Divyashree Ravishankar <sup>1</sup>, Amita Mehmi <sup>1</sup> , Medha Sonavane <sup>1</sup>, Anika Salim <sup>1</sup>, Rajendran Vaiyapuri <sup>2</sup>, Karthik Lakshminarayanan <sup>2</sup>, Thomas M. Vallance <sup>1</sup>, Andrew B. Bicknell <sup>3</sup>, Steven A. Trim <sup>4</sup> , Ketan Patel <sup>3</sup> and Sakthivel Vaiyapuri <sup>1,\*</sup> 

<sup>1</sup> School of Pharmacy, University of Reading, Reading RG6 6UB, UK; harrylayfield@gmail.com (H.J.L.); harry@toxiven.com (H.F.W.); divyasri.april86@gmail.com (D.R.); A.Mehmi@student.reading.ac.uk (A.M.); m.sonavane@pgr.reading.ac.uk (M.S.); anika.salim@pgr.reading.ac.uk (A.S.); T.M.Vallance@pgr.reading.ac.uk (T.M.V.)

<sup>2</sup> Toxiven Biotech Private Limited, Coimbatore, Tamil Nadu 641042, India; raj@toxiven.com (R.V.); karthik@toxiven.com (K.L.)

<sup>3</sup> School of Biological Sciences, University of Reading, Reading RG6 6UB, UK; a.b.bicknell@reading.ac.uk (A.B.B.); ketan.patel@reading.ac.uk (K.P.)

<sup>4</sup> Venomtech Limited, Sandwich, Kent CT13 9ND, UK; s.trim@venomtech.co.uk

\* Correspondence: s.vaiyapuri@reading.ac.uk

† These authors contributed equally to this paper.

Received: 16 April 2020; Accepted: 7 May 2020; Published: 9 May 2020



**Abstract:** Snakebite envenomation causes over 140,000 deaths every year, predominantly in developing countries. As a result, it is one of the most lethal neglected tropical diseases. It is associated with incredibly complex pathophysiology due to the vast number of unique toxins/proteins present in the venoms of diverse snake species found worldwide. Here, we report the purification and functional characteristics of a Group I (PI) metalloprotease (CAMP-2) from the venom of the western diamondback rattlesnake, *Crotalus atrox*. Its sensitivity to matrix metalloprotease inhibitors (batimastat and marimastat) was established using specific in vitro experiments and in silico molecular docking analysis. CAMP-2 shows high sequence homology to atroxase from the venom of *Crotalus atrox* and exhibits collagenolytic, fibrinogenolytic and mild haemolytic activities. It exerts a mild inhibitory effect on agonist-induced platelet aggregation in the absence of plasma proteins. Its collagenolytic activity is completely inhibited by batimastat and marimastat. Zinc chloride also inhibits the collagenolytic activity of CAMP-2 by around 75% at 50  $\mu$ M, while it is partially potentiated by calcium chloride. Molecular docking studies have demonstrated that batimastat and marimastat are able to bind strongly to the active site residues of CAMP-2. This study demonstrates the impact of matrix metalloprotease inhibitors in the modulation of a purified, Group I metalloprotease activities in comparison to the whole venom. By improving our understanding of snake venom metalloproteases and their sensitivity to small molecule inhibitors, we can begin to develop novel and improved treatment strategies for snakebites.

**Keywords:** *Crotalus atrox*; metalloprotease; snake venom; neglected tropical disease; rattlesnake; batimastat; marimastat; antivenom

**Key Contribution:** This study details the purification of a Group I (PI) snake venom metalloprotease (SVMP) from the venom of *Crotalus atrox* venom and the efficacy of various proposed inhibitors on this isolated SVMP in comparison to the whole venom. Both batimastat and marimastat, commercially

available matrix metalloprotease inhibitors, effectively abrogate the metalloprotease activity of the isolated SVMP and whole venom.

---

## 1. Introduction

In 2017, snakebite envenomation (SBE) was reinstated to the list of neglected tropical diseases by the World Health Organisation [1,2]. SBE is estimated to occur in at least 1.8–2.7 million people, resulting in around 80,000–137,000 deaths and over 400,000 amputations worldwide per year [3]. The distribution of fatalities is primarily concentrated in rural tropical areas that are some of the world's poorest and most healthcare deprived communities [1,4,5]. Prompt access to antivenom therapy and appropriate medical facilities is crucial in order to protect victims from death, potential extensive limb injuries and the possibility of subsequent, long-term disabilities [4]. The current antivenoms are considered to be sub-optimal in preventing venom-induced tissue damage due to their inability to access the affected local tissues [4,5]. Hence, the development of small molecules that are able to neutralise the locally acting venom components would be highly beneficial in treating SBE, specifically SBE-induced muscle damage and/or tissue necrosis.

Snake venoms are a complex mixture of bioactive proteins and peptides that have evolved over time to assist in subduing and killing prey as quickly as possible, as well as having a secondary role in prey digestion and defence [5]. The clinical effects of SBE range from mild local reactions to more serious life-threatening conditions depending on a variety of variables including the size, species and locality of the snake [6,7], ontogeny [8,9], body mass and health of the victim and the total volume of venom injected [1,10]. Snake venoms are composed of both enzymatic and non-enzymatic components. The enzymatic components of viper venoms primarily include the snake venom metalloproteases (SVMPs), serine proteases and phospholipase A<sub>2</sub> (PLA<sub>2</sub>), whereas non-enzymatic venom components include three-finger toxins, C-type lectins and disintegrins amongst many others [5]. The western diamondback rattlesnake, *Crotalus atrox* (*C. atrox*) is likely to be responsible for the majority of SBE-induced fatalities in Northern Mexico [11]. *C. atrox* venom has an abundance of two major protein families, SVMPs and serine proteases, which together account for approximately 70% of the total protein found within the venom [12].

SVMPs are zinc-dependent enzymes that vary in molecular mass from approximately 20 to 100 kDa and are responsible for the haemorrhagic effects and local tissue damage frequently seen upon viper envenomation [13,14]. SVMPs are classified into PI to PIV depending on the presence of additional domains [15]: PI—only a metalloprotease domain; PII—a metalloprotease and a disintegrin domain; PIII—a metalloprotease domain, a disintegrin-like and a cysteine-rich domain; PIV—two C-type lectin domains in addition to all the domains present in PIII. SVMPs are involved in a wide range of toxic activities, including the degradation of collagen and other basement membrane components, fibrinogen and a range of other proteins [13]. The peptidomimetic molecules, batimastat and marimastat are broad-spectrum matrix metalloprotease (MMPs) inhibitors [16] that have been proposed as next generation treatment options for the SVMP-induced effects of SBE [17]. This inhibition is achieved by mimicking the cleavage site of natural substrates and binding to the zinc ion found in the active site of these proteases. In this way, batimastat and the orally bioavailable and similar compound, marimastat are able to inhibit both matrix metalloproteases as well as SVMPs [5]. An improved understanding of MMPs, their inhibitors, and their relationship with SVMPs will aid in the development of improved therapeutic strategies for SBE.

SVMPs in *C. atrox* venom account for 49.7% of total venom, which breaks down further to 22.4% PI and 27.3% PIII SVMPs [12]. In order to determine the therapeutic potential of batimastat and marimastat against PI venom metalloproteases, here, we report the purification and functional characterisation of a PI metalloprotease with a molecular weight of around 23 kDa from the venom of *C. atrox*. The sensitivity of the purified protein to inhibition by batimastat and marimastat was established in comparison to the

whole *C. atrox* venom. Together, this study supports the potential beneficial effects of these molecules against the broad spectrum of pathological effects induced by SVMPs.

## 2. Results

### 2.1. Purification and Identification of CAMP-2

To purify a PI SVMP from the venom of *C. atrox*, we deployed a two-dimensional chromatography approach. Initially, 50 mg of whole *C. atrox* venom was applied to a cation-exchange (SP-HP) chromatography column (Figure 1A) followed by the analysis of collected fractions using SDS-PAGE (Figure 1B). Due to the abundance of the target protein at a molecular weight of around 23 kDa (typical for a PI SVMP [18]), the selected fractions (6–9) were further fractionated by gel filtration (Superdex 75, 1.6 × 70 cm) chromatography (Figure 1C). Following SDS-PAGE analysis (Figure 1D), selected fractions (67–72) were further run through the same gel filtration column to remove any impurities from the protein of interest (Figure 1E,F). Finally, a pure protein with a molecular weight of approximately 23 kDa was isolated, which we henceforth refer to as CAMP-2 (denoting the second SVMP that we have isolated from the venom of *C. atrox*). The molecular weight of the isolated protein was confirmed under native conditions using chymotrypsinogen A (25 kDa) as a marker in gel filtration chromatography (indicated with an arrow in Figure 1C,E) and under denaturing (reduced) conditions using SDS-PAGE (Figure 1F).

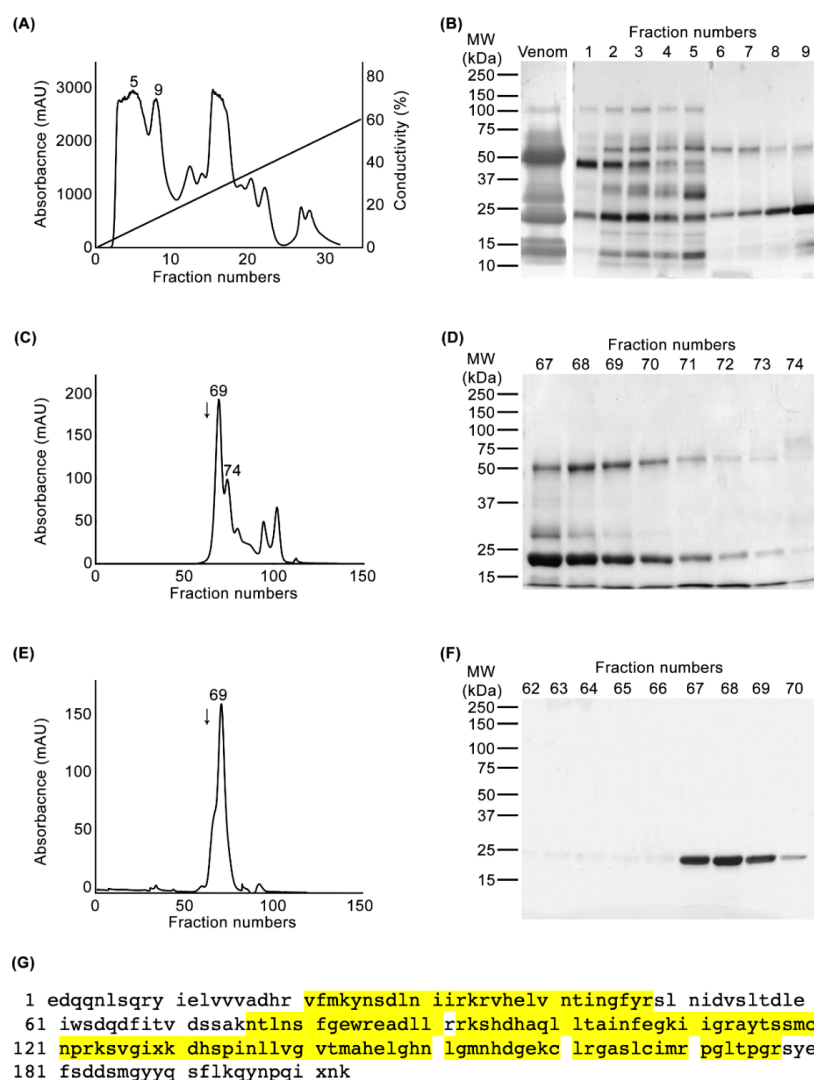


**Figure 1.** Purification and identification of CAMP-2. 50 mg of whole *C. atrox* venom was fractionated

using a cation exchange chromatography column (A) And the collected fractions were analysed by SDS-PAGE (B). (C) A chromatogram showing the gel filtration chromatography profile of fractions 6 to 9 collected from the cation exchange column. (D) SDS-PAGE analysis of selected fractions resulting from the gel filtration chromatography. (E) The chromatogram from the second run of gel filtration chromatography using fractions 67–72 from the previous run, and SDS-PAGE analysis showing the purified protein (F). The gels shown were stained with Coomassie brilliant blue. The arrow in (C) and (E) indicates the position of chymotrypsinogen A (25 kDa), which was used as a molecular weight marker in the same gel filtration column. (G) Tryptic digested peptides of the purified protein were analysed by mass spectrometry and the data show 52.2% identity to a previously sequenced PI SVMP, atroxase, from *C. atrox* venom. The mass spectrometry-identified peptide sequences of purified protein are shown in yellow on the sequence of atroxase.

To determine the identity of the purified protein, it was subjected to trypsin digestion and subsequent analysis by mass spectrometry (Figure 1G). Mascot analysis of the MS/MS data suggested that the isolated protein possesses a high sequence identity to atroxase, a 23 kDa SVMP from the venom of *C. atrox* [19,20]. The peptide sequences resulting from the mass spectrometry covered 52.2% of atroxase, suggesting that the purified protein is highly likely to be atroxase although we cannot confirm this due to the lack of complete sequencing from this study. However, these data confirm that the purified protein is a PI SVMP with a molecular weight of 23 kDa, and it is likely to be atroxase, which was previously purified and characterised as a non-haemorrhagic protease with fibrin(ogen)olytic activities [20–23].

## 2.2. CAMP-2 Exerts Collagenolytic, Fibrinogenolytic and Haemolytic Activities

To determine the roles of CAMP-2, various functional assays using synthetic and natural substrates were performed in comparison to the whole *C. atrox* venom. Fluorogenic substrates such as DQ-gelatin and EnzCheck™ lipid-based substrate were used to assess if CAMP-2 possesses metalloprotease (collagenolytic) and PLA<sub>2</sub> activities, respectively. Similar to the whole *C. atrox* venom (Figure 2A), CAMP-2 (Figure 2B) exhibited strong collagenolytic activity. While the whole *C. atrox* venom showed clear PLA<sub>2</sub> activity, CAMP-2 did not display any PLA<sub>2</sub> activity (Figure 2C). These data not only suggest that CAMP-2 is an SVMP, but it is also free from any PLA<sub>2</sub> impurities which have a similar molecular weight. Moreover, human fibrinogen, a plasma protein which is a natural substrate for some SVMPs, was incubated with CAMP-2, before the digest was analysed by SDS-PAGE to determine its effects on fibrinogen. This analysis showed that CAMP-2 has fibrinogenolytic activity and notably, it exerts high specificity for the A $\alpha$  chain of fibrinogen, as it was completely digested within 10 min (Figure 2D) although over a longer time (e.g., 12 h), it also began to degrade the B $\beta$  chain while the  $\gamma$  chain of fibrinogen remained largely unaffected. Similarly, CAMP-2 showed a mild haemolytic effect compared to the whole venom when incubated with human red blood cells over 24 h (Figure 2E). These data suggest that CAMP-2 is a collagenolytic, fibrinogenolytic and mildly haemolytic enzyme.

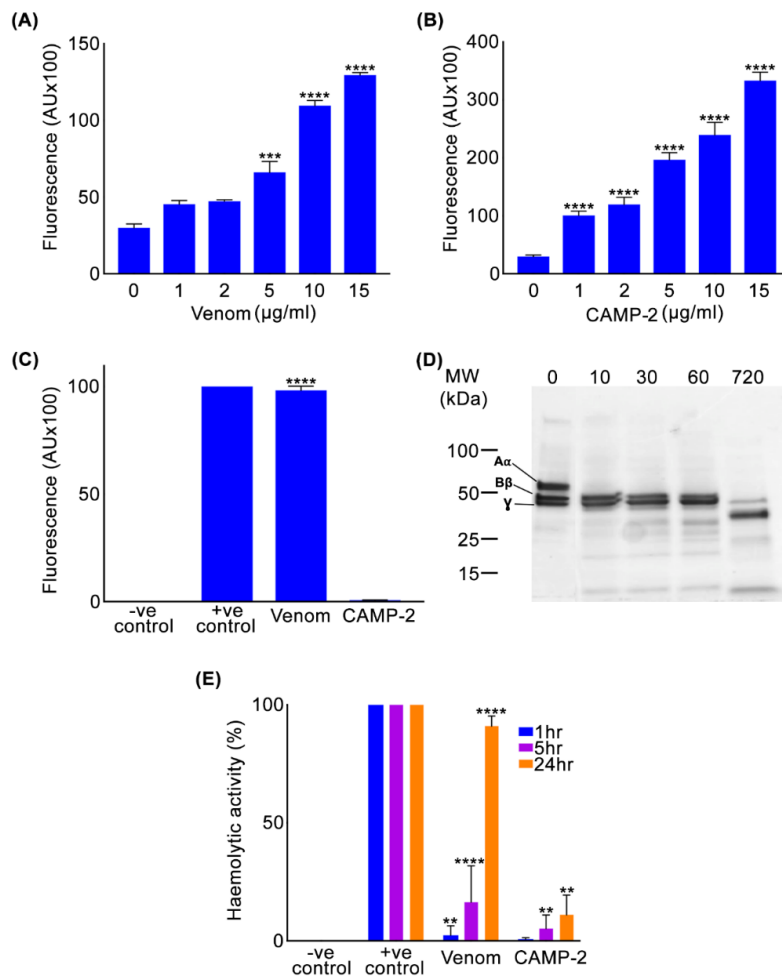


**Figure 2.** Functional characterisation of CAMP-2. The metalloprotease (collagenolytic) activity of different concentrations of whole *C. atrox* venom (A) and CAMP-2 (B) was assessed using DQ gelatin (a fluorogenic substrate). (C) the PLA<sub>2</sub> activity of whole *C. atrox* venom and CAMP-2 was analysed using EnzCheck™ lipid-based substrate. (D) The fibrinogenolytic activity of CAMP-2 was analysed by incubating it with human fibrinogen and the samples collected at different time points (0–720 min as indicated at the top) were assessed by SDS-PAGE and Coomassie staining. (E) Haemolytic activity of whole *C. atrox* venom and CAMP-2 was analysed by incubating them with human red blood cells and analysing the cell-free supernatant by spectrometry. The positive (+ve) control represents the complete lysis achieved using 1% (*v/v*) Triton-X in PBS. Data represent mean  $\pm$  S.D. ( $n = 3$ ). The  $p$ -values shown were calculated using one-way ANOVA followed by posthoc Tukey's test using GraphPad Prism (\*\*  $p \leq 0.01$ , \*\*\*  $p \leq 0.001$  and \*\*\*\*  $p \leq 0.0001$ ).

### 2.3. CAMP-2 Inhibits Human Platelet Aggregation

To determine if CAMP-2 is able to affect human platelet function, platelet aggregation assays using platelet-rich plasma (PRP) and isolated platelets from human whole blood were used. CAMP-2 at both low (3 µg/mL) and high (10 µg/mL) concentrations did not induce platelet aggregation on its own (indicated as 0–5 min in aggregation traces shown in Figure 3). However, 10 µg/mL CAMP-2 inhibited (Figure 3A,B) platelet aggregation (by around 25%) induced by a cross-linked collagen-related peptide (CRP-XL) when isolated platelets were used, although the low concentration did not show any significant effect. This inhibitory effect was absent when PRP (i.e., in the presence of plasma proteins) was used (Figure 3C,D). When the whole *C. atrox* venom was used, at a low concentration (3 µg/mL) it displayed mild inhibitory effects on CRP-XL induced platelet aggregation, although at a higher (10 µg/mL) concentration it has possibly lysed (even in the absence of an agonist as shown in

the aggregation traces between 0 and 5 minutes) the platelets when both isolated platelets (Figure 3E,F) and PRP (Figure 3G,H) were used. These results demonstrate that although CAMP-2 is able to display a minimal inhibitory effect on platelet aggregation when isolated platelets were used, it is unable to affect their function in the presence of plasma proteins, indicating that this may not be its primary role in humans. However, the whole venom may induce the lysis of platelets based on the concentrations injected during the bite.

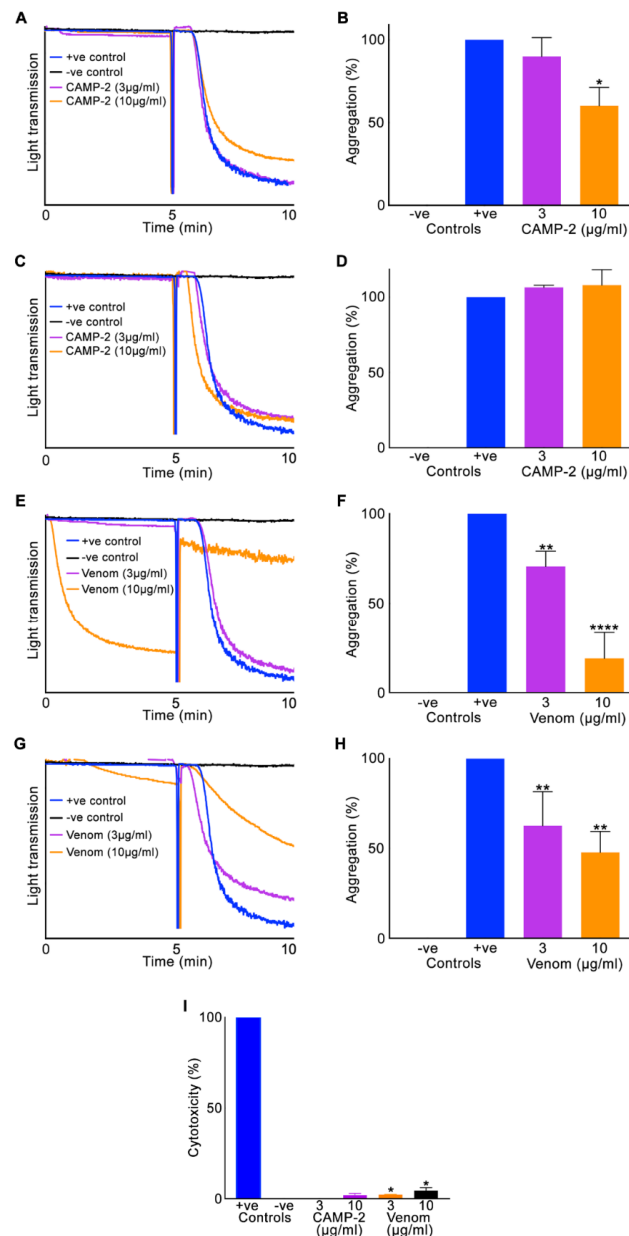


**Figure 3.** Effect of CAMP-2 on human platelets. The effect of CAMP-2 on human isolated platelets (A,B) and platelet-rich plasma (PRP) (C,D) was analysed in the presence and absence of a platelet agonist, cross-linked collagen-related peptide (CRP-XL) by aggregometry. Similar experiments using isolated platelets (E,F) and PRP (G,H) were performed using the whole *C. atrox* venom. The aggregation traces shown are representative of three separate experiments. (I) The cytotoxicity of CAMP-2 and the whole venom was determined by incubating them with human platelets for 30 min and analysing using a lactate dehydrogenase (LDH) assay kit by spectrometry. The positive (+ve) control (100% cytotoxicity) was achieved using a lysis buffer provided in the kit. Data represent mean  $\pm$  S.D. ( $n = 3$ ). The  $p$ -values shown were calculated using one-way ANOVA followed by a posthoc Tukey's test using GraphPad Prism (\*  $p \leq 0.05$ , \*\*  $p \leq 0.01$ , and \*\*\*\*  $p \leq 0.0001$ ).



In order to assess if CAMP-2 and the whole venom are able to exert direct cytotoxic effects on platelets, lactate dehydrogenase (LDH) assay using human isolated platelets was performed. These results indicated that CAMP-2 does not have any cytotoxic effects on platelets at the concentrations tested in this study, although the whole venom displayed a mild (around 10% at 10  $\mu\text{g}/\text{mL}$ ) cytotoxic effect on platelets (Figure 3I) similar to its effect on platelet aggregation (Figure 3E–H).

#### 2.4. Chlorides and a Metal Chelator Affect Metalloprotease Activity of CAMP-2

As zinc-dependent proteases, SVMPs rely on free divalent cations such as calcium for catalysis, the impact of various metal chlorides on the metalloprotease activity of CAMP-2 was assessed. Diverse concentrations of both zinc and calcium chloride were used to assess if they would interfere with the metalloprotease (collagenolytic) activity of CAMP-2 and the whole *C. atrox* venom. The results demonstrate that while zinc chloride significantly reduced the metalloprotease activity observed with both the whole venom (Figure 4A) and CAMP-2 (Figure 4B), calcium chloride potentiated this activity of whole venom (Figure 4C) and CAMP-2 (Figure 4D).

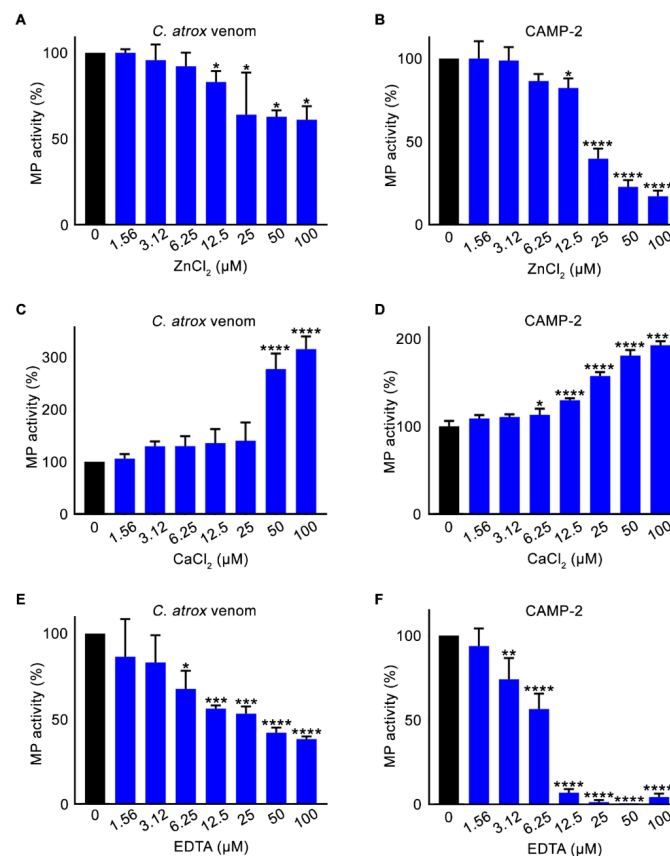


**Figure 4.** The effect of chlorides and a metal chelator on the metalloprotease activity of CAMP-2. The effect of different concentrations of zinc chloride on the metalloprotease (collagenolytic) activity of whole venom (A) and CAMP-2 (B) was analysed using DQ-gelatin as a substrate by spectrofluorimetry. Similarly, the effect of various concentrations of calcium chloride (C,D) and a metal chelator, EDTA (E,F) on whole *C. atrox* venom, as well as on CAMP-2, was analysed. Data represent mean  $\pm$  S.D. ( $n = 3$ ). The  $p$ -values shown are as calculated by one-way ANOVA followed by posthoc Tukey's test using GraphPad Prism (\*  $p \leq 0.05$ , \*\*  $p \leq 0.01$ , \*\*\*  $p \leq 0.001$  and \*\*\*\*  $p \leq 0.0001$ ).

Similarly, the effect of a metal chelator on proteolytic activity was assessed using ethylenediaminetetraacetic acid (EDTA). The metalloprotease activity of both whole venom (Figure 4E) and CAMP-2 (Figure 4F) was strongly inhibited by different concentrations of EDTA, further corroborating that CAMP-2 is a metalloprotease and sensitive to metal chelators such as EDTA.

### 2.5. Marimastat and Batimastat Inhibit the Activity of CAMP-2

After confirming the biological actions of CAMP-2, the effects of MMP inhibitors, batimastat and marimastat on this protein in comparison to the whole *C. atrox* venom were analysed. Different concentrations of these inhibitors were incubated with 2 µg of CAMP-2 or whole venom for 5 min prior to analysing their metalloprotease (collagenolytic) activity using DQ-gelatin by spectrofluorimetry. The results suggest that marimastat (Figure 5A,B) and batimastat (Figure 5C,D) are able to inhibit the metalloprotease activity of both the whole venom and CAMP-2. A concentration of around 3 µM was able to completely inhibit the activity of both the whole venom and CAMP-2. Moreover, neither marimastat nor batimastat exerted any cytotoxic effects on human platelets, as analysed by an LDH assay (Figure 5E,F). These data suggest that these two MMP inhibitors are effective at inhibiting PI SVMPs such as CAMP-2, and they do not possess any cytotoxic activities.

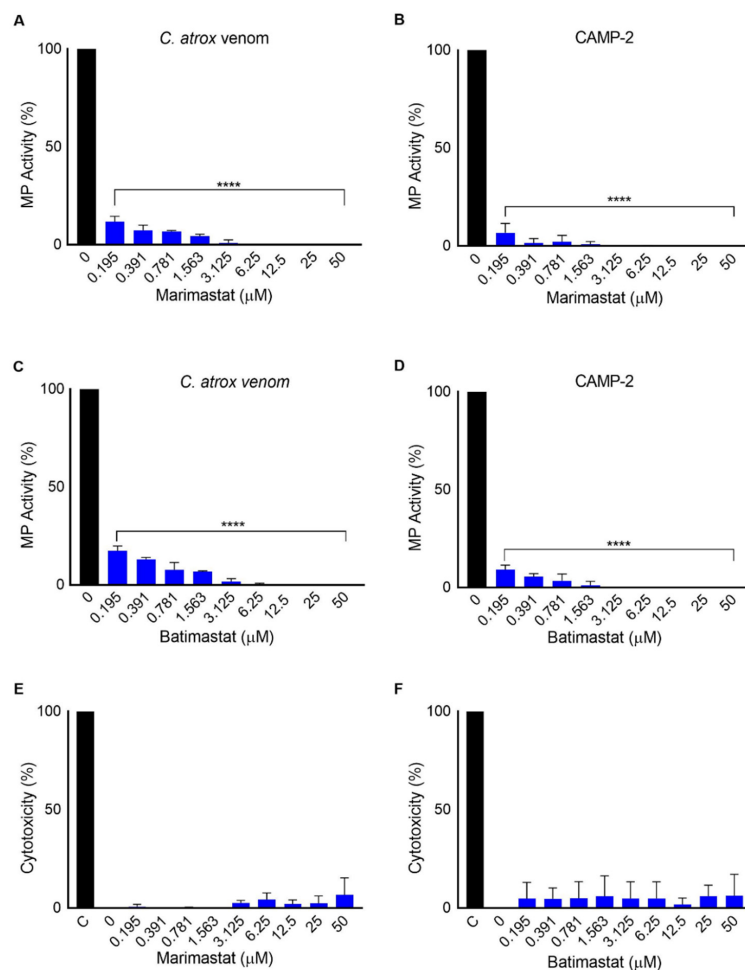


**Figure 5.** Inhibitory effects of marimastat and batimastat on metalloprotease activity of CAMP-2 and whole *C. atrox* venom. The inhibitory effects of various concentrations of marimastat (on whole *C. atrox* venom (A) or CAMP-2 (B)) and batimastat (on whole *C. atrox* venom (C) or CAMP-2 (D)) were quantified in vitro using a fluorogenic substrate, DQ-gelatin by spectrofluorimetry. The inhibitors were incubated with the whole venom or CAMP-2 for 5 min prior to the addition of DQ-gelatin and further incubation of 30 min prior to measuring the level of fluorescence by spectrofluorimetry. The cytotoxicity of marimastat (E) and batimastat (F) on human platelets was also assessed using a lactate dehydrogenase (LDH) assay. C represents the positive control (100% lysis) achieved using the lysis buffer provided in the kit. Data represent mean  $\pm$  S.D. ( $n = 3$ ). The  $p$ -values shown are as calculated by one-way ANOVA followed by posthoc Tukey's test using GraphPad Prism (\*\*\*\*  $p \leq 0.0001$ ).

## 2.6. Interactions of CAMP-2 with Batimastat and Marimastat

The mass spectrometry (Figure 1G) and functional data suggested that CAMP-2 is highly likely to be a previously characterised PI SVMP, atroxase, from the venom of *C. atrox*. Hence, we have used the complete sequence of atroxase (Uniprot accession number: Q91401) as CAMP-2 in this study for further analysis. Sequence analysis confirmed that CAMP-2 displayed approximately 74% and 50% identity with other metalloproteases, atrolysin C (PI SVMP; PDB accession numbers: 1DTH and 1ATL) and catrocollastatin (PIII SVMP; PDB accession number: 2DW0), respectively, from the same *C. atrox* venom. A three-dimensional structure of CAMP-2 was generated using homology modeling in Swiss Model Server [24] based on the template of adamalysin II (PDB accession number: 4AIG) from the venom of *Crotalus adamanteus*. A pairwise sequence alignment confirmed that CAMP-2 exhibited 83% identity with adamalysin II and, therefore, this protein has been used as a template instead of atrolysin C to develop the structure of CAMP-2. The superimposing of CAMP-2 with the structure of adamalysin has displayed a minimum rmsd of 0.142 Å, which further emphasises the reliability of this model.

Following the validation of the modeled structure of CAMP-2, molecular docking analysis was performed using AutoDock 4.2 [25] with the chemical structures (obtained from PubChem) of batimastat and marimastat. Three-dimensional atomic coordinates of these compounds were generated using the Online SMILES Translator and Structure File Generator (NCI NIH server (<https://cactus.nci.nih.gov/translate/>)). Subsequently, the compounds were subjected to energy-minimization using the PRODRG server. The docking analysis revealed that both the inhibitors exhibited comparable binding energy and reliable hydrogen bond interactions with the active site residues of CAMP-2 (Table 1). While batimastat possessed slightly higher binding energy and inhibitory constant, marimastat formed a greater number of hydrogen bonds and hydrophobic interactions with CAMP-2 (Figure 6A–D). Notably, batimastat was found to interact with one of the catalytic triad residues, His 154, through its backbone nitrogen, while marimastat formed a bifurcated hydrogen bond interaction with the active site, Glu 145, through its sidechain oxygen (Table 1). These results are in line with the inhibitory effects observed in the metalloprotease assay (Figure 5A–D).

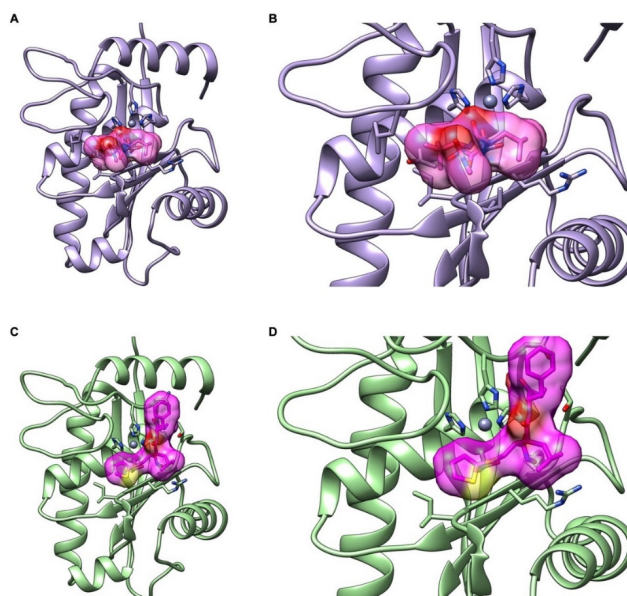


**Figure 6.** Interactions of marimastat and batimastat with the modeled structure of CAMP-2. The structure of CAMP-2 was modeled using the crystal structure of adamalysin II, a highly (83%) similar SVMP from the venom of *Crotalus adamanteus* as a template. This structure was used for molecular docking analysis (using AutoDock) to evaluate the interactions of marimastat (A,B) and batimastat (C,D) with CAMP-2. The structures shown in (B,D) are enlarged views of the docking complex (catalytic site with the small molecule inhibitors batimastat and marimastat).

**Table 1.** Results of molecular docking of CAMP-2 with the inhibitors batimastat and marimastat using AutoDock (a molecular docking tool).

Compound	Binding Energy (kcal/mol)	Ligand Efficiency (kcal/mol)	Inhibitory Constant ( $\mu$ M)	H Bond Interactions (D-H ... A)	Distance (Å)
Batimastat	−5.59	−0.17	79.37	ALA 114 N-H ... O	2.8
				HIS 154 N-H ... O	2.8
Marimastat	−5.29	−0.23	132.52	N-H ... O LYS 109	3.2
				ILE 111 N-H ... O	3.2
				GLY 112 N-H ... O	3.0
				N-H ... O(E2) GLU 145	2.6
				O-H ... O(E2) GLU 145	3.1

### 3. Discussion

Common effects of SBE caused by vipers include haemorrhage, rhabdomyolysis, oedema and severe muscle damage, and often these result in permanent disabilities [1]. These consequences can trigger serious lifestyle and socio-economic ramifications for victims, particularly those in rural areas with difficulty in accessing affordable and effective antivenom [26,27]. The most abundant proteins within viper venoms that are responsible for many of these consequences are SVMPs [13]. The currently used antivenom therapy has proven to be largely ineffective in treating local tissue damage induced by SVMPs due to their inability to access the damaged site because of the large size of antibodies and damaged/blocked blood capillaries around the bite site [5]. As a result, clinicians are forced to employ surgical procedures such as fasciotomy, debridement or limb amputation in severe cases to treat/remove the affected tissues [27]. Therefore, developing an alternative therapy is critical to prevent/treat SBE-induced muscle damage and subsequent disabilities. The use of MMP inhibitors such as batimastat and marimastat has been proposed to inhibit the activities of SVMPs from various venoms [5]. These drugs were originally developed for cancer but failed in clinical trials—batimastat due to its poor solubility and low oral bioavailability, and marimastat, although it showed much promise and reached phase II and III clinical trials, was eventually discontinued after failing to demonstrate a survival benefit [28]. Its longer-term use also leads to debilitating “musculoskeletal syndrome” [29]. Despite these failings, their applications (particularly, orally bioavailable marimastat) in treating the acute local effects induced by SBE would be greatly beneficial to prevent SBE-induced disabilities. Hence, in this study, we have evaluated the efficacy of batimastat and marimastat, specifically on a purified PI SVMP from the venom of *C. atrox*.

We have previously used the two-dimensional chromatography approach (e.g., a combination of ion exchange and gel filtration) as an effective method to purify various venom components, including a 50 kDa PIII SVMP CAMP from the venom of *C. atrox* [14,30]. Here, we have deployed a similar approach to purify a PI SVMP with a molecular weight of 23 kDa from the venom *C. atrox*. The mass spectrometry analysis of this purified protein (entitled CAMP-2) suggests that this is highly likely to be a previously sequenced protein, atroxase, from the same venom. Further functional assays confirmed that CAMP-2 is a collagenolytic, fibrinogenolytic and mildly haemolytic enzyme. At a relatively high concentration, CAMP-2 was also found to inhibit human platelet aggregation. These functions of CAMP-2 are very similar to the ones that have been reported for atroxase (a non-haemolytic protease with fibrin(ogen)olytic activity) [20,23]. Although the complete sequence of CAMP-2 was not obtained in this study, based on the mass spectrometry and functional data, this protein is highly similar, if not identical, to atroxase.

Given that SVMPs directly and indirectly mediate local tissue damage, the inhibition of these enzymes is likely to reduce SBE-induced local tissue damage [13]. Here, the sensitivity of CAMP-2 to MMP inhibitors (batimastat and marimastat) was tested in comparison to the whole *C. atrox* venom. There is a great degree of both structural and functional homology between SVMPs and human variants of MMPs [31]. This implies that substrate/inhibitor interactions between these subfamilies are likely to be similar [31]. Marimastat is a hydroxamic acid derivative which exerts broad-range metalloprotease

inhibition by mimicking the cleavage site of collagen substrates [31]. When comparing the structural differences between these two compounds, marimastat has an additional hydroxyl group, increasing its hydrophilicity and thus, improving its pharmacokinetic properties [32]. Although they are likely to inhibit the majority of SVMPs, the additional domains found in PII, PIII, and PIV SVMPs would most likely be unaffected by these inhibitors. Indeed, batimastat and marimastat have already been reported to inhibit SVMPs in various venoms under *in vitro* and *in vivo* [33–35] settings. Similar to previous studies, the metalloprotease activity of both whole venom and CAMP-2 were almost completely inhibited by MMP inhibitors at around 3  $\mu$ M. Notably, as a PI SVMP, CAMP-2 possesses only the metalloprotease domain. These data emphasise that batimastat and marimastat are both likely to act as broad-spectrum inhibitors for SVMPs including the PI SVMP analysed in this study. In contrast to these inhibitors, which target only the metalloprotease domain of SVMPs, antivenoms, on the other hand, are probably capable of binding all, or many of, the domains including the metalloprotease domain in SVMPs. While the large size of antibodies affects their ability to reach the bite site in time to prevent local tissue damage, the small molecule inhibitors are likely to reach and act rapidly for SBE-induced tissue damage. Multiple injections of these inhibitors have also been suggested to treat SBE, although the consequences of inhibiting human MMPs in the body are yet to be elucidated.

In the past, EDTA has been used to treat SBE under clinical/*in vivo* settings [36]. As a chelating agent, it binds to divalent cations and therefore affects the catalytic activity of metalloproteases. Several studies have reported the impact of EDTA on venom and other human metalloprotease activities [36]. In this study, EDTA has inhibited the metalloprotease activity of both the venom and CAMP-2; however, its use is problematic, and being orally bioavailable, marimastat is a far better clinical approach, especially considering the passing of stage II clinical trials. Similarly,  $ZnCl_2$  has proven to be a successful inhibitor of SVMPs through its ability to cause stereochemical and structural instabilities of metalloproteases when used in excess [37,38].  $ZnCl_2$  has also shown a significant inhibitory effect on the metalloprotease activity of whole venom and CAMP-2 at many of the concentrations tested. Another observation is that the plateau of the SVMP activity observed at 25, 50 and 100  $\mu$ M concentrations when the whole venom was used. This may be as a result of  $Zn^{2+}$  saturation, which may have caused  $Zn^{2+}$  to bind to other ions and proteins within the whole venom, rather than just the metalloproteases [39].

As marimastat and batimastat have proven to be effective in the inhibition of SVMP activity of CAMP-2, a cytotoxicity assay was completed to establish whether they are cytotoxic to human cells, such as platelets. As the LDH cytotoxicity assay measures whether the plasma membrane is damaged, this can be correlated with the effects that the compounds would have on other cells in the human body. If they present signs of cytotoxicity, they would not be appropriate for human use. However, both marimastat and batimastat showed no significant cytotoxic effects on platelets at the numerous concentrations tested and also passed phase I safety trials in humans [28]. This highlights their potential for further development into next-generation treatments for SBE in humans. However, the long-term side effects of their use and dosage requirements are still unknown and demand extensive *in vivo* research before they can be fully supported as an adjunctive treatment for SBE. The use of structural biology to screen and identify small molecules that are likely to affect venom toxins is also beneficial in finding alternative treatments for SBE. In this study, the structure of CAMP-2 was modeled and used in a docking analysis with batimastat and marimastat. Batimastat possessed higher binding energy and inhibitory constant, whereas marimastat has formed multiple hydrogen bonds with the active site of CAMP-2. While batimastat was found to interact with one of the catalytic triad histidine (His 154) residues through its backbone nitrogen, marimastat was observed to form a bifurcated hydrogen bond interaction with another active site residue, glutamate (Glu 145), through its sidechain oxygen. Due to the easy access and robustness of these *in silico* approaches, they can be used to analyse the binding efficiencies of these and other similar molecules with SVMPs from diverse venoms to determine their potential in treating SBE.

SVMPs play important roles in the overall pathophysiology of viper envenoming by inducing local tissue damage and haemorrhage, which can be primarily attributed to their potential to degrade basement membrane components and affect coagulation factors [18,40]. SVMPs activate two key coagulation factors, factor X and prothrombin, to exhibit their procoagulant effects. SVMPs are also known to digest plasma fibrinogen, which may induce clotting effects in some cases, but, largely, it induces the consumption coagulopathy by reducing the functional fibrinogen levels in the plasma, which subsequently results in bleeding. CAMP-2 has also exerted its ability to degrade fibrinogen, specifically the A $\alpha$  chain, with delayed/minimal effect on B $\beta$  chain. SVMPs [18,40], as well as venom serine proteases [41], show varying specificity to cleave the A $\alpha$  and/or B $\beta$  chains of fibrinogen with rarely an effect on the  $\gamma$  chain. Therefore, in addition to their impact on local tissue damage, the effects of SVMPs on the blood coagulation factors, specifically fibrinogen, should also be reduced in order to combat SBE-induced pathological complications.

In conclusion, SVMPs are one of the key venom toxins that should be neutralised as quickly as possible following a snakebite, particularly in the case of vipers. The inability of antivenoms to counteract the effects of SVMPs, particularly at the local bite site, emphasises the urgent need to develop alternative, small molecule-based treatments to minimise SBE-induced tissue damage, which often results in permanent disabilities. In this study, we give a comprehensive analysis of the applications of batimastat, marimastat, EDTA and ZnCl<sub>2</sub> in inhibiting a purified PI SVMP, CAMP-2, in comparison to the whole *C. atrox* venom. The cytotoxic effects of batimastat and marimastat were also analysed. Hence, this study demonstrates a robust method to screen small molecule inhibitors for therapeutic utility against venom toxins using a spectrum of functional assays and *in silico* techniques in order to develop alternative therapies for SBE.

## 4. Materials and Methods

### 4.1. Protein Purification

Lyophilised *C. atrox* venom (50 mg) (Sigma Aldrich, Dorset, UK) was dissolved in 1 mL of 20 mM Tris.HCl (pH 7.4) (ThermoScientific, Loughborough, UK), and after centrifugation at 5000 $\times$  g for 5 min to remove the undissolved materials, the supernatant was applied to a 5-mL HiTrap™ Sepharose (SP) HP cation exchange chromatography column (GE Healthcare, Amersham, UK) and fractionated using an Akta Purifier (GE Healthcare, Amersham, UK). Fractions were collected at a rate of 1 mL/min using 20 mM Tris.HCl pH 7.4 (Buffer A) and 1 M NaCl prepared in Buffer A (Buffer B) with a gradient reaching 60% Buffer B over 30 min. All fractions containing the target protein were pooled together, desalted and concentrated using Vivaspin ultra-centrifugal filtration tubes (Sartorius, Epsom, UK), and applied to a gel filtration column (Superdex 75) to further purify the target protein. Fractions were collected at a rate of 1 mL/min using 20 mM Tris.HCl (pH 7.4).

The fractions were stored on ice and analysed by Bradford protein assay according to the manufacturer's protocol (ThermoScientific, Loughborough, UK) and SDS-PAGE, as described previously [42]. The protein assay was run, and the intensity of the color developed was measured at 600 nm using an Emax spectrophotometer (Molecular Devices, Wokingham, UK). Bovine serum albumin (BSA) (ThermoScientific, Loughborough, UK) was used as a standard in the protein assay. For SDS-PAGE, the proteins were denatured using reducing sample treatment buffer (RSTB) (10% (*w/v*) SDS (ThermoScientific, Loughborough, UK), 10% (*v/v*)  $\beta$ -mercaptoethanol (Sigma Aldrich, Dorset, UK), 1% (*w/v*) bromophenol blue (Sigma Aldrich, Dorset, UK), 50% (*v/v*) glycerol (ThermoScientific, Loughborough, UK) and 20 mM Tris.HCl (pH 7.4)) and heating at 90 °C for 10 min. Samples (30  $\mu$ L from each fraction) were loaded into precast gradient (4–15%) Mini-PROTEAN® TGX™ gels (Bio-Rad, Watford, UK) alongside a protein molecular weight marker (Bio-Rad, Watford, UK) and resolved using a Mini-Protean II apparatus (Biorad, Watford, UK). Gels were immersed in a staining solution (0.1% (*w/v*) Coomassie Brilliant blue R250 (Sigma Aldrich, Dorset, UK) dissolved in 10% (*v/v*) acetic acid (ThermoScientific, Loughborough, UK), 40% (*v/v*) methanol (ThermoScientific, Loughborough, UK)

and 50% deionized water) for 1 h on a plate shaker, washed 3x with deionised water for 5 min and destained (10% (v/v) acetic acid, 10% (v/v) methanol and 80% deionized water) for 3 h or until protein bands became clear.

#### 4.2. Mass Spectrometry Analysis

A gel slice (from SDS-PAGE) containing CAMP-2 was subjected to tryptic digestion before undergoing mass spectrometry analysis at Alta Bioscience (Birmingham, UK), as we described previously [14]. Both MS and MS/MS scans were cross-referenced against the Uniprot protein database using the Sequest algorithm (Thermo fisher PD 1.4) in order to determine the identity of the purified protein.

#### 4.3. Fluorogenic Assays

The metalloprotease (collagenolytic) activity of the venom or the purified protein (CAMP-2) was measured using a fluorogenic substrate, DQ<sup>TM</sup>-gelatin (ThermoScientific, Loughborough, UK). Several concentrations of the purified protein or venom (with and without different concentrations of batimastat, marimastat, EDTA, ZnCl<sub>2</sub> and CaCl<sub>2</sub> (Sigma Aldrich, Dorset, UK)) were added to a black 96-well plate in triplicates along with appropriate controls. Then DQ-gelatin (10 µg/mL) was added to each well, and following mixing, the plate was incubated at 37 °C and the level of fluorescence was measured at various time points using an excitation of 485 nm and emission wavelength of 520 nm in a FLUOstar OPTIMA (BMG Labtech, Ortenberg, Germany) spectrofluorimeter. To determine PLA<sub>2</sub> activity, an EnzChek<sup>TM</sup> Phospholipase A<sub>2</sub> Assay Kit (ThermoFisher Scientific, Loughborough, UK) was used in accordance with the manufacturer's instructions.

#### 4.4. Fibrinogenolytic Assay

CAMP-2 (1 mg/mL) was mixed with fibrinogen (10 mg/mL) (Sigma Aldrich, Dorset, UK) in PBS and incubated at 37 °C for various time points. Samples (50 µL) were taken at time intervals of 10, 30 and 60 min and then again after 12 h and immediately mixed with 25 µL of RSTB before boiling at 90 °C for 10 min. Each sample was then analysed by SDS-PAGE, as explained above.

#### 4.5. Human Blood Collection, Platelet Preparation and Aggregation Assay

Blood samples from healthy human volunteers were obtained in accordance with the approved procedures by the University of Reading Research Ethics Committee (UREC 17/17 approved: 10 May 2017) and after obtaining written informed consent. The platelets were prepared, as described previously [42]. Blood was collected using venepuncture into vacutainers containing 3.2% (w/v) citrate. For PRP, blood samples were centrifuged at 102× g for 20 min at 20 °C. PRP was rested for 30 min at 30 °C in a water bath before use. For isolated platelets preparation, the PRP was mixed with 3 mL of acid citrate dextrose (ACD) and 10 ng/mL prostacyclin (PGI<sub>2</sub> dissolved in EthOH) (Sigma Aldrich, Dorset, UK) and mixed gently by inversion and centrifuged at 1413 g. Modified tyrodes-HEPES buffer (1 ml with 5 mM glucose) was added together with 150 µL of ACD to the platelet pellet to resuspend the pellet, and the final volume was made up to 25 mL using a pre-warmed modified tyrodes-HEPES buffer. A further 3 mL of ACD and 10 ng/mL prostacyclin was added prior to centrifuging at 1413× g for 10 min at 20 °C. Finally, the supernatant was discarded, and the platelets were resuspended in modified tyrodes-HEPES buffer at a density of 4 × 10<sup>8</sup> platelets/mL. The aggregation assays were performed using isolated platelets or PRP with 0.5 µg/mL CRP-XL (obtained from Professor Richard Farndale, University of Cambridge, UK) as an agonist. The level of aggregation in the presence and absence of different concentrations of venom or CAMP-2 was monitored using an optical aggregometer (model 700, Chrono-log, USA).

#### 4.6. Haemolytic Assay

Human erythrocytes were collected from the dense red blood cells found in the bottom of vacutainers following centrifugation for the collection of PRP, as mentioned above. These erythrocytes were then washed three times by mixing with an equal volume of PBS, centrifuging at  $2000\times g$  for 2 min, and discarding the supernatant. The haemolytic activity was measured using these washed human erythrocytes suspended in calcified phosphate-buffered saline (PBS). The erythrocytes were treated with different concentrations of CAMP-2 or venom and incubated at  $37\text{ }^{\circ}\text{C}$  for various time points. A detergent, Triton X-100 (1%) (Sigma Aldrich, Dorset, UK), and PBS were used as a positive and negative control, respectively. Following incubation, the samples were centrifuged at  $2000\times g$  for two minutes and  $50\text{ }\mu\text{L}$  of supernatant was pipetted into a 96-well plate and the absorbance was measured at 540 nm using a spectrophotometer.

#### 4.7. LDH Cytotoxicity Assay

An LDH cytotoxicity assay kit (ThermoFisher, Loughborough, UK) was used in accordance with the manufacturer's instructions. Briefly, human platelets were incubated at  $37\text{ }^{\circ}\text{C}$  for 30 min prior to incubation with different concentrations of venom or CAMP-2 or small molecule inhibitors for five minutes. These results were compared with those from the positive control (100% lysis) achieved using the lysis buffer provided. The substrate mix from the kit was added to the platelets and incubated for another 30 min and subsequently stopped using the stop solution provided. The level of absorbance was read at 490 and 650 nm using a Fluostar Optima (BMG Labtech, Ortenberg, Germany) spectrofluorimeter. The assay was performed in duplicates using platelets obtained from three individual donors.

#### 4.8. Structure Modelling and Molecular Docking

A three-dimensional structure of CAMP-2 was developed using homology modeling in the Swiss Model Server [24] based on the crystal structure of adamalysin II (PDB accession number: 4AIG) from the venom of *Crotalus adamanteus* as a template. Before proceeding to the docking simulation, protein preparation steps such as fixing charge for the  $\text{Zn}^{2+}$  metal ion, adding solvation parameters and polar hydrogens to the metalloprotease were carried out. AutoDock [25] necessitates pre-calculated grid maps for each type of atom present in the ligand molecule being docked because it stores the potential energy produced from interacting with the macromolecule. This grid surrounds the region of interest (active site) of the macromolecule. A grid box of size  $50 \times 50 \times 50\text{ }\text{\AA}$  with a spacing of  $0.375\text{ }\text{\AA}$  was prepared at the active site of CAMP-2 metalloprotease. The Lamarckian genetic algorithm was used to identify the best conformers. Throughout the docking process, a maximum of 15 conformers was considered per compound. AutoDock (version 4.0 SRC, California, USA) was compiled and run under Microsoft Windows XP operating system.

#### 4.9. Statistical Analysis

All statistical analyses were performed with GraphPad Prism (version 7.0, Graphpad Prism, California, USA, 2018). For most of the data, the statistical significance was analysed using one-way ANOVA, which was followed by a posthoc Tukey's test.

**Author Contributions:** Conceptualization, S.V., R.V. and H.F.W.; Methodology, K.L., S.V.; Software, K.L.; Formal Analysis, K.L., H.J.L., H.F.W., S.V.; Investigation, H.J.L., M.S., D.R., A.S., H.F.W. and T.M.V.; Resources, S.A.T., A.B.B., K.P. and S.V.; Writing-Original Draft Preparation, H.J.L., H.F.W., A.M. and S.V.; Writing-Review & Editing, All authors.; Supervision, R.V., H.F.W., S.V., S.A.T., A.B.B. and K.P. All authors have read and agreed to the published version of the manuscript.

**Funding:** This research received no external funding.

**Conflicts of Interest:** The authors declare no conflict of interest.



## References

1. Gutierrez, J.M.; Calvete, J.J.; Habib, A.G.; Harrison, R.A.; Williams, D.J.; Warrell, D.A. Snakebite envenoming. *Nat. Rev. Dis. Primers* **2017**, *3*, 17079. [[CrossRef](#)]
2. Chippaux, J.P. Snakebite envenomation turns again into a neglected tropical disease! *J. Venom. Anim. Toxins Incl. Trop. Dis.* **2017**, *23*, 38. [[CrossRef](#)]
3. Kasturiratne, A.; Wickremasinghe, A.R.; de Silva, N.; Gunawardena, N.K.; Pathmeswaran, A.; Premaratna, R.; Savioli, L.; Lalloo, D.G.; de Silva, H.J. The global burden of snakebite: A literature analysis and modelling based on regional estimates of envenoming and deaths. *PLoS Med.* **2008**, *5*, e218. [[CrossRef](#)] [[PubMed](#)]
4. Williams, D.; Gutierrez, J.M.; Harrison, R.; Warrell, D.A.; White, J.; Winkel, K.D.; Gopalakrishnakone, P. The Global Snake Bite Initiative: An antidote for snake bite. *Lancet* **2010**, *375*, 89–91. [[CrossRef](#)]
5. Williams, H.F.; Layfield, H.J.; Vallance, T.; Patel, K.; Bicknell, A.B.; Trim, S.A.; Vaiyapuri, S. The Urgent Need to Develop Novel Strategies for the Diagnosis and Treatment of Snakebites. *Toxins (Basel)* **2019**, *11*, 363. [[CrossRef](#)] [[PubMed](#)]
6. Sunagar, K.; Undheim, E.A.; Scheib, H.; Gren, E.C.; Cochran, C.; Person, C.E.; Koludarov, I.; Kelln, W.; Hayes, W.K.; King, G.F.; et al. Intraspecific venom variation in the medically significant Southern Pacific Rattlesnake (*Crotalus oreganus helleri*): Biodiscovery, clinical and evolutionary implications. *J. Proteom.* **2014**, *99*, 68–83. [[CrossRef](#)] [[PubMed](#)]
7. Fry, B.G.; Winkel, K.D.; Wickramaratna, J.C.; Hodgson, W.C.; Wüster, W. Effectiveness of Snake Antivenom: Species and Regional Venom Variation and Its Clinical Impact. *J. Toxicol. Toxin Rev.* **2003**, *22*, 23–34. [[CrossRef](#)]
8. Pla, D.; Sanz, L.; Sasa, M.; Acevedo, M.E.; Dwyer, Q.; Durban, J.; Perez, A.; Rodriguez, Y.; Lomonte, B.; Calvete, J.J. Proteomic analysis of venom variability and ontogeny across the arboreal palm-pitvipers (genus *Bothriechis*). *J. Proteom.* **2017**, *152*, 1–12. [[CrossRef](#)]
9. Modahl, C.M.; Mukherjee, A.K.; Mackessy, S.P. An analysis of venom ontogeny and prey-specific toxicity in the Monocled Cobra (*Naja kaouthia*). *Toxicon* **2016**, *119*, 8–20. [[CrossRef](#)]
10. Harrison, R.A.; Hargreaves, A.; Wagstaff, S.C.; Faragher, B.; Lalloo, D.G. Snake envenoming: A disease of poverty. *PLoS Negl. Trop. Dis.* **2009**, *3*, e569. [[CrossRef](#)]
11. Yanez-Arenas, C.; Peterson, A.T.; Mokondoko, P.; Rojas-Soto, O.; Martinez-Meyer, E. The use of ecological niche modeling to infer potential risk areas of snakebite in the Mexican state of Veracruz. *PLoS ONE* **2014**, *9*, e100957. [[CrossRef](#)] [[PubMed](#)]
12. Calvete, J.J.; Fasoli, E.; Sanz, L.; Boschetti, E.; Righetti, P.G. Exploring the venom proteome of the western diamondback rattlesnake, *Crotalus atrox*, via snake venomomics and combinatorial peptide ligand library approaches. *J. Proteome Res.* **2009**, *8*, 3055–3067. [[CrossRef](#)] [[PubMed](#)]
13. Gutierrez, J.M.; Rucavado, A. Snake venom metalloproteinases: Their role in the pathogenesis of local tissue damage. *Biochimie* **2000**, *82*, 841–850. [[CrossRef](#)]
14. Williams, H.F.; Mellows, B.A.; Mitchell, R.; Sfyri, P.; Layfield, H.J.; Salamah, M.; Vaiyapuri, R.; Collins-Hooper, H.; Bicknell, A.B.; Matsakas, A.; et al. Mechanisms underpinning the permanent muscle damage induced by snake venom metalloprotease. *PLoS Negl. Trop. Dis.* **2019**, *13*, e0007041. [[CrossRef](#)]
15. Fox, J.W.; Serrano, S.M. Structural considerations of the snake venom metalloproteinases, key members of the M12 repolysin family of metalloproteinases. *Toxicon* **2005**, *45*, 969–985. [[CrossRef](#)]
16. Rasmussen, H.S.; McCann, P.P. Matrix metalloproteinase inhibition as a novel anticancer strategy: A review with special focus on batimastat and marimastat. *Pharm. Ther.* **1997**, *75*, 69–75. [[CrossRef](#)]
17. Knudsen, C.; Laustsen, A.H. Recent Advances in Next Generation Snakebite Antivenoms. *Trop. Med. Infect. Dis.* **2018**, *3*, 42. [[CrossRef](#)]
18. Markland, F.S., Jr.; Swenson, S. Snake venom metalloproteinases. *Toxicon* **2013**, *62*, 3–18. [[CrossRef](#)]
19. Baker, B.J.; Wongvibulsin, S.; Nyborg, J.; Tu, A.T. Nucleotide sequence encoding the snake venom fibrinolytic enzyme atroxase obtained from a *Crotalus atrox* venom gland cDNA library. *Arch. Biochem. Biophys.* **1995**, *317*, 357–364. [[CrossRef](#)]
20. Willis, T.W.; Tu, A.T. Purification and biochemical characterization of atroxase, a nonhemorrhagic fibrinolytic protease from western diamondback rattlesnake venom. *Biochemistry* **1988**, *27*, 4769–4777. [[CrossRef](#)]

21. Tu, A.T.; Baker, B.; Wongvibulsin, S.; Willis, T. Biochemical characterization of atroxase and nucleotide sequence encoding the fibrinolytic enzyme. *Toxicon* **1996**, *34*, 1295–1300. [[CrossRef](#)]
22. Baker, B.J.; Tu, A.T. Atoxase—A fibrinolytic enzyme isolated from the venom of western diamondback rattlesnake. Isolation, characterization and cloning. *Adv. Exp. Med. Biol.* **1996**, *391*, 203–211. [[PubMed](#)]
23. Willis, T.W.; Tu, A.T.; Miller, C.W. Thrombolysis with a snake venom protease in a rat model of venous thrombosis. *Thromb. Res.* **1989**, *53*, 19–29. [[CrossRef](#)]
24. Waterhouse, A.; Bertoni, M.; Bienert, S.; Studer, G.; Tauriello, G.; Gumienny, R.; Heer, F.T.; de Beer, T.A.P.; Rempfer, C.; Bordoli, L.; et al. SWISS-MODEL: Homology modelling of protein structures and complexes. *Nucleic Acids Res.* **2018**, *46*, W296–W303. [[CrossRef](#)] [[PubMed](#)]
25. Morris, G.M.; Huey, R.; Olson, A.J. Using AutoDock for ligand-receptor docking. *Curr. Protoc. Bioinform.* **2008**, *24*, 8.14.1–8.14.40. [[CrossRef](#)] [[PubMed](#)]
26. Vaiyapuri, S.; Vaiyapuri, R.; Ashokan, R.; Ramasamy, K.; Nattamaisundar, K.; Jeyaraj, A.; Chandran, V.; Gajjeraman, P.; Baksh, M.F.; Gibbins, J.M.; et al. Snakebite and its socio-economic impact on the rural population of Tamil Nadu, India. *PLoS ONE* **2013**, *8*, e80090. [[CrossRef](#)]
27. Williams, H.F.; Vaiyapuri, R.; Gajjeraman, P.; Hutchinson, G.; Gibbins, J.M.; Bicknell, A.B.; Vaiyapuri, S. Challenges in diagnosing and treating snakebites in a rural population of Tamil Nadu, India: The views of clinicians. *Toxicon* **2017**, *130*, 44–46. [[CrossRef](#)]
28. Winer, A.; Adams, S.; Mignatti, P. Matrix Metalloproteinase Inhibitors in Cancer Therapy: Turning Past Failures Into Future Successes. *Mol. Cancer Ther.* **2018**, *17*, 1147–1155. [[CrossRef](#)]
29. Vandenbroucke, R.E.; Libert, C. Is there new hope for therapeutic matrix metalloproteinase inhibition? *Nat. Rev. Drug Discov.* **2014**, *13*, 904–927. [[CrossRef](#)]
30. Vaiyapuri, S.; Hutchinson, E.G.; Ali, M.S.; Dannoura, A.; Stanley, R.G.; Harrison, R.A.; Bicknell, A.B.; Gibbins, J.M. Rhinocetin, a venom-derived integrin-specific antagonist inhibits collagen-induced platelet and endothelial cell functions. *J. Biol. Chem.* **2012**, *287*, 26235–26244. [[CrossRef](#)]
31. Howes, J.M.; Theakston, R.D.; Laing, G.D. Neutralization of the haemorrhagic activities of viperine snake venoms and venom metalloproteinases using synthetic peptide inhibitors and chelators. *Toxicon* **2007**, *49*, 734–739. [[CrossRef](#)] [[PubMed](#)]
32. Rasmussen, H.S. Batimastat and Marimastat in Cancer. In *Antiangiogenic Agents in Cancer Therapy*; Teicher, B.A., Ed.; Humana Press: Totowa, NJ, USA, 1999; pp. 399–405.
33. Rucavado, A.; Escalante, T.; Gutiérrez, J.M.A. Effect of the metalloproteinase inhibitor batimastat in the systemic toxicity induced by Bothrops asper snake venom: Understanding the role of metalloproteinases in envenomation. *Toxicon* **2004**, *43*, 417–424. [[CrossRef](#)] [[PubMed](#)]
34. Rucavado, A.; Escalante, T.; Franceschi, A.; Chaves, F.; León, G.; Cury, Y.; Ovadia, M.; Gutiérrez, J.M. Inhibition of local hemorrhage and dermonecrosis induced by Bothrops asper snake venom: Effectiveness of early in situ administration of the peptidomimetic metalloproteinase inhibitor batimastat and the chelating agent CaNa2EDTA. *Am. J. Trop. Med. Hyg.* **2000**, *63*, 313–319. [[CrossRef](#)] [[PubMed](#)]
35. Escalante, T.; Franceschi, A.; Rucavado, A.; Gutiérrez, J.M.A. Effectiveness of batimastat, a synthetic inhibitor of matrix metalloproteinases, in neutralizing local tissue damage induced by BaP1, a hemorrhagic metalloproteinase from the venom of the snake Bothrops asper. *Biochem. Pharm.* **2000**, *60*, 269–274. [[CrossRef](#)]
36. Ainsworth, S.; Slagboom, J.; Alomran, N.; Pla, D.; Alhamdi, Y.; King, S.I.; Bolton, F.M.S.; Gutierrez, J.M.; Vonk, F.J.; Toh, C.H.; et al. The paraspecific neutralisation of snake venom induced coagulopathy by antivenoms. *Commun. Biol.* **2018**, *1*, 34. [[CrossRef](#)] [[PubMed](#)]
37. Cordeiro, F.A.; Coutinho, B.M.; Wiesel, G.A.; Bordon, K.F. Purification and enzymatic characterization of a novel metalloprotease from *Lachesis muta rhombata* snake venom. *J. Venom. Anim. Toxins Incl. Trop. Dis.* **2018**, *24*, 32. [[CrossRef](#)] [[PubMed](#)]
38. Gomez-Ortiz, M.; Gomis-Ruth, F.X.; Huber, R.; Aviles, F.X. Inhibition of carboxypeptidase A by excess zinc: Analysis of the structural determinants by X-ray crystallography. *Febs Press* **1997**, *400*, 336–340. [[CrossRef](#)]
39. Takeda, S. ADAM and ADAMTS Family Proteins and Snake, Venom Metalloproteinases: A Structural Overview. *Toxins* **2016**, *8*, 155. [[CrossRef](#)]
40. Kini, R.M.; Koh, C.Y. Metalloproteases Affecting Blood Coagulation, Fibrinolysis and Platelet Aggregation from Snake Venoms: Definition and Nomenclature of Interaction Sites. *Toxins (Basel)* **2016**, *8*, 284. [[CrossRef](#)]

41. Yamazaki, Y.; Morita, T. Snake venom components affecting blood coagulation and the vascular system: Structural similarities and marked diversity. *Curr. Pharm. Des.* **2007**, *13*, 2872–2886. [[CrossRef](#)]
42. Vaiyapuri, S.; Sage, T.; Rana, R.H.; Schenk, M.P.; Ali, M.S.; Unsworth, A.J.; Jones, C.I.; Stainer, A.R.; Kriek, N.; Moraes, L.A.; et al. EphB2 regulates contact-dependent and contact-independent signaling to control platelet function. *Blood* **2015**, *125*, 720–730. [[CrossRef](#)] [[PubMed](#)]



© 2020 by the authors. Licensee MDPI, Basel, Switzerland. This article is an open access article distributed under the terms and conditions of the Creative Commons Attribution (CC BY) license (<http://creativecommons.org/licenses/by/4.0/>).